AD NUMBER

AD915581

LIMITATION CHANGES

TO:

Approved for public release; distribution is unlimited.

FROM:

Distribution authorized to U.S. Gov't. agencies only; Test and Evaluation; AUG 1973. Other requests shall be referred to Rome Air Development Center, Attn: TUTV, Griffiss AFB, NY 13441.

AUTHORITY

RADC ltr, 8 Jul 1983

AD 915 581

AUTHORITY: RADC, USAF
ltr, 8 Jul 83

RADC-TR-73-233
Final Report
August 1973

PRECISION ANTENNA MEASUREMENT SYSTEM (PAMS)

Actron Industries, Inc.

Rome Air Development Center
Air Force Systems Command
Griffiss Air Force Base, New York

PRECISION ANTENNA MEASUREMENT SYSTEM (PAMS)

Graham A. Walker

Actron Industries, Inc.

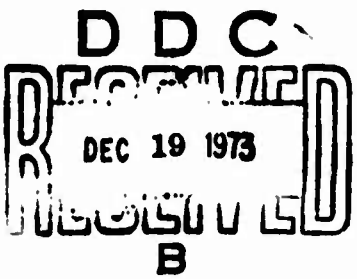

FOREWORD

This document is the Final Technical Report for the design, development, and fabrication of a Precision Antenna Measurement System (PAMS). This report covers work accomplished by Actron Industries, Inc., 700 Royal Oaks Drive, Monrovia, California under Contract Number F30602-70-C-0011. The effort reported herein was performed during the period January 1970 - February 1972 ,Job Order No.: 65100015.

It should be noted that at the time of contract award Tridea Electronics was the program contractor. References here and elsewhere in this report to Actron reflects the fact that, on 1 June 1971, Tridea Electronics was merged into Actron Industries, Inc., a subsidiary of the McDonnell Douglas Corporation.

This Final Technical Report was submitted by Actron Industries, Inc. in fulfillment of Contract Number F30602-70-C-0011 and was written by Graham A. Walker.

Acknowledgement is made here to R. L. Mitchell of the Technology Service Corporation, Santa Monica, California of his efforts in the preparation of the "Active RCS Measurements With PAMS" Report Number TCS-PD-342-1, dated 21 February 1972, which is included as the appendix to this report.

The principal contributors to the development of the system described and discussed herein are: Robert J. Schlesinger and William B. Whistler who directed the system design, Edward S. Peltzman and Graham A. Walker who executed the Logic and RF design, respectively, and William E. Ellau who did the mechanical design.

Special appreciation is extended to Mr. M. E. Cook of the Rome Air Development Center for his tireless and enthusiastic support of the program from its very inception, and for his valuable guidance and direction during the development and checkout phase.

This technical report has been reviewed and is approved.

Approved: Merton E. Cook

MERTON E. COOK
Project Engineer

Approved: Quentin J. Porter

QUENTIN J. PORTER
Chief, Technical Support Div

FOR THE COMMANDER: Carlo P. Crocetti

CARLO P. CROCETTI
Chief, Plans Office

ABSTRACT

This technical report documents the design, development, and performance of a Precision Antenna Measurement System (PAMS) which is used to perform dynamic measurements and evaluate the radiation characteristics of airborne antennas.

The PAMS operates over the frequency range of 100 MHz through 18 GHz and can be used to measure the cross section of aircraft and chaff. The system is slaved to either a MSQ-1A or FPS-16 track radar for aircraft acquisition.

The report details the design parameters and covers the data acquisition and computer programs used in the data reduction. The system performance is presented and actual antenna patterns given for various antenna configurations on a C-131 aircraft.

EVALUATOR'S MEMO ON FINAL REPORT

This technical report documents the design, development and performance of a Precision Antenna Measurement System (PAMS).

The PAMS is a operational passive measurement system located at the Rome Air Development Center Test Annex, Verona, NY. The system, slaved to the AN/FPS-16 tracking radar, provides the capability to conduct engineering evaluations of airborne antennas designed for use on tactical aircraft equipped with ECM and associated penetration aids. The facility operates over the frequency range of 0.1 - 18 GHz and is capable of receiving AM, FM, CW or pulse type signals of any polarization. Measurements are correlated with the aircraft attitude and are conducted on a real time radiated basis. Types of measurements include power (peak signal amplitude), density (peak signal amplitude X the IF Bandwidth) and integrated (integrated amplitude over octave or increments of an octave bandwidth in terms of DBW/MHZ). The final plotted data can be outputed in polarization, rectangular or three dimension.

Several objectives were met during the system development which are, collection of high densities of data with a minimum of flying time, multiple (12) frequency evaluations during a single flight, collection of antenna pattern and cross section data simultaneously, and a timely output of processed data.

Merton E Cook

MERTON E. COOK
Project Engineer

TABLE OF CONTENTS

TABLE OF CONTENTS (CONTINUED)

TABLE OF CONTENTS (CONTINUED)

TABLE OF CONTENTS (CONTINUED)

LIST OF ILLUSTRATIONS

LIST OF ILLUSTRATIONS (CONTINUED)

LIST OF ILLUSTRATIONS (CONTINUED)

LIST OF TABLES

SECTION I

INTRODUCTION AND REPORT SUMMARY

1.1 INTRODUCTION

This technical report documents the design, development, and performance of a Precision Antenna Measurement System (PAMS) which is used to perform dynamic measurements and evaluate the radiation characteristics of airborne RF antennas.

1.2 REPORT SUMMARY

PAMS receives RF radiation over the frequency range of 0.1 GHz through 18 GHz and with suitable illuminators can also be used to measure reflectivity and radar cross-section of aircraft and chaff. PAMS has the capability to monitor and collect data on twelve signals simultaneously in either vertical and horizontal polarization, or right- and left-hand polarization, or a combination of both. Target acquisition is obtained by slaving PAMS to an AN/MSQ-1 or an AN/FPS-16 track radar.

Data storage and reduction is accomplished by an HP2116B computer with 24K memory and dual HP7970A digital tape decks. Real time printout of the received signal is available during test on an HP2778A line printer. The reduced data may be displayed in either two-dimensional rectangular or polar formats on a Cal Comp 565 drum plotter and three-dimensional plots on the line printer. Interface with the computer and the operator is via teletype.

Section II of this report deals with the overall objectives of the development program; the system requirements are covered, and all of the features required for optimum system performance are described.

System considerations are investigated in Section III and operating parameters which are consistent with the contractual requirements are defined. Computer interface and programming requirements are also described in this Section.

Section IV describes the PAMS configuration. The basic theory of operation is covered and detailed block diagrams of the system are presented. Interface with the computer and data storage and reduction are also described in detail in Section IV.

Operational results of the PAMS system during Final Acceptance Tests conducted at the Verona Annex of Rome Air Development Center, Rome, New York are covered in Section V. The test program consisted of performing static tests using known emitters operating from a van located approximately eight miles from the Verona site. Flight tests, using RADC aircraft, were made to evaluate the dynamic performance of PAMS. Both the AN/MSQ-1 and the AN/FPS-16 were used as the track radar during the flight test program.

Performance of the PAMS is analyzed in Section VI with respect to the operational results. The problem of determining an error allowance to various portions of the system is also addressed and the effect of the system error is analyzed with respect to the operational data. Overall accuracy of the PAMS is then dictated and boundary

conditions set to ensure optimum performance of the system. Section VII summarizes the PAMS program to date and draws some final conclusions on the operational capability of the system and recommends procedures to improve system accuracy.

The Appendix to this report contains a tutorial discussion of reflectivity and radar cross-section with specific application to the PAMS.

SECTION II

PROGRAM OBJECTIVE AND REQUIREMENTS

2.1 OBJECTIVE

The objective of the PAMS program was, as briefly covered in the introduction to this report, to develop an electronics system capable of performing precision measurements of the radiation characteristics of airborne RF antennas. In the past it was the practice to test antennas on a partial mockup of the aircraft or to use scale models of the aircraft and its antenna complement. However, this method has not provided enough realistic data on the antennas and the effect of the aircraft on the antenna characteristics. The development of the Precision Antenna Measurement System (PAMS) was undertaken to provide the type of data that is needed to accurately describe the effective radiation profile of airborne antenna systems.

2.2 REQUIREMENTS

The basic requirements of the PAMS were that the system be capable of performing dynamic measurements of airborne RF radiating systems and reflectivity/cross-section measurements of airborne vehicles and chaff. In general, it was required that the data be recorded in the following manner.

a. Two- and three-dimensional radiation patterns. These patterns to include rectangular, polar, and contour plots of single and multiple sources.

b. Power density measurements in watts per megahertz. The data to be correlated with the attitude of the aircraft and plotted with respect to the aircraft heading, with a final resolution of ±0.5 db and ±0.5 degree.

The requirements of the PAMS appear relatively simple; however, they require a very complex system with multiple capabilities. These basic requirements must be met over a frequency range of 0.1 GHz through 18 GHz. In addition, the measurements must be made simultaneously in both vertical and horizontal polarizations, or in right-hand and left-hand circular polarizations. The signals may be CW, AM, pulse, Doppler, or noise. To ensure valid data, the system must incorporate an automatic calibration system with ±0.1 percent frequency accuracy and ±0.5 db amplitude accuracy. The ability to collect, measure, and store all of these data automatically requires the incorporation of a computer into the system. The computer is then used to control the system during data collection.

2.3 CAPABILITIES

The concept of the PAMS is illustrated in figure 1. It was determined that the PAMS would comprise four groupings which would consist of (1) the Antenna and Pedestal, (2) the Receiver Group, (3) the Control and Display Console, and (4) the Computer Group, as shown. It was further determined that, to meet the system operational requirements, each of these groups would have specific capabilities, as are detailed in paragraphs 2.3.1 through 2.3.5.

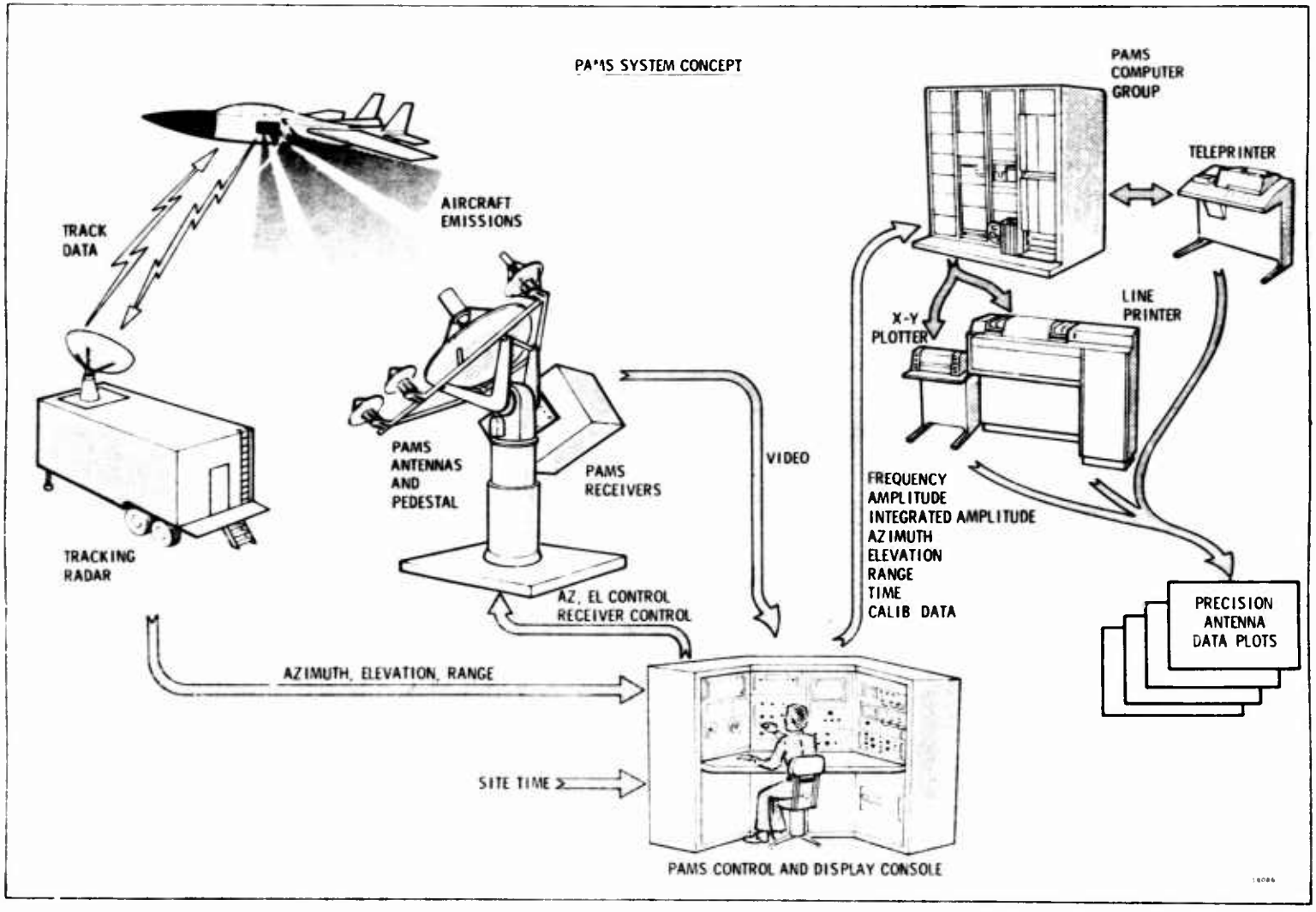

Figure 1. PAMS System Concept

2.3.1 Antennas

The PAMS antenna system would be required to operate over the frequency range of 0.1 GHz through 18 GHz. (The antenna used to cover the 100 MHz to 1000 MHz range would be furnished by the contracting agency.) The antennas would be capable of operating in both linear or both circular polarizations simultaneously. The gain, beamwidth, and side lobe characteristics would be such as to minimize multipath and undesired reflections.

2.3.2 Pedestal

The Pedestal and control unit would have the following characteristics:

Function	Capability
Azimuth Rotation	Continuous
Elevation Rotation	±90 degrees
Positional Accuracy	±1 mil
Tracking Rates:	
Azimuth	10 degrees/sec
Elevation	5 degrees/sec
Acceleration	
Azimuth	5 degrees/sec
Elevation	5 degrees/sec
Operating Modes	
Slave	External Track Radar
Manual	No Handwheels

2.3.3 Receivers

It was determined that the Receiver Group would consist of dual channel receivers covering the frequency range of 0.1 GHz through 18 GHz and would be designed to meet the following specifications.

Receiver Parameter	Specification
Sensitivity	-100 dbm minimum (unity signal to noise with a 1.5 MHz bandwidth).
Image and Spurious	-60 db minimum from the response at center frequency.

Tuning	Automatic electronic tuning, with adjustment over 0 to 100 percent of the operating bandwidth. Manual tuning to any single frequency would be available.
Automatic Frequency Control (AFC)	Selectable AFC incorporated in each receiver.
IF Bandwidth	Each receiver to have the capability of providing IF bandwidths of 1.5, 3.0, 6.0, and 10.0 MHz.
Signal Outputs	Both video and analog signal voltages to be made available.
Calibration	Each receiver to incorporate automatic calibration circuitry for both amplitude and frequency. The accuracy to be ±0.5 db in amplitude and 0.1 percent in frequency.

2.3.4 Control and Display Console

The Control and Display Console would have the capability to display all signal data, initiate commands, and control all antenna, receiver, and computer functions. In particular, the console would provide the following:

a. Panoramic frequency display with logarithmic amplitude.

b. Analysis display to show the signal characteristics of modulated signals.

c. A control panel to operate and select all receiver functions.

d. Antenna control panel.

e. Receiver test panel.

f. Numeric display of all system parameters.

g. Mode control panel.

h. Signal processor/computer interface.

2.3.5 Computer Group

The Computer Group would consist of all of the instrumentation necessary to collect, store, reduce, and record the measured data. In addition, the Computer Group would initiate all automatic calibrations upon command and store and display the results.

The Computer Group would cause displays to be activated during data acquisition to show all measured parameters. The modes of operation would be: the calibration mode, the calibration record mode, the data acquisition mode, the record mode, and the manual input mode.

A teletype would be provided as part of the Computer Group to interface with the computer for the purpose of inputting header data, compiling programs, and initiating programs. The additional hardware comprising the Computer Group would include magnetic tape decks, line printers, and an X-Y recorder. All software required to operate in the modes described above would be furnished with the system.

Figure 2 illustrates the required PAMS basic building blocks. Detailed characteristics and requirements of the four groups are discussed in Section III.

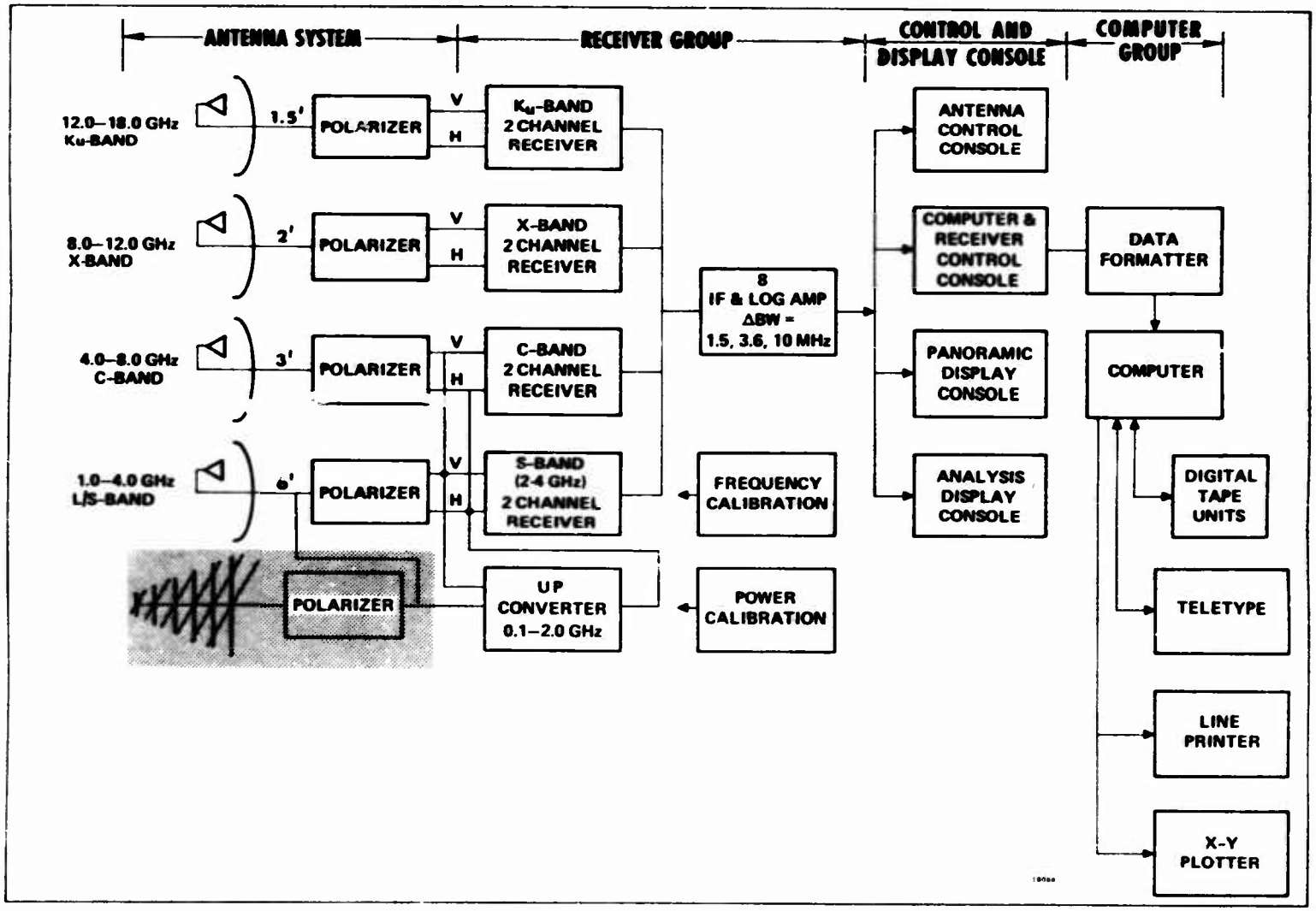

Figure 2. PAMS Block Diagram

SECTION III

SYSTEM CONSIDERATIONS

3.1 INTRODUCTION

The previous Section discussed a number of requirements that the PAMS would be required to meet in order to achieve the objectives of the program. This Section discusses those requirements and presents a conceptual analysis of the operation of the PAMS from a system viewpoint. The ensuing discussion takes on the following order.

Antennas
Receivers
Console/Processor
Computer

3.2 ANTENNA REQUIREMENTS

As previously noted, the required operating frequency ranges from 100 MHz through 18 GHz. Consideration was given first to the investigation of the required antenna performance in terms of gain and beamwidth over the RF frequency range, including the problems of parallax and sidelobes. Once these characteristics were defined the antenna configuration could be determined.

3.2.1 Antenna Gain

An initial program requirement was that the system operate with a minimum transmitted power of 50 watts at a maximum range of 100 nautical miles. These figures were used to calculate the required antenna gains needed by the PAMS. Several assumptions were also made here as to the received power level and transmit antenna gains. The antenna gains for airborne systems vary over a very wide range from 0 dbi (db above isotropic) at the low frequencies to 30 dbi at the high end of the frequency band. Not knowing exactly what antennas were to be evaluated the following assumptions were made:

Frequency (GHz)	Gain (dbi)
.1 - 1.0	0
1.0 - 2.0	3
2.0 - 4.0	6
4.0 - 8.0	8
8.0 - 12.0	12
12.0 - 18.0	15

These assumptions were based on the fact that most broadband antennas are useful up to 8.0 GHz. Above that, more directive antennas are employed over narrower bands with the resulting higher gains.

It was further assumed that a received signal of -95 dbm at the input to the receiver would be available at the receiver input terminals. This would provide a minimum signal-to-noise ratio for wide-bandwidth signals at the higher frequencies and somewhat larger signal-to-noise ratios for narrow-bandwidth signals at lower frequencies. The one way range or beacon equation is

$$P_R = \frac{P_T G_T G_R \lambda^2}{(4\pi R)^2} = \frac{P_T G_T G_R C^2}{(4\pi RF)^2} \quad (1)$$

where

P_R = received signal power at the receiver terminals

P_T = Transmitted power

G_T, G_R = Transmit and receive antenna gains

C = Speed of light: 3×10^8 meters/sec

F = Frequency

R = Range

Equation (1) can be expressed in a more convenient form as follows:

$$P_R = P_T + G_T + G_R + 37.86 - 2R - 2F \quad (2)$$

where

P_R = Power at receiver terminals in dbm

P_T = Transmitted power in dbm

G_T, G_R = Transmit and receive antenna gain in db

R = Range in db above 1 foot

F = Frequency in db above 1 MHz

Rearranging equation (2) to solve for G_R we have

$$G_R = P_R + 2R + 2F - G_T - 37.86 - P_T \quad (3)$$

The required gain over the operating frequency band was determined to be as shown in figure 3.

The gains shown by Curve Number 1 in figure 3 are those required to receive a signal at -95 dbm. However, at least 25 db dynamic range is required for antenna patterns in order to properly define the beamwidth and sidelobe characteristics. Curve Number 2 in figure 3 then is the actual gain to be furnished by the receive antenna system.

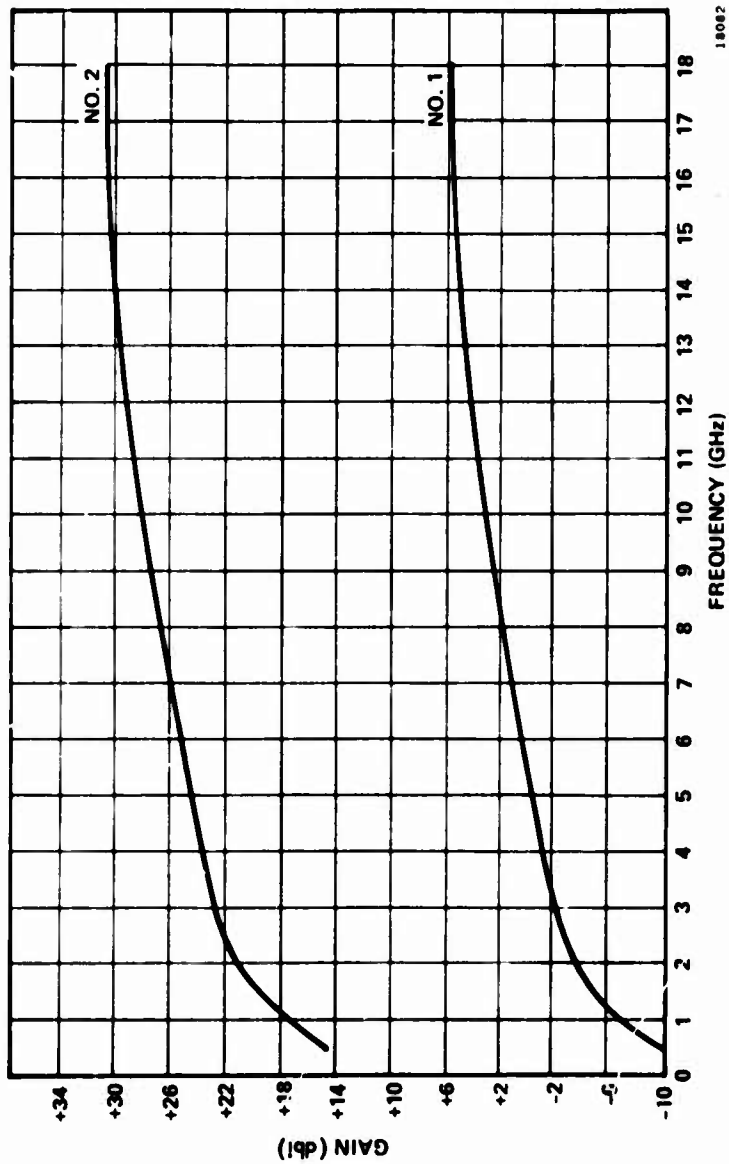

Figure 3. Antenna Gain vs Frequency

It should be mentioned here that the loss due to atmospheric absorption was neglected in the foregoing gain calculations. This loss factor is quite complex and is dependent upon both frequency and elevation ray angle. For example, at a range of 100 nautical miles and an elevation angle of one degree the atmospheric attenuation is approximately 1.4 db at a frequency of 10 GHz. When the ray elevation angle is increased to ten degrees the loss drops to 0.30 db. For lower frequencies, at elevation angles greater than three degrees, and ranges less than one hundred nautical miles, the atmospheric absorption can be considered negligible. For frequencies greater than 10 GHz the absorption is extremely sensitive to the water vapor density. The water vapor loss is directly additive to the oxygen contribution and is directly proportional to the water vapor density. A range for water vapor density of about 2 to 20 grams per cubic meter may be observed, corresponding to dry winter air and moist tropical air. Below 10 GHz, however, most of the loss is due to oxygen, which is relatively constant for various locations and times. The absorption losses due to rain are too variable a phenomenon to have been considered at the time the gain calculations were made.

3.2.2 Beamwidth

The second parameter of interest was the beamwidth characteristic. In particular the 0.25 db beamwidth would be the most critical for the PAMS since the system would be slaved to a track radar. At a radar range of 100 miles the beamwidth would have to be broad enough to maintain a field of view with minimum amplitude variation. If the beamwidth were very narrow the target might swing up and down on the slope of the pattern causing large amplitude variations in the received signal. This, in turn, would put severe requirements on the tracking radar. A secondary parameter of interest was channel tracking. Since the PAMS would operate in dual polarization it would be necessary to maintain close amplitude tracking in both polarizations to avoid ambiguities when the input channels were reversed.

The above discussion indicated a conflict with gain and beamwidth. Since the overall accuracy of the PAMS is paramount it was concluded that a reduction in range was dictated for the low power sources that were under consideration. Reducing the range in half provided a six-decibel improvement which would provide adequate gain for the most severe case under consideration.

3.2.3 Parallax

In addition to the long range case there was the problem of minimum range. The proposed physical layout of the PAMS and the track radars was such that there would be approximately a 300-foot baseline separation between the PAMS and the MSQ-1 and 600 feet for the FPS-16. This separation introduced the problem of parallax if the vehicle of interest was less than some minimum range. See figure 4 for a typical layout for a fly-by. It was assumed that the difference in the height of the PAMS and the track radar would be insignificant in the established configuration. Consequently, the problem could be reduced to a two-dimensional case. Then the parallax angle α is specified by

$$\alpha = \tan^{-1} AD/BC \qquad (4)$$

A solution for (4) is given in figure 5 for various separations between the PAMS and the track radar. For the separation in question it is seen from figure 5 that the

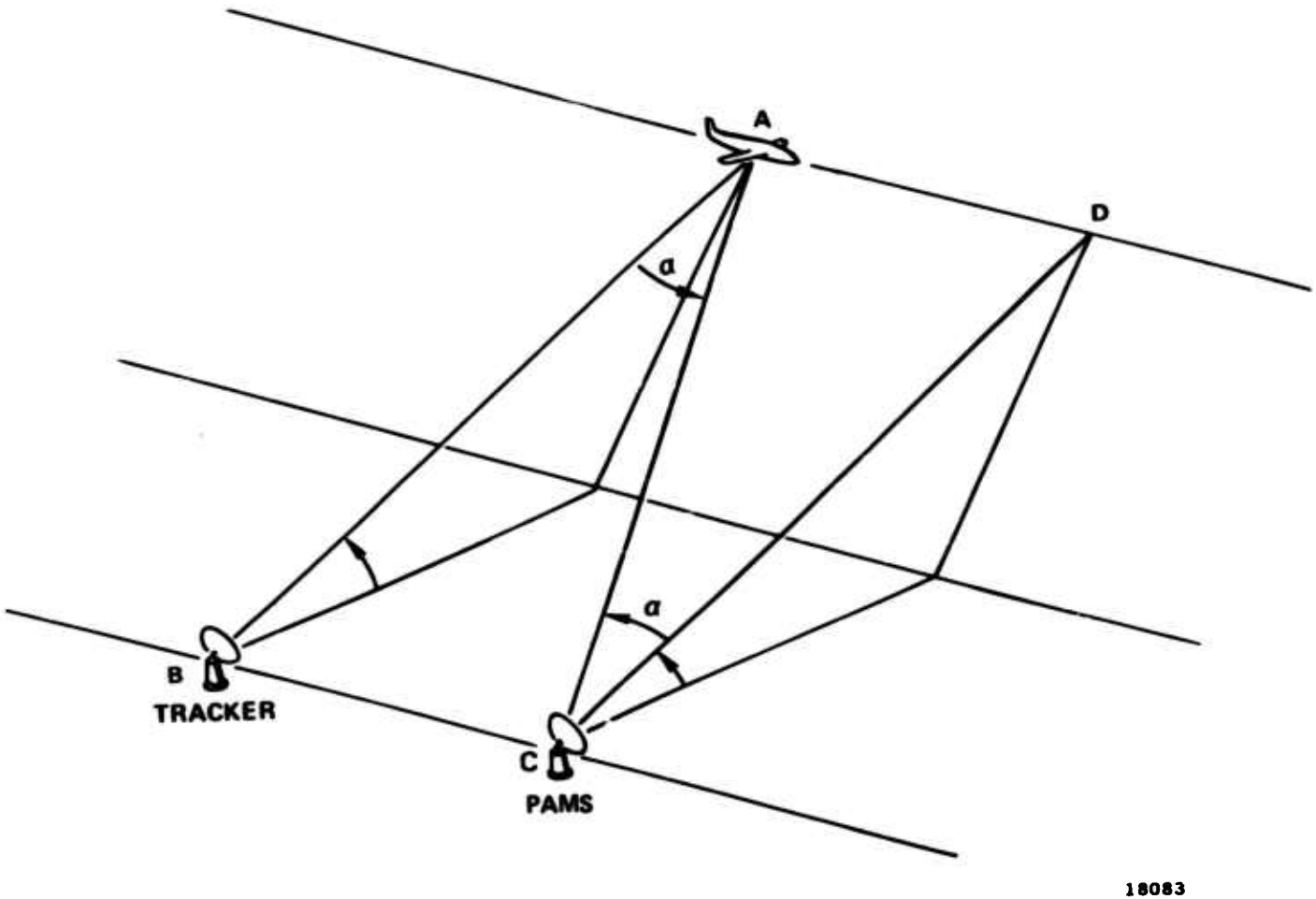

Figure 4. PAMS Tracking Geometry

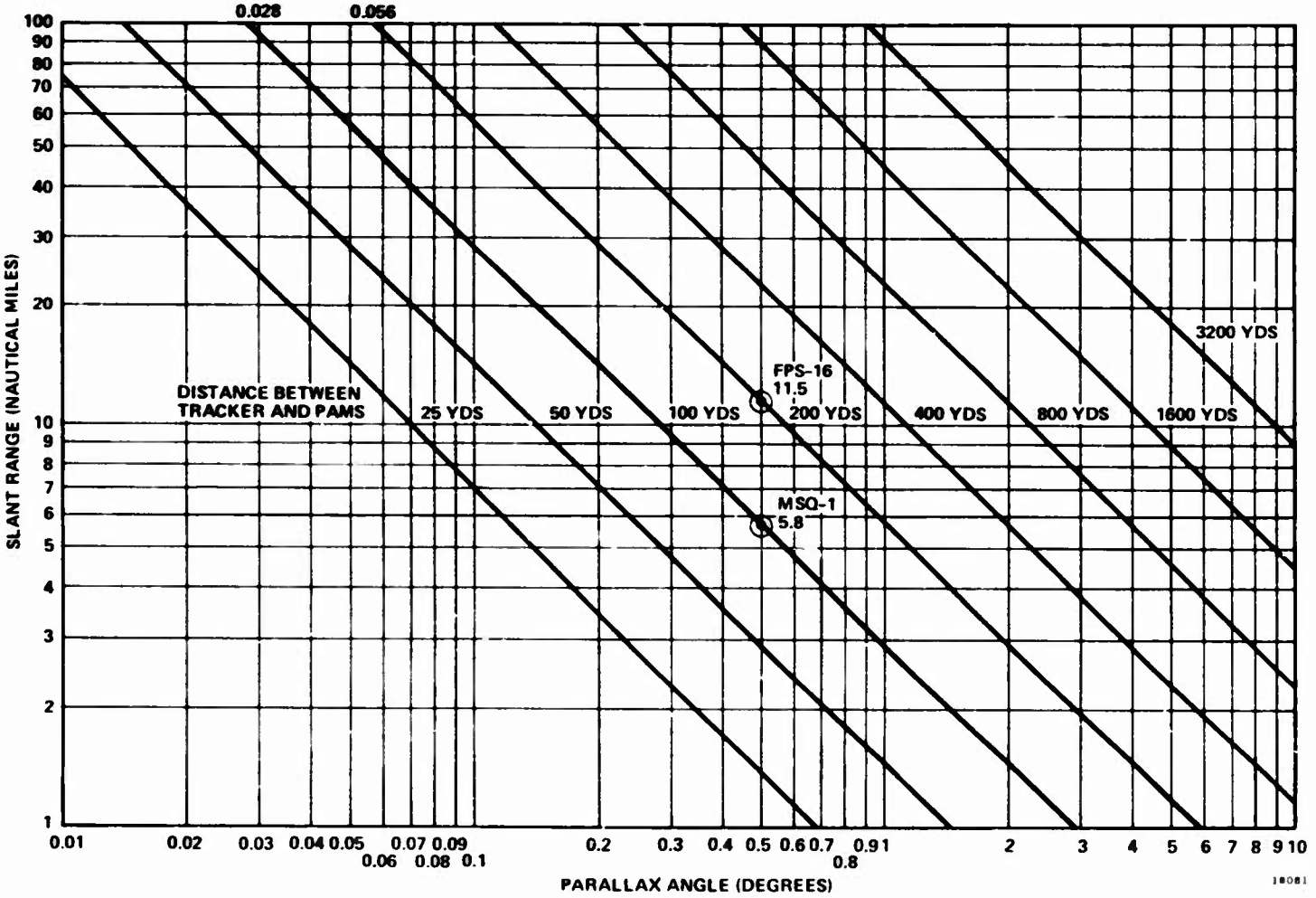

Figure 5. PAMS Parallax

minimum range that could be flown and maintain a parallax error of 0.5 degree was 5.8 miles for the MSQ-1 and 11.5 miles for the FPS-16. This also pointed up the need to maintain a 0.25 decibel beamwidth that was not too narrow. If the beamwidth were one-half that specified previously, the minimum ranges would be 11.5 and 23 miles respectively, since this is equivalent to reducing the parallax error to 0.25 degree.

3.2.4 Sidelobe Levels

The last parameter of interest in the performance of the receive antenna was the sidelobe level. The primary area of concern here was the effect of multipath on the amplitude of received energy. In order to minimize the effects of multipath it was desirable to keep the sidelobe level as low as possible in order to avoid ambiguities in signal level. However, a compromise had to be made due to the large bandwidths covered and the dual polarization requirements. Practical sidelobe levels for the application of the PAMS were -15 decibels. The effect on the system operation is covered in the analysis portion of Section VI.

3.2.5 Antenna Parameters

The preceding paragraphs have described the requirements of the antenna array for the PAMS. It was determined, as a result of the previous investigations and analyses, that the antenna parameters defined for the PAMS were relatively standard and could be obtained with available hardware. In order to take advantage of this, the bands were divided as shown in the following tabulation. Included are the other parameters of interest.

Freq. (GHz)	Gain (dbi)	.25 Beamwidth (Deg)	3 db Beamwidth (Deg)	Channel Tracking (db)	Sidelobe Level (db)
0.1 - 1.0	7.0	20	60	±0.5	-15
1.0 - 4.0	20.5 - 32.0	3.4 - 0.85	12.0 - 2.8	±0.5	-15
4.0 - 8.0	27 - 30	1.7 - 0.85	6.0 - 2.5	±0.5	-15
8.0 - 12.0	29 - 32	1.3 - 0.85	4.0 - 3.0	±0.5	-15
12.0 - 18.0	30 - 33	1.2 - 0.75	3.7 - 2.9	±0.5	-15

The antenna hardware and configuration is described in Section IV.

3.3 SITE INTERFERENCE

This Section details the investigation of the Radio Frequency (RF) environment that the PAMS would be expected to encounter at the Verona Test Annex of Rome Air Development Center (RADC). There are a large number of active RF systems at Verona covering an extremely broad frequency spectrum. Consequently, this Section deals only with those systems which operate in the same frequency range as the PAMS.

The equipments and their locations were obtained from data provided by RADC. The distances from the PAMS to the various sites were scaled from the Plot Plan - Verona Test Annex, figure 6. The scaled distances were considered to have sufficient accuracy for this investigation. The sites and their distances from the PAMS are given in

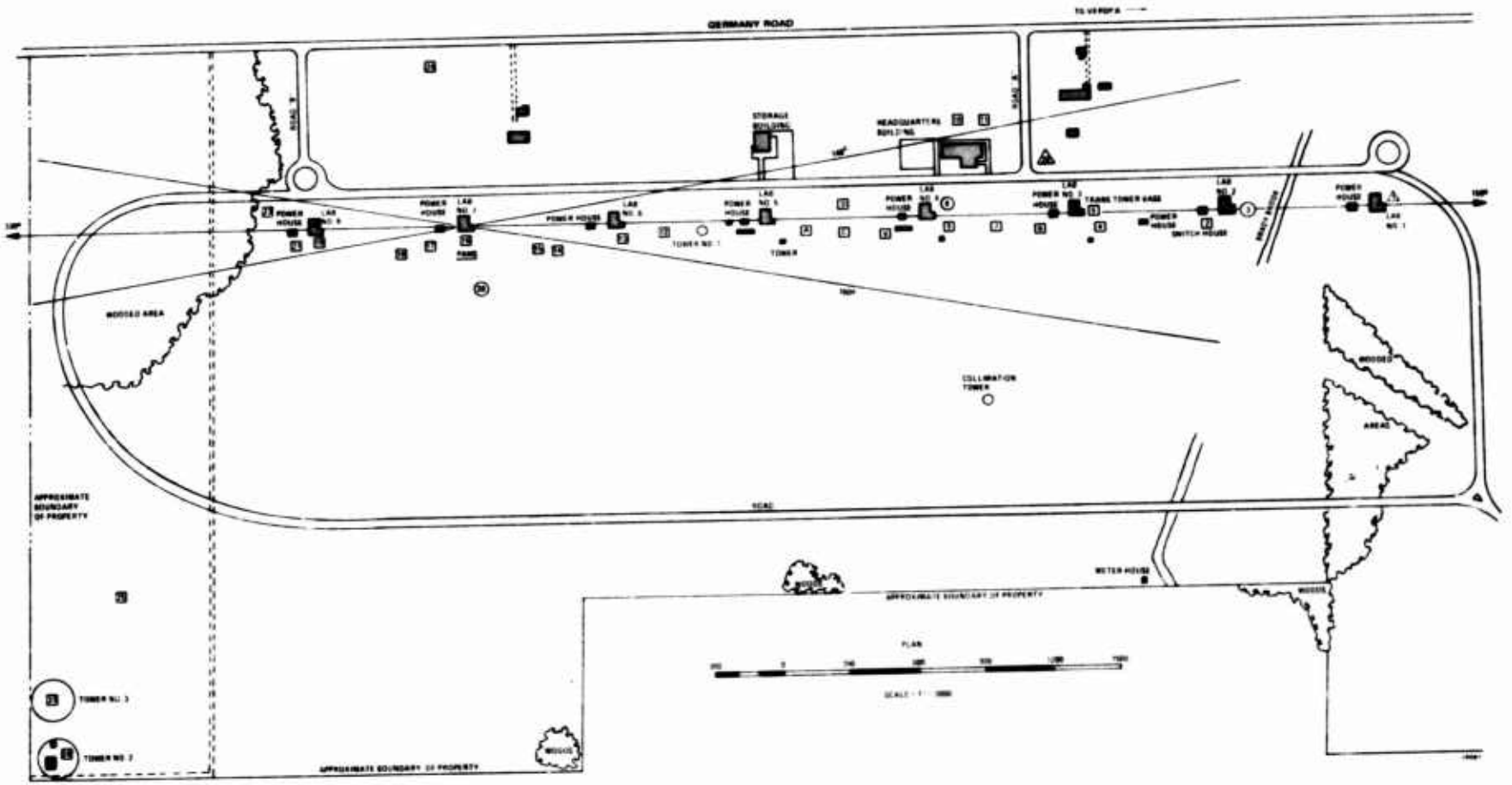

Figure 6. Plot Plan - Verona Test Annex

table I. The beacon equation stated in paragraph 3.3.2 was used to describe the worst case condition of RF interference. It is then shown how the worst condition was modified in normal operation by the effects of receiver selectivity and antenna beam shape. The results of the computer calculations and the discussion on the PAMS were used as the basis for recommendations to optimize the accuracy and performance of the PAMS.

TABLE I

EMITTER LOCATIONS

Bldg.	Site	Emitter	Unit	Dist. to PAMS (ft)
1	1	1	FPS-74	4060*
	1	2	MRC-113	3260*
2	2	1	MRC-98	3410*
3	4	1	SPS-8	2810*
	5	1	SPS-30	2735*
	6	1	TPS-40/MPS-16	2530*
4	7	1	FPS-6	2215*
	8	1	FPS-65	2065*
	9	1	FPS-67	2095*
Hdqtrs.	10	1	URN-3	2220*
	11	1	GRC-27	2220*
	11	2	GRC-27	2220*
	11	3	GRC-27	2220*
	11	4	GRC-27	2220*
	11	5	GRC-27	2220*
	11	6	GRC-27	2220*
	11	7	GRC-27	2220*
	11	8	RT-723	2220*
	11	9	RT-723	2220*
	11	10	RT-723	2220*
Tower 1	12	1	K-Band	965
	12	2	Q-Band	965
6	13	1	FPS-16	640*
	14	1	SG1-B	400*
	15	1	HF XMTR.	156
7	16	-	PAMS	0
	17	1	MPQ-29	130*
	18	1	MSQ-1A	320*
	18	2	MSQ-1A	320*
8	19	1	TROPO	670*
	20	1	TROPO	605*
	21	1	SCR-584	770*
Tower 2	26	1	FRT-60	3000*
	26	2	S-Band Breadboard	3000*
	28	-	H.F. Trans. TWR	150

*Operate in the PAMS frequency range.

TABLE I (CONTINUED)

EMITTER LOCATIONS

Bldg.	Site	Emitter	Unit	Dist. to PAMS (ft)
Mobile 1	30	1	**TPS-1D	4000*
Mobile 2	31	1	**TRAIL III	4000*
A	32	1	NIKE "X"	1450*
B	33	1	NIKE "X"	1695*
C	34	1	NIKE "S"	1570*

*Operate in the PAMS frequency range.
**These are mobile units - 4000 feet was assumed distance from the PAMS site. Only those sites known to have an active source are listed.

3.3.1 RF Site Analysis

The first part of the analysis was to establish what the worst case RF conditions would be at the PAMS site. To accomplish this, it was assumed that the PAMS and the interfering emitter would be aligned with each other along the RF axis. The effects of ground reflections and multipath propagation were not taken into account for this analysis due to the complexity of the multiple site environment. The beacon equation was used to calculate the power received at the PAMS antenna. Of the emitters listed in table I and shown in figure 6, those identified as being in the same frequency range as the PAMS have been asterisked.

3.3.2 Computer Program and Calculations

The equation used to determine the RF power at the input terminals was somewhat unwieldly and time consuming in its general format as can be seen below:

$$P_R = \frac{P_T G_T G_R \lambda^2}{(4\pi)^2 R^2} \tag{5}$$

where

P_R = Receive power at antenna in watts

P_T = Transmitter power in watts

G_T = Transmit antenna gain

G_R = Receive antenna gain

λ = Free space wavelength in meters

R = Range between sites in meters

To simplify the calculations and reduce the time required, equation (5) was transformed to a decibel (db) format and is shown in equation (6).

$$P_{R(dbm)} = P_{T(dbkw)} + G_{T(db)} + G_{R(db)} - 2F_{(dbMHz)} - 2R_{(dbFt)} + 97.876 \qquad (6)$$

Although the above equation proved to be relatively simple to use, the number of calculations required suggested the use of a computer. Therefore, equation (6) was programmed using BASIC computer language. The data for P_T, F, and R were entered in the program in kilowatts, MHz, and feet, and the log functions were calculated in the program. The gain G was entered in db. The computer program is shown in table II. Table III illustrates the input data used in the program. The elapsed processor time for this program was 0.32 second.

The output data from the computer program are given in table IV. The power received by the PAMS antenna, P_R (DBM), was quite high for a number of the sites. Those sites which were considered objectionable are identified in paragraph 3.3.3.

3.3.3 Potential Interference Sites

For the purpose of this analysis peak pulse power greater than 500 watts and continuous wave (CW) power greater than 1000 watts were considered to be detrimental to the PAMS performance. The limiting characteristics of the Yttrium-Iron-Garnet (YIG) filter accounted for the low level of peak pulse power used above. The ability of YIG devices to limit pulse power is dependent on the rise time of the leading edge of the pulse. A very fast rise time allows considerable peak power to leak through to the receiver(s) while a slower rising pulse can be limited rather effectively. Since the pulse characteristics were not known for the emitters in question, the somewhat pessimistic value of 500 watts was used in this analysis.

Based on the above definitions there were 15 emitters which fell into the classification of an objectionable source. These were the emitters at sites 4, 5, 6, 7, 8, 9, 13, 17, 18, 20, 21, 26, 32, 33, and 34. (When site 20 was in a CW mode of operation, it was not considered to be a threat.) Site 30, which was mobile, was a potential interfering source when the distance between it and the PAMS was 1000 feet or less. Referral to the site locations given in figure 6 shows that most of the emitters considered in the analysis were on or very close to the headings 150 degrees - 330 degrees true. If an arc of ±5 degrees to the indicated headings were considered, all but sites 13, 14, 17, 18, 21, and 26 were enclosed. The high concentration of RF sources in the indicated zones effectively restricted any measurement activity in that area. However, sites 13, 14, 17, 18, 21, and 26 presented an interference problem to the PAMS during measurements. All of the cited emitters could degrade the PAMS receiver performance up to and including crystal burnout, unless adequate precautions were taken. These problems and recommended solutions are covered in the following paragraphs.

3.3.4 Effect on PAMS

The ability of the PAMS in gathering data to accurately define the radiation characteristics of airborne antennas, aircraft cross-section, and cross-section per unit volume of radar clutter was determined to be primarily a function of antenna and receiver performance. The following sections evaluate what interference effects the nearby RF systems would have on the PAMS.

TABLE II

BEACON EQUATION - COMPUTER PROGRAM

```
10 DIM A(50),B(50),X(50),Q(50),G(50),H(50),T(50),W(50),R(50),P(50)
20 DIM F(50)
30 FILES EMITT
40 DEF FNA(P)=10*(LOG(P)/LOG(10))
50 DEF FNB(F)=20*(LOG(F)/LOG(10))
60 DEF FNC(R)=20*(LOG(R)/LOG(10))
70 I=I+1
80 INPUT#1,A(I),B(I),P(I),G(I),H(I),F(I),R(I)
90 Q(I)=FNA(P(I))
100 T(I)=FNB(F(I))
110 W(I)=FNC(R(I))
120 X(I)=Q(I)+G(I)+H(I)-T(I)-W(I)+97.876
130 IF END #1 THEN 150
140 GO TO 70
150 FOR K=1 TO 5
160 PRINT
170 NEXT K
180 PRINT USING 190
190:SITE EMITT  PR(DBM)    PT(DBKW)   GT(DB)   GR(DB)   F(DBMC)    R(DBF
    T)
200 PRINT
210 FOR M=1 TO (I)
220 PRINT USING 230,A(M),B(M),X(M),Q(M),G(M),H(M),T(M),W(M)
230:###   ###  -##.####   -##.####   -##.##   -##.##   -##.####   -##.##
    ##
240 NEXT M
250 FOR J=1 TO 5
260 PRINT
270 NEXT J
280 END
```

TABLE III

INPUT DATA

```
10 1,1,1000,28,29.5,2800,4060
40 4,1,1200,37,31.5,3500,2810
50 5,1,2500,42,31.5,3500,2735
60 6,1,1000,42,29,5290,2530
70 7,1,5000,40,29.5,2800,2215
80 8,1,2000,36,23,1300,2065
90 9,1,2000,35,23,1300,2095
100 10,1,7.5,7.5,21.7,1151,2220
110 11,1,.1,0,6,262.5,2220
120 11,2,.1,0,6,294.6,2220
130 11,3,.1,0,6,319.6,2220
140 11,4,.1,0,6,341.6,2220
150 11,5,.1,0,6,349.6,2220
160 11,6,.1,0,6,383,2220
170 11,7,.1,0,6,384.8,2220
180 11,8,.025,0,6,123.2,2220
190 11,9,.025,0,6,123.4,2220
200 11,10,.025,0,6,139.8,2220
210 13,1,1000,42,29.5,5600,640
220 14,1,50,25.5,30,3050,400
230 17,1,30,35,30,8700,130
240 18,1,300,35,29.5,2800,320
250 19,1,5,23,6,303.5,670
260 20,1,3,54,32,7900,605
270 21,1,250,33,29.5,2800,770
300 26,2,1500,34,30,3000,3000
310 30,1,400,27,23,1290,4000
320 31,1,2.2,38,32.5,6250,4000
330 32,1,250,43,30,9000,1450
340 33,1,250,43,30,9000,1695
350 34,1,500,30,31.5,3300,1570
```

TABLE IV

BEACON EQUATION DATA OUTPUT

SITE	EMITT	PR(DBM)	PT(DBKW)	GT(DB)	GR(DB)	F(DBMC)	R(DBFT)
1	1	44.2623	30.0000	28.00	29.50	68.9432	72.1705
4	1	57.3123	30.7918	37.00	31.50	70.8814	68.9741
5	1	65.7349	33.9794	42.00	31.50	70.8814	68.7391
6	1	56.3445	30.0000	42.00	29.00	74.4691	68.0624
7	1	68.5151	36.9897	40.00	29.50	68.9432	66.9075
8	1	61.3090	33.0103	36.00	23.00	62.2789	66.2984
9	1	60.1838	33.0103	35.00	23.00	62.2789	66.4237
10	1	7.6780	8.7506	7.50	21.70	61.2215	66.9271
11	1	-21.4336	-10.0000	.00	6.00	48.3826	66.9271
11	2	-22.4357	-10.0000	.00	6.00	49.3847	66.9271
11	3	-23.1432	-10.0000	.00	6.00	50.0921	66.9271
11	4	-23.7214	-10.0000	.00	6.00	50.6704	66.9271
11	5	-23.9225	-10.0000	.00	6.00	50.8714	66.9271
11	6	-24.7150	-10.0000	.00	6.00	51.6640	66.9271
11	7	-24.7557	-10.0000	.00	6.00	51.7047	66.9271
11	8	-20.8839	-16.0206	.00	6.00	41.8122	66.9271
11	9	-20.8980	-16.0206	.00	6.00	41.8263	66.9271
11	10	-21.9818	-16.0206	.00	6.00	42.9101	66.9271
13	1	68.2886	30.0000	42.00	29.50	74.9638	56.1236
14	1	48.6385	16.9897	25.50	30.00	69.6860	52.0412
17	1	56.5780	14.7712	35.00	30.00	78.7904	42.2789
18	1	68.1011	24.7712	35.00	29.50	68.9432	50.1030
19	1	27.7010	6.9897	23.00	6.00	49.6432	56.5215
20	1	55.0596	4.7712	54.00	32.00	77.9525	55.6351
21	1	57.6824	23.9794	33.00	29.50	68.9432	57.7298
26	2	54.5521	31.7609	34.00	30.00	69.5424	69.5424
30	1	39.6436	26.0206	27.00	23.00	62.2118	72.0412
31	1	23.8414	3.4242	38.00	32.50	75.9176	72.0412
32	1	52.5432	23.9794	43.00	30.00	79.0848	63.2274
33	1	51.1872	23.9794	43.00	30.00	79.0848	64.5834
34	1	52.0774	26.9897	30.00	31.50	70.3703	63.9180

3.3.4.1 Receiver

The concentration of high power emitters posed a potential threat of damage to the receiver crystals. The consequences of high power range from degradation of crystal performance, to actual burn-out of the crystal. YIG preselectors have an inherent limiting characteristic and limit signal level to approximately +16 dbm. The limiting action occurs through the precessing magnetization of the YIG crystal. Unfortunately, there is a time lag involved with the initial absorption which gives rise to some spike leakage, as shown in figure 7.

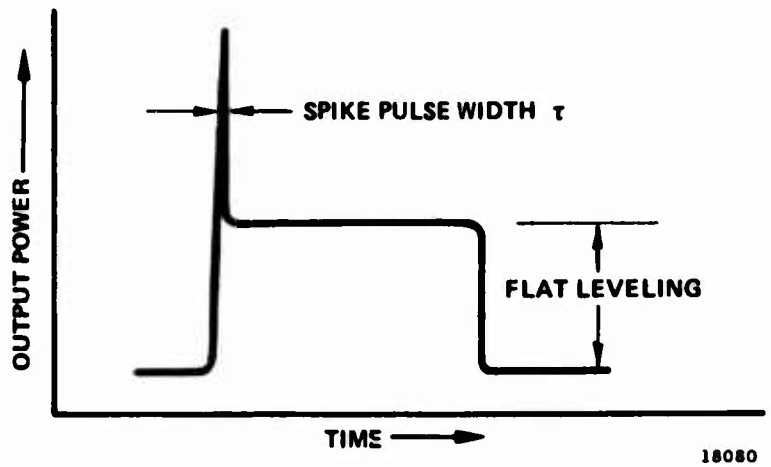

Figure 7. YIG Limiting Characteristics

This spike is equivalent to the spikes encountered in the early radars which were due to the ionization time of the Transmit-Receive (TR) and Anti Transmit-Receive (ATR) tubes. It has been shown that the pulse energy ($P_k \tau$) associated with such a spike is actually more detrimental to crystal life than CW levels of several watts. For YIG devices, the pulse width τ of the spike can range from 10^{-7} to 10^{-11} seconds and is a function of the doping characteristics of the YIG crystal, the physical size of the sphere, magnetic field, and the leading edge rise time of pulse signals.

In order to see what could happen due to the leakage spike, consider the following example. Assume the received power from site 13 (FPS-16) was attenuated 3 db by transmission line and polarizer losses. The approximate peak power at the receiver input would then be 3.4 kilowatts. If the pulse width τ of the spike were 10^{-9} seconds, the pulse energy at the mixer crystals would be on the order of 34 ergs which would be catastrophic. Even with τ equal to 10^{-10} seconds the pulse energy would be 3.4 ergs which could degrade crystal performance when subjected to such energy levels over a period of time. Safe values of spike pulse width would be in the range of $0.5 \times 10^{-11} < \tau < 0.5 \times 10^{-10}$ for peak power values in the range of 1 to 10 kilowatts.

In addition to the problem of crystal damage, the nearby emitters also presented a potential interference problem which could degrade measurement accuracy. Fortunately, this problem could be reduced considerably by the combination of receiver selectivity and antenna directivity. The receiver preselector, a multi-pole YIG

filter, would provide 60 db attenuation to the image frequency 200 MHz away. Signals further away than the image would be attenuated 60 to 80 db. An unwanted signal might be detected during the sweep mode but would not interefere with the signal of interest. This would be the result of the 60-db attenuation if the undesired signal were outside the ±200 MHz band. If the signal were less than ±200 MHz from the desired signal the intermodulation products would be very low until the signals were within one or two MHz of each other. In addition, the YIG preselector would limit on the largest signal and would not affect the smaller signal. Consequently, if a signal from a nearby emitter were detected within the ±200-MHz band the signal would be limited to a point (approximately +16 dbm for strong signals) where the possibility of receiver saturation would be eliminated. In normal operation, the interfering signal would be the result of reflections or spillover and consequently, the problem of the high peak powers with the resultant pulse spike would not be present.

3.3.4.2 Antenna

The antenna system of the PAMS plays an important role in reducing the problems of crystal damage and interference. Paragraph 3.3.3 established that most of the emitters at the site were on the heading 150 degrees - 330 degrees true. This is considered a "dead zone." If one takes a ±5 degree arc from the "dead zone" (145 degrees - 155 degrees and 325 degrees - 335 degrees) 80 percent of the emitters are enclosed and basically eliminated from the interference problem. Those emitters outside the ±5 degree arc are potential sources of interference. If the emitters exceed power levels specified in paragraph 3.2.2 (500 watts peak pulse power or 1000 watts CW) they are also classified as potential sources of crystal damage. The sites which fell into one or both of these catagories are listed below. (Refer to table 1 for nomenclature).

1. Site 13, C band - This was a source of both interference and crystal damage.

2. Site 14, S band - Source of interference.

3. Site 17, X band - Source of interference and crystal damage.

4. Site 18, S band - Source of interference and crystal damage.

5. Site 19, UHF - This site was included as a potential interference source due to the broad beamwidth of the Band 1 antenna.

6. Site 21, S band - Source of interference and crystal damage.

7. Site 26, S band - Source of interference and crystal damage. The characteristics of the second emitter at this site (FRT-60) were not known at the time, however, it was included in the survey. This site was located in an area where the PAMS would be conducting a number of measurements and the probability of interference was extremely high.

In order to attenuate the level of the interfering signals, isolation is obtained by the directivity and pattern shape of the PAMS antenna as well as the antenna of the undesired emitter. With the exception of the UHF antenna (Band 1) the antennas making up the PAMS array are parabolic reflectors. Figure 8 is the theoretical secondary pattern for a circular-aperture antenna with a tapered primary illumination function. The

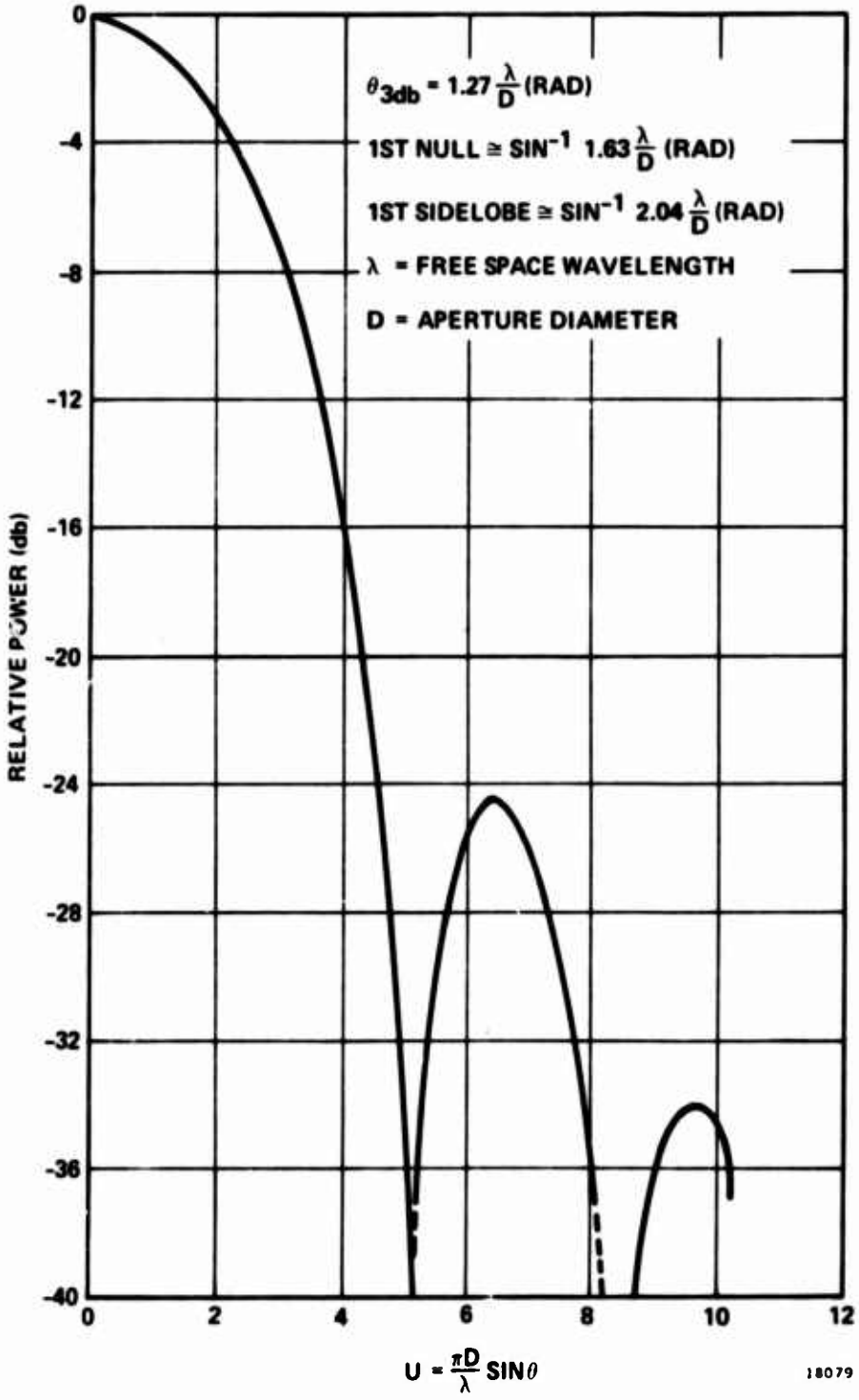

Figure 8. Secondary Radiation Pattern - Circular Aperture

pattern is pencil shaped and has theoretical sidelobes of 24 db below the peak of the beam. (The sidelobes on the PAMS array will nominally be 20 db due to reflector diameter, Focal Length/Diameter (F/D) ratio, and amplitude taper of the primary feed.) The positions of the nulls and sidelobes are a function of U where U is defined as being equal to $\frac{\pi D}{\lambda} \sin \theta$.

The positions of the first null and first sidelobe are given by:

$$\text{1st Null} \cong \sin^{-1} 1.63 \frac{(\lambda)}{D} \text{ radians} \tag{7}$$

and

$$\text{1st Sidelobe} \cong \sin^{-1} 2.04 \frac{(\lambda)}{D} \text{ radians} \tag{8}$$

where

λ = free space wavelength

D = diameter of parabolic reflector

λ and D are in the same units, i.e., meters, inches, feet

Examination of (7) and (8) shows their position to be frequency dependent moving toward the major axis with increasing frequency (beam narrowing characteristic). For example, the reflector is 6 feet in diameter and operates over the range of 1.0 to 4.0 GHz. At 1.0 GHz, the 10 db beamwidth and first null are at 15 degrees and 20 degrees respectively, and at 4.0 GHz the corresponding values are 5 degrees and 3.9 degrees. In other words 10 db attenuation could be achieved by moving the peak of the beam 10 degrees. The same value could be achieved with only 2.5 degrees beam offset at 4.0 GHz. If the emitter antenna had similar characteristics approximately 40 db attenuation could be obtained at 4.0 GHz by offsetting each antenna about 3 degrees in opposite directions. Applying the results of the above discussion to the seven emitters listed as problem sites, approximately 15 to 20 db of signal attenuation could be achieved by offsetting the beams of the PAMS antenna ±10 degrees from the 150 degree - 330 degree heading. The broad beamwidth of the Band 1 antenna would require a larger offset to obtain results comparable to the rest of the system. The undesirable effects of site 26 could not be eliminated with the technique of beam offset. Additional limiting could be achieved with passive PIN diode limiters placed in the receiver front end. Although the insertion loss of these devices would degrade receiver performance to some degree the increased protection would be worth the price when operation would be required in a high emitter density environment.

3.4 RECEIVERS

Receivers for the PAMS would require the maximum possible sensitivity in order to accurately record the radiation characteristics of the emitters over the entire range of interest. Furthermore, the radiations under evaluation could have spectral widths from near zero to a full octave, and modulation characteristics from noise to CW.

3.4.1 Sensitivity

In order to achieve maximum sensitivity there were three system parameters which had to be optimized. First, the system noise figure had to be minimized. Secondly, the image noise had to be suppressed as fully as possible. Lastly, the combined RF and IF bandwidth had to be restricted to the fundamental spectral lobe of the information signal. These processes would minimize the noise bandwidth and maximize the signal-to-noise ratio on the standard pulse or CW modulated signals. However, system sensitivity to the radiated noise source required maximizing the source-noise to system-noise ratio which is slightly different from the preceding.

Maximizing sensitivity to a noise-type signal still required a minimum system-noise figure and image-noise suppression. Image suppression not only lowered the system noise, but also prevented signal noise at the image frequency from introducing ambiquities. Variations in the RF - IF bandwidth would not increase system sensitivity since this would simultaneously vary the signal and system-noise bandwidth, producing a change in selectivity only. Consequently, there was no effect on the noise-to-noise ratio or sensitivity to a signal from a noise source. However, noise-to-noise sensitivity could be greatly improved by first; selecting the IF bandwidth no narrower than required to obtain the desired frequency resolution, second; slowing the system spectral scan rate as slow as possible without creating indicator flicker, and then narrowing the video bandwidth to conform with the time it would take the frequency to traverse one frequency resolution cell. This process would create a spectral envelope of the noise signal and would enhance the sensitivity by the equivalent IF to video bandwidth ratios.

The available noise power of a receiver was calculated from the following equation:

$$P_n = KTB \tag{9}$$

where

P_n = noise power in watts

K = Boltzman's constant - 1.38×10^{-23} watt/sec/°K

T = Temperature in degrees Kelvin

B = Bandwidth in Hertz

Equation can be stated in a more usable form as:

$$P_n \text{ (dbm)} = -114 + 10 \log B + NF \tag{10}$$

where

P_n = Absolute noise threshold

B = Bandwidth in Megahertz

NF = Receiver noise figure in db

Using equation (10) and a bandwidth of 1.5 MHz the absolute noise threshold is

$$P_n = -112.24 \text{ db} + NF$$

Therefore in order to achieve unity signal-to-noise of -100 dbm it was determined that a receiver noise figure of 12.24 db would be required.

A worst case analysis was performed on the receiver front end based on preliminary data from component manufacturers. The results were as follows:

Freq. Band	LO Mixer Power	Mixer Pre-Amp. NF	Isol. Loss	YIG Loss & Ripple	Cable, Conn.	Tuner NF
S	+3 dbm	8.5 db	1.0 db	4.75 db	1.0 db	15.75 db
C	-3 dbm	9 db	1.0 db	4.5 db	1.5 db	16.5 db
X	+2 dbm	10 db	1.0 db	4.5 db	2.3 db	18.3 db
Ku	+2 dbm	12 db	1.0 db	4.5 db	2.5 db	20.5 db

As can be seen, the required noise figure was exceeded in all bands using the present day components. However, as mentioned previously, noise-to-noise sensitivity could be improved by the proper combination of IF bandwidth, scan rate, and video bandwidth.

To cite an example, if a noise or CW signal were to be evaluated with a desired 10 MHz resolution in Ku band, and if a 24 millisecond sweep were assumed for the 6000 MHz dispersion, the following conditions would prevail. The video signal would have approximately a 0.1 microsecond grain; however, it would take 40 microseconds for the sweep to transverse the 10 MHz window. Thus, a video filter smoothing the noise structure to the 0.1 microsecond grain compatible with the system resolution would improve the sensitivity by the ratio of 40 to 0.1 or approximately 26 db. However, the filter would have to be switched out during pulse reception to prevent serious signal distortion.

When receiving pulse signals, the receiver would be operated in either a fixed-frequency mode or would utilize a fixed portion of the sweep period. Figure 9 illustrates the type of scan determined to be required by the PAMS receivers.

During pulse reception the video filter would be deactivated and the signal path would be through a pulse stretcher and a gated peak detector would be used to maximize sensitivity. The pulses would be detected and averaged for a specified period of time and then "dumped" into computer storage upon command. This technique of post-detection integration would improve the over-all receiver sensitivity to an acceptable level when operating with pulsed signals.

3.4.2 Image and Spurious Signals

In order to eliminate erroneous data from being displayed and processed by PAMS all image and spurious signals would have to be suppressed by at least 60 db, the dynamic range of the receivers.

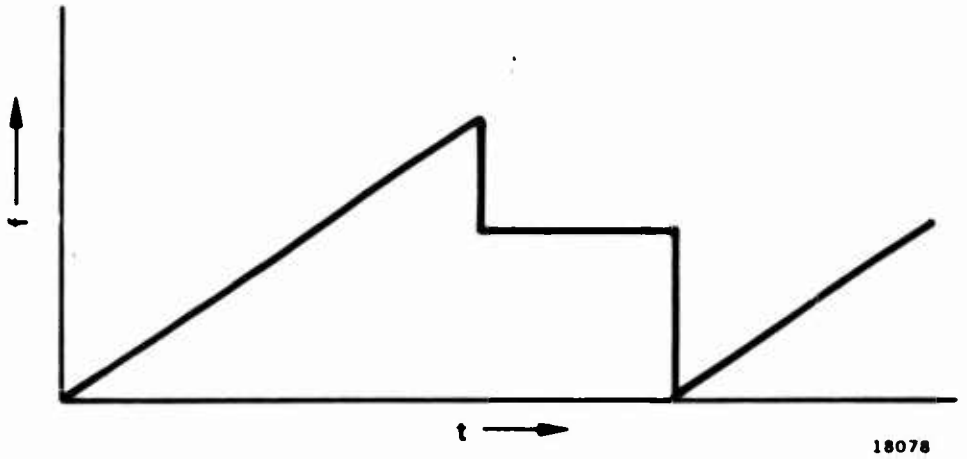

Figure 9. Sweep Configuration

Image rejection would best be accomplished using preselection techniques. Sufficient image rejection could be achieved by this method providing the IF frequency were high enough to provide maximum frequency separation between the fundamental and image frequencies without requiring excessively steep preselector skirt selectivity to pass a 10 MHz bandwidth signal and simultaneously attenuate the image by 60 db. In order to produce a full panoramic display of all radiation within each octave band the preselector would have to be swept across the RF band in synchronism with a sweeping local oscillator. The preselectors selected for the PAMS were Yttruim Iron Garnet (YIG) filters, with 18 to 24 db per octave skirt selectivity and sweep drivers. These devices would provide the required image rejection of 60 db and in addition would provide some receiver protection to high level signals due to the limiting characteristics of YIG devices.

It can be noted here, with reference to figure 17 showing the layout of the YIG preselector assembly used in the PAMS receivers, that the basic overall system bandwidth of 10 MHz includes the tuned circuits of the YIG preselectors, preamplifier, and logarithmic amplifier. Consequently, the skirt selectivity of the basic 10 MHz bandpass filter is very steep due to the multiple tuned circuit configuration of the filter selection box. However, the narrowband modes of 1.5, 3, and 6 MHz are created by injecting a narrow filter into the basic receiver circuitry. Thus, the selectivity within the 10 MHz domain is solely a function of the filter skirts. The narrowband filter is inserted prior to the logarithmic amplifier since signal sampling is obtained from each IF stage, thus, the signal spectral width entering each stage should be identical to ensure proper combining.

3.4.3 Calibration

In accordance with system requirements, the amplitude and frequency calibration modes of the PAMS were required in both manual and automatic modes of operation. The manual calibration of both amplitude and frequency would not be as accurate as the automatic mode primarily because the operator would be required to make all adjustments and interpret the display outputs. However, the manual mode would

permit amplitude readings of ±3 db and frequencies to be read within several percent. The automatic mode of calibration required much higher accuracy. Here the amplitude and frequency requirements would be ±1.0 db and one-tenth percent respectively. This accuracy would require special circuitry and interface with the computer. The conceptual approach to amplitude and frequency calibration circuits are discussed here briefly and are treated in greater detail in Section IV.

3.4.3.1 Amplitude Calibration

The automatic amplitude calibration would require an overall accuracy of ±1.0 db over the dynamic range of the receiver. The calibration would be done from -40 dbm to -99 dbm, a 59 db range. Both coarse and fine attenuation control would be used. The coarse control would consist of 10 db steps and the fine control would be in 1 db increments. The calibration system would employ a balanced mixer operating as an up-converter. A 100 MHz signal would be mixed with a portion of the local oscillator (LO) power. The output of the up-converter would contain the upper and lower sidebands plus the LO frequency. The undesired sideband and LO frequency would be reasonably attenuated by the main receiver YIG filters. The AGC circuitry would need the capability to regulate the power of the desired frequency to a few tenths of a db. However, it would be difficult to suppress unwanted signals of the up-converter by 10 db or more over an octave band. An unwanted signal in the calibration channel suppressed by only 10 db would cause a power monitoring error of approximately 0.5 db. To eliminate this error, it was decided that a third YIG filter be placed ahead of the power monitor detector which tracks the input receiver filters. The AGC would thus respond only to the desired calibration signal and not to a spur. The AGC calibration loop would regulate the amplitude of the RF calibration signal over a 10 db range in 1 db steps. A voltage control signal would be provided which would match the RF detector power curve over a 10 db range. This control signal would be compared with a sensitive low drift operational amplifier. The output of this amplifier would drive the AGC control of a 100 MHz amplifier. The IF amplifier would need to have adequate gain in order that the 10 db control range plus the variations in loss through the up-converter, YIG filter, and other components could be compensated for. The calibrated amplitude data would be stored by the computer to be compared with measured data during final data reduction.

3.4.3.2 Frequency Calibration

It was required that the automatic frequency calibration have an accuracy requirement of 0.1 percent over the entire operating frequency range. To obtain this accuracy a harmonic generator would be used to inject a train of RF input signals every 100 MHz over the frequency band of interest. During the swept mode of operation the voltage at each frequency increment would be measured using zero crossover techniques. These voltage points would be stored in the computer and compared with measured frequency voltages during data reduction. In order to obtain the accuracy required, an automatic frequency control/IF amplifier assembly would be used to generate an error signal which would be sensed by the computer. The error signal would be derived from a ratio detector and would be coupled into a difference video amplifier. The gain of the amplifier would be adjustable and would provide an output error sensitivity slope of 0.5 volt per megahertz or greater. This would provide an extremely accurate voltage point for the computer to extrapolate against. For automatic

calibration during the fixed frequency mode the computer would sense the voltage at the fixed tuned frequency and then measure several points above and below that point to ensure adequate data for the computer.

3.4.4 Low Frequency Operation

The requirement for frequency coverage from 100 MHz through 2000 MHz was introduced after the development and fabrication of the S- through Ku-band receivers. The broad frequency band precluded the use of a single receiver to cover the range. In addition the use of YIG preselectors below 500 MHz is not too practical at this time. However, the frequency range could be covered by a single unit utilizing up-conversion techniques. The output of the up-converter could then be switched into one or more of the existing receivers. It was decided that up-conversion to all receivers was not practical since frequency multipliers and more complex circuitry would be required. On the other hand the use of only one receiver would limit the efficiency of the system. The use of two receivers however, would provide a good compromise. In order to use readily available hardware, S- and C-band receivers were selected for integration with the up-converter. The input to the YIG preselectors of S and C band would serve to suppress any unwanted image by at least 60 db.

The actual up-converter would use thin film preamplifiers which have extremely stable gain characteristics. A 4 GHz crystal controlled oscillator would be used in conjunction with a pair of mixers to provide a difference output of 2.0 GHz to 3.8 GHz and a sum output of 4.2 GHz to 6.0 GHz. The difference output would then be used in conjunction with the S-band receiver while the sum output would be fed to the C-band receiver. Since the frequency scales for the up-converted signals would not be the same as those of the receivers, some correction factors would be required to provide correct frequency conversion. Input terminals for the 100 MHz to 1000 MHz band would be provided; however, the antenna would not be a part of the present PAMS.

3.4.5 Mismatch Considerations

The VSWR characteristics of the antenna, YIG filter, and mixer-preamplifier would produce large gain variations as a function of frequency if these items were connected directly together by cable. This effect could be suppressed by inserting attenuation between the components. However, attenuators in the receiving channel prior to signal amplification would degrade the system sensitivity. Thus, isolators would be placed between the antenna and YIG filter and between the YIG filter and mixer-preamplifier. The attenuation of this device to signals traveling from the antenna through the receiving channel would be only 0.4 decibel, creating only a minor degradation in sensitivity. However, reflected signals traveling back towards the antenna would be attenuated by at least 18 decibels in the isolator. When this attenuated signal would be again reflected forward in the receiving channel and phase combined with the incoming signals, it would be too small to cause large variations in signal amplitude.

The two isolators in each receiving channel would also further suppress leakage of the local oscillator signal to the antenna by at least 36 decibels, and thus would reduce RF emission to approximately minus 90 dbm.

The VSWR characteristics of the up-converter, YIG filter, and AGC leveling detector in the calibration channel would also be counteracted by placing isolators between these components to prevent amplitude-frequency variations in the precision calibration signal.

Since the up-converter in the calibration channel would generate an on-frequency RF signal at a -20 dbm level and a common local oscillator would be used for the up-converter and the dual high-sensitivity receiving channels, the receiving channel mixers would have to be highly isolated from signals within the up-converter. The inherent isolation within the mixers, hybrid couplers, and up-converter would be inadequate to prevent cross-talk between channels. Thus, two isolators would be included in the local oscillator line to the up-converter. This would adequately suppress RF cross-talk. However, a high-pass filter would also be required to eliminate 100 MHz cross-talk since these coaxial type components would not properly isolate the large 100 MHz CW signal in the up-converter.

3.4.6 Signal Routing

The method of signal routing as conceived for PAMS required a number of parameters to be investigated. There were several options available in the system design. These were; (1) route all RF signal data to the receivers which would be located in the Control Console and, (2) place the receiver assemblies on the antenna pedestal and route low frequency video signals down to the Control Console.

The first approach would require a multiple channel rotary joint in order not to restrict pedestal rotation in the azimuth plane. Since each receiver would be a dual-channel unit the rotary joint would require eight signal channels plus two additional channels for the amplitude and frequency calibrate signals. However, ten channel rotary joints are not readily available. The number of channels could be reduced with multiplexing, but this approach would be quite complicated and the multiplexer would have to have very stringent specifications on maintaining phase and amplitude levels over an extremely broad frequency band. The attenuation of fifty to sixty feet of coaxial cable would also degrade receiver sensitivity by three to ten decibels, dependent upon frequency. The problem of procuring an adequate rotary joint, and the RF attenuation due to cable losses made it apparent that this approach could not be practically implemented.

The second option was to place the receiver assemblies on the elevation axis of the antenna pedestal. This would make greater demands on the physical structure of the pedestal and its associated servo system. However, such an approach would permit all the RF to be processed in close proximity of the antennas and eliminate the long cable runs and rotary joint. The video output signals and all analog control voltages could then be routed through a conventional slip ring assembly. These assemblies are readily available and can be provided with both dc and high-frequency capability. Most slip ring assemblies can handle frequencies up to 50 MHz without any signal distortion. The attenuation of low frequency video signals is approximately 1.2 db per hundred feet of RG-58B coaxial cable. This low level of attenuation would not contribute much degradation to the overall signal level routed to the Control Console. In addition this loss could be easily compensated for in the signal conditioning section of the Control Console.

3.5 PAMS CONSOLE

To provide a control center for the PAMS, a four-bay rack connected together to form a semi-circular console was considered to be the best design approach. In the conceptual layout, an effort was made to optimize the location of each control function to

minimize the reach distance and to provide the operator the best monitoring angle for the various displays. The console would perform functions and contain controls as follows:

Produce the system timing signals.
Process the receiver video and frequency data.
Display the video data.
Establish the cursor system.
Display the numerical equivalent of pertinent data.
Provide for manual calibration signals.
Contain the computer control.
Contain the receiver controls.
Contain the pedestal controls.
Interface with the FPS-16 and MSQ-1 tracking radars.
Interface with the site real-time standard.
Include outputs for video recorders and receiver test.

3.5.1 System Timing (Figure 10)

Since the final design of the PAMS system timing remains as it was planned in the conceptual phases of the program, it is briefly discussed here in the light of its present operating configuration. As shown in figure 10, the PAMS system is cycled at a rate of 30 Hz. Each receiver is operated in two modes during each cycle, a swept and a fixed frequency. A settling time is provided before each mode of receiver operation is begun. This is required to give the receiver YIGS time to tune to the selected frequency. A receiver sweeps through a preselected frequency band for 24 ms after a 0.8 ms settling time. Up to twelve frequency data points can be recorded in the computer. A 4.0 ms settling time is then required to allow the YIGS to reach the specified fixed frequency level. Data can then be taken for the next 4.5 ms. The fixed frequency data are transferred to computer during the last 0.125 ms. The 30 Hz rate is synchronized with the power line to minimize flicker when data are displayed on the oscilloscope.

3.5.2 Receiver Video and Frequency Data Processing (Figure 11)

The functions of receiver video and frequency data processing are also discussed in the light of their present operational configuration for the same reason previously mentioned for system timing. (Refer to figure 11, the signal processing block diagram.) Each receiver generates four signals: two are the polarized video, the third is the frequency, and the fourth is the discriminator output. The discriminator is used for frequency calibration and automatic frequency control.

Both of the video signals are terminated into a 50 ohm impedance-matching load in the processor section of the console. The signals are then fed to a differential input instrument amplifier. This was done to give 60 db of common mode noise rejection. The output of the amplifier is fed to a data gate either directly or through a 100 KHz filter. If data are to be taken during the sweep mode, then a 100 KHz filter is used to improve the signal detection. Up to twelve frequency points are selected by the cursors described in paragraph 3.5.4. The cursor opens the data gate for 100 μsec, feeding the filtered video to a peak detector. Since only 100 μsec of the signal is sampled, the peak detector actually acts as a sample hold. The cursor system flags the computer to read the peak detector output and convert the analog voltage to a 12-bit digital word.

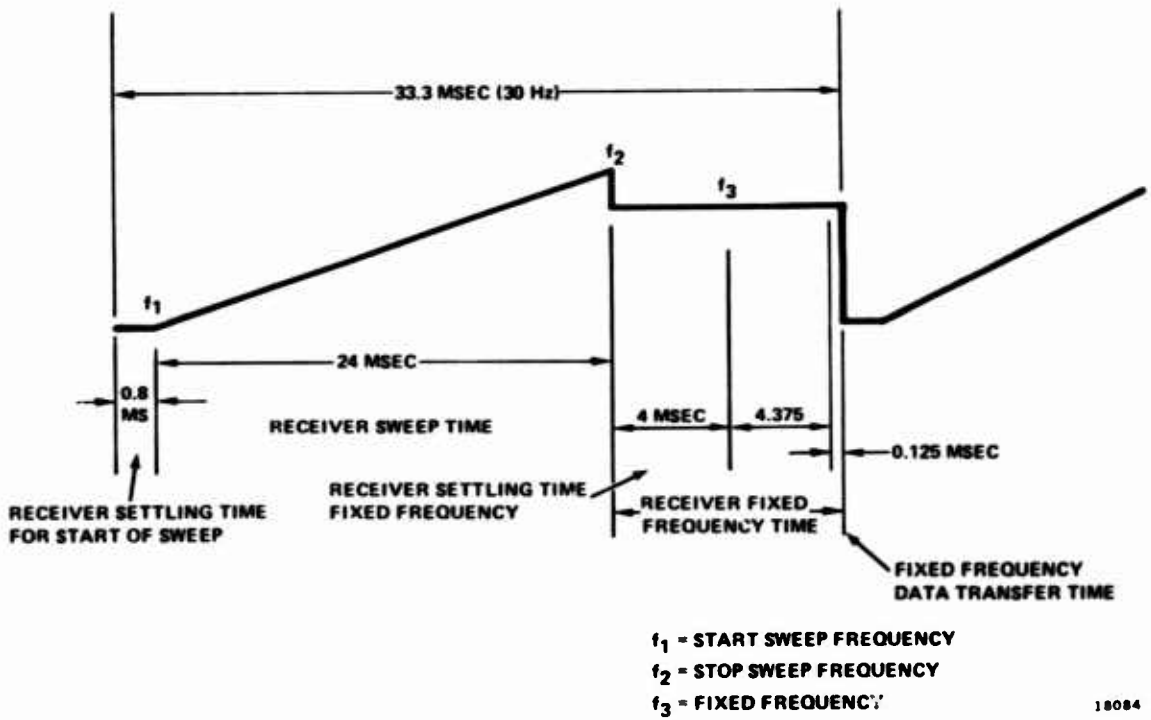

Figure 10. System Timing - Receiver Sweep Pattern

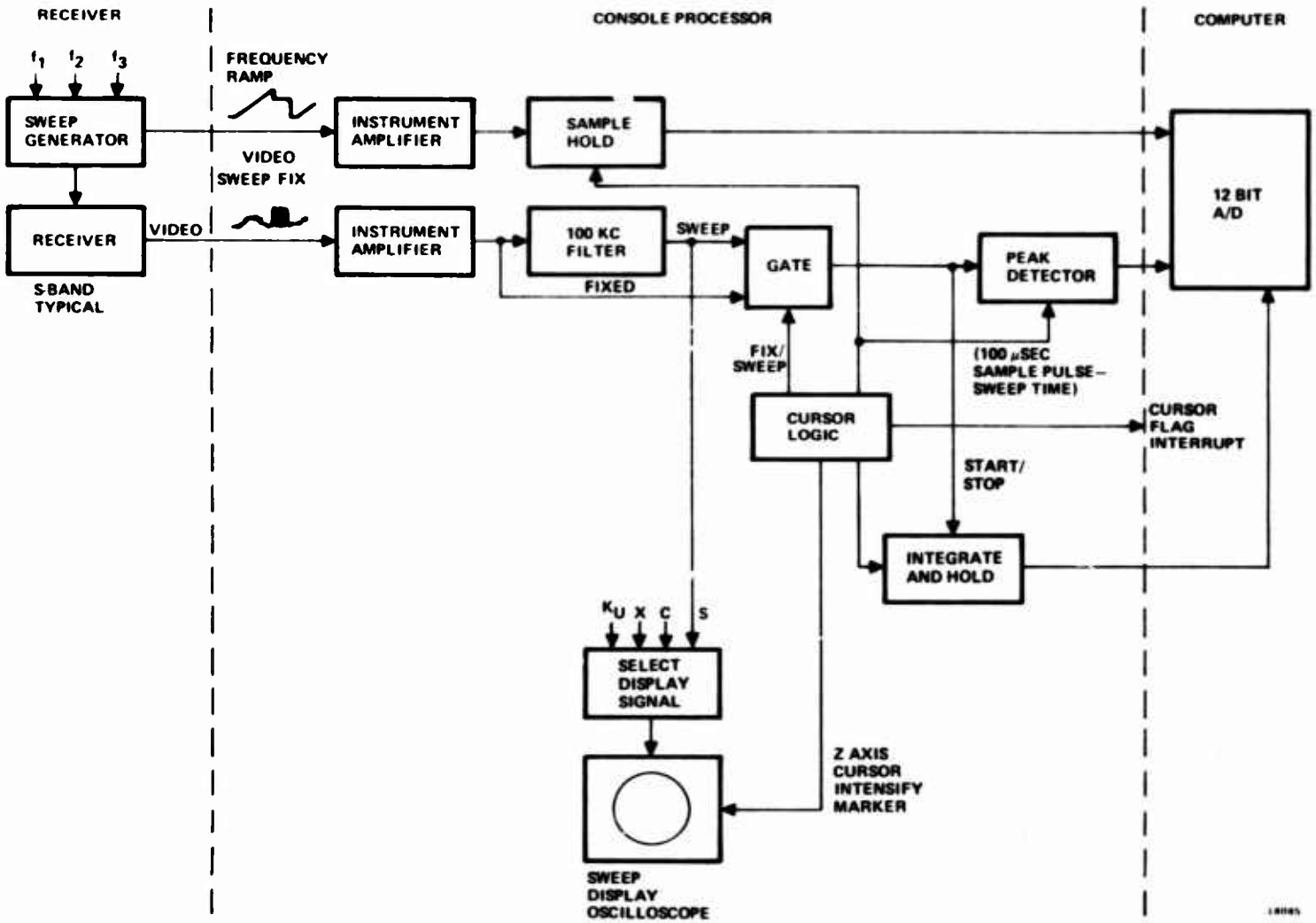

Figure 11. Signal Processing - Block Diagram

If the signal characteristics of a radar operating at a single frequency are to be analyzed then the fixed frequency mode of each sweep is utilized. In this case, the unfiltered video is fed to the peak detector for 4.375 ms.

The 4.375 ms is long enough to sample 90 percent of all known aircraft radars. The 4.375 ms time can monitor radars with repetition rates of 220 Hz or more. If a special radar with a repetition rate of lower than 220 Hz is being monitored the receivers can be set to operate in the fixed-frequency phase only. In this mode, the sample time is extended to 8.5 ms or a 175 Hz signal can be sampled.

The filtered video data can also be fed to a voltage integration and hold circuit. The integrator start and stop points are selected by cursors. The frequency at the start and stop points of the integration period are known, thus, the computer can calculate the power density of the integrated signal in watts/mc.

The frequency signal is in the form of a ramp with a step as shown in figure 10. The frequency data are buffered by an instrument amplifier then fed to a sample hold. The same cursor pulse which sets the video peak detectors also sets the sample holds. These data are then fed to the computer in the form of an analog voltage.

3.5.3 Video Signal Displays (Panoramic and Analysis)

The original design of the PAMS system required eight panoramic displays to show the swept video signal, one display for each channel of the four dual bands, KU, X, C, and S. A single large screen scope which could be switched to any band was to be used to analyze signal characteristics for fixed-frequency data, as range radar pulse widths and repetition rates. Subsequently, in the light of invoking program cost economies the number of scopes were reduced and their function modified. A compromise was made which resulted in one dual-trace 12-inch scope being selected. This scope could display either the swept receiver video, (panoramic display), or the fixed frequency video, (analyses display). For the analyses requirements, the bandwidth of this scope had to be wide enough to display pulses with a minimum width of 0.2 μs. The scope could switch to any of the four bands and display both polarized video channels at once.

The eight panoramic scopes were replaced by two dual-trace 0.5 MHz, 4-inch scopes. The lower bandwidth and less expensive scope could be used because of the lower frequency of the swept video. All swept video signals would be passed through a 100 KHz filter for signal to noise enhancement.

Each of the two smaller panoramic scopes could also be switched to monitor any band. Thus, three bands could be monitored simultaneously. An analysis of most of the PAMS applications indicated that there would be very few requirements for monitoring more than three bands simultaneously.

The scopes could also be used as standard oscilloscopes to monitor other functions or troubleshoot the PAMS.

3.5.4 Cursors

The video data to be monitored by the computer was specified by a cursor or a pair of cursors. Two types of cursors were considered for use in the PAMS. The first type of cursor would monitor the amplitudes of both video channels at a specified frequency.

With 12 cursors in all, four would operate independently and eight would operate in pairs. The four independent cursors could monitor either the swept frequency or one fixed frequency point on each receiver.

The eight cursors operating in pairs not only could monitor the video data at a specific frequency but also could integrate it. The first cursor would indicate the point to start integrating while the second cursor would indicate the stop point. The computer would then read the integrated video data. These data could be used to determine broadband jammer power density.

In order to position a cursor on a signal of interest, any of the three panoramic scopes could be used. The cursor would be superimposed upon the screen by intensifying the data at the cursor point. Cursors could be switched to any band, and up to twelve cursors could be placed on one band. Cursors could occur on multiple bands simultaneously but no one cursor could be used on more than one band and point at any one time. (The cursor system, in its operational configuration, is so designed that if required at a future time it can be expanded from twelve to at least thirty cursors.)

3.5.5 Numeric Display

A six-digit numeric display on the PAMS console would indicate the various system parameters. The display would work in conjunction with the computer to provide uncalibrated video data. Any of the twelve cursor outputs could be displayed in terms of frequency or db of signal. The frequency data would be within 0.5 percent of the true value while the video signal would be ±3 db in the range of -40 db to -85 db. The display also could indicate the tracking radar range and the site time.

3.5.6 Manual System Calibration

Two types of manual system calibration would be available on the PAMS console. One would be receiver and the second would be scope calibration.

Switches on the console would allow an operator to place the receiver in the amplitude or the frequency calibration mode. In the amplitude mode, a manually selected video level would be injected into each receiver and displayed on the scope as a dc level. This level could be compared against a signal level to accurately determine the received signal level without the use of the computer.

For the frequency calibration mode a harmonic generator would inject RF signals at 100 MHz intervals into each receiver.

The scope calibration signal would allow an operator to simultaneously observe a video signal and an amplitude calibration signal. The amplitude calibration is actually a dc signal which is gated for 400 μsec into the scope video input. The position of this signal can be adjusted to any location on the scope trace. The amplitude of the calibrated signal is adjusted by a 10-turn digital reading pot on the analysis scope control panel.

3.5.7 Computer Control and Interface

A console panel and a processor located in the console rear, would provide a computer control and interface required to input and read data from the HP2116B computer.

The console would control the operation of the computer during the data-taking mode. Five console pushbuttons would perform these functions which are described as follows:

Freq/Amp Calibrate	Initiates a computer-controlled amplitude and frequency calibration of each receiver which contains a cursor.
Run	Computer takes cursor video amplitude and frequency data, plus site time, target radar range, azimuth, and elevation data and stores it on 9-track magnetic tape.
Pause	Halts data storage on 9-track magnetic tape, but does not initiate a new data run nor terminate present run.
Stop	Computer stops taking data mode and terminates run. Teletype data input is performed at this time. Data includes cursor data types, power, power density, reflectivity, etc., and aircraft attitude, plus any other comment which would be required.
End of Flight	Computer terminates data taken for a given flight. All runs taken during this flight are combined to form the antenna pattern data.

The processor would interface with the computer input/output priority interrupt system to load or read data. Each of the twelve cursors would control an interrupt, causing the computer to read the video peak detectors and frequency sample hold circuits. The site time and tracking radar AZ, EL, and range inputs would also have interrupts. The remaining data are console controls, receiver status, computer mode controls, cursor receiver assignment, display function control, and receiver attenuation controls, which would all be scanned by the computer automatically as part of the normal program routine.

3.5.8 Receiver Control

One panel containing controls for the S-, C-, X-, and Ku-band receivers was conceived. The panel would allow an operator to control the following functions for each receiver:

IF Bandwidth	1.5 to 10 MHz

Adjust sweep bandwidth	From less than 100 MHz to full band.
Automatic Frequency Control (AFC)	Turns AFC on and selects which channel of the polarized video is to be used to control the fixed frequency pattern of each sweep.
Antenna Polarization	Select either linear or circular polarization for the antennas. The antenna channels can be interchanged. Thus, if one channel goes out, the data of interest can be switched to the operational channel.
Select Fixed Frequency	Select any frequency from minimum to maximum band for the fixed frequency part of each sweep cycle.
Power Control	Turn any one receiver on or off.

Extending the receiver frequency coverage to include L band was effected as an add-on contract to the program. To minimize cost and maintain the required performance, it was decided to share the S- or C-band receiver. The L-band signal is mixed with a 4 GHz oscillator and the difference can be fed to the S-band receiver or the sum fed to the C band. Whenever an L-band signal is to be analyzed, either the S- or C-band receiver must be utilized. The computer is informed which band has been selected by switch logic and programs the display and data reduction equations to convert the S- or C-band signals to an equivalent L band.

3.5.9 Pedestal Control

It was determined that all the pedestal controls would be contained in bay one of the console. See Section IV for a more detailed discussion of the present pedestal controls configuration.

3.5.10 Interface with the FPS-16 and MSQ-1 Tracking Radars

The azimuth and elevation inputs from both tracking radars are 16:1 synchro commands. A Northern Precision Laboratory (NPL) device converts both signals to binary outputs for the computer and the pedestal electronics. The pedestal electronics compares the trackers position with its own position using binary inputs rather than synchro data. The NPL converter also contains a decimal readout for azimuth and elevation. The tracker radar ranges are converted to binary in two different ways. The MSQ-1 has a 500:1 synchro input which the NPL unit converts to a binary number equivalent to range in yards. The FPS-16 has a serial binary number representing ranges in yards which is converted to parallel by logic in the processor. Both tracker binary numbers are converted to nautical miles by the computer and can be selected on the numeric display.

3.5.11 Site Time Standard

The console provides the interface between the RADC site time standard and the computer. The time is used to merge the data acquisition information with an airborne aircraft and attitude monitoring system which is under separate development.

3.5.12 Video Recorder Outputs and Test Panel

Each receiver's video and frequency signals have been brought to a special panel so an analog recorder may be used to record the data as it is being received. System timing signals are also available to synchronize the video data to the PAMS sweep times.

This same panel contains circuitry necessary to test any receiver using the S-band controls and reading signals on the oscilloscope displays set to S band.

3.6 COMPUTER GROUP

The computer group comprises all of the instrumentation required to store, reduce, and display all measured data. The requirements of the PAMS were investigated in order to define the computer characteristics. This analysis consisted of defining the number and type of inputs, data sampling rates, number and type of outputs, and the peripheral equipment needed to provide the required format and display of the data. From the results of the analysis above it was then possible to determine the computational rates, size of memory, and interface requirements with the PAMS. Also a factor in the selection of a data reduction system was the available software supplied as part of the system, and the ease of adding ancillary hardware at a later date. The computer and peripheral equipment are to be furnished by the Government. Options on several systems were given to Actron and based on the above requirements for the PAMS data reduction an HP 2116B computer was selected. The final equipment selected for the Computer Group is listed in paragraph 4.2.3.

SECTION IV

SYSTEM CONFIGURATION

4.1 GENERAL

This Section describes the present configuration of the Precision Antenna Measurement System (PAMS). A brief general description of the hardware making up the system is presented, followed by a more detailed discussion of the equipment, including test data of the major and critical components of the system along with a thermal analysis of the receiver housing. PAMS theory of operation is presented, and the last part of this Section lists the computer programs and their functions.

4.2 DESCRIPTION OF EQUIPMENT

As shown in figure 12, the PAMS consists of: (1) antennas and receivers mounted on an antenna pedestal, (2) a control and display console, and (3) a computer and peripheral equipment. The PAMS is a receive-only system, and a tracking radar (MSQ-1 or FPS-16), not supplied as part of the system, is necessary to the operation of the system. The tracking radar is required (1) to actively track a test aircraft (or chaff) and to slave-position the PAMS antenna array onto the target, (2) to provide target azimuth, elevation, and range data for the PAMS computer, and (3) to provide a blanking input to the PAMS to blank the acquisition of data during the transmitted pulse of the tracking radar and for a selectable length of time thereafter. The PAMS computer requires a site-time input, the source of which is not supplied as part of the system.

4.2.1 Antennas and Receivers

The array of four antennas is used to provide frequency coverage from 1 GHz to 18 GHz. Each antenna includes a polarization network which, at the operator's selection, switches the antenna from a dual linear polarization configuration (vertical and horizontal components) to a dual circular polarization configuration (right-hand and left-hand components), or decouples the antenna from the receiver. As shown in figure 12, the polarization networks for the two larger (lower-frequency) antennas are integral parts of the feed elements and the polarization networks for the two smaller (high-frequency) antennas are contained in separate enclosures behind the antennas. The antennas are positioned by azimuth and elevation drive motors in the antenna pedestal. The drive motors are controlled by a servo system which includes components in the pedestal and in the console which is described later. The antennas, polarization networks, and antenna pedestal (but not the receiver housing shown attached to the pedestal in figure 12) are manufactured by Scientific-Atlanta, Inc.

The receiver housing attached to the antenna pedestal (figure 12) is shown with cover removed in figure 13. The principal assemblies in the housing are four receivers, each of which is normally connected to one of the four antennas. The frequency bands of the receivers are 2 GHz to 4 GHz (S band), 4 GHz to 8 GHz (C band), 8 GHz to 12 GHz (X band), and 12 GHz to 18 GHz (K_u band). The frequency bands of the antennas match those of the receivers except that the S-band antenna operates from 1 GHz to

ANTENNAS/RECEIVERS

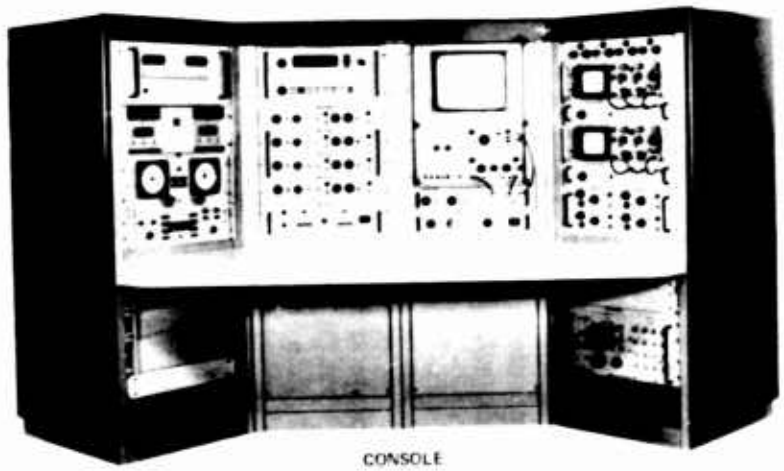

CONSOLE

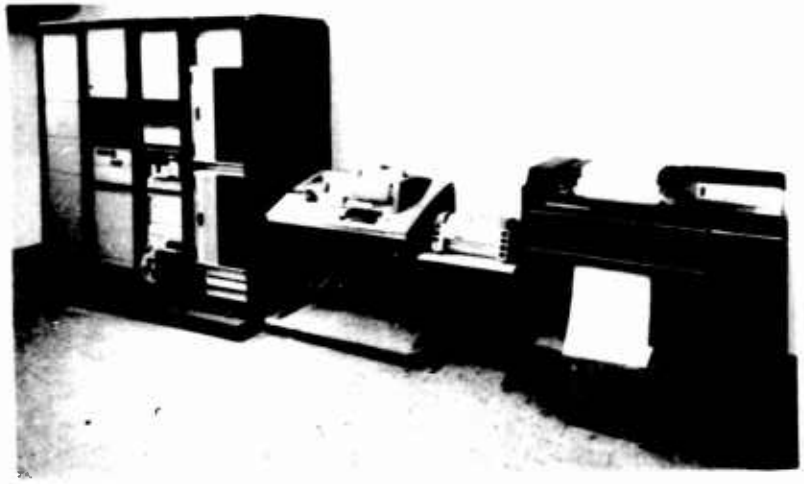

COMPUTER PERIPHERAL EQUIPMENT

Figure 12. Precision Antenna Measurement System (PAMS)

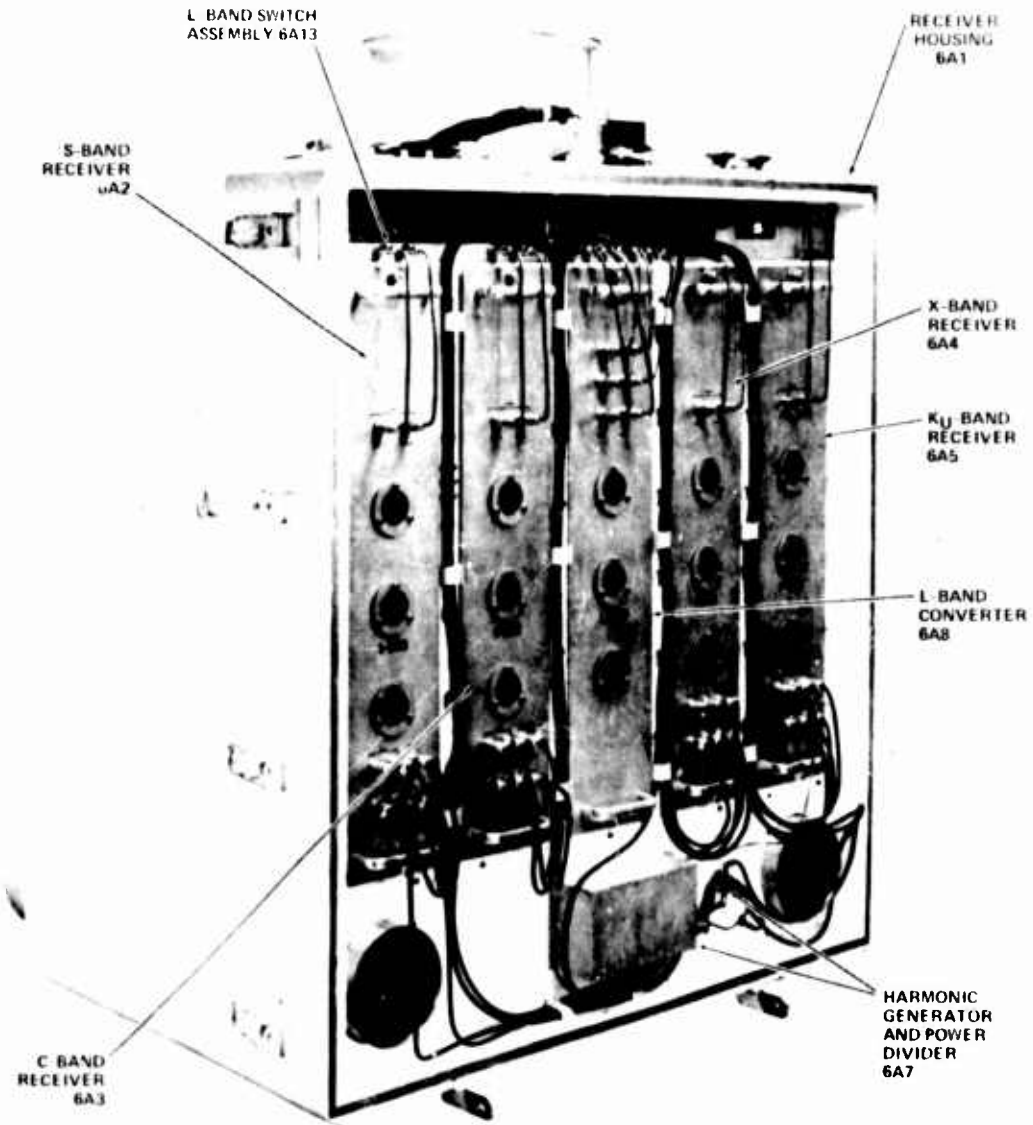

NOTE: DISTRIBUTION PANEL 6A6, MOTOR CONTROLLER 6A9, VENT MOTORS 6A10, 6A11, 6A12, THERMISTOR 6RT1, VARIACS 6T1, 6T2, 6T3, FAN 6B1, UNDERTEMP THERMOSTATS 6S1, 6S2, 6S3, HEATERS 6HR1 THRU 6HR4 ARE INSIDE THE RECEIVER HOUSING AND NOT VISIBLE IN THIS PHOTOGRAPH.

Figure 13. Receiver Housing

4 GHz. The 1-to-2 GHz band is considered part of an L band. An L-band switch assembly and L-band converter are provided to up-convert L-band signals for processing either by the S-band receiver or C-band receiver, at the operator's selection. The L-band converter is designed to operate from 0.1 GHz to 2 GHz so that an additional UHF antenna (not supplied with the system)* operating from 0.1 GHz to 1 GHz may be used. A harmonic generator and a power divider are included in the receiver housing to provide RF calibration signals to the four receivers.

All RF inputs from the antennas to the receivers are routed through connectors across the top of the receiver housing to connectors on the front of each receiver and the L-band converter (via the L-band switch assembly in some cases). The RF calibration signals are also applied to connectors on the front of each receiver. The receiver video outputs from connectors on the front of each receiver are routed through a single connector at the top of the receiver housing to the console. Power and control signals from the console are routed via connectors on the rear of the receiver housing and a distribution panel (not visible in figure 13) to the harmonic generator and to connectors on the rear of each receiver and the L-band converter. A fourth connector at the rear of the housing provides for routing power and control signals to the antenna polarization networks. The distribution panel, accessible from the bottom of the receiver housing, also provides interconnection between various other components within the receiver housing. These other components, which are listed in the note on figure 13, are concerned with air flow and temperature control. The receiver housing contains three motor-driven external vents (one at the top and two at the back) to control the flow of external air through the receiver housing. A motor controller circuit and thermistor control the three vent motors. Air movement is provided by a fan. Three variacs are required to step down the primary 208-vac line-to-line 3-phase power to 120-vac line-to-line power for the fan motor. Under-temperature thermostats and heaters are provided to supply heat to the receiver housing when the system is not in use.

4.2.2 Console

As shown in figure 14, the console includes four bays of equipment. All of the equipment in bay 1 (left-hand bay) is related to the antenna servo system. The tracker unit converts azimuth, elevation, and range synchro command signals from the tracking radar to digital signals. The two digital synchro display units convert azimuth and elevation synchro position signals from the antenna pedestal to digital signals. The synchro junction box selects synchro command signals from either the MSQ-1 or FPS-16 tracking radars. The manual command unit provides the capability of manually positioning the PAMS antenna array. The servo control unit is used to control power to the antenna servo system and to select the mode of control for the servo system. The digital comparator compares the digital azimuth and elevation command data from the tracking radar with the digital azimuth and elevation position data from the antenna pedestal to generate error signals for the antenna servo system when the PAMS antenna array is slaved to the tracking radar. The dc amplifier unit and servo amplifier unit are part of the antenna servo loop; these units operate in conjunction with power amplifiers, drive motors, and tachometers in the antenna pedestal to position the antenna array. One of two fans for the console is located at the bottom of bay 1.

*After delivery of the system, a UHF crossed log-periodic antenna has been added to the antenna mount, to extend the frequency coverage down to 0.1 GHz.

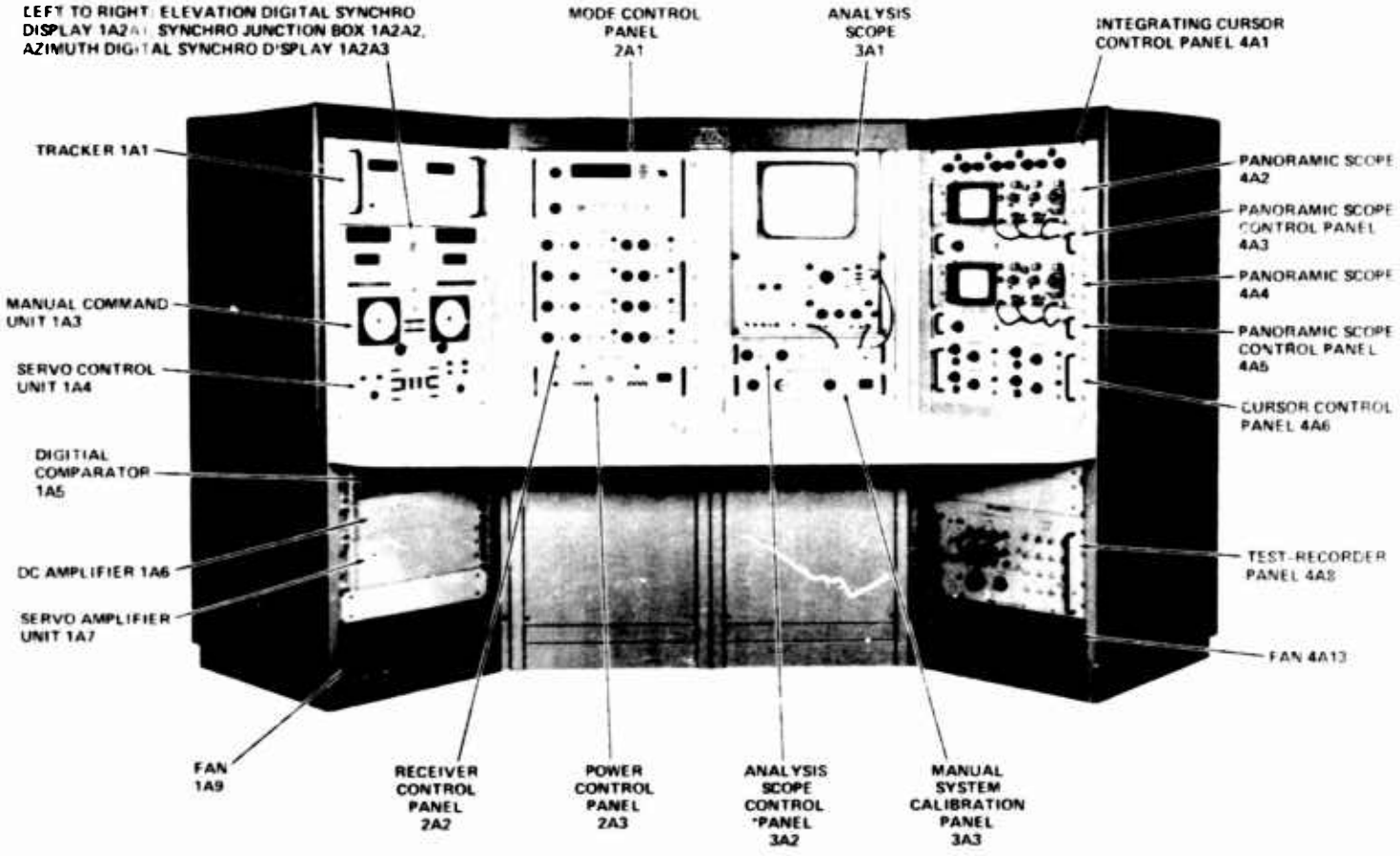

Figure 14. PAMS Console, Front View

In bay 2, the mode control panel selects the system mode of operation via the computer and selects various data from the computer for numerical display. The receiver control panel contains a set of controls for each of the four receivers. The power control panel connects primary power to the system.

In bay 3, the analysis scope is used to display the video from any of the four bands in either a panoramic or fixed-frequency display. The analysis scope control panel band-selects the video to be displayed, selects the panoramic or fixed-frequency display, and provides for connecting the selected video and horizontal sweep voltage to the analysis scope via jumper cables. The analysis scope control panel also contains radar blanking controls and test points for system timing signals. The manual system calibration panel provides for manual system calibration as opposed to automatic (computer controlled) calibration which is selected at the mode control panel in bay 2.

In bay 4, the integrating cursor control panel controls the generation of four pairs of cursors, each pair of which is (a) assigned to any of the four frequency bands, (b) superimposed on the oscilloscope display of the video for the assigned band, (c) positioned to any pair of frequencies of interest in the assigned band, and (d) used to acquire frequency and amplitude data at the two selected frequencies as well as integrated amplitude data between the two frequencies. Each of two panoramic scopes provides a panoramic display of the video from any of the four bands. A panoramic scope control panel is provided for each panoramic scope to band-select the video and to connect the selected video and horizontal sweep voltage to the scope via jumper cables. The (non-integrating) cursor control panel controls the generation of four cursors, each of which is (a) assigned to any of the four frequency bands, (b) superimposed on the oscilloscope display of the video for the assigned band, (c) positioned to any frequency of interest in the assigned band, and (d) used to acquire frequency and amplitude data at the selected frequency. The test-recorder panel is used to (a) provide all connections necessary to allow any of the four receivers to be connected to this panel for testing, (b) provide video outputs from all four bands and timing signals for recording, (c) provide connections for radar blanking inputs from the two tracking radars, and (d) provide test points for power supply voltages. The second of two console fans is located at the bottom of bay 4.

Figure 15 is a rear view of the console, showing assemblies not visible from the front. Attached to the side of bay 1 is a power control box which connects power to the antenna servo system under control of the servo control unit in bay 1. A terminal plate at the side of bay 1 provides for branching digital azimuth and elevation command data out of the servo system to the computer. The processor at the rear of bay 2 contains most of the PAMS video processing and digital control circuits on plug-in circuit cards. The processor tilts down to a horizontal position for access to the circuit cards. Attached to the side of bay 2 is a power supply assembly which contains two +28 vdc power supplies and +15 vdc and -15 vdc power supplies. The receiver interface panel at the rear of bay 3 provides all power, control, and video signal interconnections between the console and the receivers. This panel also contains three coaxial connectors used to acquire range data from the FPS-16 tracking radar in digital form. (Range data from the MSQ-1 tracking radar and azimuth and elevation data from both tracking radars are received in the form of synchro signals at the synchro junction box in bay 1.) Two computer interface panels attached to either side of bay 4 provide all digital signal interconnections between the console and the computer. (Analog inputs to the computer are routed directly from the processor to the computer.)

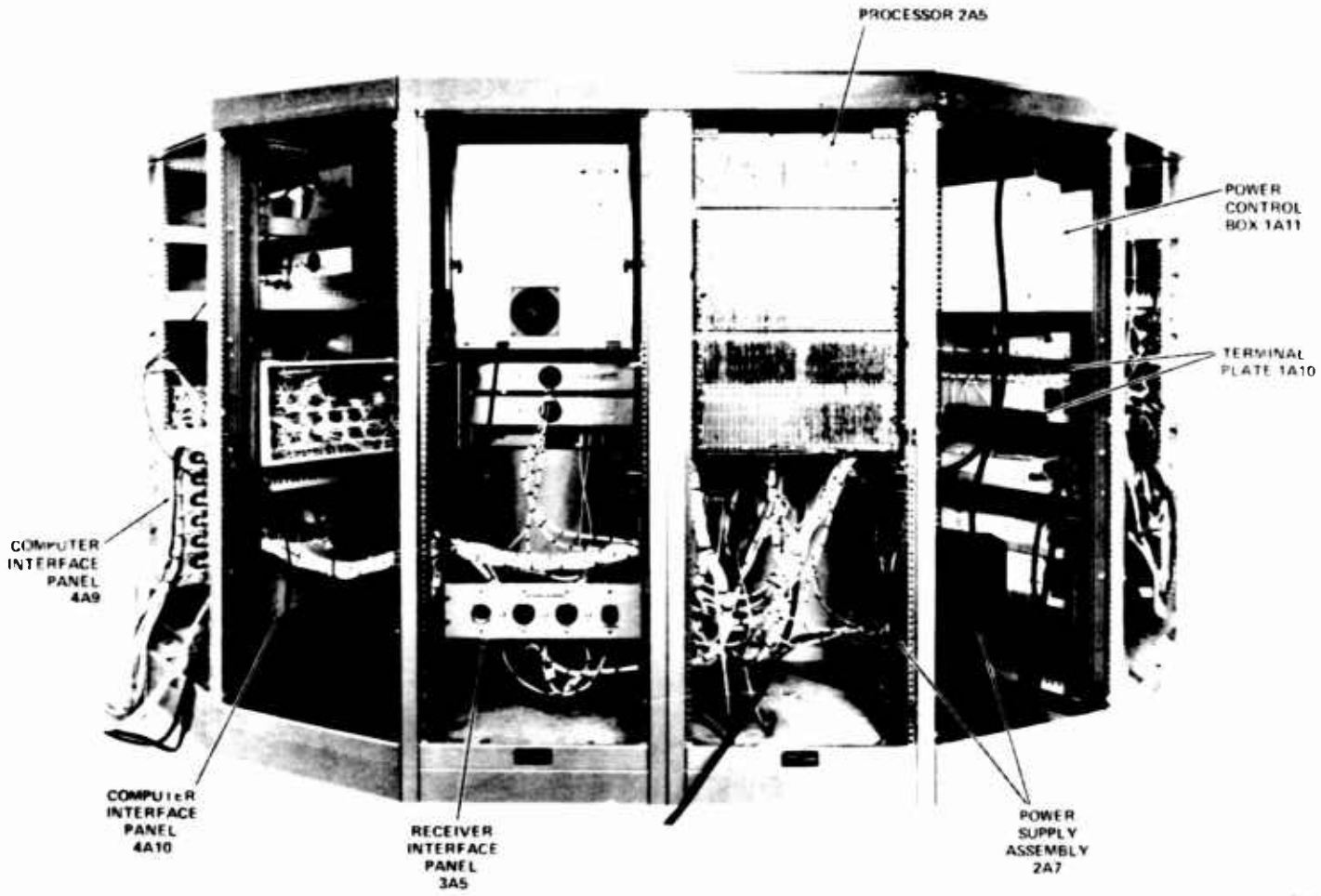

Figure 15. PAMS Console, Rear View

4.2.3 Computer and Peripheral Equipment

The computer and its peripheral equipment is shown in figure 16. The computer is an HP 2116B and is contained in three of the four bays shown in figure 16. The first bay is presently a spare. The second bay contains the following units:

HP 12539A Time Base Generator
HP 12555A Digital-to-Analog Converter (two cards)
HP 12566A Microcircuit Interface (six cards)
HP 12604B 32-Bit Data Source Interface (two cards)
HP 12556B 40-Bit Register
HP 12554A 16-Bit Duplex Register (two cards)
HP 2310B (Options 02, 16) Analog-to-Digital Subsystem

The third bay consists of the following units:

HP 2116B computer with 24,574 words of memory
HP 12579A Extended Arithmetic Unit
HP 12578A Direct Memory Access
HP 12588A Power Fail Interrupt
HP 12591A Memory Parity Check
HP 2150B (Option 01) I/O and Memory Extender
HP 2160A Power Supply
HP 2748A Paper Tape Reader (500 characters/sec)
HP 2753A Paper Tape Punch (120 characters/sec)
HP 13181A Magnetic Tape Controller
HP 12575A Paper Tape Winder

The fourth bay consists of two HP 7970A nine-track magnetic tape units. In addition to the computer there is an HP 2754B teleprinter (10 characters/sec), a HP 2778-01 Line Printer, and a Calcomp 565 X-Y Plotter with HP 12560A plotting interface.

4.3 ANTENNA/PEDESTAL SUBSYSTEM

The antenna/pedestal subsystem is shown in figure 17. This unit was procured from Scientific-Atlanta Inc. to Actron specifications. The antenna array is made up of four antennas covering the frequency range of 1 GHz to 18 GHz.* The L/S-band antenna covers the 1 GHz to 4 GHz band and consists of a six-foot parabolic reflector with a dual polarization primary feed utilizing crossed log periodic antennas. The C-band antenna is made up of a four-foot reflector and a dual polarized quadra-ridge waveguide primary feed. The X band and K_u band are both of the Cassegrain type with the X-band antenna using a two-foot reflector while the K_u band uses an eighteen-inch reflector. All four of the antennas have a polarizer unit to permit the simultaneous reception of either vertical and horizontal linear polarizations or right-hand and left-hand circular polarizations. The only difference in the polarizers is the selection of components to cover the required frequency bands. The polarizer is shown schematically in figure 18. During operation in the linear mode, the signal bypasses the hybrid and is routed directly through the transfer switch to the vertical and horizontal channels of the receiver. When circular polarization is selected by the operator, the hybrid is switched into the signal path thereby providing the required ninety-degree phase differential for right-hand and left-hand circular polarization. The

*See footnote, page 44.

Figure 16. PAMS Computer Group

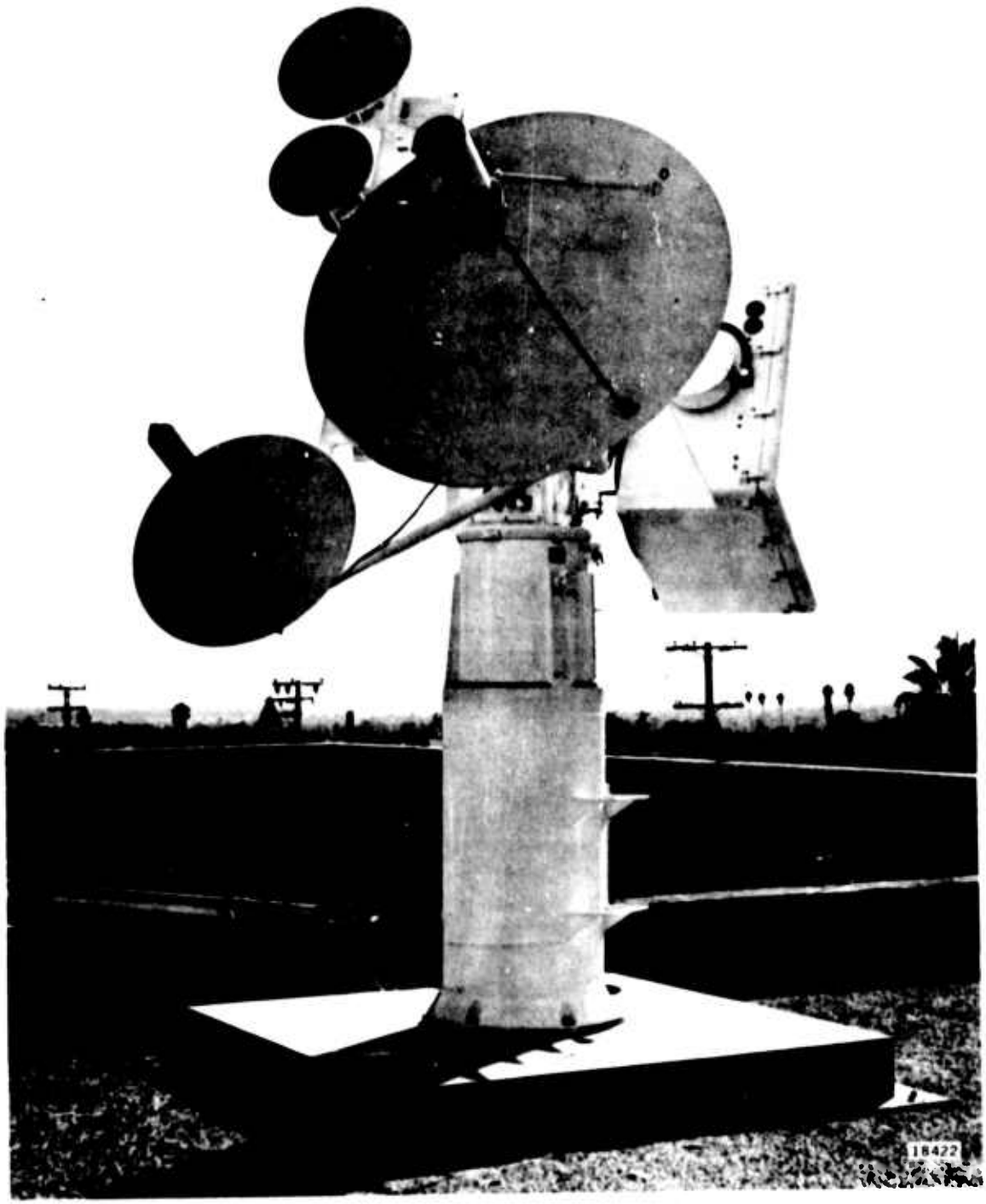

Figure 17. Antenna/Pedestal Subsystem

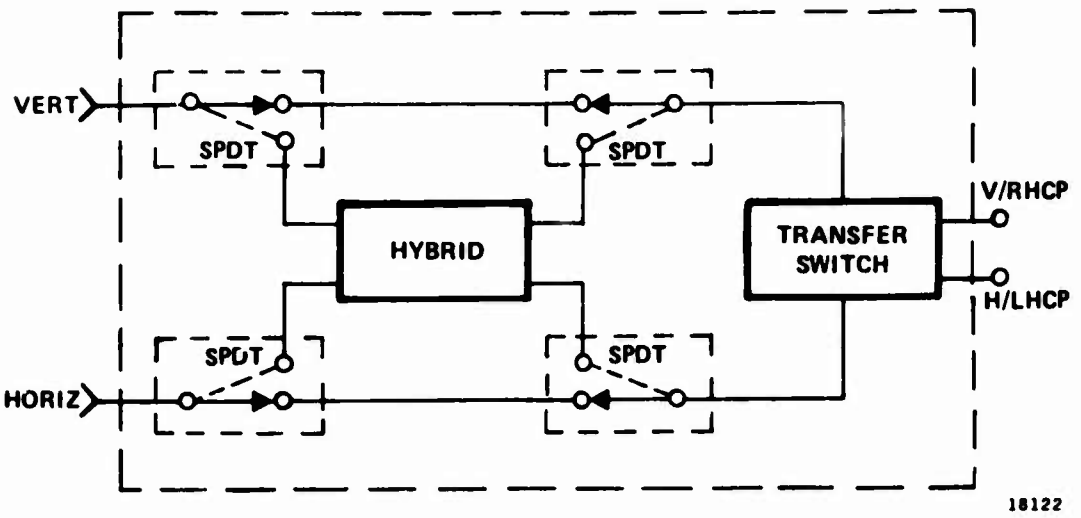

Figure 18. Polarizer Network

signal then passes through the transfer switch to the respective receiver channels. The transfer switch is used for improved reliability while operating in the linear polarization mode. Should a receiver channel fail during operation, the operator can activate the transfer switch and reverse the inputs to the receiver. This allows the data to be routed into the operating receiver channel.

4.3.1 VSWR Data

All the polarizer units were measured to determine the Standing Wave Ratio (SWR) of the unit. The maximum specified SWR for the units was 2.0:1. This limit was exceeded in all bands to some degree; however, the maximum never exceeded 2.5:1. In addition, the out-of-specification condition was over a very small portion of the frequency band. The high SWR was the result of interacting SWR s of each component in the polarizer. The SWR of the polarizer is not seen by the receiver inputs due to the attenuation of the transmission line which effectively reduces the SWR so that the effective SWR is much lower. The typical transmission line attenuation is on the order of two to four db depending on the frequency. This reduces the input SWR to approximately 1.5:1 or less in all cases. The relationship for input and load SWR as a function of attenuation is given by

$$\text{Coth}^{-1}\,\text{SWR}_{in} = \text{Coth}^{-1}\,\text{SWR}_{load} + \alpha/8.686 \qquad (11)$$

where α = line attenuation.

Figure 19 is typical of the SWR data for the polarizers. The data for the 1 GHz to 4 GHz polarizer were taken using a swept reflectometer technique. The data for the other bands were taken using a swept slotted-line technique. In the later case the scale is calibrated using known precision attenuators and then the maximum deflection is the maximum SWR and is calculated with the use of the following equation:

$$\text{SWR} = \log_{10}^{-1}\,\frac{\text{db}}{20} \qquad (12)$$

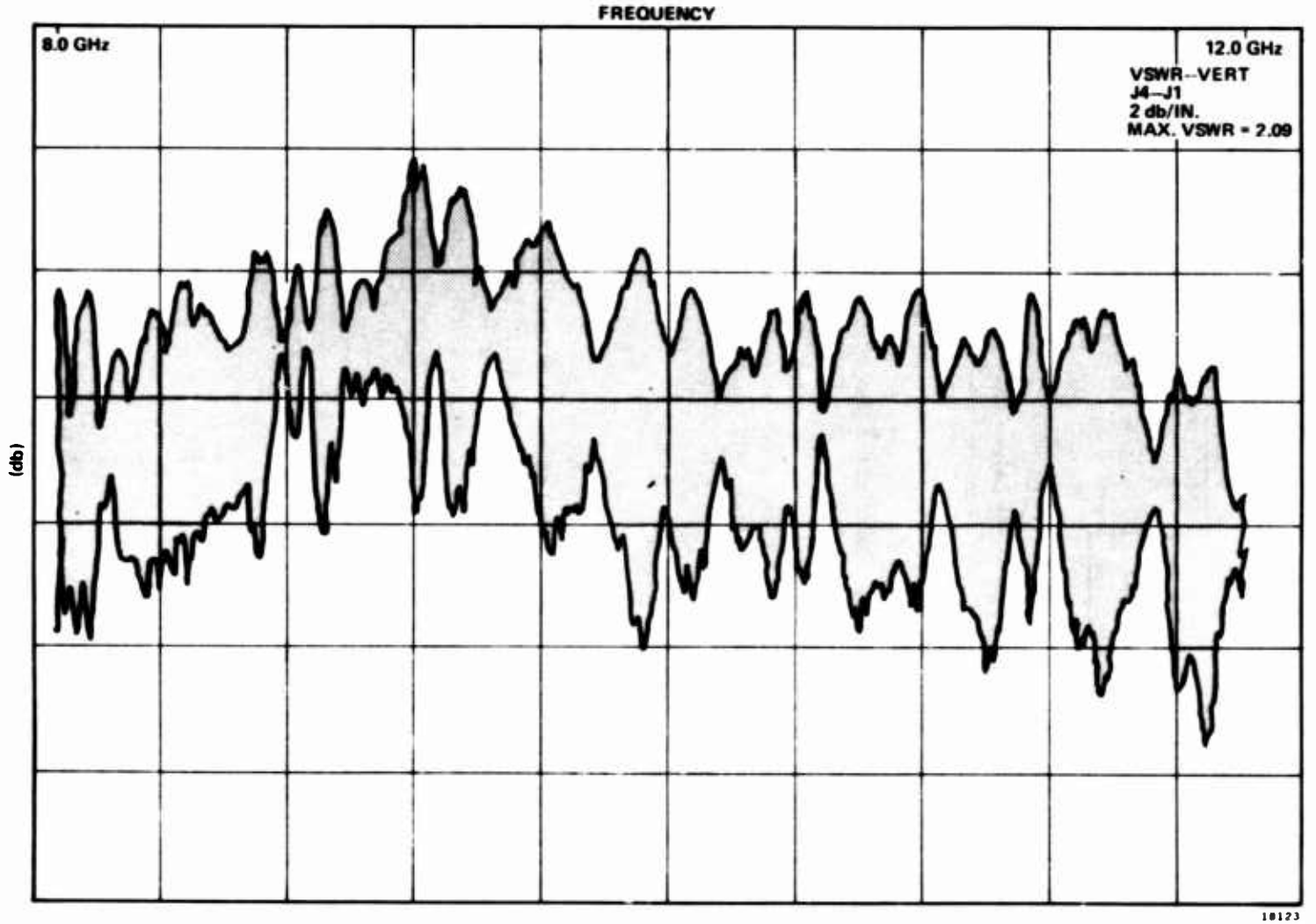

Figure 19. VSWR - X-Band Polarizer

The maximum is read in db per inch from the data and the SWR calculated. For example, referring to figure 19, the maximum excursion occurs at approximately 10.0 GHz and is 3.2 inches. The scale factor is 2 db per inch or 6.4 db. Using (12) we have

$$SWR = \log_{10}^{-1} 6.4/20 = \log_{10}^{-1} .320$$

$$SWR = 2.1:1$$

The maximum SWR in L/S band was 2.25:1, and in C band it was 2.08:1. The worst SWR was encountered in K_u band where it was 2.62:1.

4.3.2 Antenna Characteristics

The primary parameters of importance for the antennas are beamwidths, sidelobe level, gain, gain tracking for both polarizations, and axial ratio. Extensive tests were run on the antenna subsystem to ensure that these parameters conformed to the operational requirements of the PAMS.

Figures 20 and 21 are typical of the antenna pattern measurement made. All patterns of the antennas were made with the polarizers installed. As can be seen there is excellent correlation between the orthogonally polarized elements. Both the 1/4 db and 3 db beamwidths approach the calculated value. However, in general the 1/4 db beamwidths were a little broader than predicted. Fortunately, this worked to the advantage of the system by providing a larger look angle with less amplitude variation. The 0.25 db and 3.0 db beamwidths were to specification for all four bands.

The sidelobe levels were generally better than those specified (-15 db) except at two points in the C-band antenna. The S band had an average level of -20 db in the E plane and -17 db in the H plane. The C-band E plane levels were typically -20 db. However, the H plane exhibited both quadratic and cubic phase error in the phase distribution. This caused the sidelobe level to increase to -12.5 db at two points. As the amplitude level is detected over the 0.25 db beamwidth the high sidelobe level does not interfere with the measurements providing the elevation angle is greater than one beamwidth. For low elevation angles care is required to minimize the effects of multipath. The measured sidelobe levels in both X and K_u bands were an average of -16 db in both the E and H planes.

The measured gains are shown in figures 22 through 25. The channel tracking was one of the more stringent requirements. As can be seen from the figures, the worst case encountered was ±0.5 db while the typical value was ±0.25 db or better. The S- and C-band gains met or exceed the gain requirements in both planes. There was a hole in the C-band gain curve due to the phase error which caused the beams to spread and reduce the gain. However, the gain decrease at the one frequency did not affect performance as there was surplus gain available in this band. The minimum gain required at this frequency was 27.5 db and the measured gain was 29.75 db. In general, the gain in both X and K_u bands was not as good as expected. This was due primarily to the small parabolic reflectors used with the Cassigrain feeds. The final design was a compromise in order to best optimize the beamwidth, sidelobe level, and gain without sacrificing any one parameter.

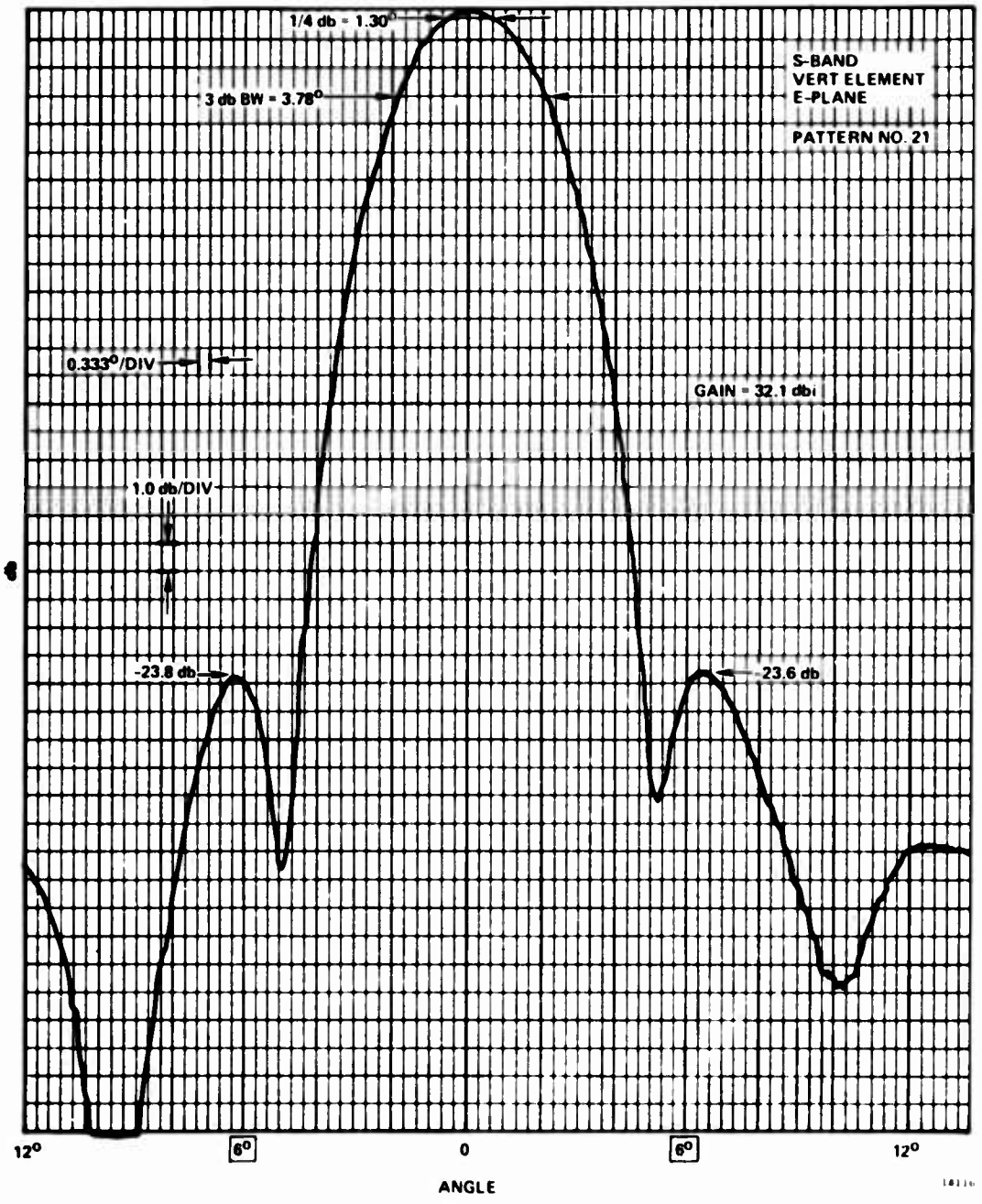

Figure 20. E-Plane Pattern - Vertical Element

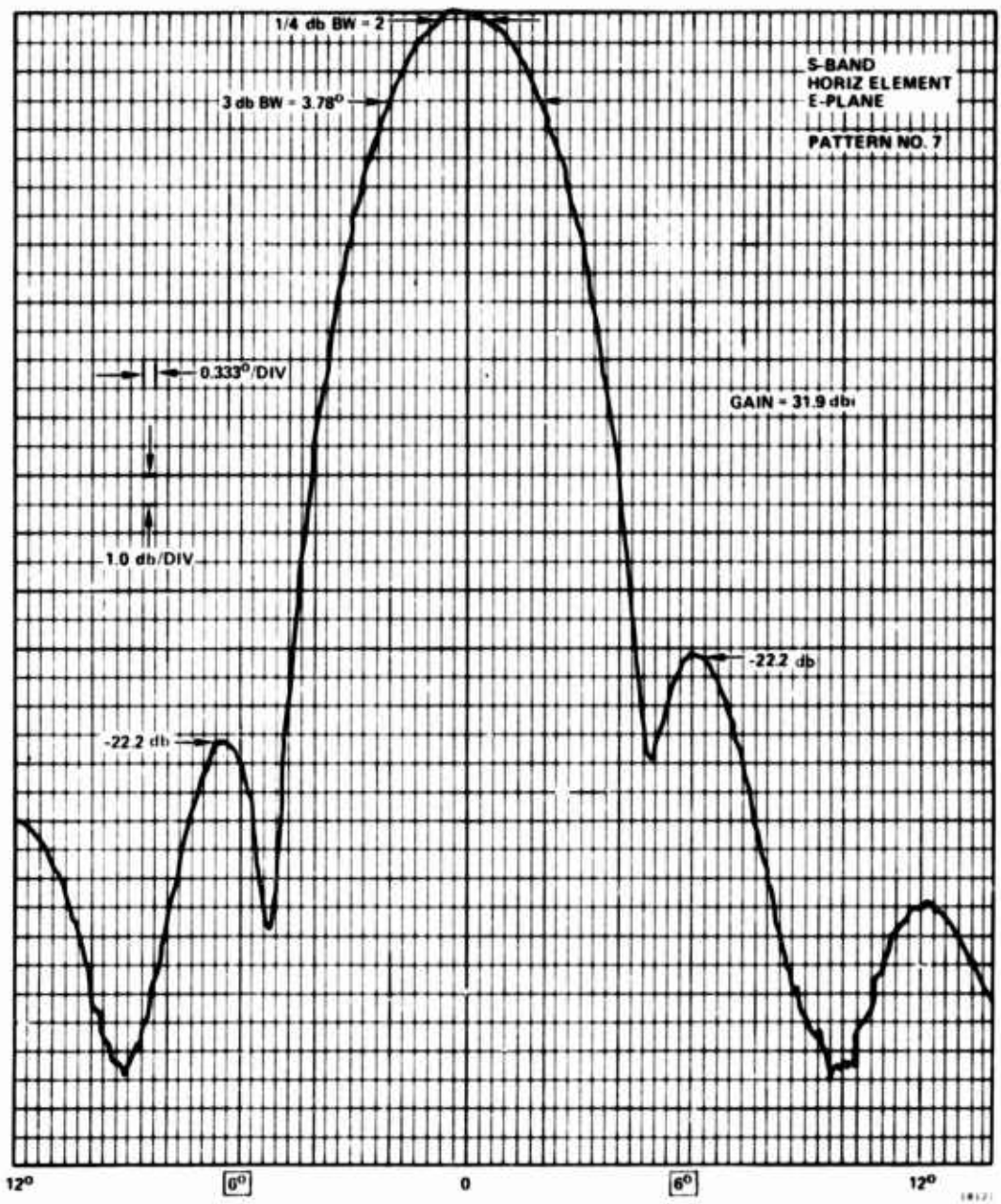

Figure 21. E-Plane Pattern - Horizontal Element

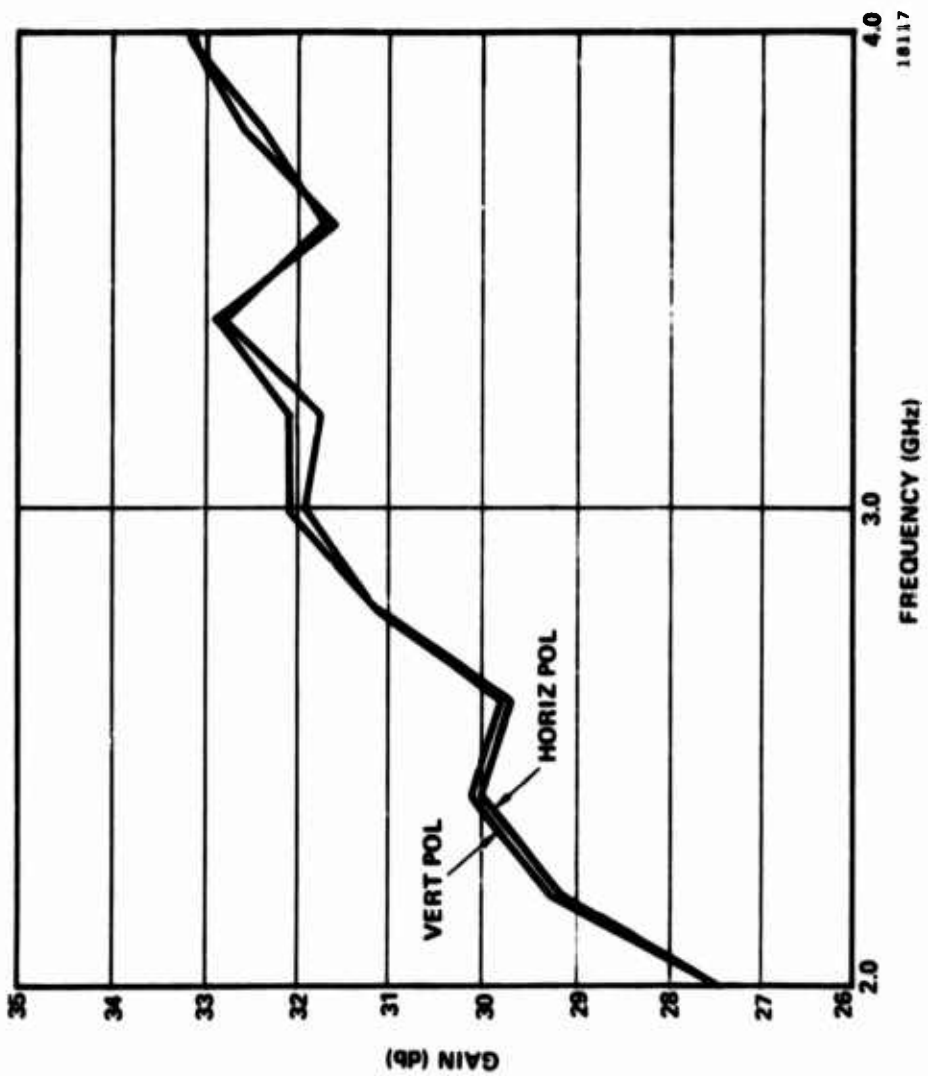

Figure 22. S-Band Antenna Gain

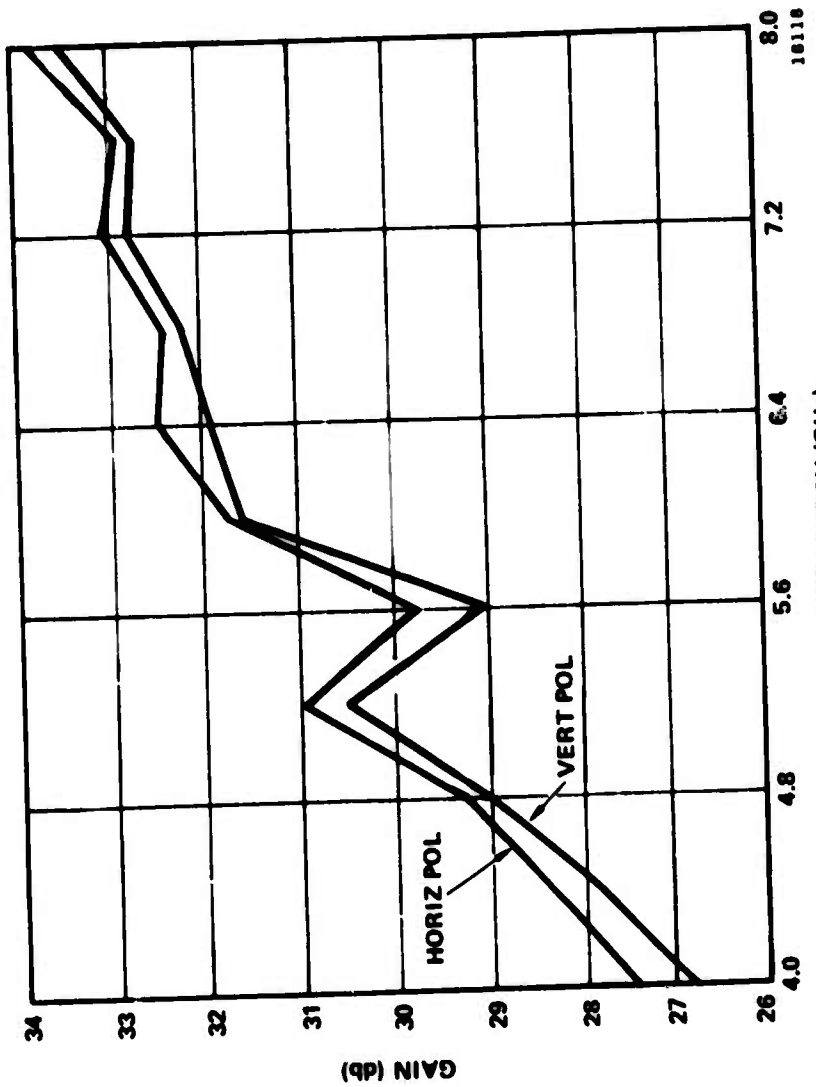

Figure 23. C-Band Antenna Gain

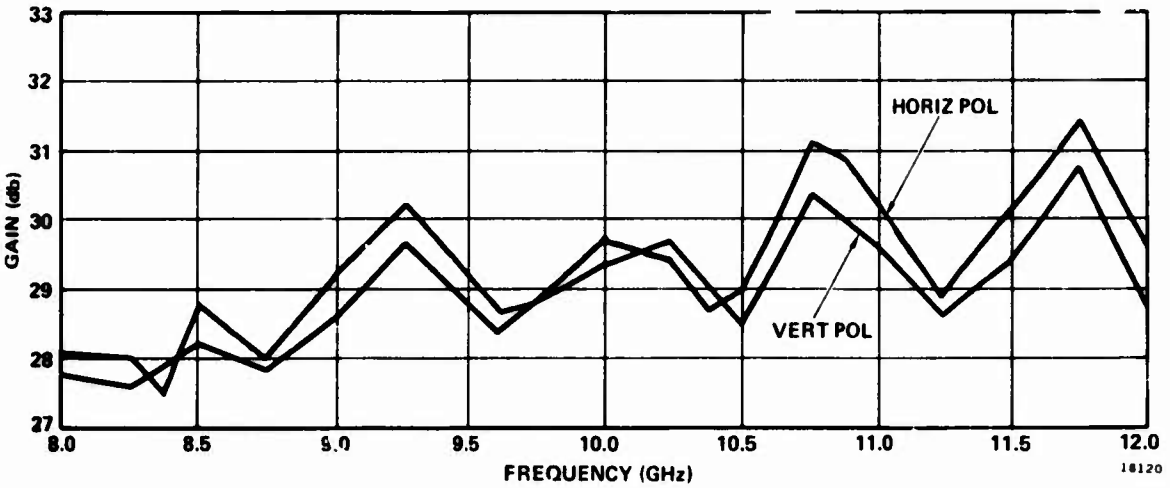

Figure 24. X-Band Antenna Gain

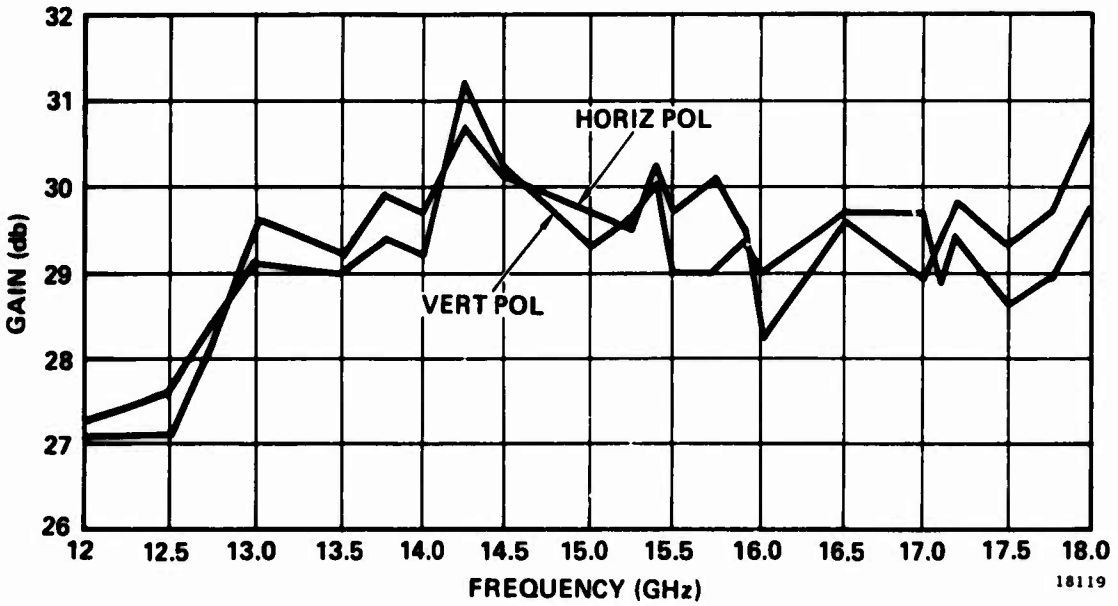

Figure 25. K_u-Band Antenna Gain

The performance of the antennas in the circular polarized mode was very good. The axial ratio for both the S- and C-band units were considerably under the 2.0 db requirement, being 1.5 db and 1.8 db respectively. The X-band antenna was 2.0 db or less across the band. The axial ratio of the K_u-band antenna was within the required 2 db with the exception of 18 GHz where it increased to 3 db. The percentage change in the ratio of E_{max}/E_{min} for a corresponding change in axial ratio from 2 db to 3 db is small and will not affect the overall performance of PAMS when operating in the circular mode.

4.3.3 Antenna Pedestal

The antenna pedestal is a standard Scientific-Atlanta Inc. unit. A five foot base extension is provided to give adequate clearance for 180 degree travel in the elevation axis. A 216 slip-ring assembly is incorporated into the azimuth section of the pedestal. The assembly contains five 93 ohm coax rings and 50-ohm coax rings with the remaining rings being used for power and control. The pedestal and slip-ring assembly meet all of the specification requirements.

4.4 RECEIVER GROUP

The receiver group is made up of four receivers and an up-converter which are housed in a metal cabinet which is mounted on the elevation axis of the antenna pedestal. The receiver housing utilizes RFI gasketing and filtered connectors in order to minimize the problem of interference with the system.

4.4.1 Thermal Analysis - Receiver Housing

The following is a thermal analysis made on the PAMS receiver housing based on data taken during a two-hour temperature run. The housing and receiver drawers were instrumented with thermocouples to monitor the temperature throughout. The housing was fabricated using 0.090-inch aluminum sheet and aluminum channel, and was insulated with a one-inch polystyrene foam sheet. A dual squirrel cage blower assembly was used to circulate either internal or external air by a temperature-controlled intake/exhaust system which was adjusted to maintain an operating temperature range of +25°C to +55°C. The heat dissipation per drawer was calculated to be 350 watts. (This was based on 50 percent efficiency.) The total heat load for the four receiver drawers was, therefore, 1400 watts. The blower motor is rated at 800 watts for a total heat dissipation of 2200 watts or 7500 BTU/hour. From figure 26 it can be seen that there was a 13°F rise in temperature from the outside to inside ambient air. As the housing cover and receiver area are insulated a conservative assumption was that the total heat load would be dissipated by forced convection when external air was circulating. At 71°F and 14.7 psi (standard laboratory conditions) air has the properties

$$C_p = 0.24 \text{ BTU/lb -°F} \quad \text{(specific heat)}$$

$$\rho = 0.0747 \text{ lb/ft.}^3 \quad \text{(density)}$$

The effective flow rate can be calculated from the energy equation:

$$q \text{ (BTU/hr)} - w\, C_p\, \Delta T \qquad (13)$$

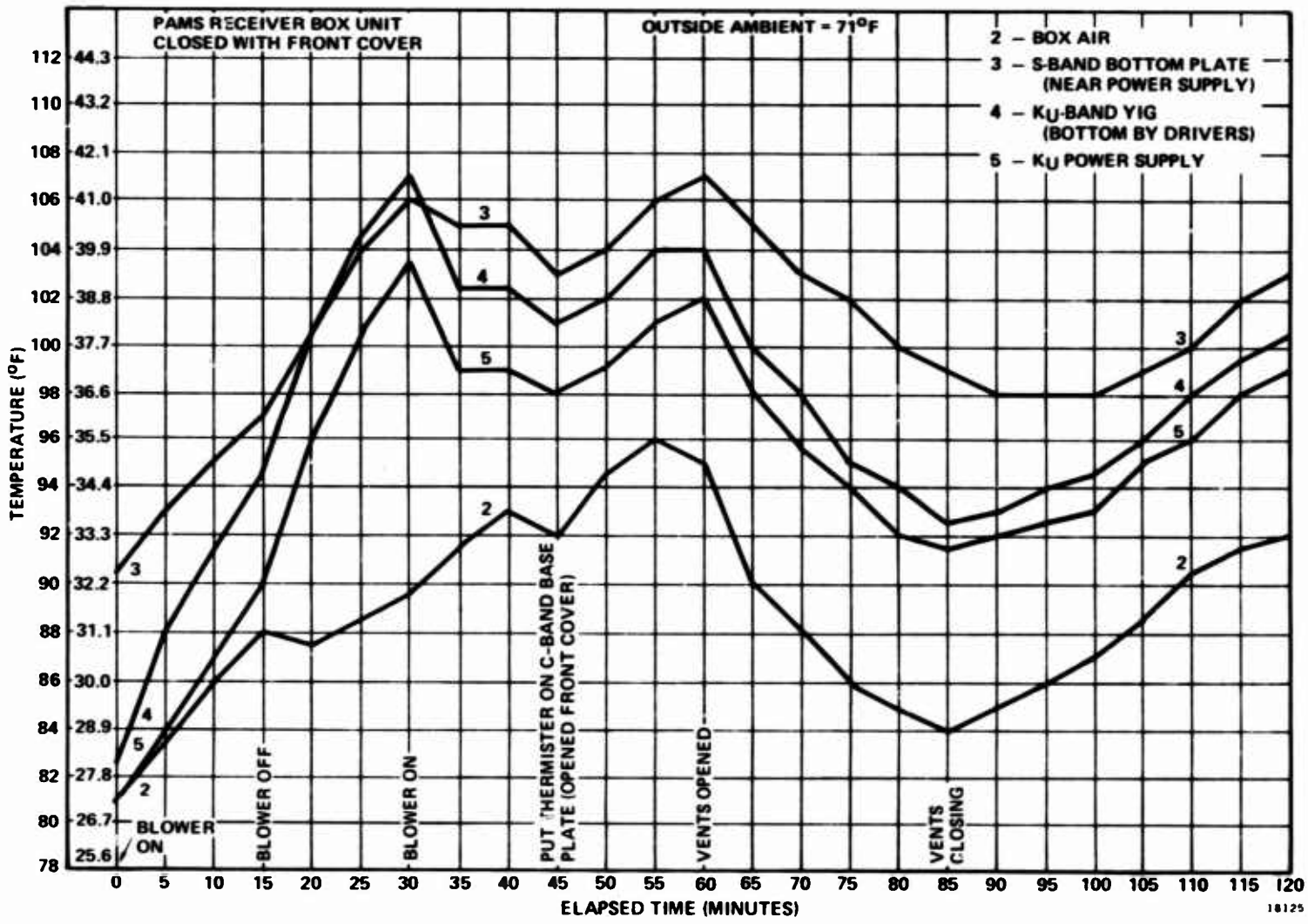

Figure 26. Receiver Housing Temperature

where w is the flow rate in lb/hr.

$$\therefore w = q/C_p \Delta T = 7500/0.24\ (13)$$

$$w = 2400 \text{ lb/hr.}$$

The volumetric flow rate is then

$$V\,(\text{cfm}) = \frac{w}{60\rho}$$

$$= \frac{2400}{60\,(0.747)} = 550 \text{ cfm}$$

This compares well with the rated output of the blower which is 1000 cfm at zero static pressure.

In order to evaluate the high temperature the data was extrapolated for an outside ambient of +105°F. Under that assumption the properties of air are:

$$C_p = 0.24 \text{ BTU/lb-°F}$$

$$\rho = 0.0702 \text{ lb/ft}^3 \qquad (14)$$

and

$$w = 60\rho V = 60\,(0.0702)\,(550) = 2320 \text{ lb/hr}$$

then

$$\Delta T = q/_{wcp} = 7500/(2320)\,(0.24) = 13.5°\text{F}$$

Therefore the internal ambient air would be

$$T = 105 + 13.5 = 118.5°\text{F}$$

From figure 26 the maximum temperature differential at the time the vents were closed was approximately 13°F. Thus the maximum expected temperature would be 118.5 +13 = 131.5°F (+55°C) at the bottom plate of the S-band drawer. This is within the maximum operating temperature range of all the receiver components. With the exterior surface of the aluminum receiver housing coated with a white paint having a low solar absorptivity to emissivity ratio ($\alpha_s/E \approx 0.28$) there would be no problem of the housing overheating at the assumed outside ambient of +105°F.

The last problem to be considered was the minimum temperature that the system could encounter during operation. The polystyrene foam insulation is very effective in reducing heat loss. The total exposed area of the receiver housing is approximately 65.5 square feet with about 10 square feet uninsulated. The minimum temperature was assumed to be -30°F with a steady wind velocity of 30 mph. Under these conditions an external coefficient of convective heat transfer of $h_o = 9.6$ BTU/hr -ft^2 -°F

was estimated. The internal air was assumed to be held at a minimum of 70°F with an average 2 feet per second estimated velocity. The internal coefficient of heat transfer is then $h_i \approx 0.69$ BTU/hr -ft^2 -°F. Using the above values the heat losses were calculated to be 643 BTU/hr from the uninsulated surfaces and 970 BTU/hr from the insulated area for a total dissipation of 1613 BTU/hr. The additional loss by radiation is less than six percent of the convective loss, and the conduction loss at the mounting surface to the antenna pedestal is also relatively small. Consequently, the total heat loss to the cold ambient air is less than the 7500 BTU/hr that is generated by the system. Therefore, it appeared that provisions for providing additional heat to operate would not be required.

The above example assumed a minimum internal operating ambient air temperature of 70°F. However, in normal operation it would be required to bring the internal temperature up to approximately 60°F from -20°F. The time for this can be estimated from the following:

$$q = W C_p \Delta T / \Delta\theta \tag{15}$$

where

W = weight of structure in pounds ≈ 500

C_p = specific heat of aluminum ≈ 0.24 BTU/lb-°F

ΔT = differential temperature ≈ 80°F

$\Delta\theta$ = time in hours

then

$$\Delta\theta = W C_p \Delta T / q = \frac{(500)(0.24)(80)}{7500}$$

$$\Delta\theta \approx 80 \text{ minutes}$$

Consequently, it appeared that it would be beneficial to strategically locate some heaters inside the receiver housing to reduce the warm-up time. This would also help to minimize any condensation that could occur.

4.4.2 Receiver Housing Configuration

In order to decrease the warm-up time indicated by the above analysis strip heaters with a total capacity of 500 watts were installed in the receiver housing. The heaters are mounted directly under the receiver drawers for maximum effect. The additional heat serves to reduce the warm-up time to less than an hour. The heaters are thermostatically controlled to come on at temperatures less than 10°C and remain on until the internal temperature reaches approximately 50°C. An under-temperature condition is indicated on the console via a panel lamp. In addition, the heaters may be left on overnight by leaving the pedestal power on. This reduces the temperature gradient that has to be overcome. The receivers have provisions for an over-temperature condition also. When the receiver base plate exceeds approximately 70°C a thermostat is energized and automatically removes power from the receiver which has exceeded

the limit. The receiver automatically comes back on line when the temperature is reduced to approximately 65°C. The over-temperature condition indicator is also located on the console.

4.4.3 Receiver

A basic receiver drawer is shown in figure 27. The receiver is a two-channel YIG preselected superheterodyne with a common YIG tuned local oscillator operating 100 MHz above the input. The receiver is illustrated schematically in figure 28. All components of the receiver are interchangeable except for the RF components. The RF components consist of the ferrite isolators, PIN limiters, YIG assembly, mixer preamplifier, local oscillator coupling circuits, and the up-converter. J10 is the signal connector that brings the control signals into the drawer. Connector J11 is the input for the three-phase 60 hertz power. Connectors J1 through J8 are the coaxial inputs and outputs located on the front of the drawer.

The RF input signal is via J1 and J2 and then is routed through a switch matrix, ferrite isolator and PIN limiter to the YIG assembly. Each RF input is filtered with a 3- or 4-ball (dependent upon frequency band) voltage tuned YIG filter. The filter is designed to have a pass band flat to 1.0 db over 10 MHz with an insertion loss of 3 to 4 db. See table V for measured insertion loss and noise figure of the RF components. The selectivity of the filter is sufficient to eliminate the image signal which is 200 MHz from the desired signal. The filter has a minimum attenuation for the image of 60 db which is the dynamic range of the receiver. The S band YIG assembly was furnished by Ryka Scientific Inc., the C-band unit by Physical Electronics Labs, and the X and K_u-band assemblies were from YIG-TEK.

The mixer assemblies are fairly standard balanced mixers with a 25 to 30 db IF preamplifier included in one package. YIG filters are used to suppress the image frequency. Therefore, no particular design criteria is placed on the mixer for image suppression such as a double balanced mixer would provide. The most important specification of the mixers is the noise figure.

Optimum mixer performance requires a local oscillator of +5 dbm or greater. The solid state local oscillator must drive three mixers as shown in figure 28. Under this configuration, the minimum power supplied to the receiver mixers will be +1 to +5 dbm as shown by table V. The mixers were biased to overcome the low local oscillator power in C band. Without bias, the noise figure drops off rapidly with a local oscillator power below 1 milliwatt. With the proper bias, the noise figure can be maintained to about 1 db greater than that with optimum LO power. The mixers selected while operating with the LO power available have noise figures of 7.5 to 8.5 db as indicated in table V.

The local oscillator for each band is a voltage-tuned YIG oscillator. In S band, the oscillator is a transistor oscillator. The transistor oscillator circuit is built into a basic YIG filter structure with the tank circuit of the oscillator coupled to the YIG ball. As the magnetic field applied to the YIG ball is changed, the resonant frequency of the oscillator tank circuitry changes. This method provides an oscillator whose frequency is directly proportional to the current applied to the magnetic coils and has the same linear transfer function as the YIG filters. A voltage-to-current driver for the oscillator and each filter is built into the YIG assembly. The power available from the S-band oscillator is +10 dbm which will provide at least 3 db at the mixer input

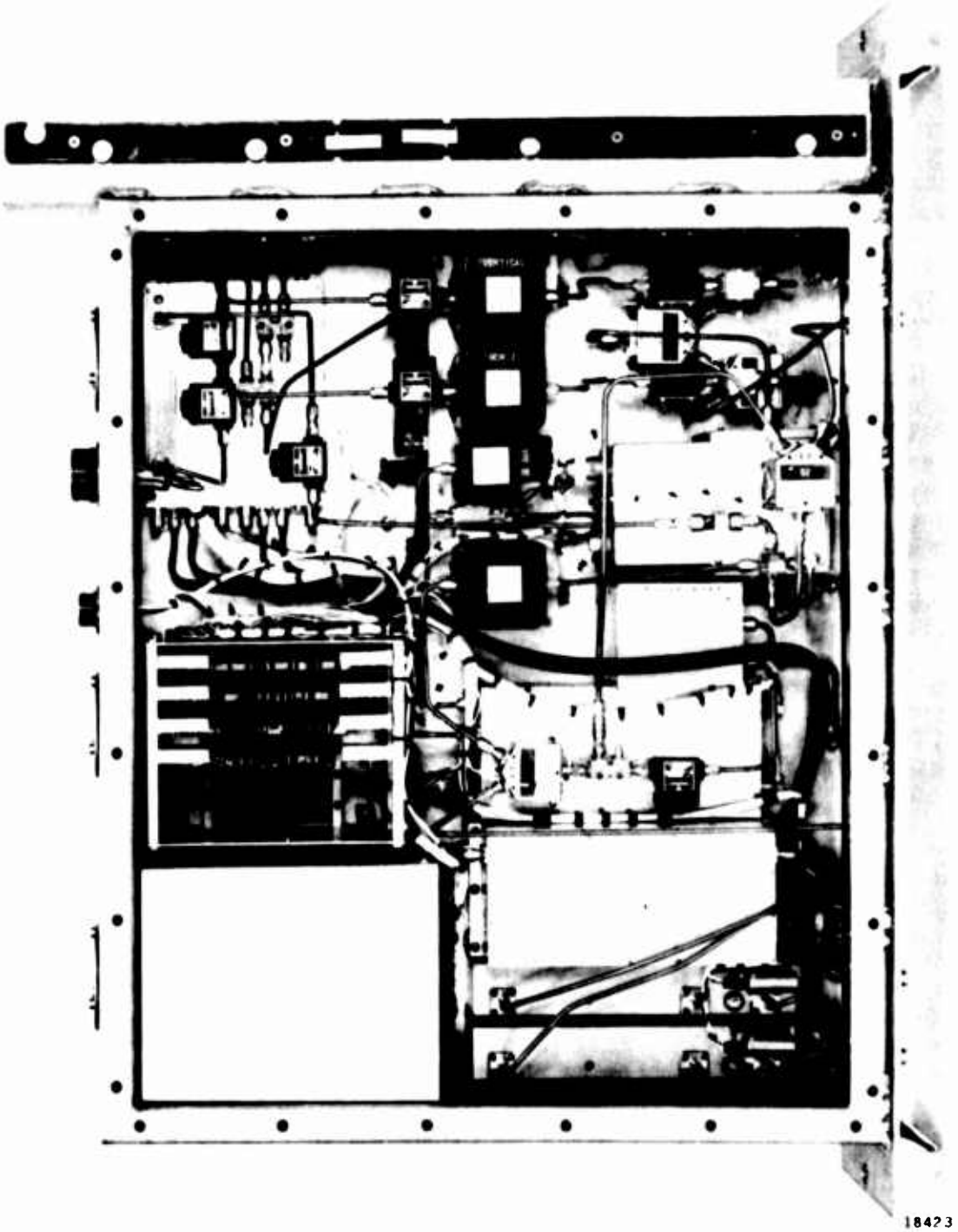

Figure 27. Receiver - C-Band

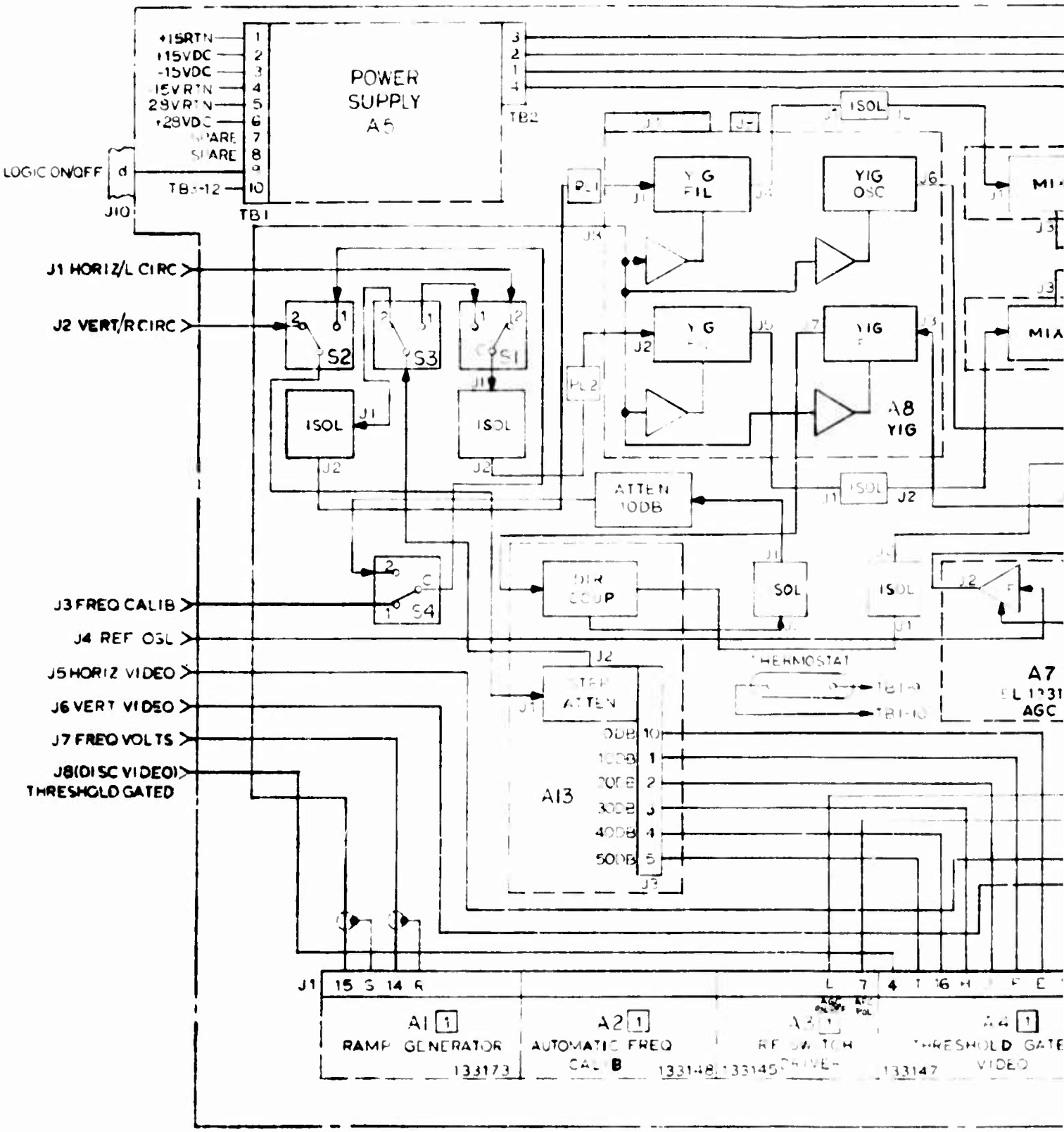
POWER SUPPLY A5
+15RTN
+15VDC
-15VDC
-15VRTN
28VRTN
+28VDC
SPARE
SPARE
LOGIC ON/OFF
TB1-12
J10
TB1
TB2
J1 HORIZ/L CIRC
J2 VERT/R CIRC
J3 FREQ CALIB
J4 REF OSC
J5 HORIZ VIDEO
J6 VERT VIDEO
J7 FREQ VOLTS
J8(DISC VIDEO) THRESHOLD GATED
S1
S2
S3
S4
ISOL
YIG FIL
YIG OSC
A8 YIG
ATTEN 10DB
DIR COUP
SOL
THERMOSTAT
A13
A7
AGC
J1 15 S 14 R
A1 RAMP GENERATOR 133173
A2 AUTOMATIC FREQ CAL B 133148
133145
133147
VIDEO

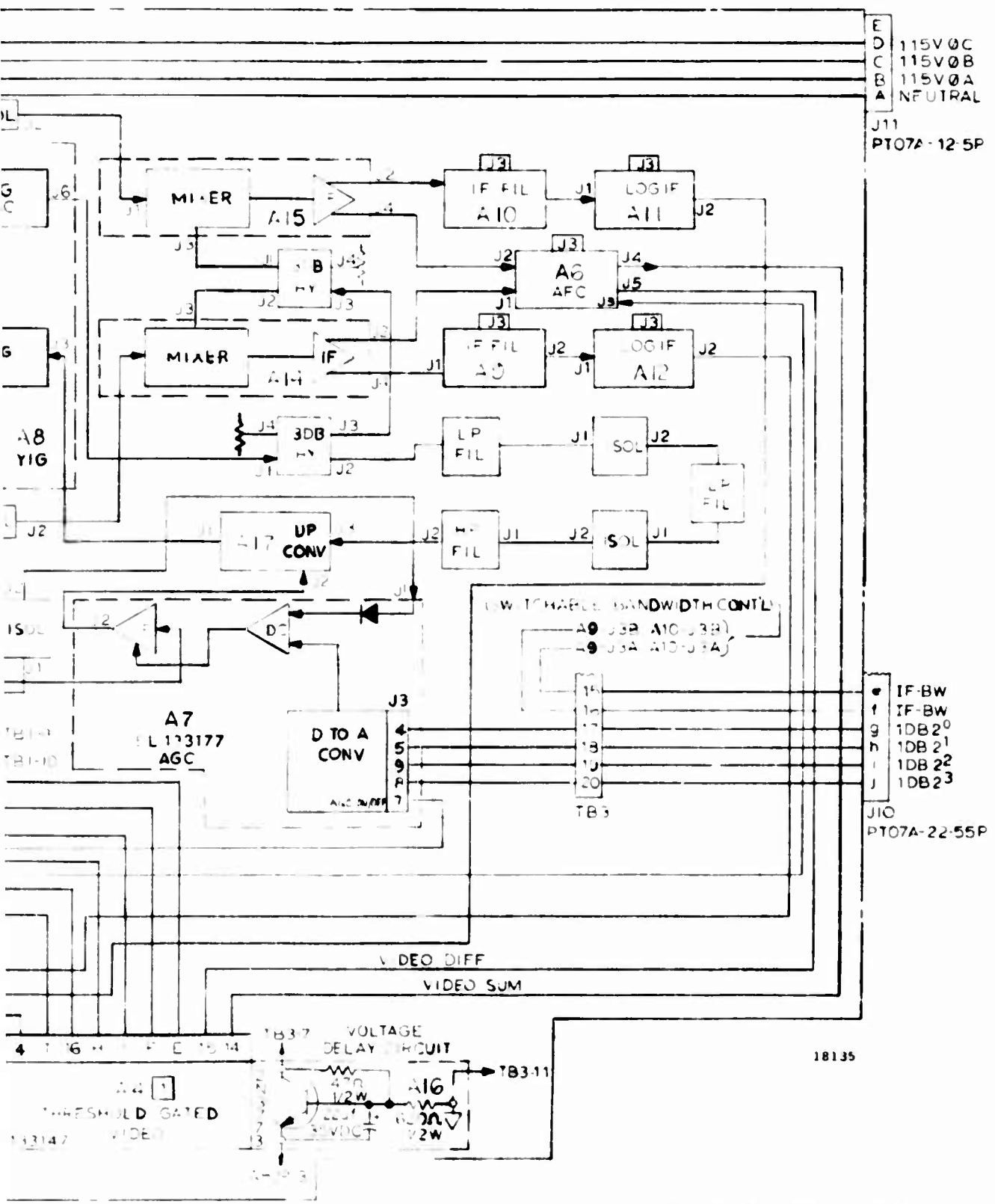

Figure 28. Receiver Schematic

TABLE V

RF FRONT END ATTENUATION NOISE FIGURES

Component	Receiver			
	S Band	C Band	X Band	K_u Band
Coaxial Switch (db)	0.3	0.4	0.5	0.6
Step Attenuator (db)	0.4	0.6	0.7	0.8
Coaxial Switch (db)	0.3	0.4	0.5	0.6
Isolator (db)	0.3	0.4	0.5	0.6
Pin Limiter (db)	0.8	1.4	2.3	2.0
YIG Filter (db)	3.7	2.8	2.2	2.8
Isolator (db)	0.3	0.4	0.5	0.6
Mixer Preamp (db)	7.5	7.5	8.5	8.5
Cable Loss (db)	0.5	0.7	0.9	1.1
Total Loss (db)	14.1	14.6	16.6	17.6

after the power splits. The C-band oscillator provided the most problems from a power output standpoint. The frequency range of 4 to 8 GHz was too high for present transistors and too low for efficient operation of Gunn diodes. A transistor oscillator and doubler was used in the C-band YIG oscillator to provide a minimum power of +5.5 dbm with a resulting mixer LO power of +1 dbm. The X and K_u bands were ideally suited for Gunn diode oscillators. Power outputs in excess +10 dbm are available from both of these oscillators. The output of the YIG filter channels are coupled to the IF filter selector unit. The IF filter switch assembly has selectable bandpass filters which determine the final IF bandwidth of the PAMS receiver. The assembly was manufactured by Zeta Labs to Actron specifications.

The assembly consists of three programmable, 100 MHz IF filters and filter bypass having the following bandwidths:

1.5 MHz ±0.1 MHz
3 MHz ±0.1 MHz
6 MHz ±0.2 MHz
Bypass Position: Flat from 95 to 105 MHz

Each filter has a Gaussian type response with 9 db per octave roll off. A combination of attenuators and amplifier are used to maintain unity input to output gain for

all filter positions. The desired filter is selected by two logic signals which are generated at the control console when a particular bandwidth is selected via the bandwidth select switch located on the receiver panel.

After the desired bandwidth has been selected the signal then passes on to the logarithmic IF amplifier. The log IF amplifier is a 100 MHz amplifier whose voltage output is proportioned to the logarithmic power input. The assembly was manufactured by RHG Electronics Lab., Inc., to Actron's specifications.

The log IF amplifier uses a successive detection technique in which a detector is placed at each IF interstage to provide a video sample. These samples are then added in a summing network. Thus, a composite signal is developed which provides a linear voltage output for a logarithmic power input. The amplifier's optimum operating range is for input power levels between -80 dbm to -20 dbm. This is equivalent to the PAMS receiver input of -100 dbm to -40 dbm. Within this dynamic range, the amplifier has an accuracy of ±1/2 db from a best straight line for logarithmic power input to linear to voltage output. See figure 29 for a typical output of the amplifier. To a lesser degree of accuracy, the amplifier has an extended dynamic range between -95 dbm to -15 db.

The output of the amplifier assembly is directly coupled to ensure fidelity of both continuous wave (CW) and pulse type input signals. The 50 ohm, low output impedance will minimize excessive pick-up possible over the long cable runs to the signal conditioner and processor.

An output of the mixer/preamplifier is routed to the Automatic Frequency Control IF amplifier assembly. The 100 MHz AFC/IF amplifier assembly provides an output voltage which is proportional to a change in input frequency. This is accomplished with a four-stage 100 MHz IF amplifier followed by a 100 MHz ratio detector. Additional circuit features are included to provide electrical system interface. These include (1) a PIN diode switch which selects one of two 100 MHz inputs, (2) a sum video amplifier which provides a minimum of +2.5 volts dc output when a signal between 95 and 105 MHz is present and, (3) a difference video amplifier which provides the ±dc error voltage versus a change in input frequency. The assembly is manufactured by Zeta Labs to Actron's specification.

The amplifier is comprised of four amplifiers tuned to 100 MHz with an overall 3 db bandwidth of 15 MHz. The low-noise first amplifier stage is designed to limit when the input signal level reaches 20 millivolts rms (approximately -20 dbm). This is done to ensure optimum signal-to-noise ratio at low levels. The second, third, and fourth amplifier stages operate as limiting amplifiers with their gains adjusted to ensure that hard limiting occurs (constant amplitude signal at the IF amplifier output) for input signals of -50 dbm and greater. The output drives the 100 MHz ratio detector. The ratio detector is used as a frequency discriminator because of its inherent amplitude limiting. The combination of the limiting amplifiers with the ratio detector ensures a minimum of discriminator output voltage changes versus input signal level changes. The ratio detector features a peak-to-peak separation of 10 MHz.

The error signal from the ratio detector is fed into the difference video amplifier. The amplifier is direct coupled and has a 3 db bandwidth of 5 MHz. Its gain is adjustable to provide an output error sensitivity slope of 0.5 volt/MHz or greater. The video amplifier output impedance is very low, allowing it [illegible] a 50 ohm load with

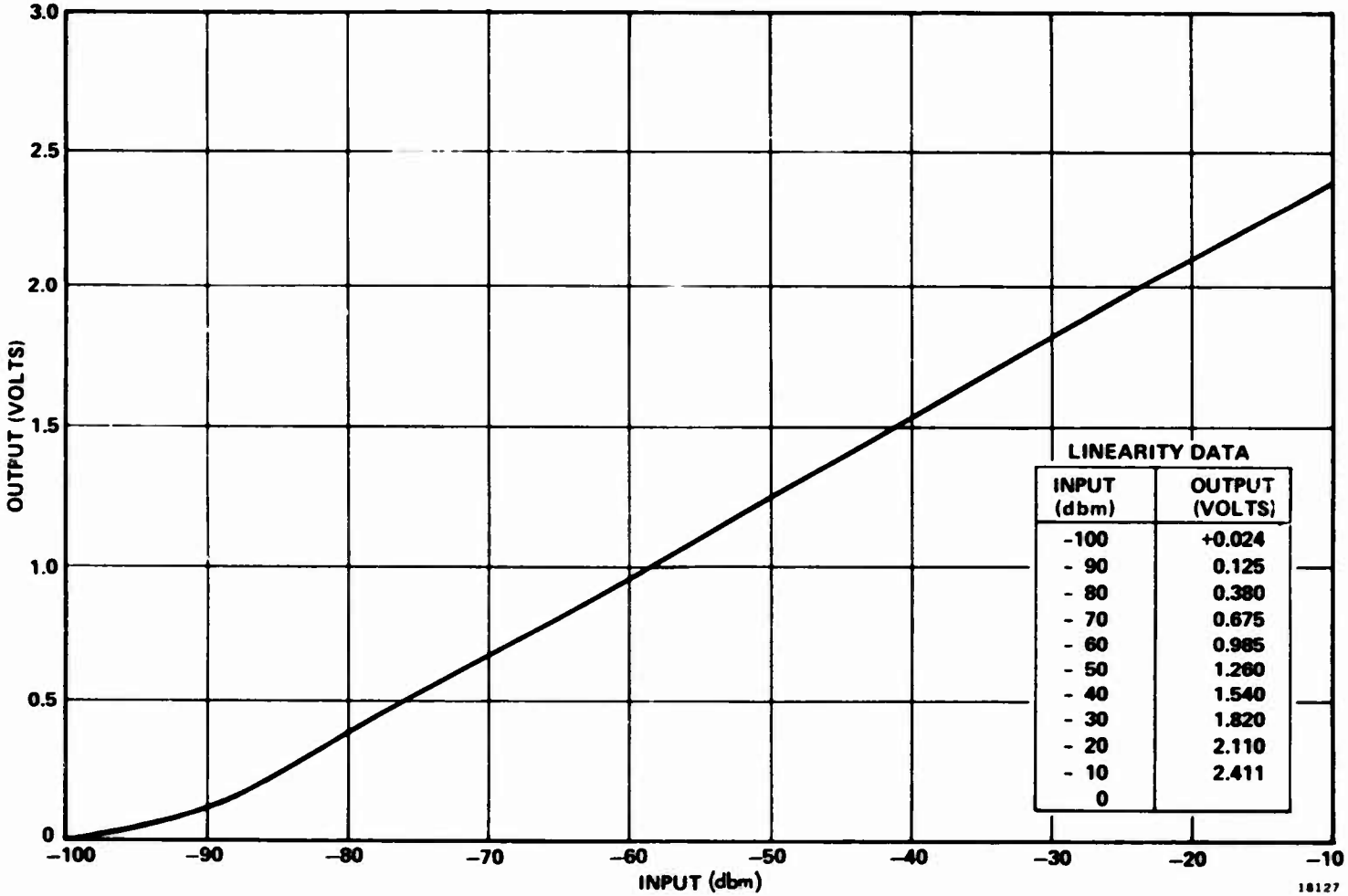

Figure 29. Log IF Response Curve

a 5 volt peak-to-peak signal without pulse waveform distortion. The output linearity is within ±5 percent (best straight line fit) over the input frequency range of 97 to 103 MHz. The response curve for frequency input versus video voltage output is shown in figure 30 below.

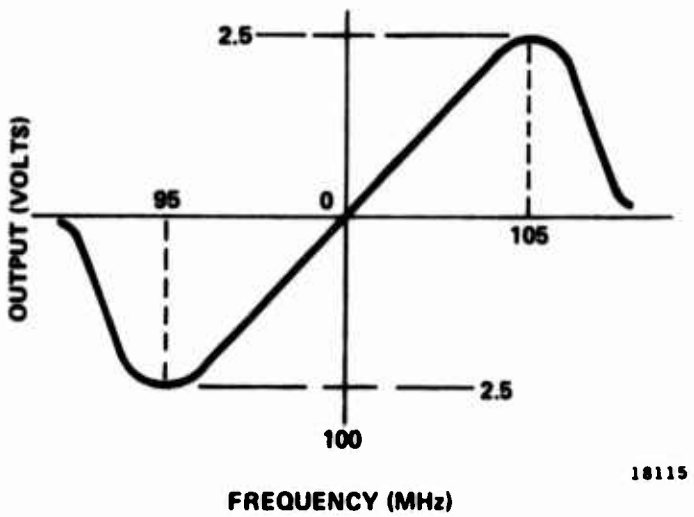

Figure 30. Receiver Error Signal

A dc offset is provided so that the difference output may be adjustable to zero (0) volts at 100 MHz. Symmetry of the response curve, as shown above, will be maintained after this adjustment. The frequency drift will not exceed 10 KHz/°C within the specified operating temperature range.

The sum video amplifier will provide a 2.5-volt dc output across 50 ohms when the input signal is between 95 and 105 MHz and its level is -50 dbm or greater. The sum signal is required to gate the difference signal so as to improve discrimination between noise signals and error signals, particularly near the crossover frequency.

The input switch selects one of two 100 MHz signals to be fed to the IF amplifier. This electronic switch using PIN diodes provides a switch cycling life much greater than electro-mechanical relays. It also provides isolation of greater than 30 db between the two 100 MHz inputs. The switch requires an actuating level of +5 volts dc.

Since the operation of a standard superheterodyne receiver is generally well known, no further details on the receiver will be given. Instead, the theory of operation will be presented and this will incorporate the hardware which makes up the control console. No attempt is made to describe the derivation of all the timing signals and various logic states. Standard circuit and logic techniques are used, the details of which are not pertinent to the report.

4.5 THEORY OF OPERATION

Figure 31 is an overall functional block diagram of the PAMS. As the MSQ-1 or FPS-16 tracking radar actively tracks a test aircraft, target azimuth, elevation, and range data are applied to the PAMS antenna servo system. The antenna servo system slaves the PAMS antenna array to the tracking radar in azimuth and elevation, and provides target azimuth, elevation, and range data to the computer in digital form. The computer samples the azimuth, elevation, and range data, as well as site time data, each time it samples frequency and amplitude data, as controlled by cursors described in subsequent paragraphs.

The four PAMS antennas receive RF emissions and reflections from the aircraft throughout the frequency range of 1 GHz to 18 GHz in four bands: 1 GHz to 4 GHz (S band), 4 GHz to 8 GHz (C band), 8 GHz to 12 GHz (X band), and 12 GHz to 18 GHz (K_u band). The RF signals from each antenna are processed separately and simultaneously in the data acquisition circuits. A polarizer for each band separates the signal into two polarized components, providing either vertical and horizontal linear polarization or right-hand and left-hand circular polarization.

A receiver for each band processes the two polarized signal components in parallel. The receiver video outputs are applied to scope control circuits which select the two polarized components of any band to be displayed on any of three dual-trace scopes. Each receiver operates sequentially in a swept-frequency mode and then in a fixed-frequency mode every 33.3 ms. Two of the scopes are panoramic scopes which display the video during the swept-frequency periods or the fixed-frequency periods.

Cursor circuits generate 12 cursors, any or all of which may be applied to any of the four bands to control the application of data to the computer during the swept-frequency periods. The cursors selected for a given band are superimposed on the panoramic scope display of that band so that the operator may position the cursors to the frequencies of interest in the band. At the same time, gates generated by the cursors are used in the data acquisition circuits to acquire frequency and video amplitude data at the frequencies of interest for application to the computer. The amplitude data include data for both polarized components. Eight of the cursors (cursors 5 through 12) are also used in pairs to acquire integrated amplitude data between two frequencies, in addition to the amplitude data at the discrete frequencies.

To acquire frequency and amplitude data at the fixed-frequency setting of any band, an assigned cursor is set to the fixed-frequency position. Cursors 1 through 4 may be assigned to the K_u, X, C, and S bands, respectively, for acquiring frequency and amplitude data during the fixed-frequency periods.

Cursor data are applied to the computer to tell the computer when to "look at" the input lines containing the acquired data (including azimuth, elevation, range and time data). The cursor data include other information, such as cursor numbers and whether the cursor is being used for the swept-frequency periods or the fixed-frequency periods. Also applied to the computer as inputs to the program from the data acquisition circuits are data concerning the settings of various manual controls. System timing is determined by timing circuits which synchronize the data acquisition circuits, cursor circuits, and scope control circuits.

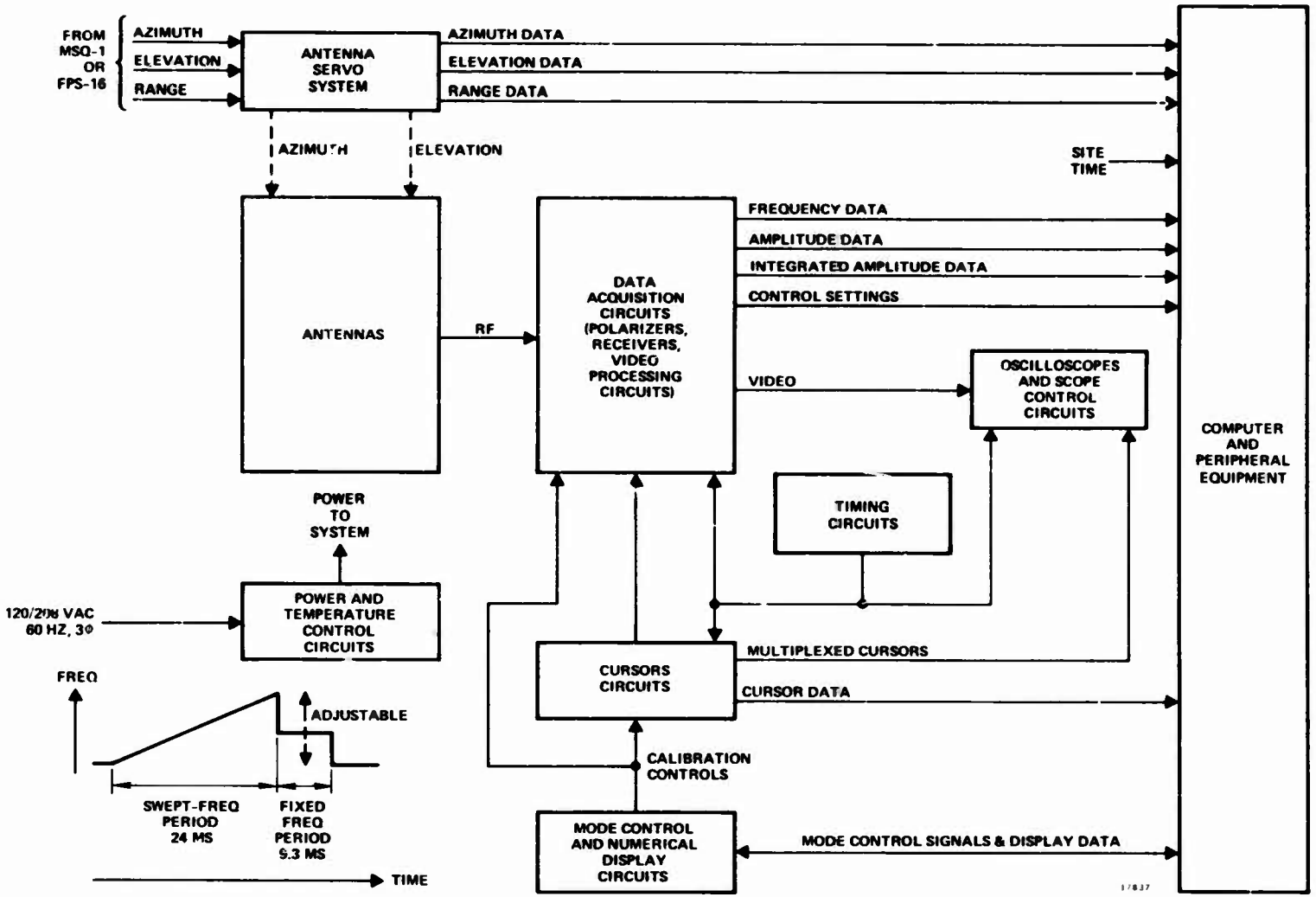

Figure 31. PAMS Functional Block Diagram

In addition to the data acquisition operations described above, the system operates in an automatic calibration mode whereby frequency and amplitude calibration data are applied to the computer in lieu of the operational data acquired from the received signals. These calibration data are stored by the computer. Then, during normal operation, the computer compares the acquired data with the calibration data to achieve high-accuracy measurement of the acquired frequency and amplitude data. Automatic calibration is initiated at the console in the mode control circuits and then controlled by the computer. Provision is also made for manual calibration. The mode control circuits also provide other mode inputs to the computer program (run, pause, stop, end flight).

Numerical display circuits provide for the selection and display of acquired frequency or amplitude data corresponding to any of the 12 cursors, as well as site time or tracker radar range data. These data are applied to the display circuits from the computer. (Azimuth and range data are displayed on units in the antenna servo system.)

Primary power for the system is 120/208 vac, 60 Hz, 3 phase. Power and temperature control circuits distribute power to the various portions of the system and also control the temperature of the receivers, which are mounted on the antenna pedestal.

As mentioned above, the S-band antenna frequency range is 1 GHz to 4 GHz. However, the S-band receiver operates only in the frequency range of 2 GHz to 4 GHz. The signals in the range of 1 GHz to 2 GHz are considered L-band signals. An L-band converter is included in the receiver circuits to up-convert the signals in the range of 1 GHz to 2 GHz from the S-band antenna. In addition, the L-band converter is designed to accept and up-convert signals in the range of 0.1 GHz to 1 GHz from a fifth (UHF) antenna (not provided with the system).* These L-band signals from either antenna, in the range of 0.1 GHz to 2 GHz, are up-converted to the range of, and processed by, either the S-band receiver or the C-band receiver, at the operator's selection. Thus, the S-band and C-band receivers may process either the 2 to 4 GHz and 4 to 8 GHz signals from the S-band and C-band antennas, respectively, or the up-converted L-band signals. As opposed to the S-band antenna and receiver, the C-band, X-band, and K_u-band antennas and receivers are matched in frequency range.

4.5.1 Antenna Servo System.

Figure 32 is a functional block diagram of the antenna servo system. The units used in the servo system are supplied by Scientific-Atlanta, Inc., and Northern Precision Laboratories, Inc. These units are: two digital synchro display units (elevation and azimuth), manual command unit, servo control unit, digital comparator unit, dc amplifier unit, servo amplifier unit 1, and antenna pedestal, all supplied by Scientific-Atlanta, Inc., and the tracker unit supplied by Northern Precision Laboratories, Inc. The antenna servo system operates in three modes, as manually selected at the servo control and manual command unit: digital slave mode, manual position mode, and manual rate mode.

4.5.1.1 Digital Slave Mode

The digital slave mode is the normal operating mode of the servo system, whereby the PAMS antenna array is slaved to azimuth and elevation inputs from the MSQ-1 or FPS-16. Although not directly concerned with the antenna servo system, application of target azimuth, elevation, and range data to the computer is also covered in this

*See footnote, page 44.

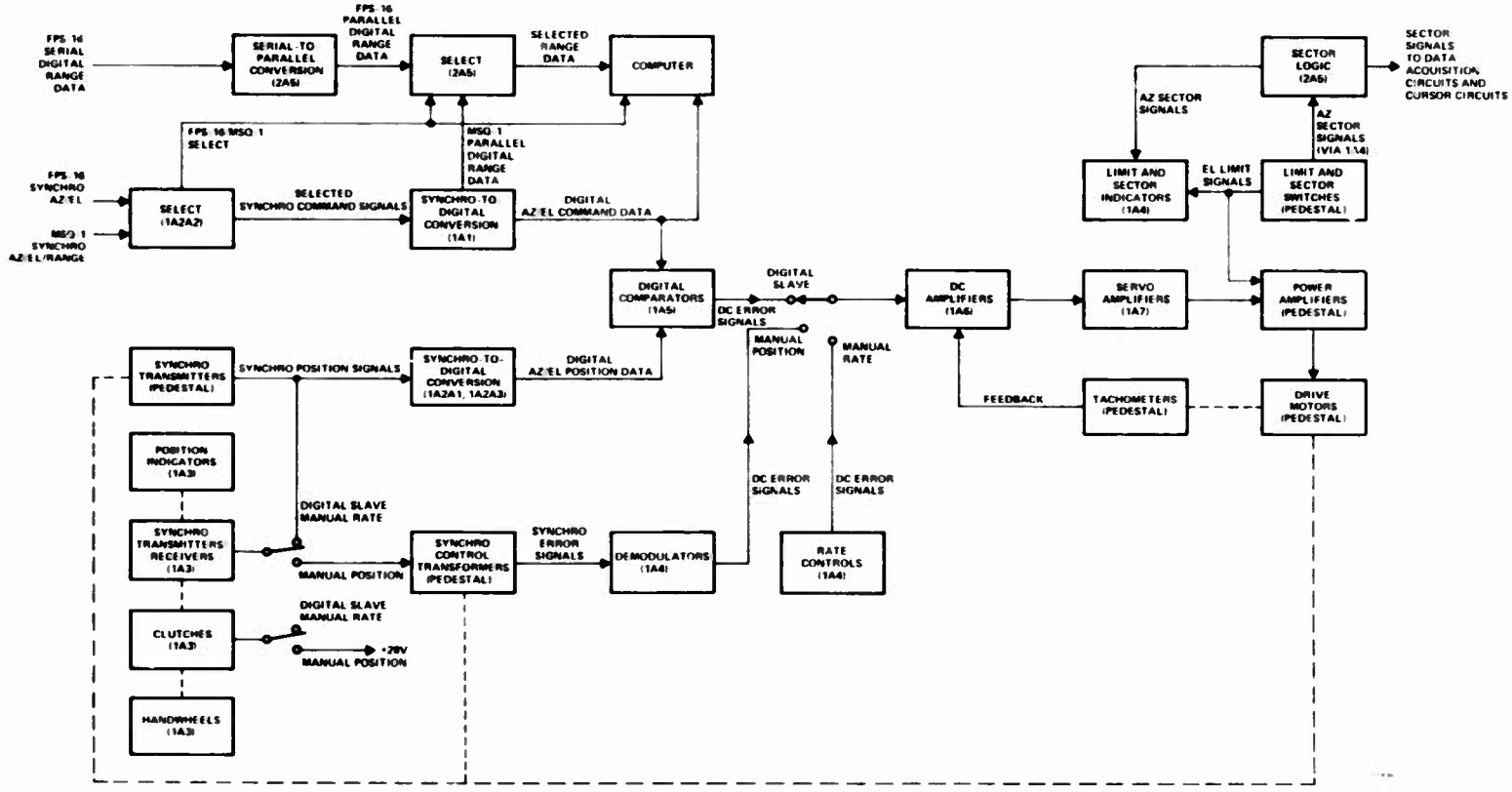

Figure 32. Antenna Servo System

discussion. MSQ-1 azimuth, elevation, and range data are all received in synchro form at the (SELECT) synchro junction box. FPS-16 azimuth and elevation data are also received in synchro form at the synchro junction box but FPS-16 range data are received in serial digital form.

Concentrating on azimuth and elevation data for now, the MSQ-1 or FPS-16 command synchro signals are selected in the synchro junction box by the FPS-16/MSQ-1 switch, which also signals the selection to the computer. The selected synchro signals are applied to synchro-to-digital conversion circuits in the tracker unit. The digital azimuth and elevation command data are then applied to the digital comparator where these data are compared with the PAMS antenna position data. The PAMS antenna azimuth and elevation position data are obtained from synchro transmitters mechanically connected to the antenna drive motors in the antenna pedestal. These synchro signals are converted to digital data in the digital comparator unit. The position synchro transmitters in the antenna pedestal also drive synchro transmitters/receivers (operating as receivers in the digital slave mode) in the manual command unit to control azimuth and elevation position indicators. The digital comparator unit detects differences between the command data and position data and generates appropriate dc error signals to control azimuth and elevation drive motors in the antenna pedestal via the dc amplifier, servo amplifier, and power amplifiers in the pedestal. The antennas are driven in azimuth and elevation in the directions which tend to cancel the dc error signals out of the digital comparator unit. Thus, the PAMS antenna position is slaved to the command inputs from the MSQ-1 or FPS-16.

Azimuth sector switches in the antenna pedestal can be actuated by cams adjusted to define an azimuth sector where the PAMS is susceptible to high-energy transmissions from adjacent radars. Either actuated sector switch decouples the receivers from the antennas to protect the receivers, and inhibits the application of cursor data to the computer so that the computer will not acquire invalid data while the receivers are decoupled.

Besides being used to control the PAMS antenna pedestal, the digital azimuth and elevation command data from the tracker unit are also applied to the computer. The computer reads the azimuth and elevation data each time it reads frequency and amplitude data, as described in later paragraphs dealing with the data acquisition circuits and cursor circuits. When MSQ-1 inputs are selected at the synchro junction box, relays apply MSQ-1 synchro range data to the synchro-to-digital conversion circuits in the tracker unit. The digital range data are applied to select circuits in the processor in parallel form. The serial digital FPS-16 range data are applied to the select circuits in the processor via serial-to-parallel conversion circuits, also in the processor. The selection function in the processor is controlled by the select switch on the synchro junction box.

When the MSQ-1 data are selected, the MSQ-1 select signal from the synchro junction box enables gates in the select circuits to which 16 bits of parallel range data and a range flag are applied from the tracker. The 16 bits of MSQ-1 range data exclude the three least significant bits (2^0, 2^1, and 2^2) and the bits more significant than 2^{18}. The reason for excluding the least significant bits of both the FPS-16 and the MSQ-1 data is that these bits represent range accuracy beyond the needs of the PAMS. The reason for excluding the most significant bits is that the long ranges represented by these bits are not considered of interest to the PAMS.

The scale factors for the FPS-16 and MSQ-1 data are 1.95 yards/bit and 0.975 yard/bit, respectively. That is, for the FPS-16 data, the 2^n bit represents a range increment of 2^n times 1.95 yards, and for the MSQ-1 data, the 2^n bit represents a range increment of 2^n times 0.975 yard. Note that, because of this difference in scale factors, the 2^n bit to the computer is derived from the 2^n bit of MSQ-1 data or from the 2^{n-1} bit of FPS-16 data so that the scale factor of the data to the computer is 0.975 yard/bit regardless of the data used. The computer reads the range data each time it reads frequency and amplitude data as described in later paragraphs dealing with the data acquisition circuits and cursor circuits.

In the manual position mode of the servo system, clutches in the manual command unit are engaged to enable handwheels to be used to position the synchro transmitters/receivers (used as transmitters in this mode). The outputs of these synchro transmitters are applied to synchro control transformers which are mechanically connected to the antenna drive motors in the antenna pedestal. Synchro error signal outputs from the control transformers are converted to dc error signals by demodulators in the servo control unit. These dc error signals are then used to control the antenna pedestal drive motors via the dc amplifier unit, servo amplifier unit, and power amplifiers in the antenna pedestal. The antennas are driven in azimuth and elevation in the directions which tend to cancel the error signals out of the synchro control transformers. The antenna azimuth and elevation positions are displayed by the position indicators on the manual command unit and are displayed on the digital synchro display units.

In the manual rate mode, the antenna azimuth and elevation positions are controlled by rate controls (variable resistors) on the servo control unit. When the azimuth and elevation rate controls are offset from their zero settings, they provide constant dc error signals to control the antenna pedestal drive motors via the dc amplifier unit, servo amplifier unit, and power amplifiers in the antenna pedestal.

4.5.2 Data Acquisition Circuits

Figure 33 is a block diagram of the data acquisition circuits. In simplest terms, the data acquisition circuits consist of receiver circuits controlled primarily by manual controls on the receiver control panel, and video processing circuits controlled by gates generated in the cursor circuits, which are detailed in a later paragraph. The circuits enclosed by a dashed line in figure 33 are typical of the four frequency bands; that is, the PAMS includes four sets of circuits similar to those shown within the dashed line, one set for each band. Circuits shown outside the dashed line are common to all four bands.

It will be convenient at times to relate the discussion to one specific band to avoid calling out four sets of reference designations. When this procedure is used, the K_u band will be the representative band.

This discussion deals primarily with the normal operating mode of the data acquisition circuits, as opposed to the calibrate mode. Circuits affected by the calibrate mode are noted, but details of the calibrate mode for both the data acquisition circuits and the cursor circuits are detailed in a later paragraph.

4.5.2.1 Antenna and Polarization Network

Each of the four antennas receives either linearly (vertical and horizontal) or circularly (right-hand and left-hand) polarized signals. The antennas are linearly polarized. When a circularly polarized signal is received by an antenna, a hybrid circuit in a polarization network on that antenna is switched into the signal path to convert the antenna to circular polarization. In figure 33 the abbreviation V/RH is used for the vertical/right-hand polarized signal component and the abbreviation H/LH is used for the horizontal/left-hand signal component.

The polarization networks are controlled by the ANT POL switches on the receiver control panel, which also signal the selection to the computer. If the antenna is in either azimuth sector stop or if the system is in the automatic calibration mode, the polarization selection is inhibited, and the receivers are decoupled from the antennas.

Each polarization network also includes a transfer switch which can be used to reverse the paths of the two polarized components of the signal. In case of failure of one of the two channels of a receiver, this feature allows the operator to switch the more significant signal component into the operative channel. The transfer switch is controlled by the REVERSE/NORMAL switch on the receiver control panel via an RF switch driver card in the receiver. This switch also signals the selection to the computer and lights an indicator when the reverse condition is selected.

4.5.2.2 Operate/Calibrate Switching and Attenuator

The outputs of the polarization network on the antenna are applied via an operate/calibrate switching circuit to tuners in the receiver drawer. (As indicated in figure 33, the S-band and C-band signals are routed through L-band switching and conversion circuits.) Referring back to figure 28, the H/LH RF is applied to one channel of YIG (yttrium iron garnet) tuner assembly A8 via switch S1 and an isolator. The V/RH RF is applied to the second channel of the tuner via switch S2 step attenuator assembly, A13, switch S3, power limiters, and an isolator. Power limiters PL1 and PL2 are used to limit the RF power above a preset threshold. The isolators are three-port circulators used to reduce amplitude variation as a function of frequency, to suppress cross-talk between channels, and to minimize emission of RF energy from the PAMS antennas. Switches S1, S2, and S3 are controlled by calibrate control signals via RF switch driver card A3 in the receiver to select either the RF from the antenna for normal operating mode or calibrate signals during calibrate mode. These switches are shown in the normal operating positions. The use of these switches for calibration will be discussed in a later paragraph dealing with system calibration.

The step attenuator assembly in the V/RH RF channel is used both during normal operation and during calibration. This attenuator is controlled by an ATTENUATORS IN/OUT switch on the mode control panel and by the tens-digit switch of the AMPLITUDE SIGNAL ATTENUATOR switch on the manual system calibration panel, as well as by automatic calibration control signals via calibration logic circuits in the processor. The selected binary-coded decimal attenuation setting is applied to a step attenuator control circuit in threshold-gated video amplifier card A4 in the receiver. Also applied to this card in the receiver is the attenuator in/out signal from the mode control panel, which also signals the selection to the computer.

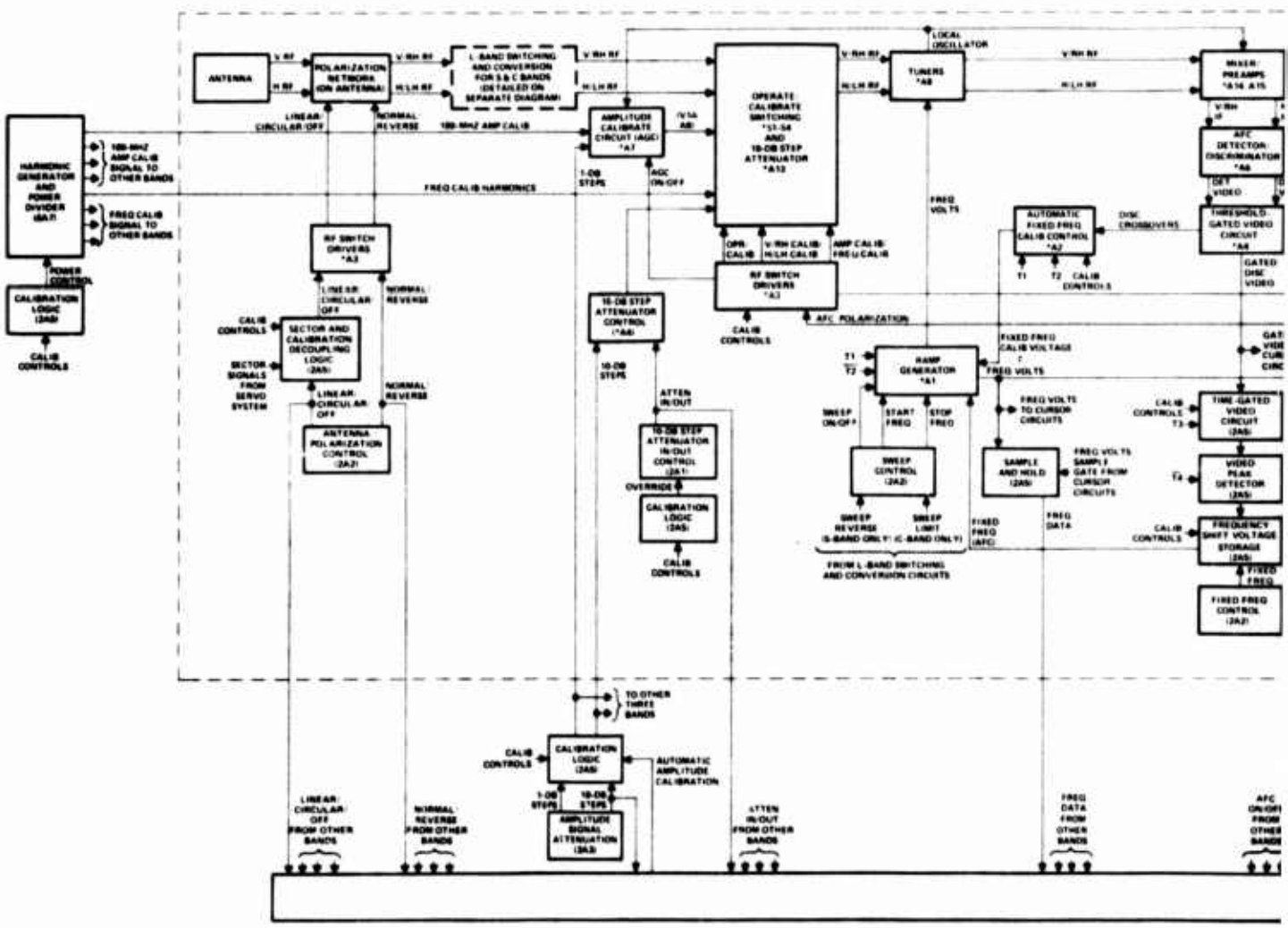
ANTENNA
POLARIZATION NETWORK (ON ANTENNA)
L BAND SWITCHING AND CONVERSION FOR S & C BANDS (DETAILED ON SEPARATE DIAGRAM)
LOCAL OSCILLATOR
TUNERS *A8
MIXER PREAMPS *A14, A15
HARMONIC GENERATOR AND POWER DIVIDER (6A7)
100-MHZ AMP CALIB SIGNAL TO OTHER BANDS
FREQ CALIB SIGNAL TO OTHER BANDS
POWER CONTROL
CALIBRATION LOGIC (2A5)
CALIB CONTROLS
LINEAR CIRCULAR OFF
NORMAL REVERSE
100-MHZ AMP CALIB
AMPLITUDE CALIBRATE CIRCUIT (AGC) *A7
AGC ON-OFF
1-DB STEPS
FREQ CALIB HARMONICS
OPERATE CALIBRATE SWITCHING *S1-S4 AND 10-DB STEP ATTENUATOR *A12
OPR CALIB
V-RH CALIB H/LH CALIB
AMP CALIB FREQ CALIB
RF SWITCH DRIVERS *A3
AFC POLARIZATION
FREQ VOLTS
AUTOMATIC FIXED FREQ CALIB CONTROL *A2
DISC CROSSOVERS
AFC DETECTOR DISCRIMINATOR *A6
DET VIDEO
THRESHOLD-GATED VIDEO CIRCUIT *A4
GATED DISC VIDEO
T1 T2 CALIB CONTROLS
RF SWITCH DRIVERS *A3
SECTOR AND CALIBRATION DECOUPLING LOGIC (2A5)
CALIB CONTROLS
SECTOR SIGNALS FROM SERVO SYSTEM
ANTENNA POLARIZATION CONTROL (2A2)
10-DB STEP ATTENUATOR CONTROL (*A6)
10-DB STEPS
ATTEN IN/OUT
10-DB STEP ATTENUATOR IN/OUT CONTROL (2A1)
OVERRIDE
CALIBRATION LOGIC (2A5)
CALIB CONTROLS
RAMP GENERATOR *A1
FIXED FREQ CALIB VOLTAGE
FREQ VOLTS
SWEEP ON-OFF
START FREQ
STOP FREQ
SWEEP CONTROL (2A2)
SWEEP REVERSE (S-BAND ONLY)
SWEEP LIMIT (C-BAND ONLY)
FROM L-BAND SWITCHING AND CONVERSION CIRCUITS
FREQ VOLTS TO CURSOR CIRCUITS
SAMPLE AND HOLD (2A5)
FREQ VOLTS SAMPLE GATE FROM CURSOR CIRCUITS
FIXED FREQ (AFC)
FREQ DATA
TIME-GATED VIDEO CIRCUIT (2A5)
VIDEO PEAK DETECTOR (2A5)
FREQUENCY SHIFT VOLTAGE STORAGE (2A5)
FIXED FREQ CONTROL (2A2)
TO OTHER THREE BANDS
CALIBRATION LOGIC (2A5)
AUTOMATIC AMPLITUDE CALIBRATION
1-DB STEPS
10-DB STEPS
AMPLITUDE SIGNAL ATTENUATION (2A3)
LINEAR CIRCULAR OFF FROM OTHER BANDS
NORMAL REVERSE FROM OTHER BANDS
ATTEN IN/OUT FROM OTHER BANDS
FREQ DATA FROM OTHER BANDS
AFC ON-OFF FROM OTHER BANDS

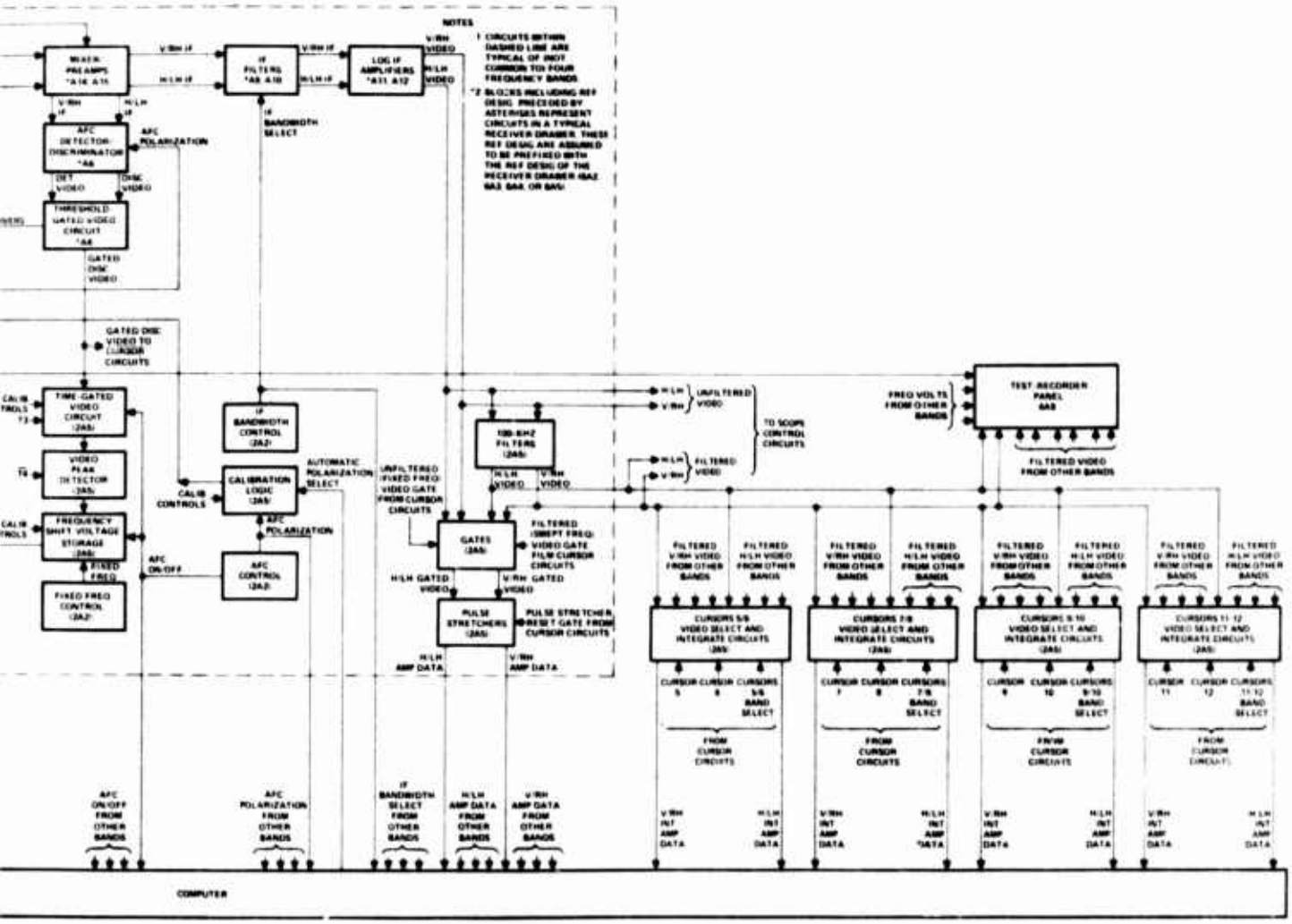

18141

Figure 33. Data Acquisition Circuits, Block Diagram

The ATTENUATORS IN/OUT switches on 2A1 can be overridden by a relay which is controlled by a calibration logic circuit consisting of a NAND gate and a relay driver on a processor card. When the system is in the amplitude calibration mode (automatic or manual), the relay is energized to override the manual setting of the IN/OUT switches. When the switches are overridden, the in/out signals to the receivers are in the "in" state so that the attenuators may be controlled by amplitude calibration signals but the in/out signals to the computer are in the "out" state so that the computer will not read the setting of the manual AMPLITUDE SIGNAL CALIBRATION switch on the manual system calibration panel. That is, the computer reads the manual attenuation setting only if the system is not in the amplitude calibrate mode and then only for those bands which have the attenuator "in".

4.5.2.3 Tuners, Ramp Generator, Frequency Data Acquisition

Referring again to figure 28, the YIG tuner assembly A8 consist of a voltage-tuned filter for each channel and a common local oscillator tuned 100 MHz above the filters. The YIG filters, with a pass band of 10 MHz, provide RF preselection to minimize susceptibility to spurious signals and to eliminate the image signal 200 MHz from the desired signal. A third filter included in YIG tuner assembly is used for calibration. Ramp generator card A1 in the receiver provides the tuning voltage to the YIG filters and local oscillator. The tuning voltage is applied to a current driver for each of the filters and the local oscillator. The current drivers tune the YIG filters and local oscillator to a frequency proportional to the tuning voltage, where the local oscillator is 100 MHz above the center frequency of the filters to provide an IF frequency of 100 MHz when the signals are mixed.

The tuners can operate sequentially in a swept frequency mode (defined by a timing signal T1) and then in a fixed frequency mode (defined by a timing signal T2), or can operate continuously in the fixed frequency mode. The ramp generator in the receiver, which provides the tuning voltage to the tuners, is controlled by SWEEP and FIXED FREQ controls on the receiver control panel. The SWEEP ON/OFF switch determines whether the tuners operate in the swept/fixed sequency (switch ON) or in the continuously fixed frequency mode (switch OFF). SWEEP WIDTH dual variable resistors are used to determine whether the tuners sweep the entire band or only some portion of the band, i.e., determine the start and stop frequency tuning voltages. (The SWEEP WIDTH controls for S band and C band are modified when the receivers are used to process up-converted L-band signals; this difference is detailed in the description of the L-band switching and conversion circuits at the end of this discussion of the data acquisition circuits.) The FIXED FREQ variable resistor determines the fixed frequency setting of the tuners. The fixed frequency setting is applied to the ramp generator via a frequency shift voltage storage circuit in the processor, which is part of the AFC loop.

The ramp generator card A1 in the receiver generates the sweep start frequency tuning voltage F1, sweep stop frequency tuning voltage F2, and fixed frequency tuning voltage F3. For operation in the swept/fixed sequence, a voltage ramp is generated followed by a fixed voltage during T2 time. The difference between F2 and F1 voltages is applied to an integrator to determine the slope of the ramp. The F1 voltage is added to the integrator output at a summer stage. Thus, during T1 time, the input to the summer is a ramp starting at the F1 voltage and sweeping to the F2 voltage. During T2 time, the F1 voltage and the integrator output are effectively disconnected from the summer. At the same time, the F3 voltage is applied to the summer. At the end of T2 time

(8.5 ms), the F3 voltage is disconnected from the summer. The F1 voltage is applied to the summer 0.8 ms before the integrator is enabled to allow the tuners to settle to the initial ramp voltage before the integrator starts. For operation in the continuous fixed frequency mode, the scan input (controlled by SWEEP ON/OFF switch on receiver control panel). Only the F3 voltage is applied to the summer.

A fourth input to the summer is an automatic fixed frequency calibration voltage. The tuning voltage (freq. volts) from the summer is applied to the YIG tuner assembly in the receiver and to a sample and hold circuit in processor at the console. The sample and hold circuit is on a frequency buffer and scope circuit card in the processor. The freq. volts signal is applied via a differential receiver buffer stage and emitter follower stage to a sample and hold circuit. Sample gates (S-H gates) generated in the cursor circuits at the frequencies of interest cause the sample and hold circuit to sample the freq. volts and then hold the sampled voltage level for reading by the computer. The freq. volts input to the sample and hold circuit is also used in the cursor circuits.

4.5.2.4 Mixers/Preamplifiers and AFC Loop

Referring again to figure 28, the outputs of the YIG filters are applied via isolators to mixer/preamplifier assemblies A14 and 15. The YIG local oscillator output is applied to the mixers via two 3 db hybrids. The local oscillator signal is also used in an amplitude calibrate circuit. The 100 MHz IF output of the mixers is amplified by 25 db IF preamplifiers within A14 and A15 and applied to IF filter assemblies A9 and A10 as well as to AFC detector/discriminator A6.

The AFC detector/discriminator selects either the V/RH IF or H/LH IF for automatic frequency control, as determined by the operator. This selection is controlled at the receiver control panel. The AFC POLARIZATION switch applies the AFC polarization signal to a calibration logic circuit in the processor as well as to the computer. The calibration logic circuit, consisting of NAND gates and a logic level converter in the processor inhibits the manual selection and enables computer selection of AFC polarization during automatic amplitude calibration. The AFC polarization signal from the calibration logic circuit is applied to the AFC in the receiver via RF switch driver card A3 in the receiver. In the RF switch driver card, besides being used for calibration control as described in a later paragraph, the AFC polarization signal converts the signal to voltage levels compatible with AFC detector/discriminator A6 in the receiver.

The AFC detector/discriminator A6 in the receiver amplifies and limits the selected IF signal, detects the presence of a signal level of -50 dbm or greater between 95 and 105 MHz to provide a detector video output, and provides a discriminator video output whose voltage and polarity is proportional to the frequency deviation from 100 MHz (0.5 v/MHz). The detector video output and the discriminator video output are applied to the threshold-gated video amplifier circuit. The discriminator video is delayed for 40 ns and applied to field effect transistor gate. While the discriminator video is being delayed, the detector video is compared with a threshold at the input of a voltage comparator. If the detector video exceeds the threshold, indicating that a discriminator video signal is present, the output enables the gate to pass the discriminator video. The purpose of the threshold gating is to exclude noise signals from further processing. The gated discriminator video is applied to a line driver for transmission to a time-gated video circuit in the processor. The line driver

output is also applied to a voltage comparator to detect discriminator crossover points for automatic fixed-frequency calibration purposes. During normal operation, AFC is enabled or inhibited by the AFC ON/OFF switch on the receiver control panel, which applies the AFC on/off status to the logic circuits and to the computer. The AFC reset and FC inputs to the logic circuits are calibration controls.

The time-gated video circuit consists of a differential receiver buffer, field effect transistor gate, and gate control transistor stages. The threshold-gated discriminator video from the receiver is applied to a transistor gate. If the AFC ON/OFF switch on the receiver control panel is ON, timing signal T3 enables a gate to pass the discriminator video to a peak detector circuit. The purpose of the time-gating function is to pass the discriminator video only during the fixed frequency period after the tuners have settled to the fixed frequency. This feature eliminates extraneous AFC signals during the swept-frequency periods; AFC is applicable only to the fixed frequency. The threshold-gated discriminator video is also applied to the cursor circuits for calibration purposes.

The peak detector circuit includes a positive peak detector, a negative peak detector, and a reset circuit. The time-gated discriminator video is applied to a voltage comparator in the positive peak detector circuit and to a voltage comparator in the negative peak detector circuit. Only the positive peak detector circuit is described here; the negative peak detector circuit operates identically except for the polarity difference. If the input video goes positive, the output goes positive and turns on a field effect transistor. A capacitor then charges in a positive direction. When the input video has passed its peak and is no longer more positive than the output of a comparator, the output goes negative and turns off the FET. The capacitor then holds the peak level. The peak level outputs are applied differentially across a balance variable resistor out to the frequency shift voltage storage circuit. The peak detector reset signal is timing signal T4 which resets the peak detectors just before each time-gated (by T3) input to the peak detectors. Timing signal T4 turns on a transistor which switches two field-effect transistors to their low impedance states to discharge peak voltage storage capacitors. The peak detector output is applied to an integrator stage whose integration rate is controlled by two resistors to determine the AFC loop gain. The integrator is enabled when the AFC ON/OFF switch on the receiver control panel is in the ON position. The fixed frequency setting from the receiver control panel is then applied to a differential receiver buffer. The outputs are summed at the input of a line driver to provide the fixed frequency/AFC input to the ramp generator in the receiver.

4.5.2.5 IF Filters and Log IF Amplifiers

Recall that the IF signals, besides being applied to the AFC loop as described above, are applied to IF filter assemblies in the receiver. The IF filter assemblies are selectable bandwidth filters controlled by the IF BANDWIDTH SELECT switch on the receiver control panel in the console. The selectable bandwidths are 1.5 MHz, 3 MHz, 6 MHz, and 10 MHz. The selection signals are also applied to the computer and the filtered IF signals are then applied to log IF amplifiers. The log IF amplifiers use a successive detection technique in which a detector is placed at each IF interstage to provide a video sample. These samples are then added in a summing network. Thus, a composite video signal is formed which provides a linear voltage output for a logarithmic input. See figure 29 for a typical IF logarithmic response curve. The video outputs of the log IF amplifiers are applied to filters and gates in the processor.

4.5.2.6 Video Amplitude Data Acquisition

The video filters and gates are located on horizontal and vertical buffer cards in the processor. The card is used for the V/RH channel video of all four bands and another card is used for the H/LH channel video of all four bands. This description applies to both channels. The video input (V/RH or H/LH) is applied via a differential receiver buffer stage. Prior to the buffer, the video is also applied to a video switch which is part of the scope control circuits described in a later paragraph. The buffer output is applied to a 100 KHz filter stage and to a gate circuit. The filter stage is an active 100 KHz low-pass filter, with an emitter follower in its feedback circuit, used to smooth the video. The filtered video is then applied to a second gate circuit. The video gates generated in the cursor circuits at the frequencies of interest during the swept frequency periods turn off a transistor stage to allow the filtered video to be applied to an output buffer. The video gates generated in the cursor circuits during the fixed-frequency periods turn off another transistor stage to allow the unfiltered video to be applied to the output buffer. The output of the buffer stage is applied to a pulse stretcher circuit. The filtered video is also applied to a test-recorder panel for monitoring and recording, video switches which are part of the scope control circuits, and video select and integrate circuits. Two identical pulse stretcher cards are used in the processor, one for the V/RH channel of all four bands and one for the H/LH channel of all four bands. This description applies to both channels. The pulse stretcher is effectively a peak detector and holding circuit which charges to the peak value of the gated video input and holds the peak level until reset. During the hold period, the computer reads the amplitude data. After the computer reads the data, the computer causes the pulse stretcher to be reset via the cursor circuits.

4.5.2.7 Integrated Video Amplitude Data Acquisition

The video select and integrate circuits consist of analog circuits on two identical video integrator cards in the processor. This description is keyed to an integrating cursor pair but is equally applicable to the circuits for the other three integrating cursor pairs. A 3-bit band select signal for the cursor pair is applied to three NAND gates on a processor card. The other input to each of these gates is the output of a latch consisting of two NAND gates on another processor card which is set by the first cursor and reset by the second cursor. Thus, the band select signals are gated into the video integrator card during the swept-frequency periods only between the frequencies at which the cursor pair is set. The first cursor also sets a flip-flop on the processor card to enable an integrator circuit. This flip-flop is reset by trailing edge of each timing signal T5 to discharge and inhibit the integrator circuit between swept frequency periods.

The filtered video inputs from all four bands are applied to two sets of video switches. Still keying to the cursor pair the H/LH and V/RH video inputs from the desired band are selected for application to the integrator stages. As indicated above, the video signals are applied to the integrators only between the frequency settings of the cursor pair. The computer reads the integrated amplitude data and then the transistor stages are turned on at the trailing edge of T5 to discharge and inhibit the integrators until the next swept-frequency period.

4.5.3 L-Band Switching and Conversion

As mentioned earlier, S-band and C-band RF signals out of the polarization networks are applied to the receiver circuits via L-band switching and conversion circuits. The

L-Band switching and conversion circuits either select the RF from the S-band and C-band antennas for application to the respective receivers, or up-convert and select L-band RF for application to either the S-band or C-band receiver. Figure 34 is a schematic diagram of the L-band switching and conversion circuits, and figure 35 is a photograph of the unit. The switches in the up-converter are controlled by the L-BAND CONVERTER switch on the mode control panel at the console, which also signals the L-band selection to the computer.

The V/RH and H/LH C-band RF signals from the C-band antenna and polarization network are applied to the coax switches. If the L-BAND CONVERTER switch at the console is not in the C position, these C-band signals are switched to the C-band receiver by another set of switches. The V/RH and H/LH S-band RF signals from the S-band antenna and polarization network are applied via RF hybrids to the switches. If the L-BAND CONVERTER switch at the console is not in the S position, these S-band signals are switched to the S-band receiver.

The frequency range of the S-band antenna is 1 GHz to 4 GHz, whereas the frequency range of the S-band receiver is 2 GHz to 4 GHz. Signals from the S-band antenna in the 1-to-2 GHz range are considered L-band signals. Thus, the second outputs from the hybrids are applied to L-band converter for up-conversion of these L-band signals from the S-band antenna. Also applied to the L-band converter are V/RH and H/LH UHF RF signals in the 0.1-to-1 GHz range from UHF antenna which may be used with the PAMS but is not supplied with the system.* The L-band inputs are applied via PIN limiters to RF amplifiers. In addition, the V/RH channels include switches used to switch 40 db attenuators in or out of the signal paths. These switches are controlled by the L ATTENUATOR IN/OUT switch on the mode control panel at the console which also signals the selection to the computer. This switch can be overridden by a relay which is controlled by a calibration logic circuit. When the system is in the amplitude calibrate mode (automatic or manual), a relay is energized to override the manual setting of the IN/OUT switch and provide an "out" signal to the C-band converter and to the computer.

The outputs of the RF amplifiers are applied, via power dividers used as combiners, to the mixers. In the mixers, the L-band signals are mixed with the output of a common 4 GHz oscillator which is applied to the mixers via 10-db attenuator. Since the combined L-band inputs to the mixers are in the 0.1-to-2 GHz range, the lower sideband of the mixer outputs is 2 GHz to 3.9 GHz, and the upper sideband of the mixer outputs is 4.1 GHz to 6 GHz. If the L-BAND CONVERTER switch at the console is in the C position, the up-converter L-band signals from the mixers are applied to the C-band receiver which uses the upper sideband. If the L-BAND CONVERTER switch at the console is in the S position, the up-converted L-band signals from the mixers are applied to the S-band receiver, which uses the lower sideband.

Note that the upper sideband signal uses only one-half the frequency range of the C-band receiver (4.1 GHz to 6 GHz versus 4 GHz to 8 GHz). To reduce the sweep width of the C-band receiver accordingly during the swept-frequency periods, the L-BAND CONVERTER switch at the console controls a C-band sweep limit circuit in the receiver control panel. When the L-BAND CONVERTER switch is in the C position, a variable resistor reduces the voltage applied across the C-band SWEEP WIDTH dual variable resistors. Note also that as the L-band signals increase in frequency, the lower sideband of the L-band mixer outputs (used by the S-band receiver) decreases in frequency. When the L-BAND CONVERTER switch is in the S position, it energizes a

*See footnote, page 44.

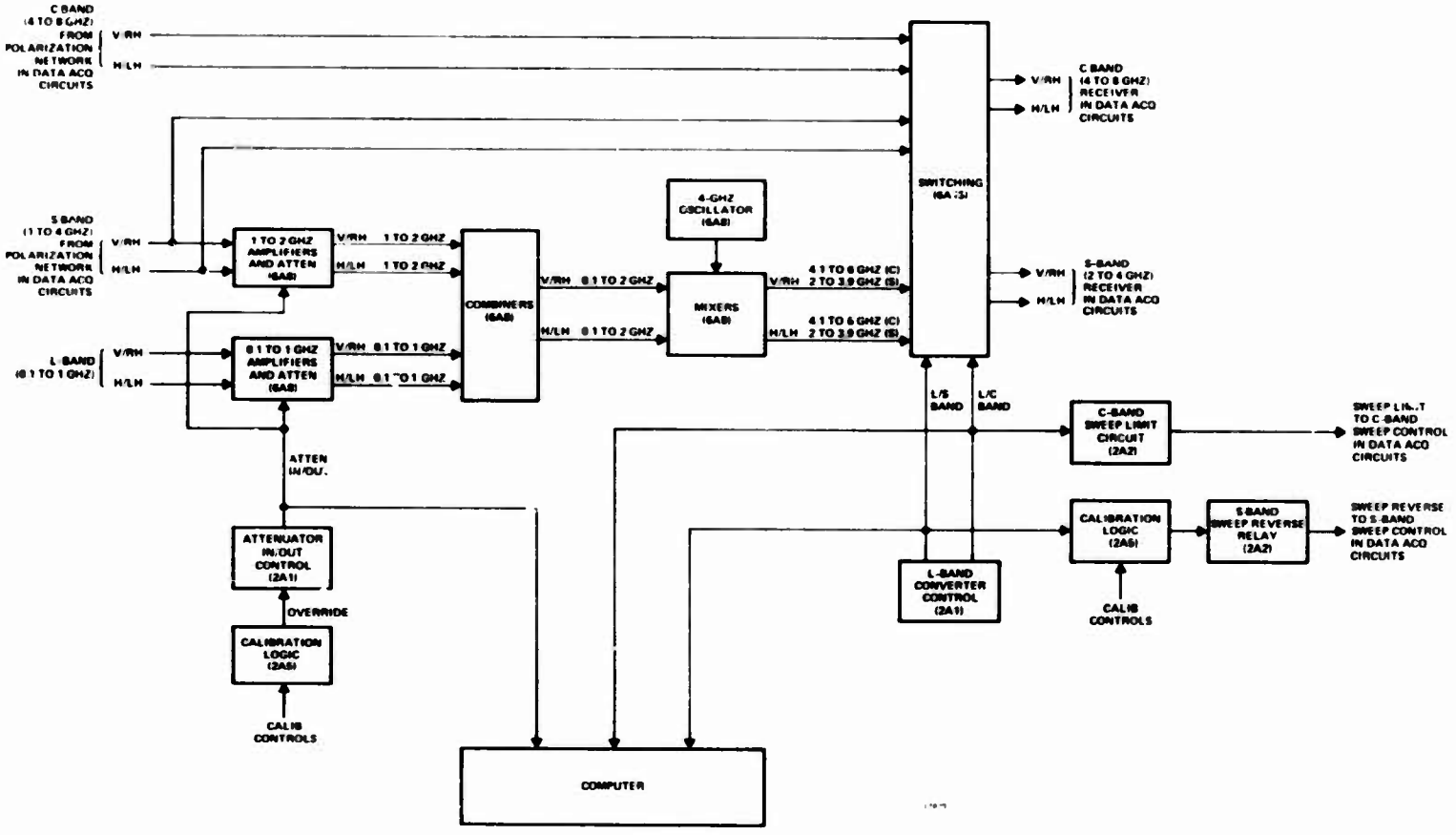

Figure 34. L-Band Switching and Conversion Circuits, Block Diagram

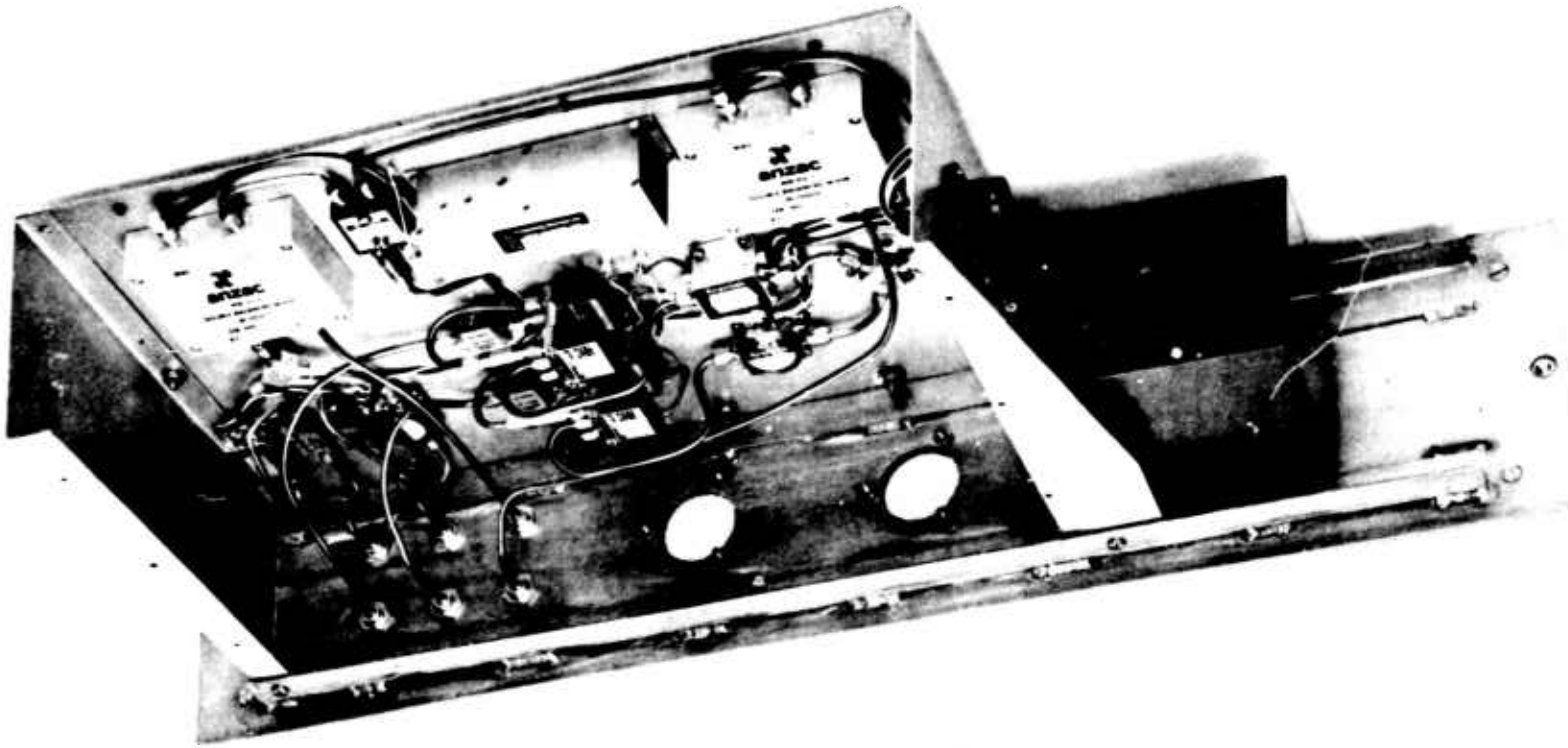

Figure 35. L-Band Up Converter

relay in the receiver control panel, via a calibration logic circuit in the processor, to reverse the roles of the S-band SWEEP WIDTH dual variable resistors. That is, the SWEEP WIDTH STOP control determines the voltage at which the tuning voltage ramp starts and the SWEEP WIDTH START control determines the voltage to which the tuning voltage ramp sweeps in the ramp generator in the S-band receiver. The calibration logic circuit in the processor is used in driving the relay in the receiver control and also to inhibit the sweep reversal when the system is in the automatic frequency calibration mode.

4.5.4 Cursor Circuits

This discussion deals primarily with the normal operating mode of the cursor circuits, as opposed to the calibrate mode. Figure 36 is a block diagram of these circuits. The calibrate mode of these circuits and of the data acquisition circuits is detailed in a later paragraph.

4.5.4.1 Non-Integrating Cursors 1 Through 4 and Common Circuits

The CURSOR NO. 1 POSITION variable resistor applies a voltage level to a voltage comparator in the processor. Also applied to this voltage comparator is the horizontal sweep voltage ramp for the pan scope displays, which is generated in the scope control circuits. This sweep voltage ramp, representing frequency, is generated during the swept-frequency periods of the receivers in synchronization with the receiver tuning voltage ramp. When the sweep voltage sweeps past the voltage level set by the POSITION control, the voltage comparator output changes from logic to set a latch. The latch output then triggers a 100 μs one-shot, provided the one-shot is not inhibited. Thus, a 100 μs cursor pulse is generated at a point in the swept-frequency period determined by the setting of the POSITION control. The latch is reset by timing signal T1 at the end of each swept-frequency period so that the cursor pulse can be generated during the next swept-frequency period. The one-shot is inhibited if the CURSOR NO. 1 BAND SELECT switch is set to OFF or K_U FIX. If the switch is set to K_U FIX, the output of a gate on the processor card not only inhibits the one-shot, but also signals the selection to the computer. (In the case of cursors 2, 3, and 4, the X FIX, C FIX, and S FIX positions, respectively, of their BAND SELECT switches correspond to the K_U FIX position for cursor 1.

Assuming the one-shot is not inhibited, the 100 μs cursor output pulse is applied to two sets of four NAND gates, set on two processor cards. The outputs of the NAND gates are applied to a set of four multiplex lines, one line for each of the four bands. One of the four gates is enabled by the setting (K_U, X, C, or S) of the CURSOR NO. 1 BAND SELECT switch to put the cursor on one of the four multiplex lines. This switch also applies a 3-bit band select signal to the computer. Also applied to the four multiplex lines are cursors 2, 3, and 4, as well as integrating cursors 5 through 12, which are described later in this discussion. Any or all of the 12 cursors may be put on any of the four multiplex lines. The cursors on each multiplex line are then used to generate the various sample gates used in the data acquisition circuits to acquire frequency and amplitude data at the frequencies of interest. The generation of these sample gates is described later in this discussion.

The outputs of the four NAND gates are applied to a second set of four multiplex lines used to superimpose the cursors on the video scope presentations. One of these four gates is enabled by the setting of the CURSOR NO. 1 BAND SELECT switch to put the

cursor on one of the four multiplex lines. If the CURSOR NO. 1 FLASHER switch is pressed, it enables a 4 Hz square wave from the timing circuits to be applied to the four NAND gates on the processor card via a NAND gate on a second processor card. The 4 Hz signal causes the cursor indication to flash so that it may be easily located on the scope presentation. Also applied to this second set of four multiplex lines are cursors 2, 3, and 4, as well as integrating cursors 5 through 12 and fixed-frequency cursors. Any or all of cursors 1 through 12 may be put on any of the four multiplex lines along with the fixed-frequency cursor. When the video for one of the four bands is selected for panoramic display on one of the scopes, the cursors on the multiplex line for that band are superimposed on that display to enable the operator to position the cursors to the points (frequencies) of interest on the display.

The 100 μs cursor 1 pulse from the one-shot in the processor is also applied to a cursor 1 flag generator circuit. This circuit consists of flip-flops and NAND gates. If the system is not in the automatic frequency calibrate mode, signals generated by NAND gates in the processor enables the cursor pulse to change the flip-flop to the 0 state. A similar relationship exists between the cursors 2, 3, and 4 flag generator circuits and the X FIX, C FIX, and S FIX positions of the BAND SELECT switches for cursors 2, 3, and 4, respectively. This flip-flop stores the cursor for transfer to the flip-flop in the processor when a flag clock occurs.

A flag clock is generated by a four-input NAND gate and, assuming that this gate is not inhibited by any of three conditions described below, the square wave output of the timing circuits is gated through as the clock input to the flip-flop setting it to a 1 state. The logic output of this flip-flop is the cursor 1 flag input to the computer, telling the computer which cursor has been generated. Another circuit applies a cursor interrupt (called flag cursor) to the computer to tell the computer to "look at" the frequency and amplitude data from the data acquisition circuits (as well as azimuth, elevation, range, and time data).

After the computer has read the data, the computer applies a cursor reset signal to the processor. This signal resets the flip-flop to terminate the cursor flag and cursor interrupt. This one-shot also applies a reset signal to the pulse stretcher reset generator circuits for all bands unless inhibited. The inhibit circuit is to prevent the computer from resetting the pulse stretchers after reading the data corresponding to a given cursor if another cursor has been generated and is ready to flag and interrupt the computer.

The generation of a flag clock to transfer a cursor flag and the flag interrupt to the computer can be inhibited or delayed by any of two conditions. These conditions are as follows. If another cursor flag (and the cursor interrupt) has been set and not yet terminated, the cursor interrupt generator circuit inhibits generation of a flag clock until the other cursor flag (and cursor interrupt) has been terminated by the computer. If the cursor reset signal from the computer is present, this logic 0 signal inhibits generation of a flag clock.

4.5.4.2 Integrating Cursors 5 through 12

The integrating cursors are used in pairs. The manual controls for cursors 5 through 12 are on the integrating cursor control panel. These controls operate in conjunction with logic circuits in the processor. In general, to avoid calling out four sets of reference designations, this portion of the discussion is keyed to one cursor pair.

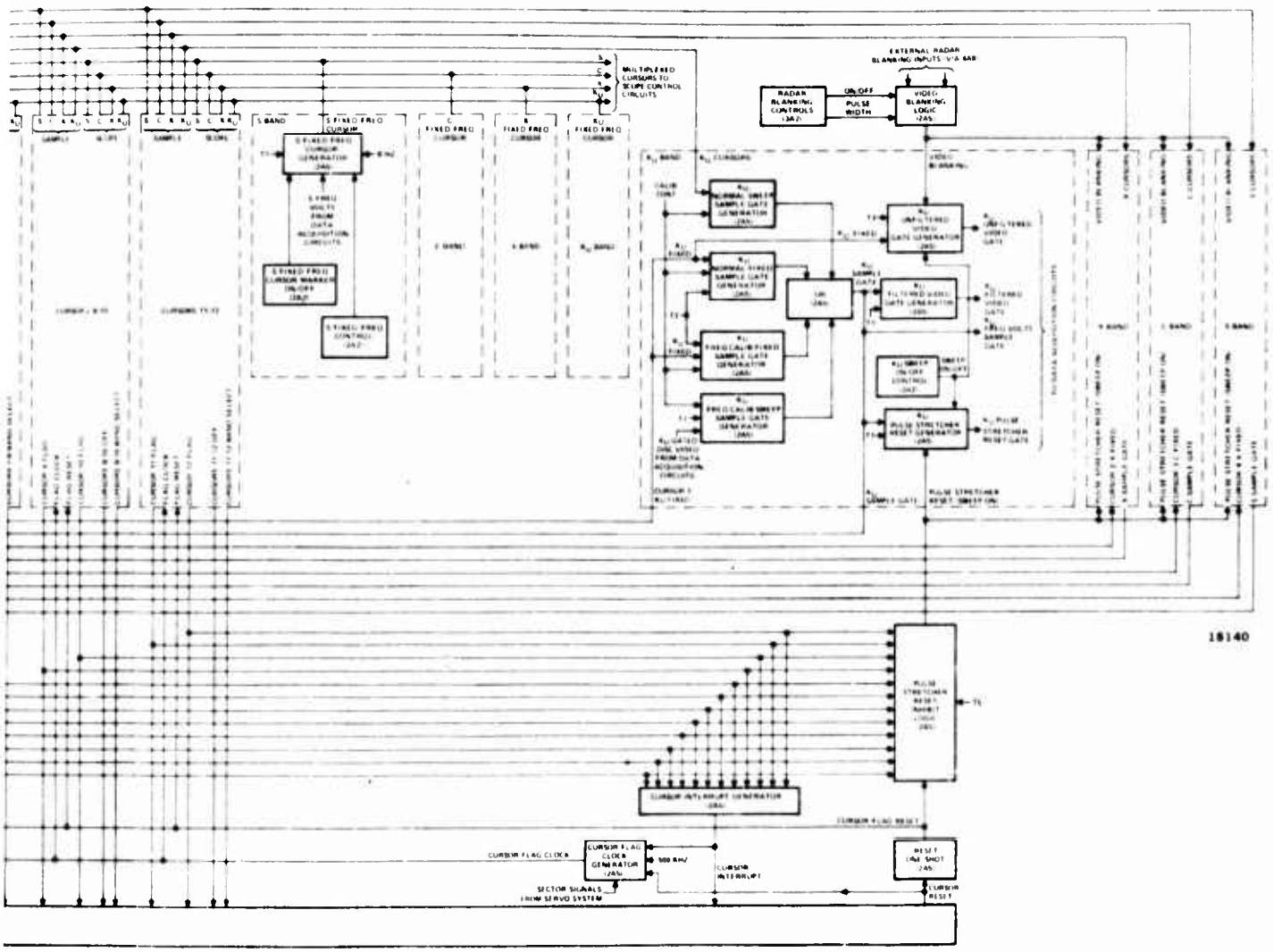

Figure 36. Cursor Circuits, Block Diagram

In many respects, the integrating cursor circuits are very similar to the non-integrating cursor circuits. The dual CURSOR START/STOP variable resistor applies voltage levels to a pair of voltage comparators in the processor. Also applied to both voltage comparators is the pan scope display horizontal sweep voltage ramp generated in the scope control circuits. When the sweep voltage sweeps past the voltage levels applied to the voltage comparators, each voltage comparator output changes from logic 1 to logic 0 to change a flip-flop to the 1 state. The output of each flip-flop then triggers a 100 μs one-shot provided the one-shots are not inhibited by CURSOR 5-6 BAND SELECT switch being in the OFF position. The flip-flops are reset by timing signal T1' (derived from T1) at the end of each swept-frequency period so that the cursor pulses can be generated during the next swept-frequency period.

The 100 μs cursor pulses from the one-shots are applied to a latch and, in addition, the first cursor pulse is applied to a flip-flop. These circuits are part of the video select and integrate circuits. The cursor pulses from the one-shots are also applied to a gate in the processor. This gate actually performs an OR function to apply the pulses for both the cursors to the band select logic circuits. The output of the gate is applied directly to one set of four gates in the processor. The one gate of these four which is enabled by the BAND SELECT switch puts the pair of cursor pulses on one of four multiplex lines. The cursors on these multiplex lines (one line for each band) are used to generate the various sample gates used in the data acquisition circuits to acquire frequency and amplitude data at the frequencies of interest.

The output of the gate is also applied to a second set of four gates in the processor via other gates in the processor where the cursor pulses are combined with a 4 Hz square-wave signal when the CURSOR FLASHER switch is pressed. This set of four gates in the processor card is used to put the pair of cursor pulses on one of the set of four multiplex lines (one for each band) which superimpose the cursors on the video scope presentations. When enabled by the FLASHER switch, the 4 Hz signal causes the cursor indications to flash so that they may be easily located on the scope presentations. In addition to controlling the two sets of four gates, the BAND SELECT switch applies a 3-bit band select signal to the computer.

The cursor 100 μs one-shot outputs are also applied to flag generator circuits. If the system is not in the automatic frequency calibrate mode, a signal enables the one-shot outputs to change the first flip-flop of each pair to the 0 state. These flip-flops store the cursors for transfer to the second flip-flops of the pairs when a flag clock occurs.

4.5.4.3 Fixed-Frequency Cursors

The purpose of the fixed-frequency cursor circuits is to provide, on the panoramic scope display for a given band, an indication of the fixed-frequency setting for that band. The manual controls for these circuits are the FIXED FREQ controls on the receiver control panel. These controls operate in conjunction with cursor generator logic circuits in the processor. As the S-band FIXED FREQ POSITION variable resistor is used to select the fixed-frequency setting of the S-band receiver, as described in the discussion of the data acquisition circuits, the fixed-frequency voltage is also applied to a voltage comparator. Also applied to this voltage comparator from the data acquisition circuits is the freq. volts ramp generated by the ramp generator in the receiver and routed via freq. buffer and scope circuit in the processor. As this ramp sweeps past the fixed frequency voltage, the output of the voltage comparator

changes from logic 1 to logic 0 to set a latch. The latch output then triggers a 100 μs one-shot, the output of which is applied to a 4-input NAND gate. This gate is enabled during the swept-frequency periods by timing signal T1, the trailing edge of which also resets the latch at the end of each swept-frequency period so that the one-shot can be triggered again during the next swept-frequency period. This gate is also controlled by the S-band FIXED FREQ CURSOR MARKER switch, which must be in the ON position to enable the gate. Also applied to this gate is the 8 Hz square wave from the timing circuits which causes a continuous flashing indication. Thus, with the gate enabled, the 100 μs fixed-frequency cursor pulse is put on the S-band multiplex line used by the scope control circuits so that this cursor, continuously flashing, is superimposed on the scope presentation.

4.5.4.4 Sample Gate Generation

The cursors on the multiplex line are applied to a NAND gate. This gate serves as the sample gate generator during swept-frequency periods of normal (non-calibrate) operation. If the system is not in the automatic frequency calibrate mode, a signal enables each cursor on the multiplex line to generate a sample gate via a four-input NAND gate, which performs an OR function. These sample gates, which are generated during the swept-frequency periods, are (a) applied to the freq-volts sample and hold circuit via a gate in the processor to sample frequency data for application to the computer, (b) applied to a gate which, when enabled by T1 and by a SWEEP ON/OFF switch in the ON position, gates filtered video amplitude data to the computer via the pulse stretchers, and (c) applied to the pulse stretcher reset generator circuit to make certain that the pulse stretchers cannot be reset while the computer is reading data, as could occur if the computer were resetting a cursor for another band.

If a CURSOR BAND SELECT switch on the cursor control panel is in the FIX position, it enables the sample gate to be generated during the fixed-frequency periods of normal operation. This sample gate performs the same function as the swept-frequency sample gates with regard to the freq. volts sample and hold and pulse stretcher reset. However, in lieu of the sample gates being used to gate filtered video amplitude data to the computer via the pulse stretchers, the FIX position of the CURSOR BAND SELECT switch enables a gate in the processor to allow a timing signal to gate unfiltered video to the computer via the pulse stretchers, unless video blanking is occurring. Either of two blanking inputs triggers a one-shot in the processor via a Schmitt-trigger circuit provided the RADAR BLANKING ON/OFF switch on the analysis scope control panel is in the ON position. The duration of the one-shot (blanking duration) is adjustable by a RADAR BLANKING PULSE WIDTH variable resistor on the analysis scope control panel. For the duration of video blanking, T3 is prevented from gating unfiltered video to the computer during the fixed-frequency periods by gates in the processor. The sample gate generated during the fixed frequency periods is also used to generate a cursor 1 flag and cursor interrupt.

The pulse stretcher reset gate is generated in the following ways. If the band SWEEP ON/OFF switch on the receiver control is in the OFF position, it enables T1 to generate a pulse stretcher reset gate for the duration of each swept-frequency period. If this switch is in the ON position, it enables a pulse stretcher reset pulse to be generated (a) each time the computer resets a cursor flag after reading the data acquired by that cursor (unless another cursor is ready to flag the computer, in which case the

pulse stretcher reset gate would be inhibited, and (b) by another timing signal to make certain that the pulse stretchers are reset just prior to acquiring amplitude data during the fixed-frequency periods.

4.5.5 Scope Control Circuits

Figure 37 is a block diagram of the scope control circuits. Reference designations shown in the blocks indicate the locations of the circuits named in the blocks. The primary purpose of the scope control circuits is to select video from one of the four bands for display on one of the three console scopes. Each scope is controlled independently so that video from any band can be displayed on any scope. When the video from a given band is selected for display on a given scope during swept-frequency periods (panoramic display), the cursors assigned to that band in the cursor circuits are superimposed on the display. The scope control circuits also provide for superimposing a calibration pulse on the displays as a means of measuring the amplitude level of a video pulse. This scope calibration function is not related to the system calibration mode described in detail in a later paragraph.

4.5.5.1 Pan Scope Control

The two pan scopes are used for panoramic display of video during the swept-frequency periods and are blanked during fixed-frequency periods. Control circuits for the two pan scopes are identical. Filtered V/RH and H/LH video signals for each band are applied to a pair of video switches for each scope. In addition to the video inputs, two other selectable inputs to the switches are (a) ground and (b) a calibration voltage set by a SCOPE CALIBRATION LEVEL DBM variable resistor on the manual system calibration panel. The video switches are controlled by manual switches on the pan scope control panels via video select logic circuits in the processor. The 3-bit video select signals from RECEIVER SELECT switches are applied to the video switches via sets of three NAND gates in the processor. These gates are in the signal path to allow the introduction of a calibration pulse as described later in this discussion. If the RECEIVER SELECT switches are set to one of the four band positions, the V/RH and H/LH video signals for the selected bands are applied to the pan scopes via connectors J1 and J2 and via jumper cables connected between these connectors and the two vertical inputs of each scope. If the RECEIVER SELECT switch is set to EXT, none of the video signals is selected for application to the corresponding scope; the ground input to the video switches is selected instead. The RECEIVER SELECT switches also control Z-axis control circuits for the scopes. The EXT position of these switches has significance to the Z-axis control circuits in allowing the scopes to be used as general purpose scopes.

If the AMP CALIB switches are ON, they enable one-shots in the processor to allow a calibration pulse to be applied to the scope presentations as follows. The SCOPE CALIBRATION POSITIONS variable resistor applies a voltage level to a voltage comparator. Also applied to this voltage comparator is the horizontal sweep voltage ramp for the pan displays. As the pan sweep voltage sweeps past the voltage set by the SCOPE CALIBRATION POSITIONS control, the voltage comparator output changes logic states to trigger the enabled one-shots. For the duration of the one-shots, the outputs of the one-shots override the band select signals at the gates in the processor and cause the outputs of these gates to select the calibration voltage input to the video switches for application to the scopes. Thus, the one-shots determine the width of the calibration pulse. The difference in one-shot durations (and resultant calibration pulse

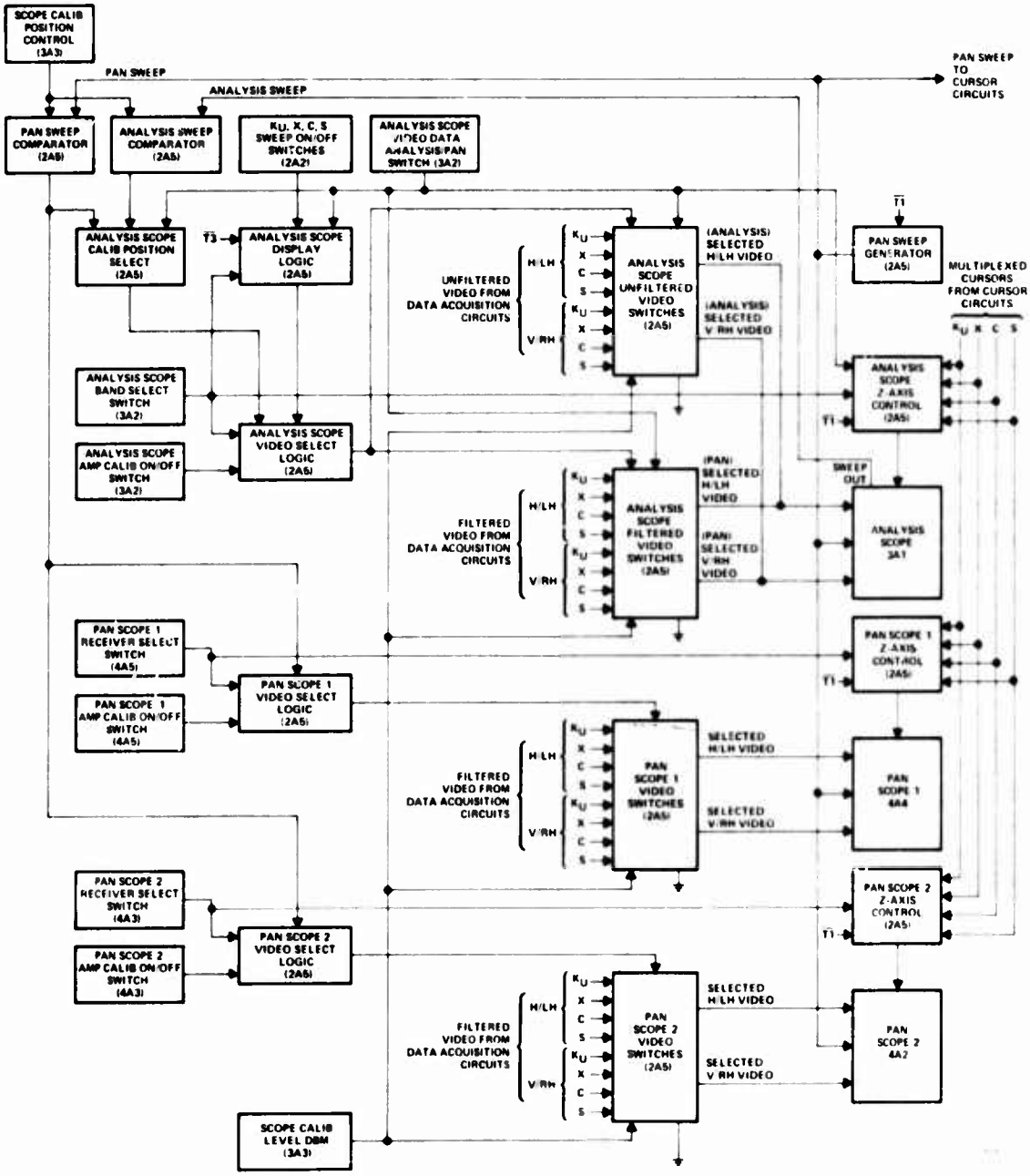

Figure 37. Scope Control Circuits, Block Diagram

widths) for the two pan scopes is not significant; the pulse width is not critical. To use the calibration pulse, the pulse is positioned next to a video pulse on the scope presentation and adjusted to the amplitude of the video pulse. Then the approximate amplitude of the video pulse in dbm is read on the SCOPE CALIBRATION LEVEL DBM control.

The pan sweep voltage used at the pan sweep comparator is the same sweep voltage used in the cursor circuits. This sweep voltage is generated on frequency buffer and scope circuit cards in the processor. The integrator stage generates a sweep voltage during the swept-frequency periods. A timing signal turns off a transistor stage to enable the integrator, and the sweep voltage is applied to pan scopes. This sweep voltage may also be used for the analysis scope when it is being used as a pan scope. The Z-axis control circuits for the pan scopes are used to intensify the sweep for cursor display and to blank the sweep during fixed-frequency periods. If the RECEIVER SELECT switches on the pan scope control panels are each set to one of the four band positions, the cursors for the selected bands are applied via gates in the processor for each scope, on the frequency buffer and scope circuits. Each cursor pulse causes a -5 volt pulse output from the amplifiers to intensify the sweep on the scopes. If the RECEIVER SELECT switch is set to EXT, the cursors and T1 are blocked at gates in the processor for the corresponding scope. That scope can then be used as a general purpose oscilloscope.

4.5.5.2 Analysis Scope Control

The analysis scope can be used either for panoramic display of video during the swept-frequency periods or for analysis display of fixed-frequency video. The use of this scope (panoramic or analysis) is selected by the VIDEO DATA switch on analysis scope control panel. When this switch is in the PANORAMIC position, operation of the analysis scope control circuits is essentially identical to that of the pan scope control circuits described above. If the BAND SELECT switch is in one of the four band positions, it applies a 3-bit band select signal to the video switches in the horizontal and vertical buffer circuits in the processor via video select logic circuits consisting of two sets of gates. The video switches in the processor are enabled only when the VIDEO DATA switch on the analysis scope control panel is in the PANORAMIC position to allow filtered V/RH and H/LH video from the data acquisition circuits to be band-selected for application to the analysis scope. Video switches in the processor are enabled only when the VIDEO DATA switch is in the ANALYSIS position to allow unfiltered V/RH and H/LH video from the data acquisition circuits to be band selected for application to the analysis scope.

The set of three gates in the signal path of the band select signals is used to determine the time that the band select signals are applied to the video switches. These gates are controlled by a display logic circuit consisting of a set of five gates in the processor, all of which are, in turn, controlled by panel switches as follows. If the VIDEO DATA switch is in the PANORAMIC position, the output of the gate in the processor card is continuously logic 1 to enable the band select signals to be applied to the video switches continuously. If the VIDEO DATA switch is in the ANALYSIS position, the output of the gate in the processor is controlled by the set of four gates also in the processor. These four gates, one for each band, are controlled by the RECEIVER SELECT switch and by the four SWEEP ON/OFF switches on the receiver control panel. If the SWEEP ON/OFF switch is OFF for the band selected by the RECEIVER SELECT switch, the output of the gate in the processor is continuously logic 1 to enable the band select signals to be applied to the video switch continuously.

This feature is related to the fact that a given receiver is tuned to the fixed frequency setting continuously if the SWEEP ON/OFF switch for that band is OFF. If the SWEEP ON/OFF switch is ON for the band selected by the RECEIVER SELECT switch, the output of the gate is logic 1 only during T3 time to enable the band select signals to be applied to the video switches only during the fixed-frequency periods. In this case, the ground input to the video switches is selected for application to the scope vertical inputs except during T3 time. The set of three gates in the signal path of the band select signals is also used to apply a calibration pulse to the scope display when the AMP CALIB switch is ON. When the VIDEO DATA switch is in the PANORAMIC position, it enables a gate to allow the calibration pulse to be introduced in the same manner as described above for the pan scopes. When the VIDEO DATA switch is in the ANALYSIS position, it enables a different gate. Applied to this second gate is the output of a voltage comparator, the inputs of which are (a) a voltage set by the SCOPE CALIBRATION POSITIONS variable resistor on the manual system calibration panel and (b) the internal horizontal sweep voltage from the analysis scope. Thus, in this case, the calibration pulse is introduced in a manner similar to that described above, except that the horizontal positioning of the pulse is based on the analysis scope internal sweep voltage rather than the pan sweep voltage. The analysis scope uses this external sweep voltage only when it is being used for panoramic display. When used for analysis display, this scope should be set up to use internal sweep. The Z-axis control circuits for the analysis scope are functionally the same as those for the pan scopes.

4.5.6 Mode Control and Numerical Display Circuits

Figure 38 is a block diagram of the mode control and numerical display circuits. Reference designations shown in the blocks indicate the locations of the circuits named in the blocks.

The mode switches on the mode control panel apply inputs to the computer via mode control logic circuits in the processor. When momentarily pressed, FREQ CALIB/AMP CALIB, RUN, PAUSE, STOP, and END FLIGHT switches set flip-flops in the processor via latches consisting of gates. The computer reads these mode inputs and can reset the flip-flops via a common reset signal. The stop and end flight modes have significance only to the computer. However, the run, pause, and freq calib/amp calib modes cause the computer to apply a 3-bit mode control output to the processor. The run and pause modes correspond to the normal data acquisition mode of the system. The RUN and PAUSE indicators are controlled via indicator logic circuits in the processor. In response to the calibrate input from the mode control panel, the computer cycles through an amplitude calibrate mode and a frequency calibrate mode as follows. The selected calibrate mode is initiated by a "set calibration control" signal from the computer and timing signal T2, which are applied to a pair of flip-flops. The purpose of these flip-flops is to synchronize the initiation of each calibrate mode with the internal system timing. The "set calibration control" signal from the computer changes the first flip-flop to a 1 state, enabling the trailing edge of the next T2 to change the second flip-flop to a 1 state. The resulting logic 0 output of the second flip-flop immediately resets the first flip-flop. Then the resulting negative-going transition of the first flip-flop changes the enabled flip-flop to the 1 state to initiate the selected calibration mode. As each of the flip-flops is set to the 1 state, its logic output lights the AMP CALIB indicator or FREQ CALIB indicator on the mode control panel via indicator logic circuits. The "set calibration control" signal from the computer also terminates each calibration mode; however, either calibration mode can be

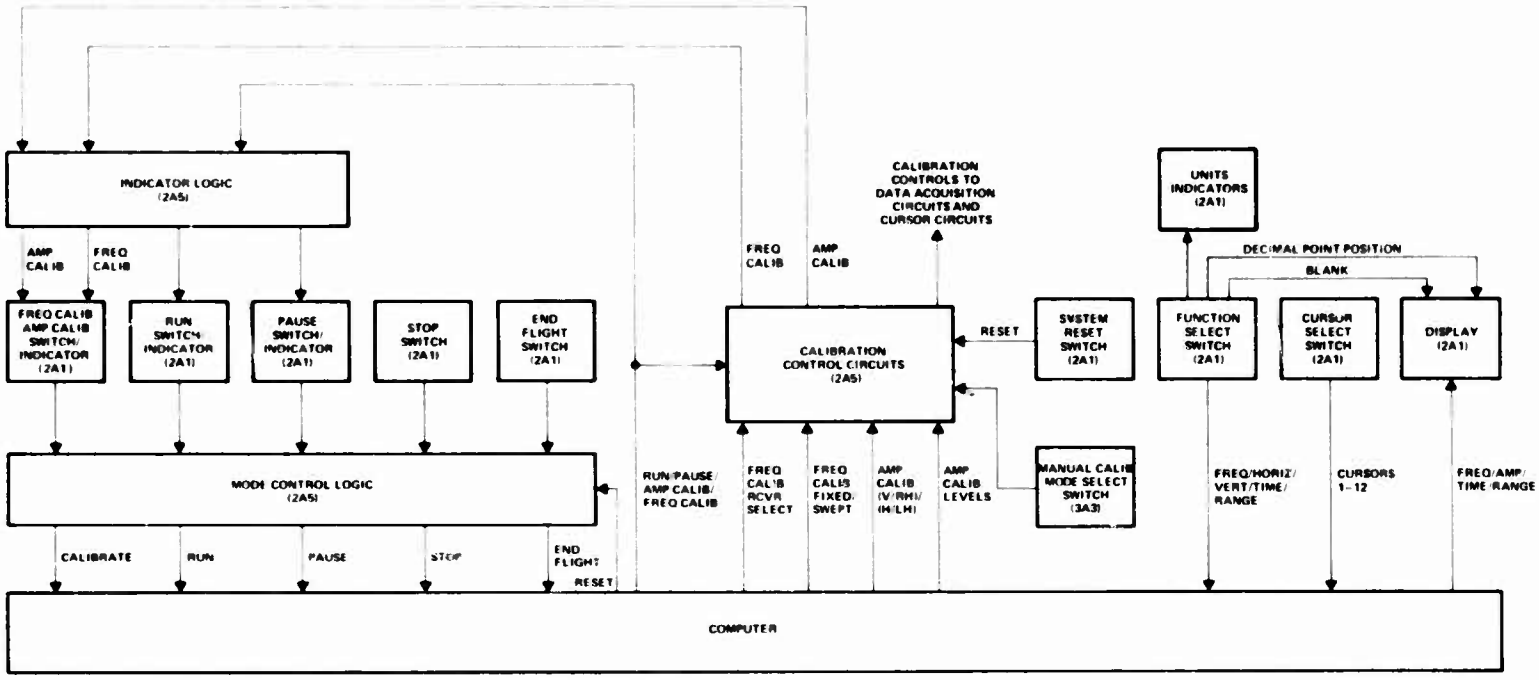

Figure 38. Mode Control and Numerical Display Circuits, Block Diagram

manually terminated by momentarily pressing the SYSTEM RESET switch on the mode control panel. Other portions of the calibration control circuits respond to various control signals from the computer to (a) select the receivers one at a time for frequency calibration, (b) select fixed and swept frequency calibration, (c) select the V/RH and H/LH channels of the receivers for amplitude calibration, and (d) provide amplitude calibration levels. In addition to these automatic or computer-controlled calibration functions, manual-controlled calibration functions can be selected at the manual system calibration panel, although computer-controlled calibration overrides manual calibration.

4.5.6.1 Numerical Display

The numerical display controls and indicators on the mode control panel select various data from the computer for an on-line six-digit display. The FUNCTION SELECT switch performs several functions: (a) applies a three-bit data select input to the computer to select FREQ (frequency), HORIZ (H/LH amplitude), VERT (V/RH amplitude), TIME, or RANGE data for display, (b) lights the appropriate units indicator, (c) positions the decimal point on the display, and (d) blanks the display when set to OFF. When frequency, H/LH amplitude, or V/RH amplitude data are selected, the displayed data are related to the cursor selected by the CURSOR SELECT switch, which applies a 4-bit binary-coded decimal (BCD) select signal to the computer. GHZ units indicator lights when frequency data are selected. DBM units indicator lights when H/LH amplitude data or V/RH amplitude data are selected. TIME units indicator lights when time data are selected; actually time is displayed in hours, minutes, and seconds (tens and units decimal digits for each). The NAUT MI units indicator lights when range data are selected. The decimal point is positioned between the third and fourth digit for all displays except time. For time, one decimal point is positioned between the second and third digit to separate hours from minutes and another decimal point is positioned between the fourth and fifth digits to separate minutes from seconds.

4.5.7 System Calibration

The system operates in two calibration modes: amplitude calibration (automatic and manual) and frequency calibration (automatic and manual). During automatic calibration, the computer acquires and stores calibration data. Then during normal operation, the computer compares acquired operational data with the calibration data to achieve high accuracy measurement of the operational data. During manual calibration, the computer does not store acquired data as calibration data. The computer does not differentiate between normal operational data and data acquired during manual calibration. The discussion includes references to appropriate portions of the discussions of the data acquisition circuits and cursor circuits where some aspects of the calibrate modes are noted.

4.5.7.1 Amplitude Calibration

Automatic amplitude calibration functions are more extensive than manual amplitude calibration functions. This discussion makes note of those functions performed only during automatic amplitude calibration and of those functions common to both automatic and manual amplitude calibration. Manual amplitude calibration is selected and initiated by setting the MODE SELECT switch to AMPLITUDE on the manual system calibration panel and controls a signal called ACM. The automatic amplitude calibration

control signals and manual amplitude calibration control signal ACM control various receiver functions via processor logic circuits. The logic circuits in the processor are described first in this discussion, followed by a description of the ultimate effects of the amplitude calibration mode in the receivers. Amplitude calibration is performed on all energized receivers simultaneously.

When the automatic amplitude calibration control flip-flop is set, the flip-flop outputs perform the following functions (in addition to lighting the AMP CALIB indicator on mode control panel). The flip-flop output is applied to a gate to decouple the receivers from the antennas during automatic amplitude calibration. The flip-flop output is also applied to four gates to inhibit manual AFC polarization selection from the receiver control, and the other flip-flop output enables computer signal H/V_{12} to select the AFC polarization during automatic (not manual) amplitude calibration. As this function implies, the two channels (H/LH and V/RH) are calibrated one at a time. During amplitude calibration (automatic or manual), the AFC polarization signals, in addition to channel-selecting the input to the AFC loop in each receiver, switch the amplitude calibration function between channels in each receiver.

An "ant amp calib" signal is generated when the system is in the automatic or manual amplitude calibration mode, except that generation of this signal is inhibited if the system is in the automatic frequency calibration mode. (This inhibition actually has significance only to manual amplitude calibration since automatic frequency and automatic amplitude calibration modes are mutually exclusive by computer control.) The "ant amp calib" signal is applied to all receivers to cause them to operate in the amplitude calibration mode.

The receiver attenuator control logic circuits are affected both by automatic amplitude calibration flip-flop outputs and by manual amplitude calibration control signal ACM. These circuits control a 1 db step attenuator (fine attenuation) in the amplitude calibration AGC circuits in each receiver and a 10 db step attenuator (coarse attenuation) which is used during both normal operation and amplitude calibration in each receiver. The fine attenuation signals are 4-bit binary-coded decimal (BCD) signals which set the fine attenuator in each receiver to any decimal setting 0 through 9 (in 1 db steps). This setting is determined either by the units digit AMPLITUDE SIGNAL ATTENUATION switch on the manual system calibration panel during manual amplitude calibration, or by signals from the computer during automatic amplitude calibration. During normal (non-calibration) operation, control signal ACM sets the fine attenuation signals to BCD 9 (maximum attenuation) to minimize cross-talk between the amplitude calibration AGC circuits and other receiver circuits.

The coarse attenuation signals are 3-bit BCD signals which set the coarse attenuator in each receiver to any decimal setting 0 through 50 (in 10 db steps). If the system is in the automatic or manual frequency calibration mode, a control signal whose derivation is described below, blocks the manual setting and sets the coarse attenuation signals to BCD 0 to select zero attenuation so that the coarse attenuator does not affect frequency calibration signals. The same circuit which generates the "ant amp calib" signal as described above also energizes a relay in the mode control panel to override the ATTENUATORS IN/OUT switches so that the coarse attenuators are "in" during amplitude calibration.

At each receiver, the amplitude calibrate and AFC polarization control signals are applied to the RF switch driver, along with a frequency calibrate control signal. These

signals control three push-pull switch driver circuits which control RF switches in each receiver. The functions of the coax switch are to (a) form part of signal path for V/RH RF signals during normal operation and (b) switch calibration RF signals between the V/RH and H/LH receiver channels during calibration. The channel switching function, performed by the AFC polarization control signal, is controlled by the computer during automatic amplitude calibration and by the AFC POLARIZATION switch for each receiver during manual amplitude calibration (as well as during frequency calibration). The AFC polarization control signal, in addition to controlling this switch driver during calibration, is level-converted for use at the AFC detector/discriminator in the receiver to channel-select the input to the AFC loop.

The function of S1 and S2, in the H/LH and V/RH input channels, is to switch between RF signals from the antenna during normal operation and calibration RF signals during calibration. The function of S4 is to switch between amplitude calibrate signals and frequency calibrate signals.

For amplitude calibration, the receivers use the continuous-wave 100 MHz reference oscillator output of the harmonic generator which is applied to all four receivers via a power divider. In each receiver, the 100 MHz reference oscillator signal is applied to an automatic gain controlled IF amplifier in AGC assembly A7. The IF amplifier output is applied to the up-converter. The local oscillator signal from the YIG tuner assembly is also applied to the up-converter via a 3-db hybrid and a series of isolators and filters. When the local oscillator signal (100 MHz above the tuner frequency) is mixed with the 100 MHz reference oscillator signal in the up-converter, the lower sideband of the up-converter output (F_{LO} - 100 MHz) is at the frequency to which the receiver is tuned. The up-converter output is applied to a YIG filter in the YIG tuner assembly which tracks the YIG filters in the V/RH and H/LH channels to select this lower sideband output.

The routing of the calibration signal out of the YIG filter differs slightly for the S-band and C-band receivers as opposed to the X-band and K_u-band receivers. In both cases the calibration signal from the YIG filter is applied to RF switch S2 via a directional coupler, an isolator, a 10 db attenuator, and RF switch S4. The only difference between the two pairs of receivers is that RF switch S4 precedes the directional coupler in the S-band and C-band receivers but follows the 10-db attenuator in the X-band and K_u-band receivers. A second output of the directional coupler is applied to the AGC assembly; the AGC circuit is discussed below. RF switch S2, which is in the 1 position for both amplitude and frequency calibration, provides a path for the amplitude calibration signal to the step attenuator. This step attenuator is controlled either manually or by the computer. The attenuator output is then applied either to the V/RH receiver channel tuner via RF switch S3 in the 2 position or to the H/LH receiver channel tuner via RF switch S3 in the 1 position and RF switch S1 in the 1 position.

The AGC assembly in each receiver varies the amplitude of the amplitude calibration signal over a 10 db range in 1 db steps and regulates the selected amplitude. (As indicated above, the 10 db step attenuator provides coarse amplitude adjustment of the amplitude calibration signal.) The amplitude calibration signal out of the directional coupler is detected and applied to a dc amplifier where it is compared with a fine attenuation level. A digital-to-analog (D to A) conversion circuit converts the BCD fine attenuation setting signals from the console to the analog attenuation level. For each 1 db change in the fine attenuation setting, the dc amplifier output changes the

gain of the IF amplifier for the 100 MHz reference oscillator signal in such a way that the output of the up-converter changes by 1 db. While a given fine attenuation setting is maintained, any tendency of the amplitude calibration signal to change in amplitude causes an AGC error voltage out of the dc amplifier to regulate the amplitude. During normal operation, an AGC on/off control signal from the RF switch driver maximizes the attenuation level applied to the dc amplifier to minimize the gain of the IF amplifier.

The 0 to 59-db amplitude variation range provided by the combination of the coarse and fine attenuators results in amplitude calibration signals over the range of -40 dbm to -99 dbm. The automatic gain controlled, precision attenuated amplitude calibration signals applied to the receiver tuners are processed by the data acquisition circuits in the same manner as operational signals. The video is selected and displayed on the oscilloscopes as previously described. Cursors are then assigned by the operator to the bands and positioned in frequency. In the case of automatic amplitude calibration, the amplitude data for each attenuation level applied from the data acquisition circuits to the computer at the frequencies selected by the cursor settings are stored as calibration data. In the case of manual amplitude calibration, the amplitude data are not stored as calibration data by the computer but the data are selectable for numerical display on mode control panel.

4.5.7.2 Frequency Calibration

Automatic frequency calibration functions are more extensive than manual frequency calibration functions. This discussion makes note of those functions performed only during automatic frequency calibration and those functions common to both automatic and manual frequency calibration. Manual frequency calibration is selected and initiated by setting the MODE SELECT switch to FREQUENCY on the manual system calibration panel. This switch controls a signal called FCM. The automatic frequency calibration control signals and manual frequency calibration control signal FCM control various receiver functions via processor logic circuits.

A signal is applied to a gate to decouple the receivers from the antennas during automatic frequency calibration. The signal is also applied to another gate to inhibit the S-band sweep reversal during automatic frequency calibration.

An "ant freq calib" signal is generated when the system is in the automatic or manual frequency calibration mode, except that generation of this signal is inhibited if the system is in the automatic amplitude calibration mode. (This inhibition actually has significance only to manual frequency calibration since automatic amplitude and automatic frequency calibration modes are mutually exclusive by computer control.) The "ant freq calib" signal is applied to all receivers to cause them to operate in the frequency calibration mode. This circuit which generates the "ant freq calib" signal also (1) enables the frequency calibration signal outputs from the harmonic generator at the receivers by energizing a +28-vdc power supply, and (2) sets the coarse attenuation signals to BCD 0 so that the coarse attenuators in the receivers do not affect frequency calibration signals.

At each receiver, the "ant freq calib" signal combines with the AFC polarization control signal to control RF switches S1 through S4 via the RF switch driver card. For automatic frequency calibration the computer does not control the AFC polarization control signal as it does for automatic amplitude calibration. Thus, frequency calibration signals are applied to the receiver channel manually selected by the AFC

POLARIZATION switch for each receiver on the receiver control panel during both automatic and manual frequency calibration. Frequency calibration RF signals are generated by the harmonic generator and applied to RF switch S4 in each receiver. These frequency calibration RF signals are continuous-wave signals at each multiple of 100 MHz throughout each of the four receiver frequency bands.

The frequency calibration RF signals are routed from RF switch S4 to RF switch S2 via a directional coupler, an isolator, and a 10 db attenuator. The frequency calibration RF signals are routed directly from RF switch S4 to RF switch S2 so that the 10 db attenuator is not in the signal path. The power levels of the harmonic generator outputs are relatively lower at the higher frequencies (X and K_u bands) and relatively higher at the lower frequencies (S and C bands) so that the 10 db attenuator is required only for the S and C bands. From RF switch S2, the frequency calibration signals are routed via the step attenuator (set to zero as mentioned above) to RF switch S3 in each receiver. RF switch S3 then routes the signals to the V/RH or H/LH channel in each receiver, as determined by the setting of the AFC POLARIZATION switch for each receiver control panel.

For manual frequency calibration, the data acquisition circuits process the frequency calibration signals the same as operational signals. The video can be selected and displayed on the oscilloscopes. A pan scope display consists of a series of pulses at 100 MHz increments of frequency. The fixed frequency setting of any receiver can be adjusted to any of the 100 MHz spaced frequencies for display on the analysis scope. Cursors can be assigned to the bands and positioned in frequency. Such data acquired during manual frequency calibration are not stored by the computer as calibration data but the data are selectable for numerical display on mode control panel.

The remainder of this discussion applies only to automatic frequency calibration, during which the data acquisition circuits and cursor circuits perform various special functions as determined by control signals from the computer. The operation of these circuits during automatic frequency calibration also differs for swept-frequency calibration as opposed to fixed-frequency calibration. Swept-frequency calibration and fixed-frequency calibration are selected in sequence from the computer.

The previous description of the data acquisition circuits is generally applicable to automatic swept-frequency calibration. For the receivers to be swept-frequency calibrated, the SWEEP ON/OFF switches on receiver control panel must be ON. The SWEEP WIDTH controls should be set to the appropriate positions before swept-frequency calibration and must not be changed during normal data acquisition. (A change in sweep width requires new calibration data.) The primary difference between normal data acquisition and automatic swept-frequency calibration is the method of generating (a) the sample gates used at the sample and hold circuits to acquire frequency data for the computer and (b) the cursor flags and interrupts applied to the computer. Although the AFC function previously described is not applicable to normal swept-frequency operation, portions of the AFC loop circuits are applicable to automatic swept-frequency calibration in that threshold-gated discriminator video is used to generate the sample gates and cursor flags and interrupts. During the swept-frequency periods, a threshold-gated video signal is generated in response to each 100-MHz spaced frequency calibrate RF signal. The nature of these video signals is as follows. As the receiver tuner sweeps through each 100-MHz spaced RF signal frequency, the video signal (a) sweeps from 0 volt to -2.5 volts at 5 MHz below the RF signal frequency, (b) crosses 0 volt at the RF signal frequency, (c) sweeps to +2.5 volts at

5 MHz above the RF signal frequency, and (d) returns to 0 volt until the next higher RF signal frequency is approached.

The threshold-gated video signals out of the buffer in video amplifier and voltage storage circuits in the processor (just prior to T3 timing gating) are applied to a voltage comparator. Also applied to this voltage comparator is a -0.5-volt reference determined by a diode and resistor in the frequency buffer and scope circuit in the processor. The voltage comparator serves as a pulse shaper. The negative half-cycle of each threshold-gated video signal causes a logic 1 pulse out of the comparator. These logic 1 pulses are applied to a gate which, when enabled, allows these pulses to be used in lieu of swept-frequency cursors from the cursor circuits to generate sample gates and cursor 1 flags and interrupts (cursor 2, 3, and 4 flags and interrupts for X, C, and S bands, respectively).

Enabling the gate to which the voltage comparator output pulses are applied involves the following functions. Timing signal T1 must be logic 1 to define the swept-frequency periods. Signal FCS, used in the circuits for all four bands, enables the gate to which the voltage comparator output pulses are applied, except for the first few milliseconds of each swept-frequency period. The trailing edge of each timing signal T2 triggers a 4.5 ms one-shot, causing FCS to be logic 0 for the first few milliseconds of each swept-frequency period. This action causes the first few voltage comparator output pulses to be ignored during each swept-frequency period. The reason for this action is to make sure that the YIG filters in the receivers are smoothly tracking the slope of the tuning voltage ramp before acquiring calibration data. The other enabling input to the gate to which the voltage comparator output pulses are applied is a band-select control signal. Automatic frequency calibration is performed on one band at a time, as determined by the computer.

Each voltage comparator output pulse then generates a sample gate which is (1) applied to the sample and hold circuit to acquire frequency data for the computer, and (2) used to generate the cursor 1 flag and interrupt for the computer. The cursor flags and interrupts are generated in a manner similar to that described previously. The frequency data acquired at each 100 MHz spaced calibration frequency are stored by the computer as calibration data. The computer relates a given sampled voltage to a given frequency by a "frequency bin" technique. That is, within each band, for each 100 MHz spaced calibration frequency, the sampled voltage is always within a predetermined voltage range known by the computer. The voltage range is referred to as the bin for that calibration frequency. The purpose of calibration is to determine the exact voltage within each bin which corresponds to each calibration frequency at a particular time and for a particular set of conditions. Then, during normal operation, acquired frequency data can be accurately measured by extrapolating between the calibration frequency voltages to determine the frequency corresponding to a sampled frequency voltage.

The "ant step AFC" pulses are used for the automatic fixed-frequency calibration in each receiver. The purpose of the circuits on the AFC card is to automatically offset the fixed-frequency timing voltage in the ramp generator to four settings corresponding to four of the 100 MHz spaced frequency calibration signals, two below the manual fixed-frequency setting and two above the manual fixed-frequency setting. The frequency data at these four fixed-frequency calibration frequencies are then acquired and applied to the computer which stores the data as calibration data. The purpose of the counter is to allow 16 fixed-frequency periods for the AFC loop to stablize at

each calibration frequency, between the time each calibration frequency is selected and the time that frequency data are acquired for the computer. Four settings are used as mentioned above so that, even if the manual fixed-frequency setting is at either extreme of the frequency band, calibration data are obtained for at least two 100 MHz spaced frequencies.

When the automatic frequency calibration mode is initiated, the frequency calibration signal allows the step ("ant step AFC") pulse, which is triggered by $\overline{FC}$, to change the logic to the 1 state. The logic 1 output enables two counter flip-flops. These two flip-flops count the step pulses which are generated by the 4-stage counter in the processor. The logic output of the flip-flop is also applied to the ramp generator card as a fixed-frequency calibration control signal. The fixed-frequency calibration control signal is applied to a gate, whose other input is logic 1 either during T2 time or continuously depending on the setting of the SWEEP ON/OFF switch on the receiver control panel. (Fixed frequency calibration can be accomplished with this switch in either position.) The resulting logic 0 output of the gate enables the fixed-frequency calibrate offset voltage to be added to the manual fixed frequency setting.

The threshold-gated video signals are applied to a voltage comparator. The nature of these video signals is similar to that described above. In this case, the receiver tuner is being "swept" by the calibration offset integrator during the fixed frequency period rather than by the normal swept-frequency ramp. The other input to the voltage comparator is a -0.5 volt reference. The negative half-cycle of the threshold-gated video signal causes a logic 0 pulse output from the comparator. The trailing edge of this pulse occurs at the 0 volt crossover of the video signal, or at a calibration signal frequency. Thus, in the automatic fixed-frequency calibration card, the trailing edge of this pulse, called a discriminator crossover pulse, is used to hold the integrator.

The first automatic fixed-frequency calibration frequency selection is accomplished as soon as automatic frequency calibration is selected by the computer. The selection process is initiated by a control signal before the computer switches from swept-frequency calibration to fixed-frequency calibration. During the fixed-frequency periods, the output of the ramp generator (a) sets the receiver tuners to the fixed-frequency calibration frequency and (b) is applied to the frequency data sample and hold circuits for frequency data acquisition. At the same time, the AFC loop locks to the fixed calibration frequency. The "AFC reset" pulse triggered by the control signal resets the voltage storage integrator on the video amplifier and voltage storage card to remove any previously stored AFC correction voltage. After a 40-μsec reset pulse terminates, the AFC loop can then lock to the first fixed-frequency calibration frequency. Note also that the logic 0 control signal enables the AFC loop regardless of the position of the manual AFC ON/OFF switch.

The nature of the AFC loop is such that while it is locked to the first calibration frequency, the discriminator video signal will tend to oscillate a small amount above and below the zero crossover point. If the discriminator video signal is slightly below the zero crossover point when the integrator is enabled to select the second calibration frequency, the discriminator crossover signal would almost immediately switch the integrator back to the hold condition, holding again at the first frequency. The delay circuit delays the enabling of the gate for approximately 110 μs after the integrator is enabled to make sure that the receiver is tuned beyond the discriminator control range for the first calibration frequency before a zero crossover signal can cause the integrator to hold. This delay function is also applicable when timing from the second to

the third and from the third to the fourth calibration frequencies. (The computer allows the sequence to be repeated several times and averages the readings.)

If the manual fixed-frequency setting is at or near the high extreme of a frequency band, the receiver may be tuned into its upper "stop" after calibration data are acquired at only two or three calibration frequencies. In this case, no discriminator crossover signal would occur while the gate is enabled and the flip-flop would not be changed to the 1 state to hold the integrator. If the output is still logic 1 when timing signal T1 occurs, the resulting logic 0 output of the gate resets the integrator to the initial offset condition. Then, calibration data are acquired again at the first (or the first and second) calibration frequencies to complete the four-step sequence. If the manual fixed-frequency setting is at or near the low extreme of a frequency band, the initial offset may tune the receiver into its lower "stop." However, the rate of the integrator is fast enough to tune the receiver up to the lowest calibration frequency within the band during T3 time so that a discriminator crossover occurs while the gate is enabled. The four-step calibration sequence is then performed at the four lowest calibration frequencies within the band, two, three, or all four of which may be above the manual fixed-frequency setting.

4.6 COMPUTER SOFTWARE

The software furnished with the PAMS consists of eight major programs and their associated subroutines as well as the software supplied with the HP 2116B. The programs for the data collection, reduction and display are listed below.

1. PAMS Data Acquisition Program
2. PAMS Tape Merge Program
3. PAMS 3-Variable Plot Program
4. PAMS 3-Variable Teleprinter Plot Program
5. PAMS 2-Variable Rectangular Plot Program
6. PAMS 2-Variable Polar Plot Program
7. PAMS 2-Variable Teleprinter Plot Program
8. PAMS Test Program

The first program is used to acquire data in real time, the second program reduces the data, and programs 3 through 7 are used to plot the data. The last program is used to test the PAMS hardware and computer interface with PAMS. The general flow of data between the programs is shown in figure 39. All of the programs with the exception of the Tape Merge Program are configured on a master magnetic tape. It was not possible to put the Tape Merge Program on the magnetic tape due to insufficient memory in the base page memory to store the required number of links and subroutine instructions. Consequently, the Tape Merge Program is furnished on a separate paper tape. All of the programs are called up via teletype entries. The function of each of the programs is described below.

4.6.1 PAMS Data Acquisition Program

The Data Acquisition Program is used to collect and store all of the data received by the PAMS on a magnetic tape. In addition the program instructs the computer to read all of the switch settings on the console and store this information. The computer is also interfaced with the track radar in order to monitor the range, azimuth, and elevation angles as the data are being collected. Prior to a data run, the computer,

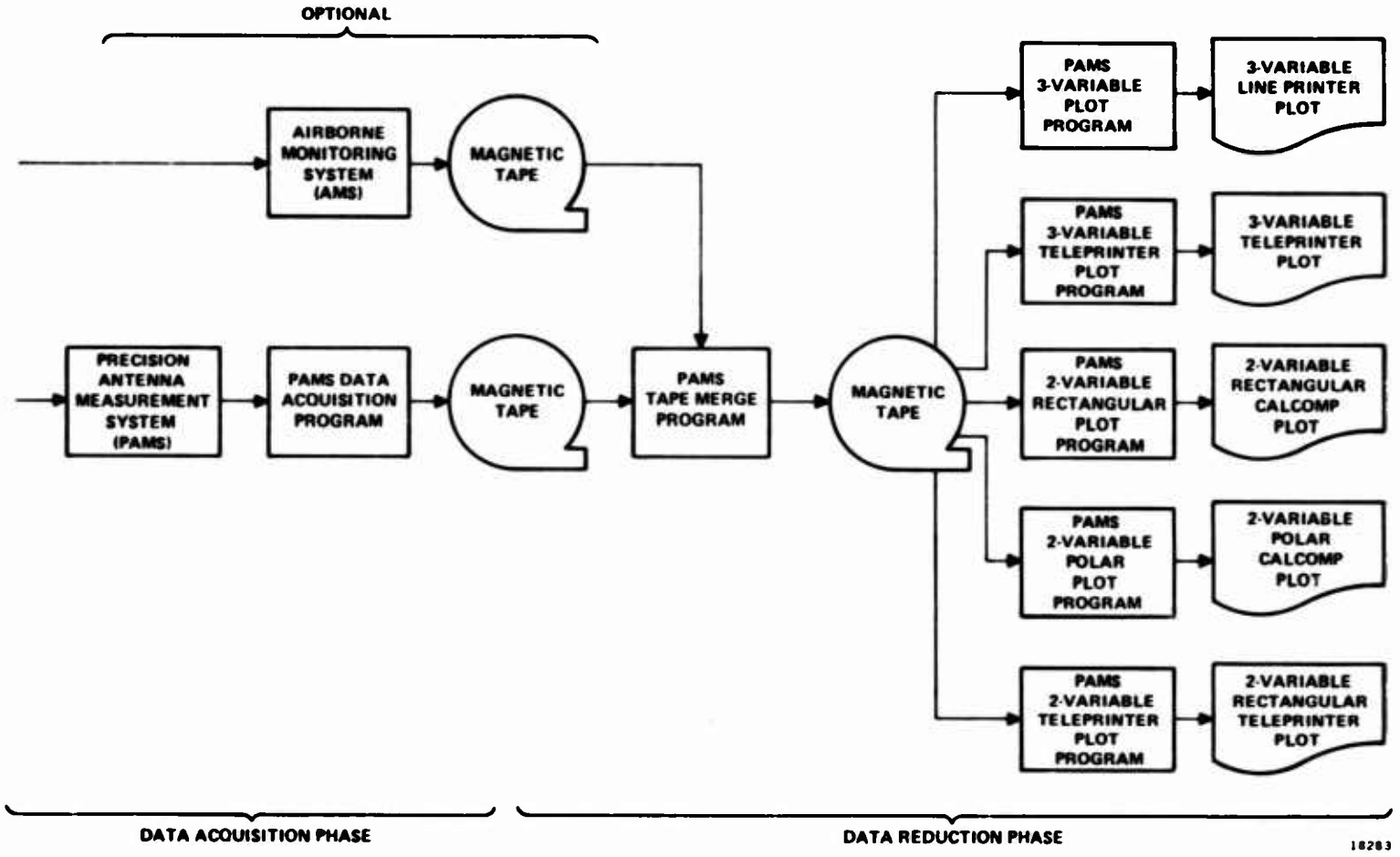

Figure 39. General Flow of Data Between Programs

upon command, initiates an automatic amplitude and frequency calibration run. Additional data such as date, aircraft type, antenna type, aircraft heading, aircraft pitch angle, and operator may be entered via the teletype. Before data are collected the operator selects the signal of interest by placing a cursor on the signal displayed on the panoramic oscilloscope. When several cursors are in use they may be sorted by pressing the flasher switch on the control panel. This causes the selected cursor to flash at a four-Hertz rate for easy identification. The system provides several options of data to be taken. These are:

1. Power (P)
2. Integrated or Power Density (Watts/MHz) (D)
3. Reflectivity (R)
4. Chaff (C)

The operator selects the type of data desired by typing in the appropriate letter for each activated cursor. Once the signals have been selected the system will begin collecting and storing data when the Start switch on the control panel is pressed. During the data collection mode it is possible to display on the line printer certain variables such as uncalibrated frequency and amplitude for each activated cursor as well as time, tracker position, and range. Data collection can be momentarily halted by pressing the Pause switch on the control panel. Data collection is resumed when the Run switch is pressed. A data run is ended by pressing the Stop switch. The Data Acquisition Program is terminated when the End of Flight switch is activated on the control panel.

4.6.2 PAMS Tape Merge Program

The Tape Merge Program performs the data reduction and prepares the data for the plotting routines. The input to this program is the magnetic tape that was recorded during data acquisition.

The program takes the angular data, aircraft heading, and aircraft pitch angle, and performs several coordinate transformations to transfer all angular data to the aircraft relative to its heading. The amplitude and frequency data are compared to the calibration data and corrected to real values. The received amplitude data are transferred, using the beacon equation, to the aircraft antenna system, resulting in an Effective Radiated Power (ERP) at the output of the antenna under test. The ERP (transmitter power at antenna input terminals x antenna gain) is then stored as a function of angular position relative to the aircraft heading. As the data are being plotted the computer prints a history of the data-taking conditions. This includes run numbers, aircraft heading and pitch angle, track radar used, cursor number and data type, frequency band, plus all other pertinent data indicated by console switch positions. The Tape Merge Program will also output error messages when there are insufficient data points, calibration errors, timing errors, and incorrect cursor information.

Provisions have been made to incorporate the output from an "Airborne Monitoring System" (AMS) to the tape merge at a later date. The AMS would be located on the test aircraft and would generate a magnetic tape with the roll, pitch, yaw, and altitude of the aircraft relative to its heading. In addition the AMS tape would include time which is synchronized with the station clock at the PAMS site. The data from the Data Acquisition tape and the AMS tape would then be merged using time as the

correlation reference. The incorporation of the AMS deletes the requirement of the operator to type in the aircraft heading and pitch angle for each data run. However, the most important function of the AMS system would be the ability to locate each data point with respect to the exact spatial position of the aircraft.

4.6.3 PAMS 3-Variable Plot Program

The 3-Variable Plot Program produces a plot of ERP as a function of azimuth (ϕ) and elevation (θ) angles. This plot is done on the HP 2778-01 line printer. The program looks for the maximum power level and then plots over a 40 db range down from that level. The power is plotted in 3 db rings with a letter from A through N assigned to each level, A being the highest. This power is decibels above one watt (dbw). The 3-variable plot is normally plotted over 360 degrees in azimuth (±180 degrees) and 180 degrees in elevation (±90 degrees). However, the operator can obtain an expanded plot by indicating the angular range of interest by teletype input. Another feature of the 3-Variable Plot Program is a data intensity plot. These plots are identical to the data plots except that the third variable represents the amount of data taken rather than the value of the data itself. Instead of a letter, the computer prints characters 1 through 9 and blank to indicate the number of data points used in the data plot. A blank indicates no data and progresses through 9 which indicates at least 100 data points were present at that point. In addition to the data plot itself the computer also prints out the elevation and azimuth angular resolution, the total number of data points in the plot and the values assigned to the letters in the plot.

4.6.4 PAMS 3-Variable Teleprinter Plot Program

This program is identical to that described in paragraph 4.6.3 with the exception that the data be plotted on the HP 2754B teleprinter. This option permits 3-variable plots to be made when the line printer is not available.

4.6.5 PAMS 2-Variable Rectangular Plot Program

The 2-Variable Plot Program produces 2-variable rectangular data plots on the Cal Comp 565 plotter according to the parameters specified by the operator via the teletype. The program searches the data tape to find the appropriate data, reads it into memory, bins the data, averages it, and then plots it. Three point interpolation is used to fill in missing data points. The operator selects either an azimuth or elevation angle as a constant. If the elevation angle is held constant the resulting plot is an azimuth pattern 360 degrees around the aircraft. When the azimuth angle is held constant an elevation pattern is plotted ±90 degrees from the nose of the aircraft. The angle is displayed on the abscissa while the power level is plotted on the ordinate of the paper. For the 2-variable plot the actual power level in dbw is used rather than a letter designation as in the 3-variable plot. In addition the frequency, frequency tolerance, polarization, receiver channel, data type, value of common angle, number of data points, and actual plotted points are printed on the plot.

4.6.6 PAMS 2-Variable Polar Plot Program

This 2-Variable Plot Program is identical to the program described in paragraph 4.6.5 with the exception that it is plotted in polar coordinates on the Cal Comp 565 rather than rectangular coordinates.

4.6.7 PAMS 2-Variable Teleprinter Plot Program

This 2-Variable Plot Program is identical to the program described in paragraph 4.6.5 with the exception that it is printed on the HP 2754B Teleprinter.

4.6.8 PAMS Test Program

The PAMS Test Program tests all of the interface hardware between the PAMS console and the computer, and certain portions of the PAMS hardware. The program was designed for preventive maintenance and partial diagnosis of hardware failures. The program is subdivided into independent test routines which test individual portions of the hardware. The test routines may be run sequentially or individually at the operators discretion. Tests that fail result in a printout on the line printer describing the conditions of the failure. The printout may be optionally suppressed by the operator. Tests 1 through 11 test to see if the proper flags are set between console and computer, time is correct, track radar range and position angles are read correctly, and that the amplitude and frequency calibration of the receivers are operating correctly. Tests 12 through 15 are special purpose looping routines for trouble shooting. These are not standard tests and will not be executed when running tests in the sequential mode of operation. These tests are selected by inputting their address into the computer via the switch register.

SECTION V

OPERATIONAL RESULTS

5.1 INTRODUCTION

This Section presents the operational results of the PAMS system tests and antenna pattern measurements conducted at the Verona Test Annex of the Rome Air Development Center, Rome, New York. The tests were conducted in three phases. The first phase consisted of tests to verify the overall receiver performance. The second phase was devoted to measuring antenna patterns in a ground range environment. The tests essentially demonstrated that the overall system was operational and that the data collection, reduction and plotting computer programs were operating correctly. The third phase was concerned with taking antenna patterns of antennas aboard an RADC KC-131 test aircraft.

5.2 RECEIVER PERFORMANCE

The receiver system was tested to define its level of performance and establish operating tolerances. The tests were conducted using calibrated amplitude and frequency signals fed into the receiver at the RF input terminals of the receiver housing. The basic test set up is shown in figure 40. The following parameters were measured during this phase of the program

1. Receiver operating bandwidth
2. Frequency accuracy
3. IF bandwidth
4. Sensitivity
5. Amplitude accuracy

The receivers were designed to have a minimum overlap of 25 MHz at each end of the band. The measured performance showed that the actual overlap was on the order of 40 MHz for each receiver. The uncalibrated frequency accurancy was measured using the 100 MHz frequency markers from the harmonic generator and comparing the console reading with the reading of the precision frequency counter. In all cases the uncalibrated accuracy was better than the design tolerance of two percent. The AFC performance was checked in a similar manner and the design goal of 0.1 percent was met for all receivers in the CW mode. The pulsed AFC error was found to be outside the tolerance initially; however, the major error was due to frequency pulling of the signal generator in the pulsed mode. The frequency pulling was partially eliminated and re-measurements indicated that the accuracy was better than 0.5 percent. Calibrated frequency accuracy using the computer was 0.1 percent or better for all receivers. The selectable IF bandwidths were measured next and the 1.5 MHz, 3.0 MHz, and 6.0 MHz bandwidths were within tolerance for all receivers. The 10 MHz bandwidth is actually a misnomer since in this position the receiver operates in basically a wide-open mode. Consequently, the bandwidth that is presented is essentially the bandpass of the YIG filter and is 13 MHz to 16 MHz for all receivers.

The specification for the receiver sensitivity was -100 dbm unity signal to noise with a 1.5 MHz IF bandwidth. The actual measured performance is shown in tables VI and VII. It can be seen from table VI that both the S- and C-band receivers exceeded the

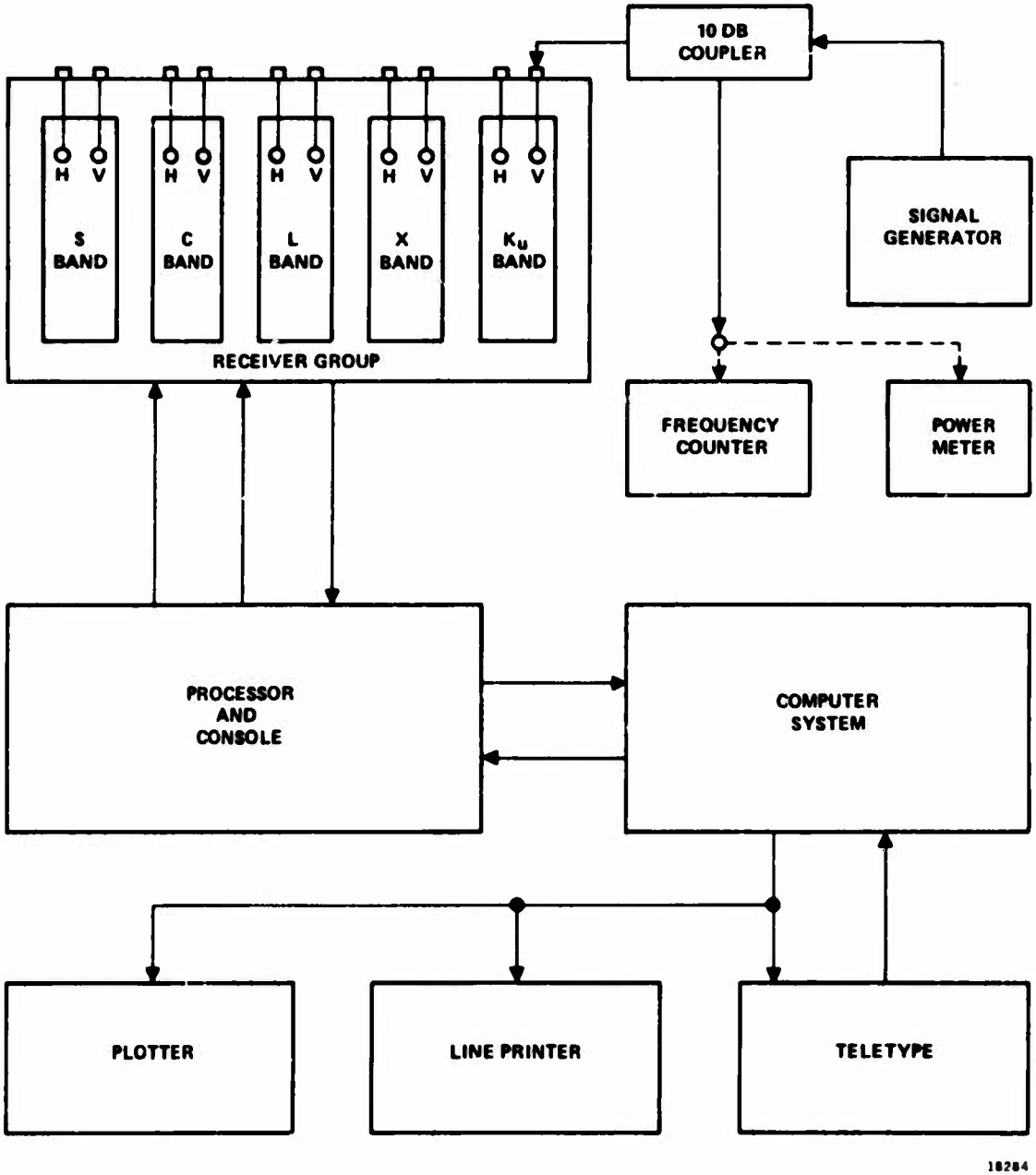

Figure 40. Equipment Configuration

TABLE VI

RECEIVER SENSITIVITIES

	Vertical S/N	Horizontal S/N
S-Band Sensitivity		
2.0 GHz	-101 dbm	-107 dbm
2.5 GHz	-103 dbm	-104 dbm
3.0 GHz	-103.6 dbm	-106 dbm
3.5 GHz	-103 dbm	-107 dbm
4.0 GHz	-106 dbm	-109 dbm
C-Band Sensitivity		
4.0 GHz	102 dbm	103 dbm
5.0 GHz	104 dbm	105 dbm
6.0 GHz	104 dbm	104 dbm
7.0 GHz	101 dbm	102 dbm
8.0 GHz	101 dbm	102 dbm
X-Band Sensitivity		
8.0 GHz	103 dbm	105 dbm
9.0 GHz	103 dbm	103 dbm
10.0 GHz	104 dbm	106 dbm
11.0 GHz	96 dbm	105 dbm
12.0 GHz	91 dbm	92 dbm
K_u-Band Sensitivity		
12.0 GHz	109 dbm	97 dbm
13.5 GHz	100 dbm	99 dbm
15.0 GHz	104 dbm	107 dbm
16.5 GHz	99 dbm	95 dbm
18.0 GHz	89 dbm	95 dbm

TABLE VII

UHF/L-BAND DOWN CONVERTER SENSITIVITIES

	Vertical S/N	Horizontal S/N
UHF/S-Band Sensitivity		
500 MHz	100.2 dbm	100.2 dbm
750 MHz	102.4 dbm	102.9 dbm
950 MHz	102.5 dbm	102.3 dbm
L/S-Band Sensitivity		
1,000 MHz	99.0 dbm	103.6 dbm
1,500 MHz	100.5 dbm	102.3 dbm
1.950 MHz	99.3 dbm	101.8 dbm
UHF/C-Band Sensitivity		
500 MHz	102 dbm	105 dbm
750 MHz	102.2 dbm	105 dbm
950 MHz	102.3 dbm	104.3 dbm
L/C-Band Sensitivity		
1,000 MHz	95.0 dbm	101.6 dbm
1.500 MHz	95.7 dbm	100.8 dbm
1.950 MHz	96.5 dbm	99.3 dbm

specification. The actual sensitivity of the S-band receiver is approximately 3.5 db better than is shown. The reduction in the basic sensitivity is due to the signal path through the L-band converter. The additional circuitry required by the converter consists of a 3 db hybrid and two coax switches ahead of the S-band receiver with 3.5 db insertion loss. The lower sensitivities at X and K_u band result from a combination of conditions. These are increased insertion loss in the YIG filters, particularly at the higher frequencies, lower local oscillator power resulting in less than optimum mixing, and increased noise figures of the mixers themselves.

The data in table VII indicates that the sensitivity of S- and C-band receivers are approximately 3 to 6 db less when used in the converter mode of operation. This reduction in sensitivity is due to the increased insertion loss of the network and the noise figure of the mixer and broadband amplifiers. The poorest sensitivity occurs when the mixer upper sidebands are used for frequency conversion. Overall, the receiver performance exceeded most of the original design goals.

The last tests made on the receiver system were uncalibrated and calibrated amplitude accuracies. The results of these tests are summarized in table VIII. The calibrated signal input was -60 dbm for all the measurements. The design goal was for uncalibrated amplitude errors of less than ±5 db and calibrated amplitude errors not to exceed ±1.0 db. As can be seen from table VIII these goals were generally exceeded. The RMS error of this data is 0.562 db. The worst case showed up in K_u band which was somewhat expected after the results of the sensitivity tests. At that, the calibrated amplitude error was excessive at only one point in the horizontal channel at 16.5 GHz.

A computer printout of calibrated amplitude and frequency is shown in table IX. The attenuator column contains the exact calibrated levels while the horizontal and vertical columns contain the values read for the calibrated inputs. These two columns then are the look-up tables used during tape merge to reduce the data. For example an amplitude with a value of -64.71 dbm recorded during data acquisition is compared against the look-up table during the data reduction and is corrected to the real value of -62 dbm. Also shown in table IX is the frequency calibration over an operating bandwidth of approximately 1700 MHz. The calibration is in 100 MHz increments from 2.3 GHz to 4.0 GHz. This is the look-up table used for frequency during data reduction. The computer uses a linear interpolation for frequencies which fall between the 100 MHz calibration points. This completed the first phase of the test program.

5.3 STATIC ANTENNA PATTERNS

The second phase of the test program consisted of taking antenna patterns of a set of horn antennas located eight nautical miles from the PAMS site. Figure 41 is an approximate profile of the test. The location of the site was not the most desirable; however, the location offered the best line of sight to the PAMS antennas. The site and the fact that it was not possible to elevate the antennas above the ground to any degree introduced some multipath and lobing problems along with some polarization skewing. These problems did not interfere with the primary purpose of this phase of the test program which was to successfully demonstrate the ability of the system to collect the data and plot an antenna pattern. The test site at Stockbridge consisted of a mobile van equipped with all of the signal sources and antennas for the tests. A mobile communication link was maintained with the PAMS site during the test. Figure 42 illustrates the field test site.

TABLE VIII

RECEIVER AMPLITUDE ACCURACY

Freq	Uncalibrated Vertical Amplitude (db)	Calibrated Vertical Amplitude (db)	Uncalibrated Horizontal Amplitude (db)	Calibrated Horizontal Amplitude (db)
S Band				
2.0	1.7	-0.3	1.9	0.0
2.5	0.95	0.5	2.4	-0.6
3.0	0.6	0.0	1.9	-0.6
3.5	0.1	0.7	0.6	0.1
4.0	2.5	-0.2	1.2	-0.5
C Band				
4.0	1.8	-0.4	1.0	0.0
5.0	-0.3	0.2	-2.8	0.2
6.0	-2.8	0.1	-2.2	-0.7
7.0	-0.5	-0.3	-0.5	-0.4
8.0	-3.0	-0.3	3.2	-0.3
X Band				
8.0	-1.4	-0.6	-0.9	-1.5
9.0	-1.0	0.2	-1.1	0.7
10.0	-1.9	0.7	-0.7	-0.2
11.0	0.1	1.2	0.2	0.0
12.0	3.0	-0.6	3.7	-0.7
K_u Band				
12.0	0.6	0.1	1.9	0.0
13.5	0.2	-0.5	1.7	-0.8
15.0	-1.5	0.0	0.0	0.0
16.5	10.0	0.2	5.0	-3.2
18.0	10.5	1.2	15.0	-0.1

TABLE IX

COMPUTER AMPLITUDE AND FREQUENCY CALIBRATION RUN

CALIBRATION DATA

CURSOR	FREQUENCY (GHZ.)	HORIZONTAL (DBM)	VERTICAL (DBM)	ATTENUATOR (DBM)
1	2.312	- 40.95	- 38.79	-40
	2.411	- 42.03	- 40.05	-41
	2.510	- 42.54	- 40.75	-42
	2.610	- 43.57	- 42.05	-43
	2.708	- 44.18	- 42.86	-44
	2.808	- 44.94	- 43.88	-45
	2.907	- 45.97	- 45.30	-46
	1.007	- 46.81	- 46.28	-47
	3.106	- 47.91	- 47.68	-48
	3.205	- 49.23	- 49.15	-49
	3.304	- 50.21	- 49.84	-50
	3.404	- 51.92	- 51.16	-51
	3.504	- 52.83	- 51.81	-52
	3.603	- 54.64	- 53.12	-53
	3.704	- 55.62	- 53.93	-54
	3.806	- 56.86	- 54.76	-55
	3.909	- 58.47	- 56.15	-56
	4.013	- 59.16	- 57.14	-57
		- 60.28	- 58.49	-58
		- 61.58	- 59.97	-59
		- 62.74	- 60.72	-60
		- 64.02	- 62.03	-61
		- 64.71	- 62.72	-62
		- 65.73	- 63.98	-63
		- 66.16	- 64.73	-64
		- 66.63	- 65.51	-65
		- 67.36	- 66.55	-66
		- 67.76	- 67.52	-67
		- 68.48	- 68.76	-68
		- 69.23	- 69.98	-69
		- 70.06	- 70.41	-70
		- 70.88	- 71.61	-71
		- 71.41	- 72.38	-72
		- 72.55	- 73.44	-73
		- 73.24	- 74.13	-74
		- 74.01	- 74.84	-75
		- 75.07	- 75.76	-76
		- 76.15	- 76.47	-77
		- 77.35	- 77.49	-78
		- 79.46	- 78.53	-79
		- 80.66	- 78.89	-80
		- 82.39	- 79.99	-81
		- 83.53	- 80.38	-82
		- 84.51	- 81.29	-83
		- 84.65	- 81.97	-84
		- 85.30	- 82.15	-85
		- 86.28	- 83.25	-86
		- 86.77	- 83.63	-87
		- 87.26	- 84.35	-88
		- 87.74	- 84.59	-89
		- 88.01	- 84.47	-90
		- 88.80	- 84.85	-91
		- 88.84	- 84.92	-92
		- 88.94	- 85.26	-93
		- 89.25	- 85.34	-94
		- 89.23	- 85.49	-95
		- 89.33	- 85.81	-96
		- 89.62	- 86.06	-97
		- 89.35	- 85.91	-98
		- 89.64	- 86.20	-99

18308

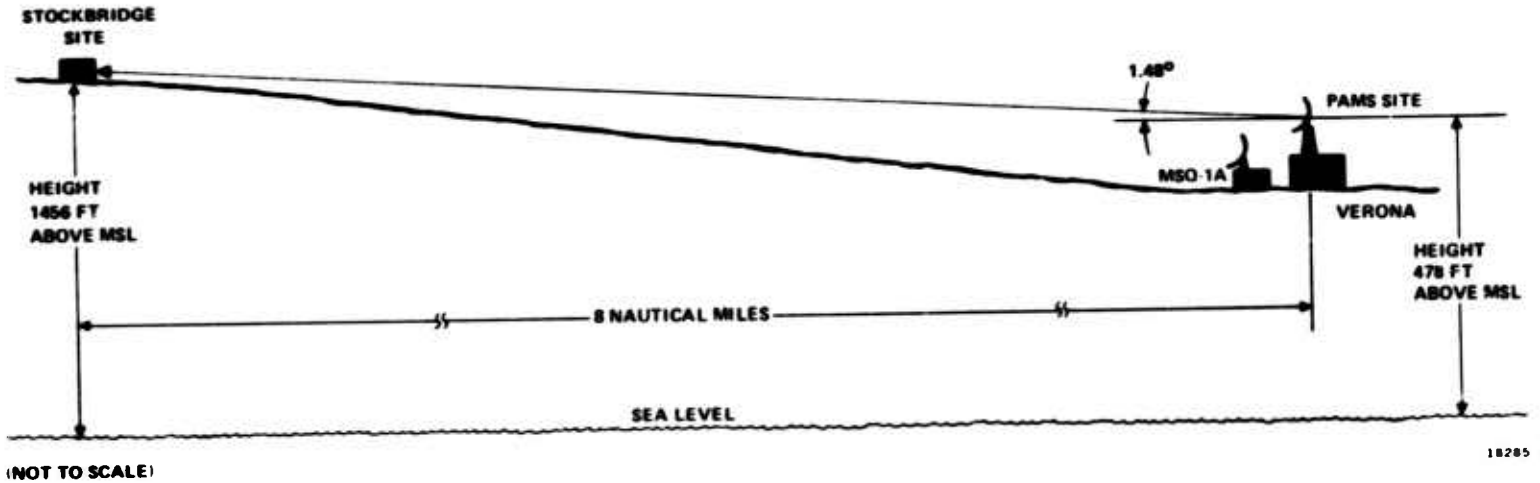

Figure 41. Antenna Pattern Range

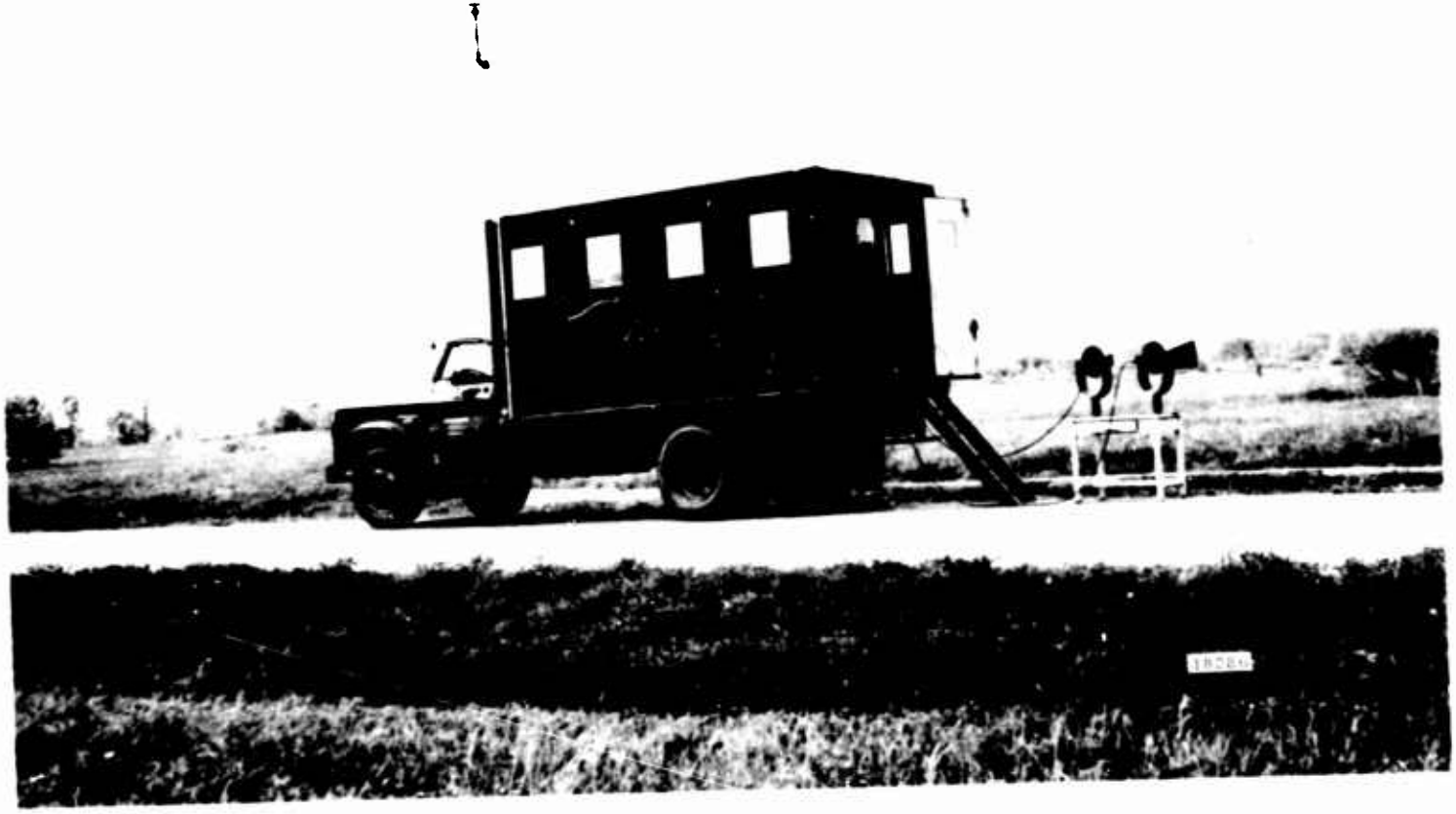

Figure 42. Stockbridge Test Site

The antennas were electrically boresighted by positioning the antennas at both sites for maximum signal strength at the PAMS receiver. The MSQ-1A track radar was used for final angular adjustment and range. The final configuration resulted in an elevation angle of 1.48 degrees. With this small elevation angle and the fact that the nominal halfpower beamwidths of the horns were nominally 20 to 30 degrees, the propagation anomalies previously mentioned were to be expected. After final alignment the horn antennas were rotated in five-degree increments ±150 to ±180 degrees from boresight. The results of these tests are shown in figures 43 through 50. The patterns are shown in both rectangular and polar coordinate to illustrate the plotting formats. As it was not possible to collect adequate data for a three-dimensional plot in this test configuration a pattern was simulated. This was accomplished by inputting amplitude data to the S-band receiver with a signal generator and varying the amplitude to approximate an antenna. The MSQ-1A angular and range data were simulated with a set of synchros. The results of this test are shown in figures 51 and 52.

The first antenna pattern pair, figures 43 and 44, shows the L-band horn pattern at 1525 MHz. The effects of multipath are readily apparent in the skewing of the pattern and sidelobe structure. The C- and X-band antennas were run simultaneously and the results given in figures 45 through 48. There was no apparent coupling between the antennas nor were any spurious or harmonic signals detected at the PAMS site. A sample of the reduced data is given in table X. The printout gives the switch settings for both receivers during the test. Also the average values for the frequency and amplitude are given for each cursor during the run. The C-band pattern was compared to a pattern of the same horn taken in an anechoic chamber prior to tests. There was excellent correlation out to the 10 db beamwidth. Beyond that point the effects of reflection and multipath entered into the picture, causing the nulls to fill in and broaden the pattern. The high noise level is the result of noise limiting in the receiver.

The X-band horn pattern as shown in figures 47 and 48 does not exhibit the effects of reflection as in the other patterns. The large backlobe is the result of energy being reflected from the side of the van as the antenna was rotated in azimuth.

The last pattern pair, figures 49 and 50, are for the K_u band horn. Here the influence of reflections is quite pronounced resulting in a scalloping effect on the pattern. During the K_u band test the received data was monitored. Table XI illustrates the format for the real time printout. If more than one cursor were activated the printout would sequentially sample the data for each cursor.

The range was not calibrated prior to the test, nor was a lobing profile made of the site. Consequently it was very difficult to predict what effects the range would have on the patterns. However, the tests did successfully demonstrate the capability of the system to plot antenna patterns which compared favorably with a pattern made in a controlled environment. Figure 51 illustrates the three-dimensional plotting capability of the system on the teleprinter. Figure 52 shows how the 3-variable plot can be expanded, giving a greater angular resolution.

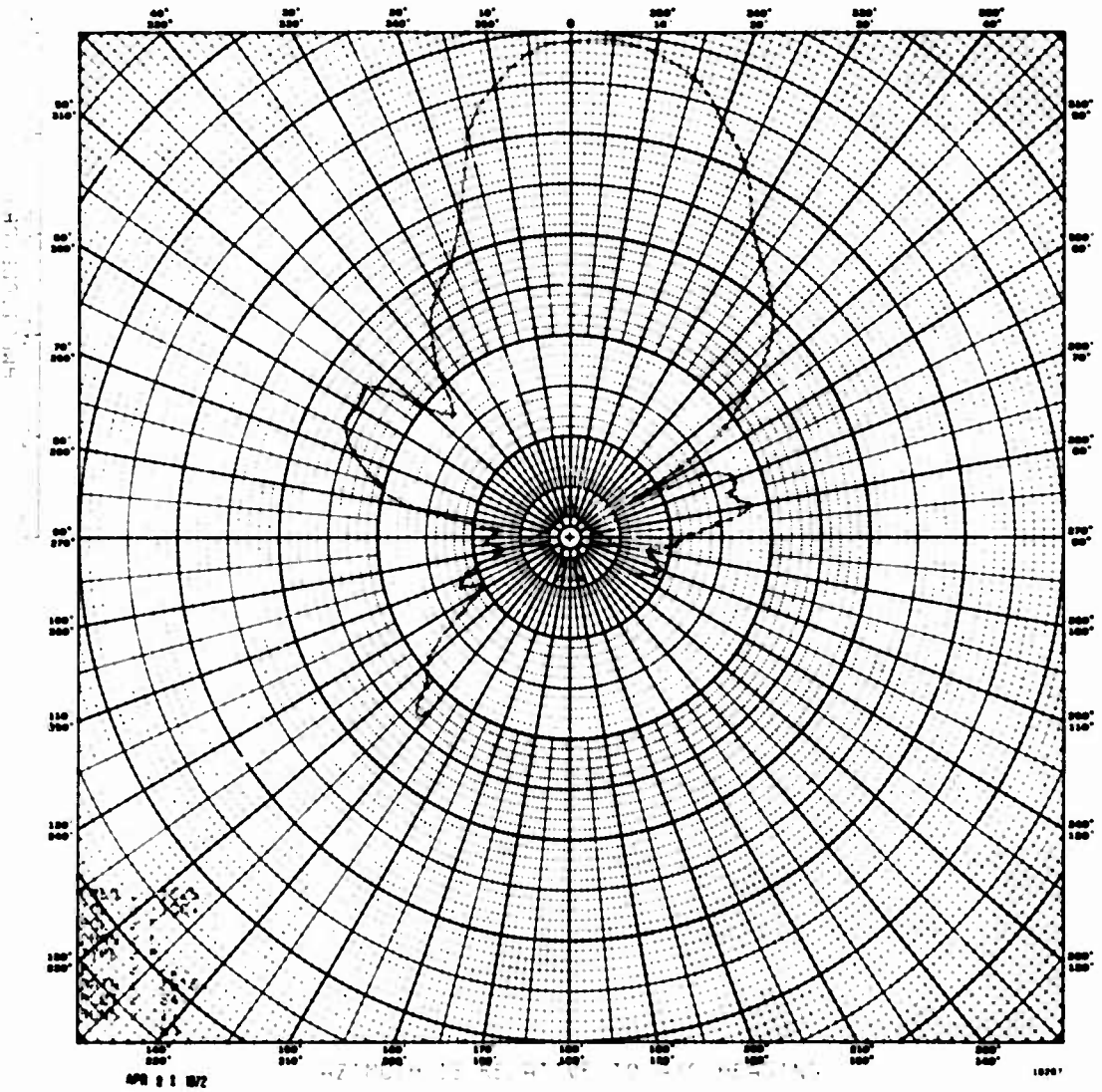

Figure 43. L-Band Horn Antenna (Polar Coordinate)

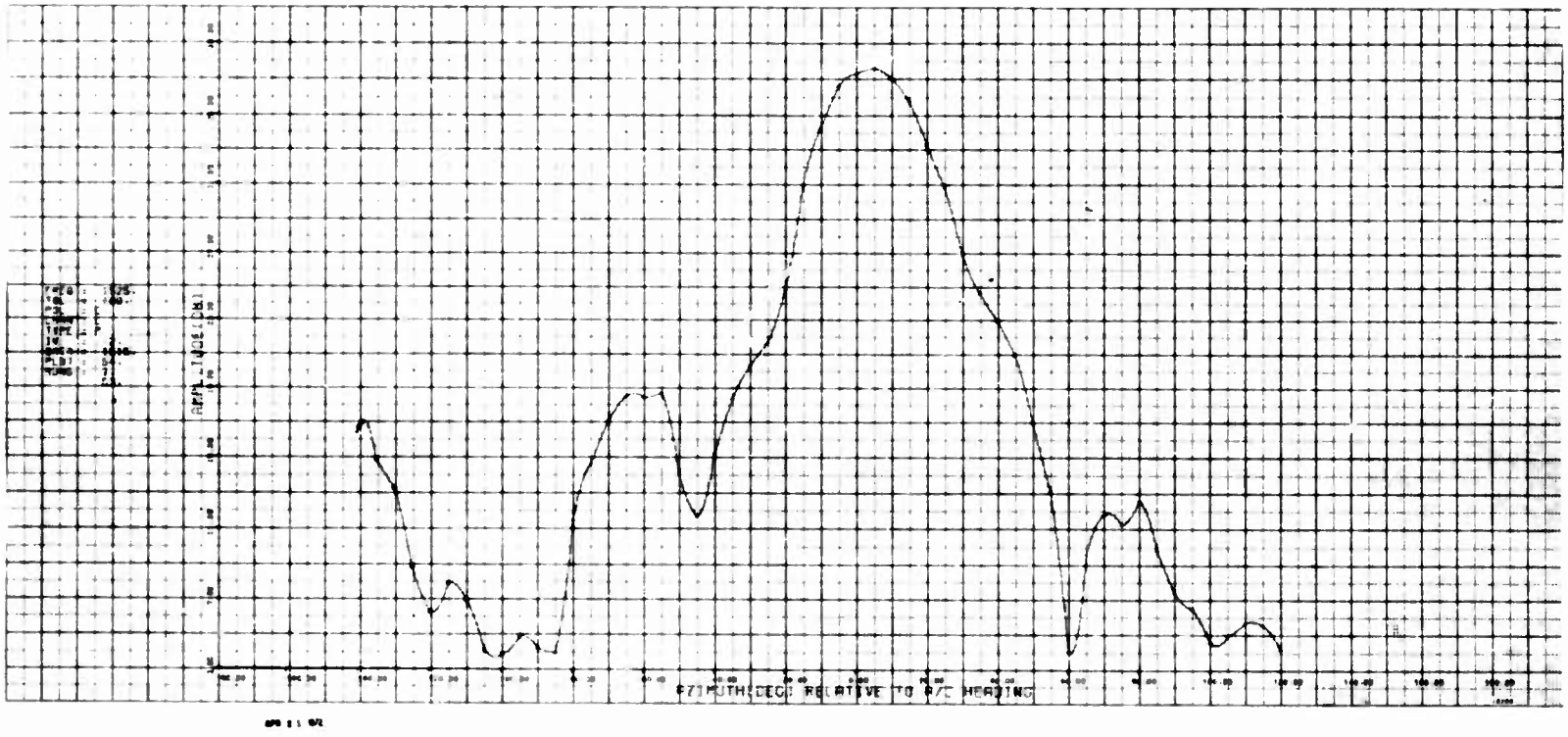

Figure 44. L-Band Horn Antenna (Rectangular Coordinate)

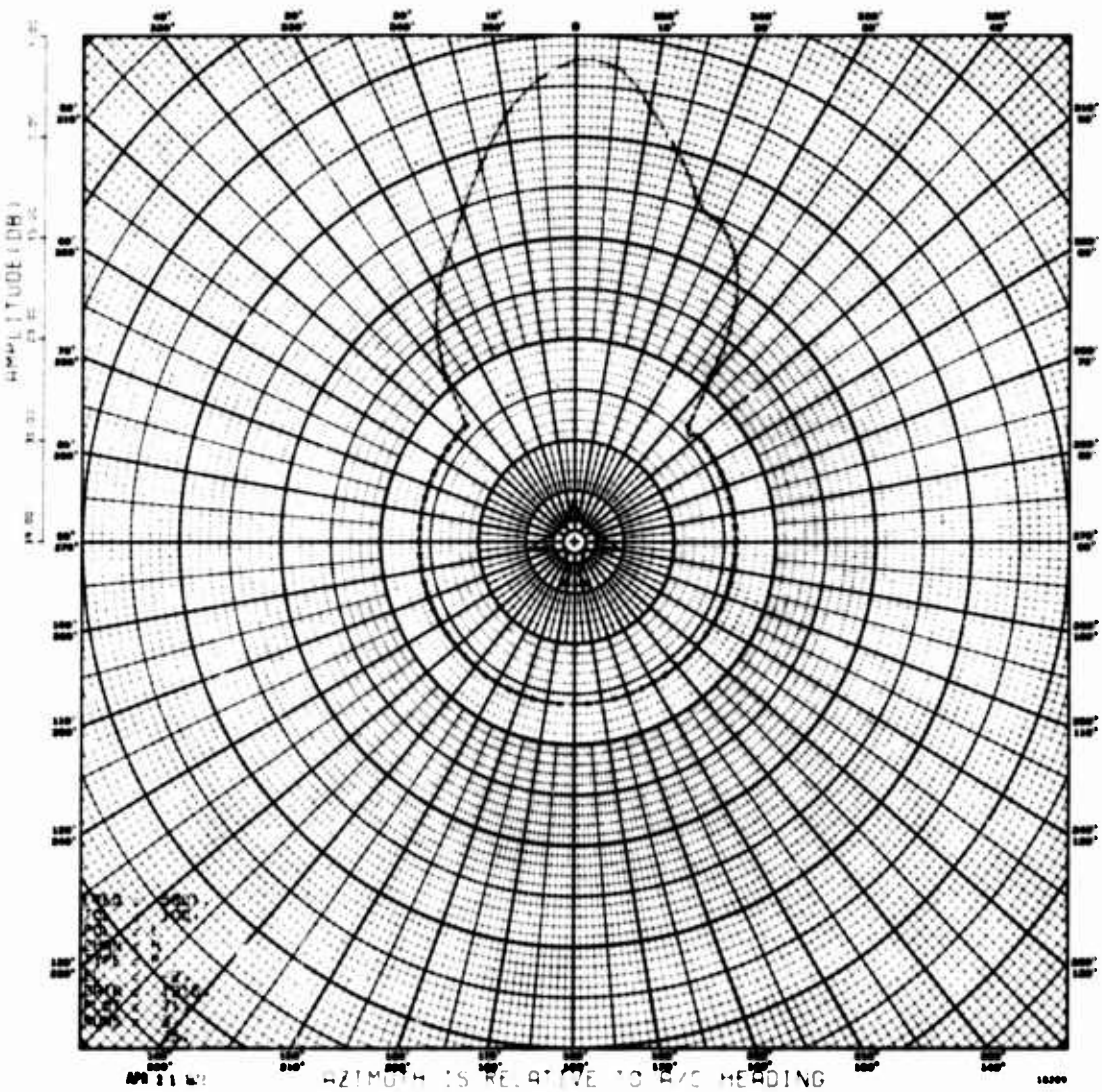

Figure 45. C-Band Horn Antenna (Polar Coordinate)

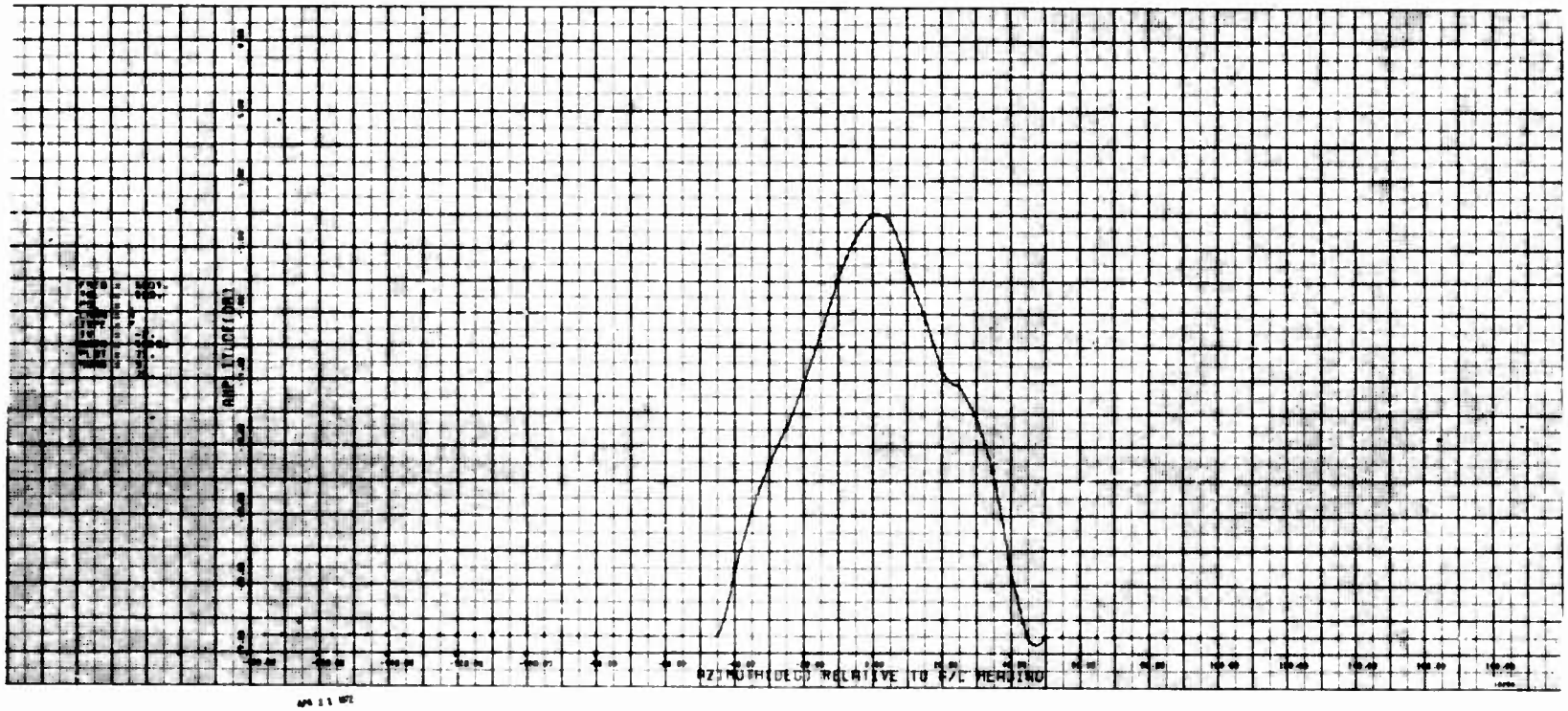

Figure 46. C-Band Horn Antenna (Rectangular Coordinate)

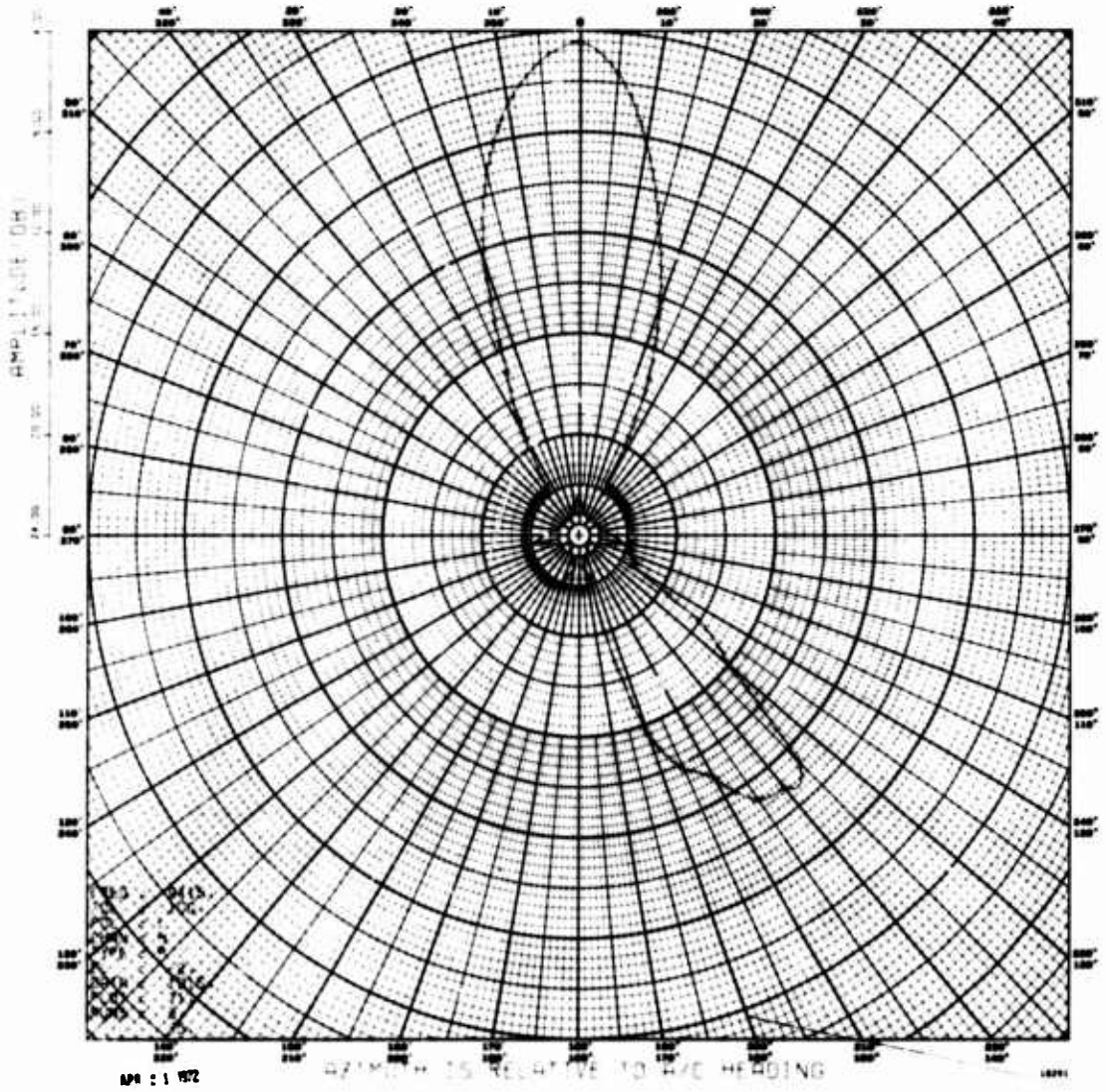

Figure 47. X-Band Horn Antenna (Polar Coordinate)

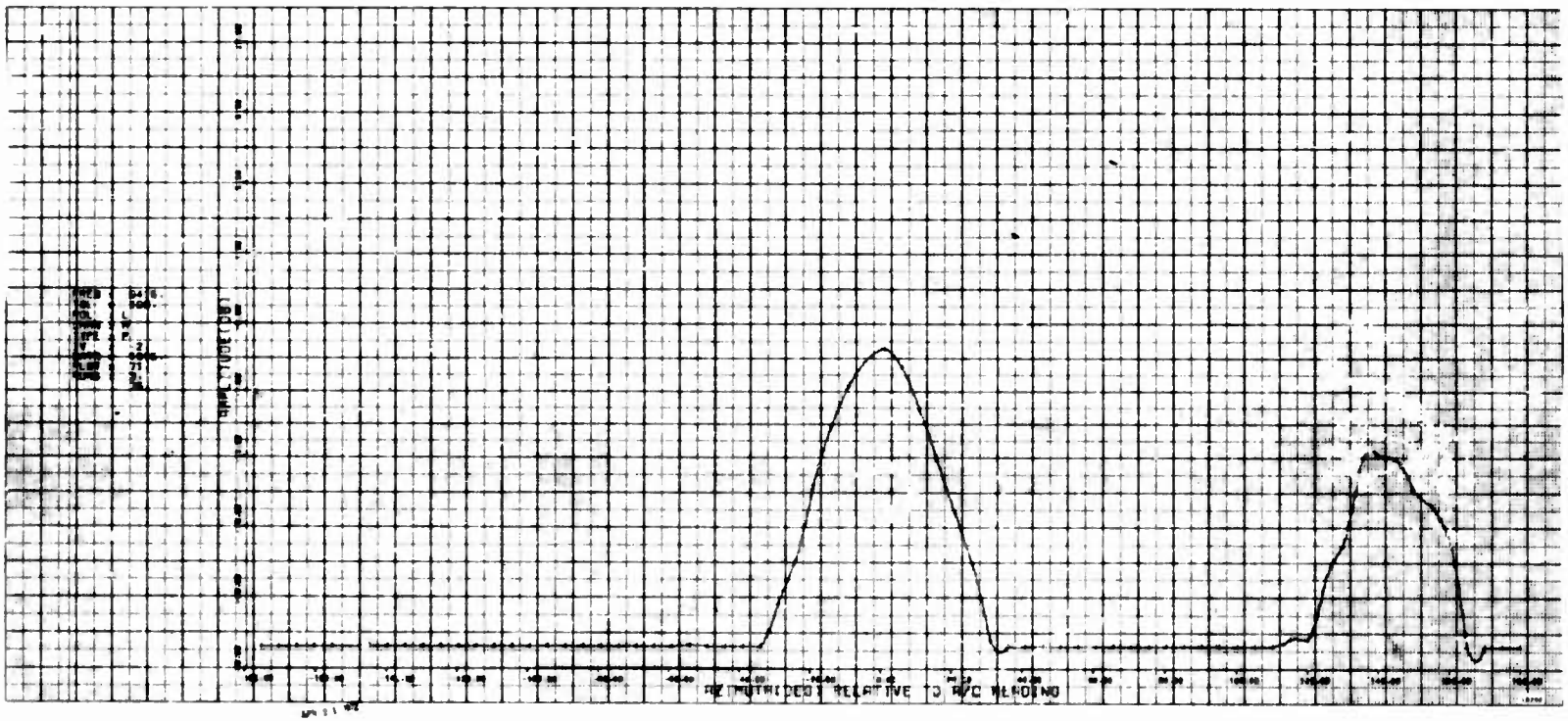

Figure 48. X-Band Horn Antenna (Rectangular Coordinate)

TABLE X

REDUCED DATA - TAPE MERGE (RUN 1, C AND X BANDS)

RUN 1

TIME: 16/43/54 TO 16/44/11
HEADING = 14.0 DEG. • PITCH = .0 DEG.
MSO-1 TRACKER

CURSOR	DATA TYPE	RECEIVER	FREQ. MODE	CHANNEL SWITCH	ATTEN. (DB)	POLAR.	IF-BAND. (MHZ)	AFC STATUS	L-BAND	TR-POWER (KW)	TR-GAIN (DB)	PULSEWIDTH (MICROSEC)	BEAMWIDTH (DEG)
1	POWER	C	SWEPT	NORMAL	:	LINEAR	6.0	OFF/HORZ	OUT	.0	.0	.0	.0
2	POWER	X	SWEPT	NORMAL	:	LINEAR	3.0	OFF/HORZ	OUT	.0	.0	.0	.0

21 APRIL 72 STOCKBRIDGE STATIC TEST. C AND X BANDS.

AVERAGE VALUES
TRACKER AZIMUTH = 193.90 DEGREES • TRACKER ELEVATION = 1.48 DEGREES • TRACKER RANGE = 8.045 NAUTICAL MILES

CURSOR	FREQ. (MHZ)	HORZ. (DBM)	VERT. (DBM)	TRANS. HORZ.	TRANS. VERT.	AZIMUTH/WIDTH (DEG) (FEET)	ELEVATION/HEIGHT (DEG) (FEET)
1	5031.	-74.773	-89.044	-.866	-15.585	-.12	-1.54
2	9414.	-83.234	-92.872	-5.006	-14.275	-.12	-1.62

18309

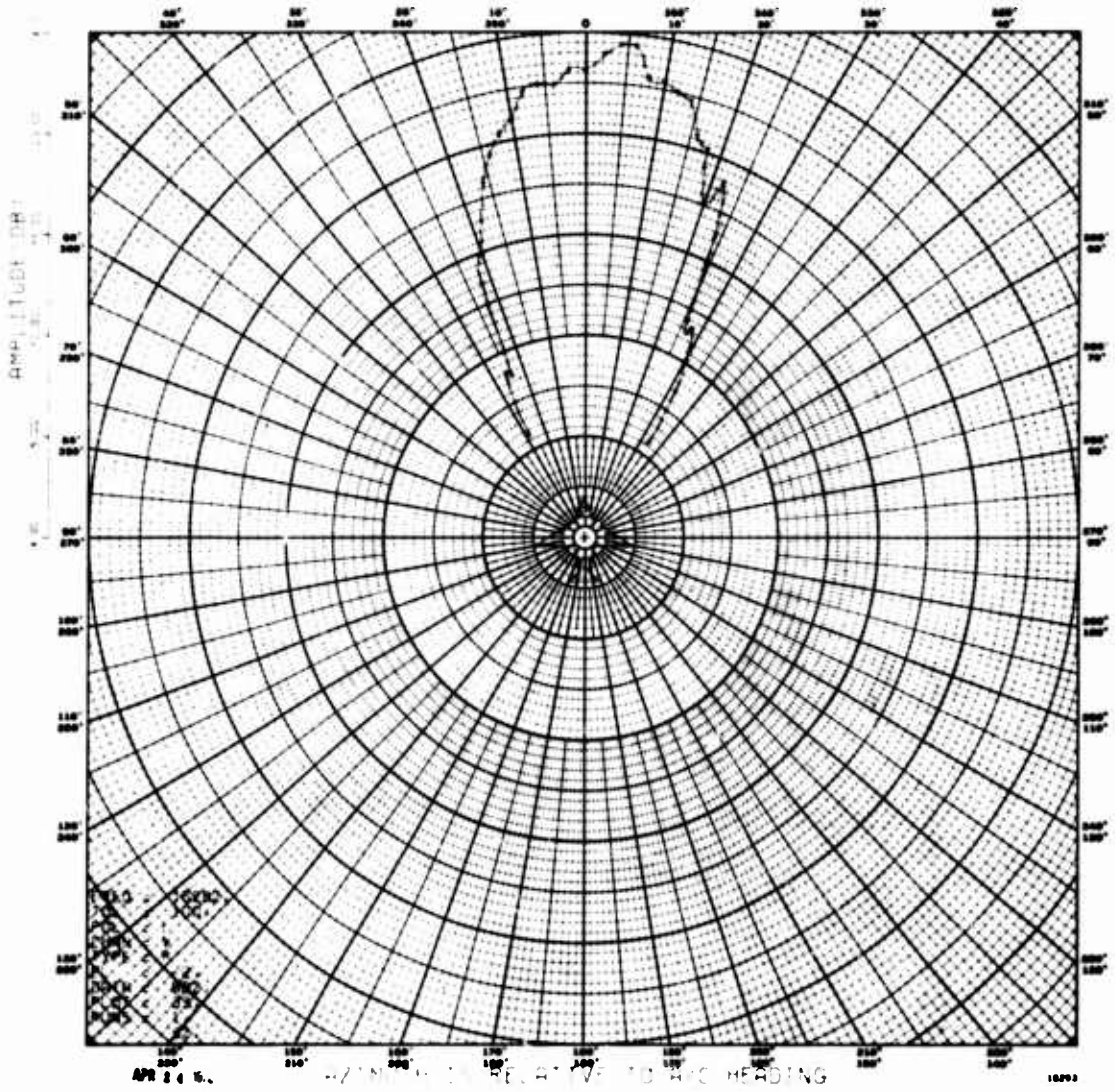

Figure 49. K_u-Band Horn Antenna (Polar Coordinate)

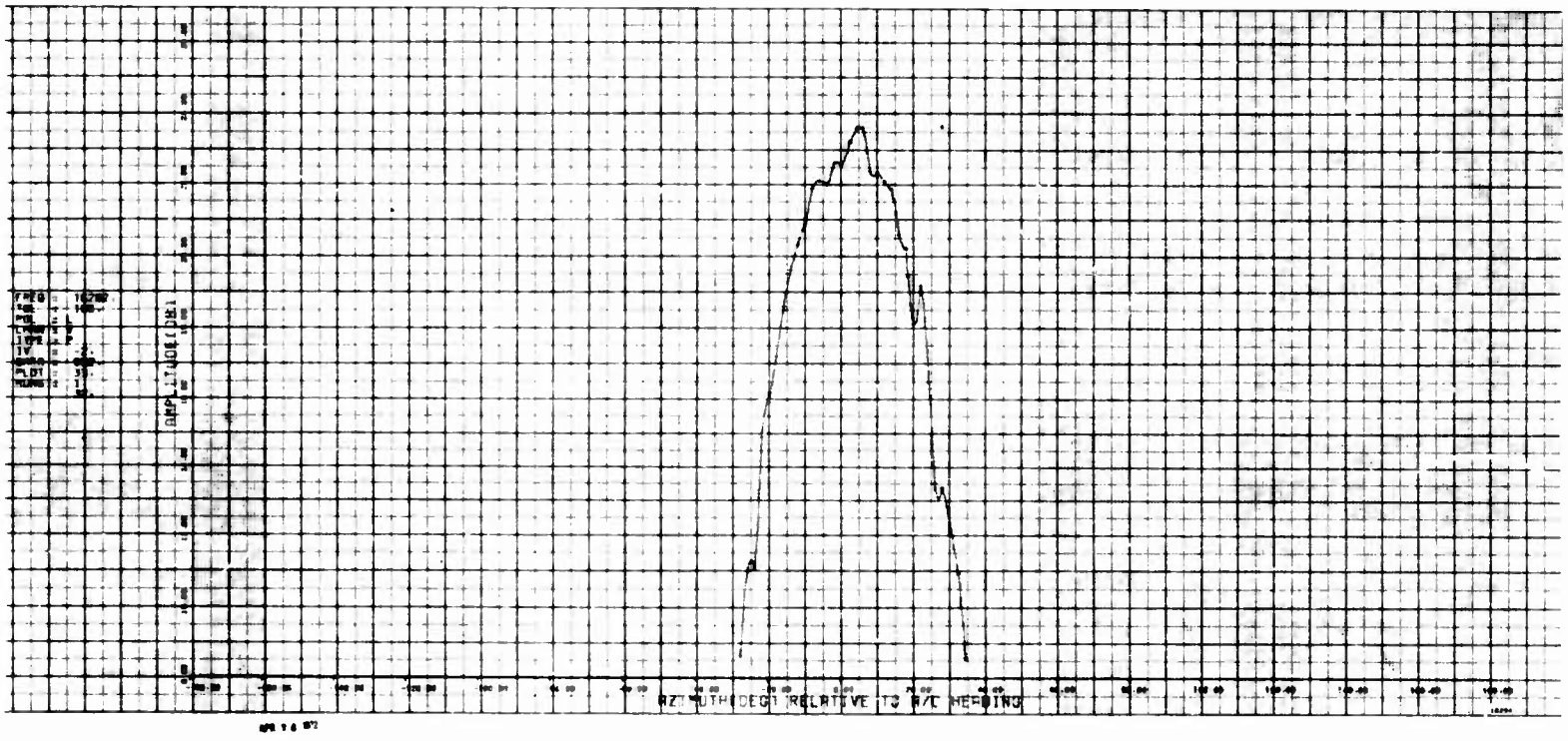

Figure 50. K_u-Band Horn Antenna (Rectangular Coordinate)

TABLE XI

REAL TIME PRINTOUT

CURSOR	FREQUENCY(GHZ.)	HORIZONTAL(DBM)	VERTICAL(DBM)	HOURS/MIN./SEC.	RANGE(N. MILES)	AZIMUTH(DEGREES)	ELEV.(DEGREES)
1	16.245	- 80.01	- 65.40	19/06/33.7	8.07	194.10	001.50
1	16.245	- 83.21	- 64.31	19/06/34.8	8.07	194.10	001.54
1	16.245	- 83.31	- 65.08	19/06/35.8	8.07	194.10	001.54
1	16.245	- 81.13	- 64.61	19/06/36.9	8.07	194.10	001.44
1	16.245	- 82.19	- 65.04	19/06/37.7	8.07	194.10	001.58
1	16.246	- 81.01	- 65.38	19/06/38.8	8.07	194.10	001.50
1	16.245	- 79.59	- 65.27	19/06/39.8	8.07	194.10	001.58
1	16.245	- 80.46	- 64.20	19/06/40.9	8.07	194.10	001.54
1	16.244	- 82.01	- 64.71	19/06/41.7	8.07	194.10	001.48

CURSOR	FREQUENCY(GHZ.)	HORIZONTAL(DBM)	VERTICAL(DBM)	HOURS/MIN./SEC.	RANGE(N. MILES)	AZIMUTH(DEGREES)	ELEV.(DEGREES)
1	16.243	- 80.58	- 66.06	19/07/24.9	8.06	194.00	001.44
1	16.245	- 80.62	- 65.22	19/07/25.9	8.06	194.00	001.44
1	16.245	- 83.27	- 65.18	19/07/26.7	8.06	194.04	001.40
1	16.245	- 82.70	- 65.63	19/07/27.8	8.06	194.04	001.38
1	16.244	- 82.96	- 64.51	19/07/28.9	8.06	194.04	001.44
1	16.245	- 84.08	- 65.12	19/07/29.9	8.06	194.04	001.40
1	16.245	- 85.55	- 63.42	19/07/30.7	8.08	194.04	001.38
1	16.245	- 81.29	- 65.36	19/07/31.8	8.09	194.04	001.44
1	16.245	- 79.91	- 65.93	19/07/32.9	8.09	194.04	001.38

CURSOR	FREQUENCY(GHZ.)	HORIZONTAL(DBM)	VERTICAL(DBM)	HOURS/MIN./SEC.	RANGE(N. MILES)	AZIMUTH(DEGREES)	ELEV.(DEGREES)
1	16.245	- 81.88	- 65.85	19/08/28.9	8.02	194.20	001.54
1	16.245	- 83.88	- 65.82	19/08/29.9	8.07	194.10	001.50
1	16.244	- 84.10	- 66.04	19/08/30.7	8.07	194.04	001.44
1	16.245	- 84.88	- 65.93	19/08/31.8	8.07	194.00	001.60
1	16.245	- 84.88	- 65.40	19/08/32.9	8.07	194.00	001.54
1	16.245	- 83.88	- 65.67	19/08/33.9	8.07	194.00	001.44
1	16.244	- 84.47	- 66.52	19/08/34.7	8.07	194.00	001.58
1	16.245	- 84.24	- 66.54	19/08/35.8	8.07	194.00	001.44
1	16.245	- 82.82	- 66.38	19/08/36.9	8.07	194.00	001.34
1	16.244	- 83.51	- 66.22	19/08/37.9	8.07	194.00	001.48

CURSOR	FREQUENCY(GHZ.)	HORIZONTAL(DBM)	VERTICAL(DBM)	HOURS/MIN./SEC.	RANGE(N. MILES)	AZIMUTH(DEGREES)	ELEV.(DEGREES)
1	16.245	- 83.72	- 66.71	19/09/01.9	8.08	194.04	001.40
1	16.245	- 83.51	- 68.09	19/09/02.7	8.08	194.04	001.50
1	16.245	- 85.20	- 66.26	19/09/03.8	8.08	194.04	001.50
1	16.245	- 84.24	- 64.47	19/09/04.9	8.08	194.04	001.50
1	16.244	- 85.85	- 66.67	19/09/05.9	8.08	194.04	001.44
1	16.245	- 85.79	- 65.97	19/09/06.7	8.08	194.04	001.40
1	16.245	- 85.51	- 67.41	19/09/07.8	8.08	194.04	001.50
1	16.244	- 84.75	- 66.12	19/09/08.9	8.08	194.04	001.54

CURSOR	FREQUENCY(GHZ.)	HORIZONTAL(DBM)	VERTICAL(DBM)	HOURS/MIN./SEC.	RANGE(N. MILES)	AZIMUTH(DEGREES)	ELEV.(DEGREES)
1	16.245	- 82.09	- 66.97	19/09/33.9	8.07	194.04	001.34
1	16.244	- 83.72	- 68.37	19/09/34.7	8.07	194.04	001.48
1	16.245	- 81.86	- 66.42	19/09/35.8	8.07	194.04	001.48
1	16.245	- 82.68	- 67.36	19/09/36.9	8.07	194.04	001.44
1	16.245	- 80.20	- 67.09	19/09/37.9	8.07	194.04	001.40
1	16.244	- 81.90	- 66.73	19/09/38.7	8.07	194.04	001.38
1	16.244	- 80.54	- 67.15	19/09/39.8	8.07	194.04	001.50
1	16.245	- 83.43	- 68.03	19/09/40.9	8.07	194.04	001.48
1	16.241	- 83.78	- 66.38	19/09/41.9	8.07	194.04	001.44
							001.34

18310

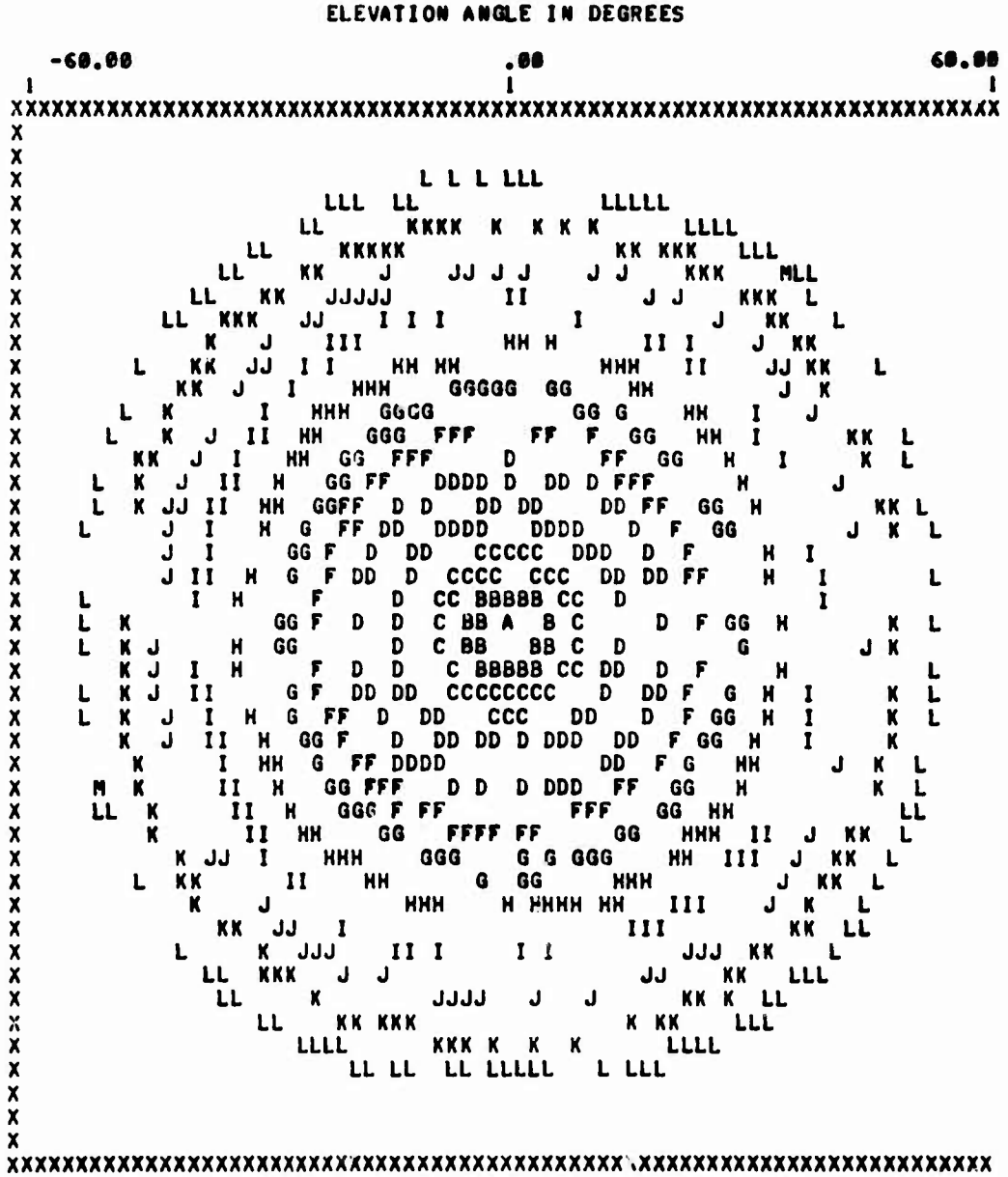

ELEVATION RESOLUTION = 1.7143 DEGREES
AZIMUTH RESOLUTION = 2.8052 DEGREES
DATA POINTS: 2967.

A	=	91.5 DBW	G	=	73.5 DBW
B	=	88.5 DBW	H	=	70.5 DBW
C	=	85.5 DBW	I	=	67.5 DBW
D	=	82.5 DBW	J	=	64.5 DBW
E	=	79.5 DBW	K	=	61.5 DBW
F	=	76.5 DBW	L	=	58.5 DBW

"A" Referenced to nose of A/C

18295

Figure 51. 3-Variable Plot

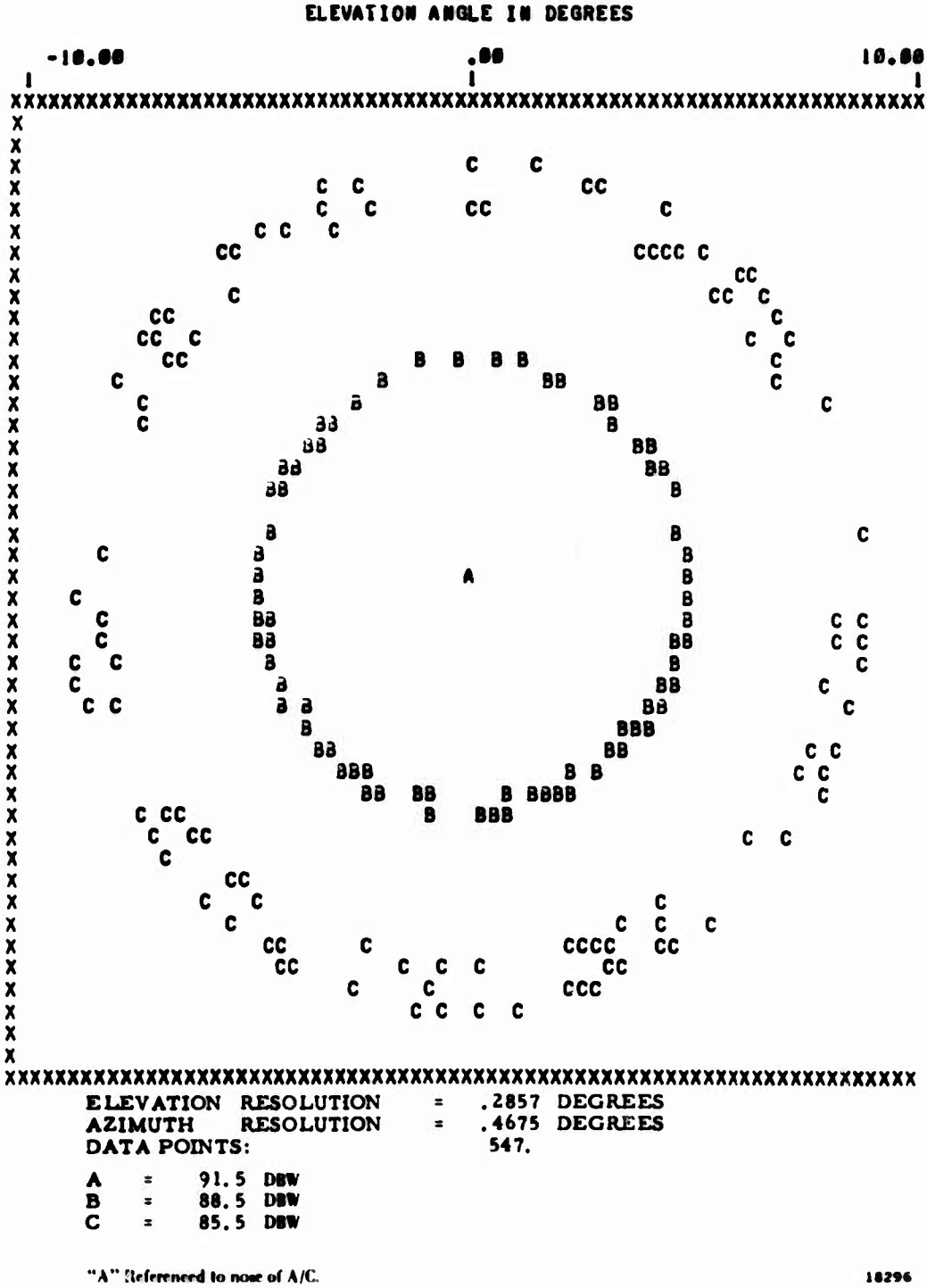

Figure 52. Expanded 3-Variable Plot

5.4 AIRBORNE PATTERNS

The performance tests were concluded with the airborne antenna pattern measurements. For this phase of the program a dual polarized log periodic array antenna was obtained and installed on the PAMS antenna array by RADC. This antenna provided frequency coverage from 0.1 GHz through 1.0 GHz. The final configuration of the PAMS antenna system is shown in figure 53. The tests were conducted using one of RADC's KC-131 test aircraft pictured in figure 54. The plane was instrumented with an assorted array of antennas for the measurement program, some of which are shown in figure 55.

Measurements of the airborne antennas were first attempted flying a cloverleaf pattern and taking data as the aircraft passed over a fixed Intercept Point (IP). This resulted in long flights and provided a limited number of data points, and the initial patterns were somewhat questionable. The problem was traced to the curve fitting subroutine used in the plotting programs. Values of missing data points are computed by quadratic interpolation using three surrounding data points. Depending on the slope and angular spacing of these three points, erroneous maximum and minimum data can be computed and plotted.

The flight pattern was changed from the cloverleaf to parallel flybys and selected radials. This increased the number of data points by an order of magnitude. Consequently, the data points are closely spaced and the curve fitting is extemely good as shown by the pattern presented here.

An L-band blade antenna was selected for the first measurement because of its predicatable properties. Consequently any unusual effects could be readily detected and analysis of problems simplified. The results of this test are given in figure 56. The calculated ERP was 12.14 dbw and the measured ERP was 9.0 dbw. There was also good correlation with the predicated pattern shape.

The second pattern consisted of two S-band blade antennas with half-wavelength spacing and fed approximately 135 degrees out of phase. The pattern shown in figure 57 is an integrated power plot over a 200 MHz bandwidth. The calculated power density was -2 dbw/MHz and the average of the measured data was -6 dbw/MHz. This is in good agreement with the calculated density particularly when the low elevation angle of -3 degrees is considered. At this frequency the minimum elevation angle of PAMS should be on the order of 10 degrees to eliminate the influence of pattern lobing.

Illustrated in figure 58 is the radiation pattern of a small aperture X-band horn antenna located near the aft end of the C-131. The transmit power was not monitored during this test; however, the pattern shape is in general agreement with what was expected. The apparent hole in the pattern at 180 degrees is due to lack of data at the tail-on aspect. The plotting routine is configured to start at 180 degrees and plot in a clockwise direction. Consequently the curve fitting will not interpolate in this range and lack of data appears as a hole in the pattern.

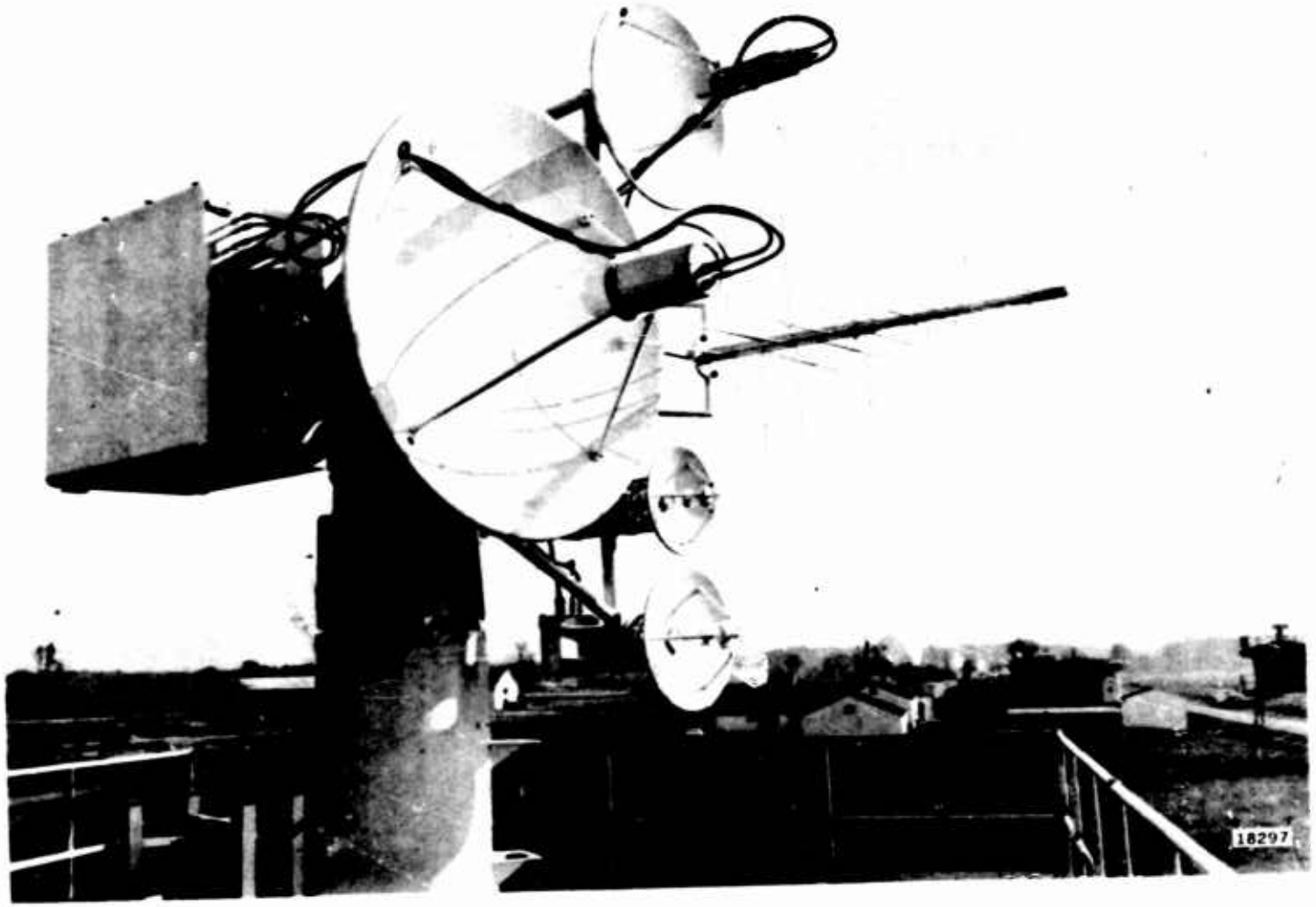

Figure 53. PAMS Antenna System With Log Periodic

Figure 54. RADC C-131 Test Aircraft

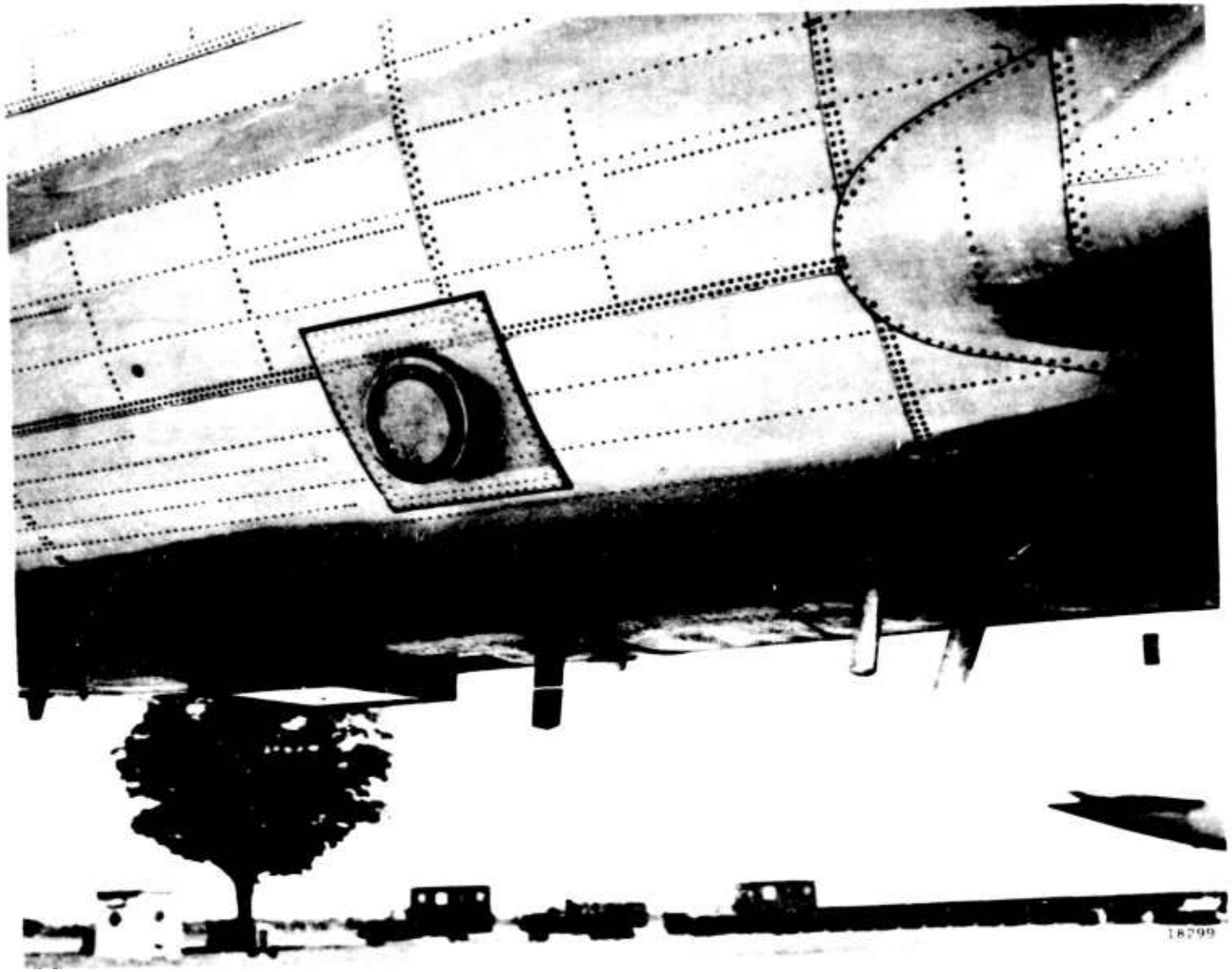

Figure 55. C-131 Antenna Complex

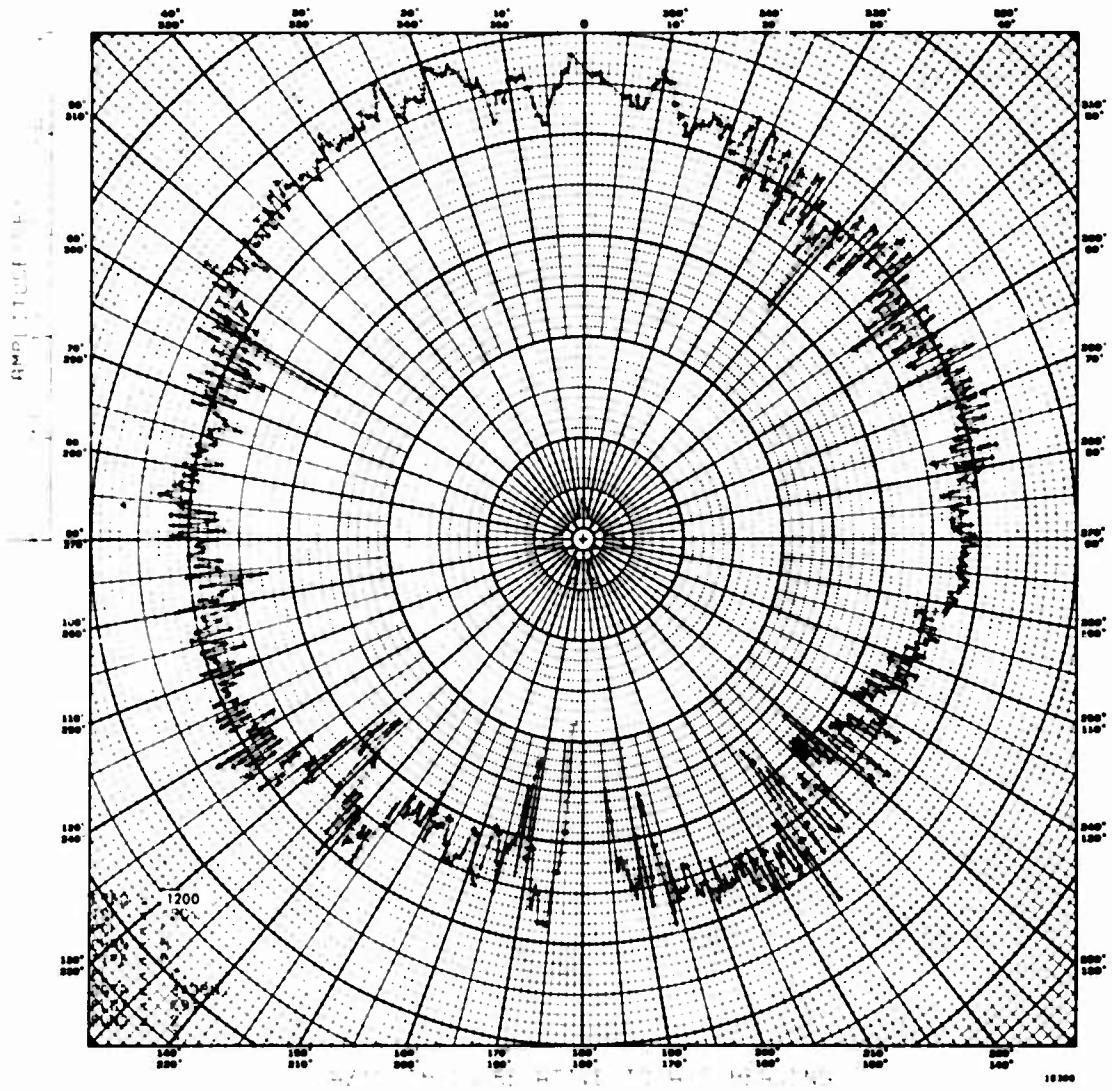

Figure 56. L-Band Blade Antenna (Polar Coordinate)

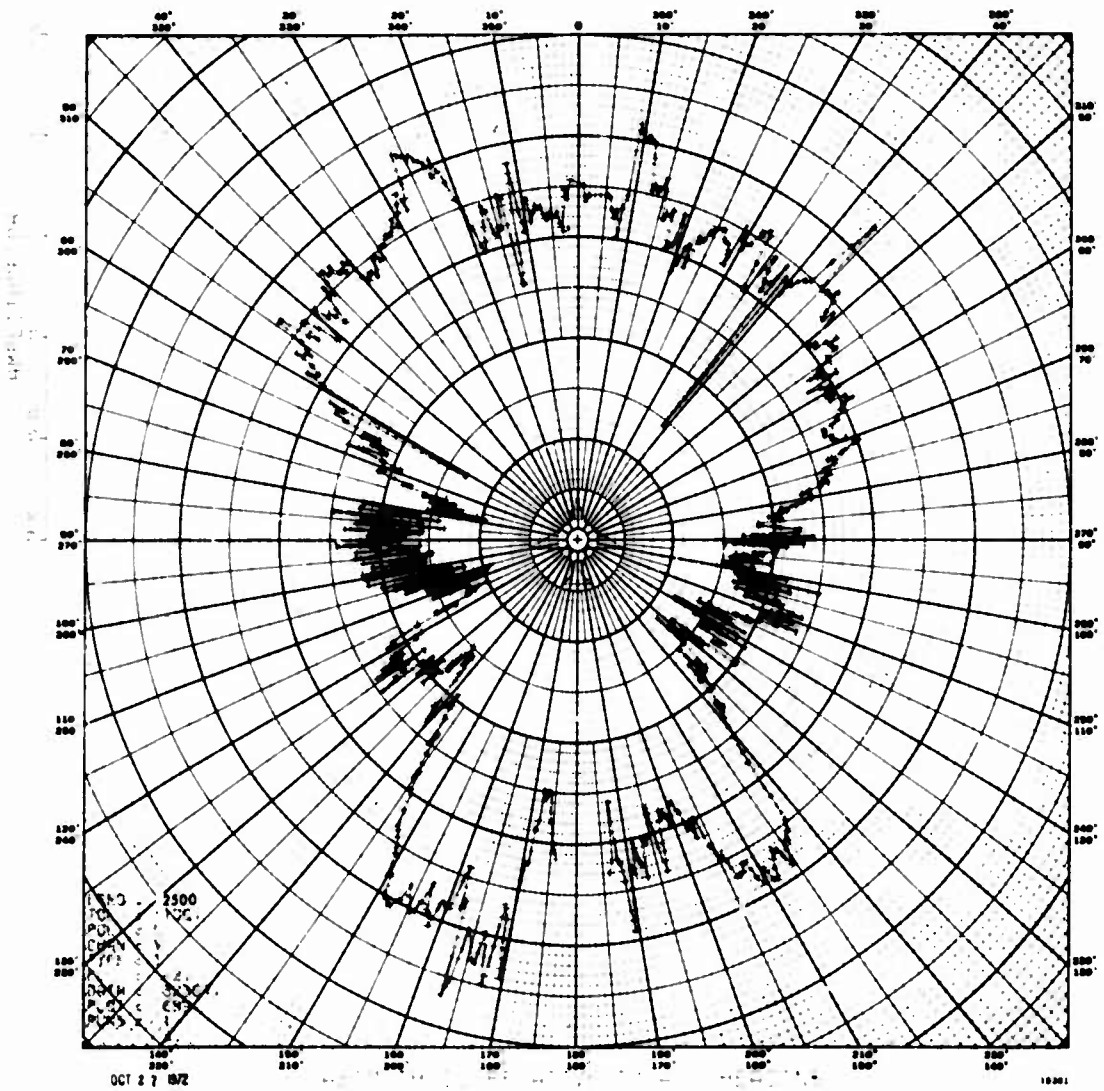

Figure 57. Two S-Band Blade Antennas With Half-Wavelength Spacing, Fed Approximately 135 Degrees Out of Phase

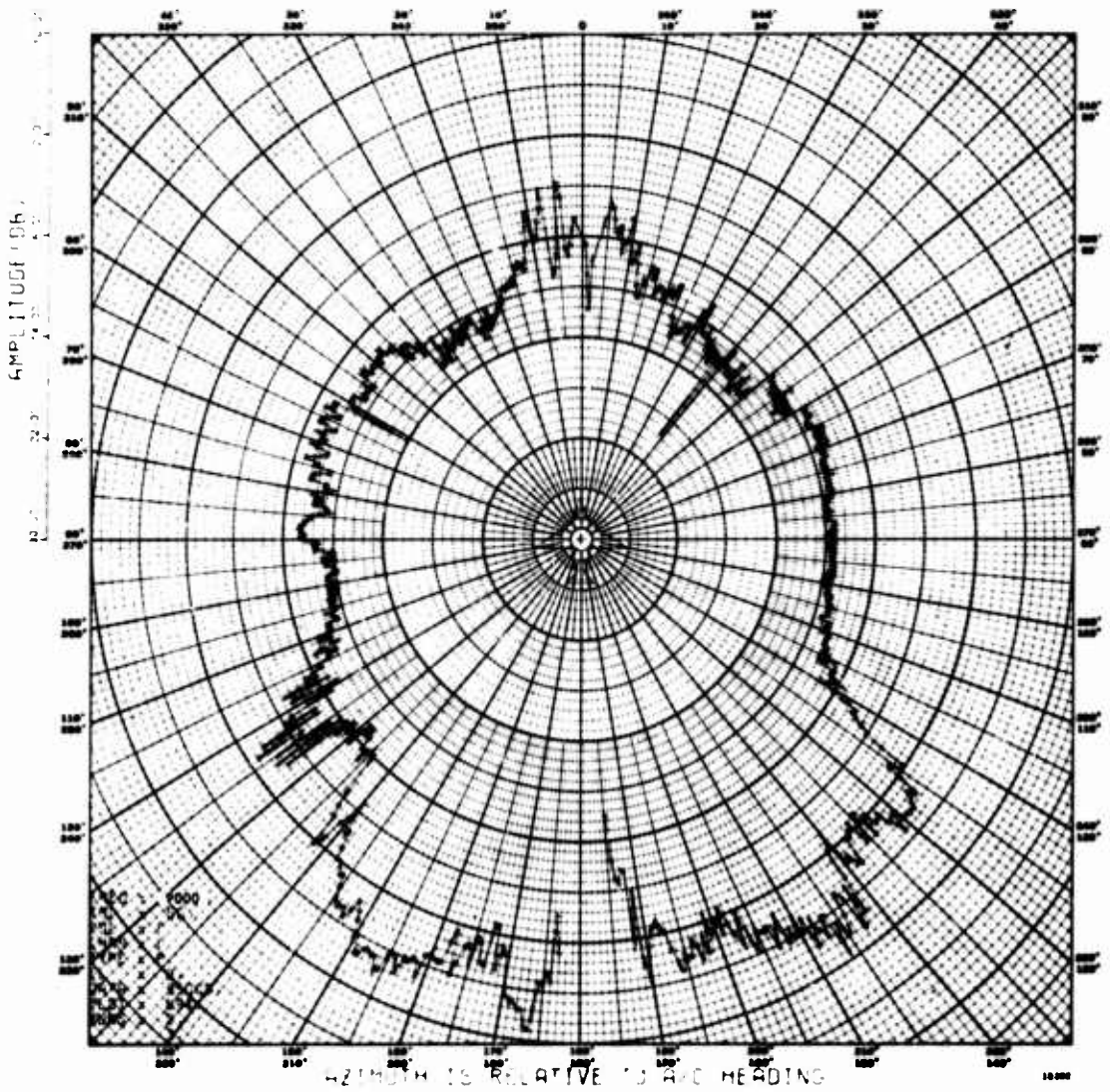

Figure 58. Radiation Pattern of Small Aperture X-Band Horn Antenna

The last measurement of the flight test program was made with two high-gain linear antennas located on each side of the aircraft. The measured data was within approximately 3.5 db of the calculated ERP. The effects of the aircraft engines and tail assembly are easily distinguishable in the pattern of figure 59. In conclusion, it has been demonstrated that PAMS is capable of measuring the radiation characteristics of airborne antennas with a high degree of accuracy. The results can be improved even further when a propagation analysis of the site is performed to define the optimum areas for uninterrupted propagation and an airborne monitoring system is installed aboard the aircraft for accurately determining the attitude of the aircraft.

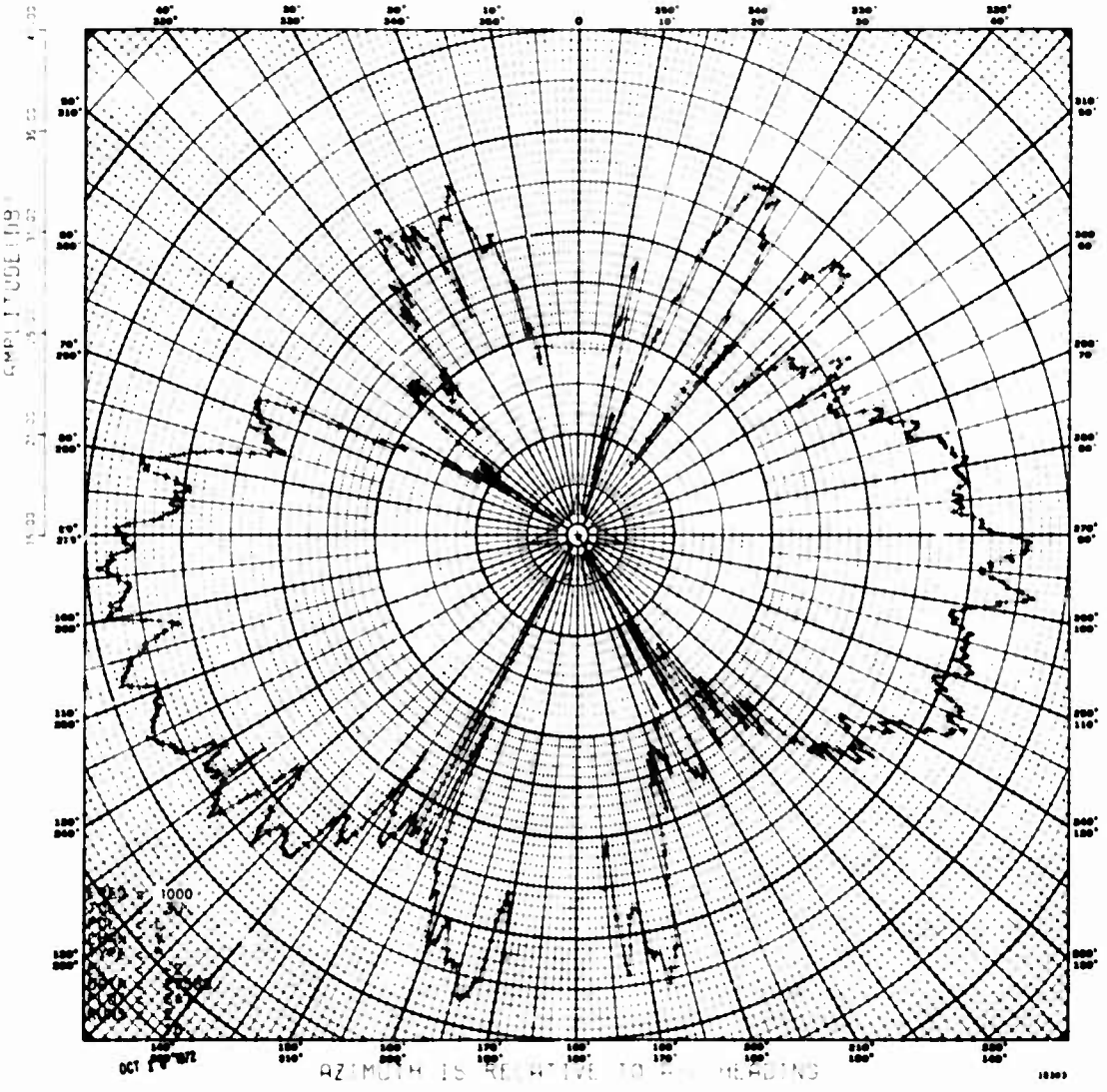

F gure 59. Radiation Pattern of Two High-Gain Linear Antennas Located on Each Side of Aircraft

SECTION VI

SYSTEM EVALUATION

6.1 INTRODUCTION

This Section will evaluate the overall performance of the PAMS and attempt to define the accumulative errors of the major subsystems. This analysis will only consider the PAMS hardware and no attempt will be made to evaluate the effect of errors introduced by the track radars, aircraft attitude, and propagation anomalies on the accuracy of the total system. For the purpose of this analysis the system will be divided into two major subsystems as follows:

1. Antenna Group
2. Receiver Group

6.2 ANTENNA GROUP

This portion of the analysis deals with the parameters which affect the beam pointing accuracy of the antenna array and its influence on the gain characteristics. The data is based primarily on test data taken during final acceptance at the facilities of Scientific-Atlanta, Inc. The analytical portion is based on methods developed by Hollis, et al [1].

The errors which contribute to the performance of the antenna system are divided into two classes, systematic and random, and are defined as follows.

Systematic Errors:	Pedestal Positioning
	Antenna Feed Alignment Error
	Array Fabrication Error
Random Errors:	Wind Loading/Deflection
	Solar Heating Effects
	Parallax
	Multipath
	Boresight Shift With Frequency

6.2.1 Pedestal Positioning

An antenna pedestal with an orthogonality error δ is pictured in figure 60. In this case it is assumed that all of the other characteristics of the system geometry are perfect. The coordinate system of the antenna coincides perfectly with the pedestal coordinate system, and the direction to the source antenna is exactly normal to the mechanical $\bar{\theta}$-axis, which will be designated as OA'. The polar ($\bar{\phi}$) axis of the antenna positioner is OZ. The mechanical $\bar{\phi}$-axis OA is displaced by an angle δ from the XY plane. If the geometry were perfect, the antenna coordinate system XYZ could be rotated about OA so that the direction OT to the source antenna would be in the plane OMZ. However, due to the orthogonality error, rotation about the $\bar{\theta}$ axis will position OT in the plane OMZ'.

[1] "Microwave Antenna Measurements" Hollis, J.S., T.T. Lyon and L. Clayton Scientific-Atlanta Inc. 1970.

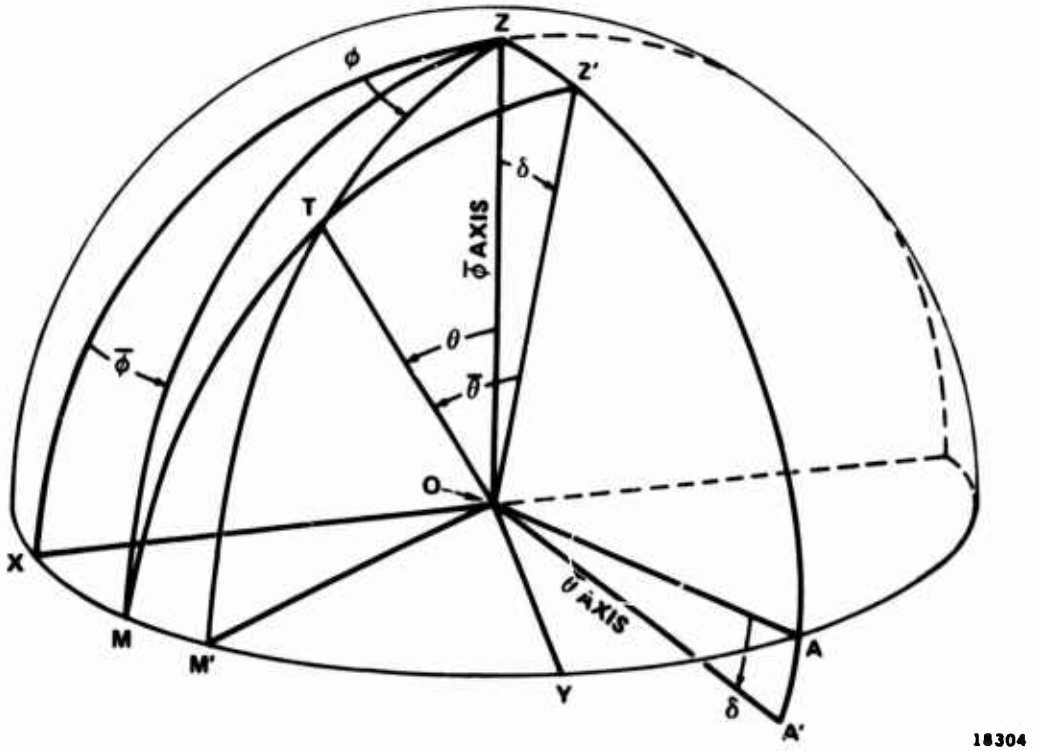

Figure 60. Antenna Positioner With Orthogonality Error

The angles or directions which will be indicated by the instrumentation equipment are $\bar{\phi}$, $\bar{\theta}$, where $\bar{\phi}$ is the rotation about the positioner polar ($\bar{\phi}$) axis and $\bar{\theta}$ is the rotation about the positioner $\bar{\theta}$ axis.

In order to position the direction OT as shown in figure 60, OT can be considered to have moved from OX to OM by rotation about the OZ axis, then from OM to OT by rotation about the OA' axis. Therefore, the direction $\bar{\phi}$ of OT is the angle between planes XOZ and MOZ.

Since $\bar{\theta}$ is a measure of the mechanical rotation about OA' it is an angle in plane MOZ', which is the plane of the great circle that is normal to OA'.

Using spherical geometry it can be shown that

$$\theta = \cos^{-1}(\cos\delta\cos\bar{\theta}) \tag{16}$$

$$\phi \doteq \bar{\phi} + \sin^{-1}(\sin\delta\cot\bar{\theta}) \quad \text{for small } \delta \text{ where } \cos^2\delta \doteq 1$$

Then the error in θ is given by

$$\epsilon_{o\overline{\theta}} = \overline{\theta} - \theta = \overline{\theta} - \cos^{-1}(\cos\delta \cos\overline{\theta})$$

and the error in $\overline{\phi}$ is given by

$$\epsilon_{o\overline{\phi}} = \overline{\phi} - \phi = \overline{\phi} - \overline{\phi} + \sin^{-1}(\sin\delta \cot\overline{\theta})$$

If we assume δ is on the order of 0.02 degree or 0.35 milliradian (typical value for the Series 3100 pedestal) we can approximate $\cos\delta$ by $1 - 1/2\ \delta^2$ which is approximately unity. Therefore, for all practical purposes $\epsilon_{o\overline{\theta}}$ can be considered to be zero. An analysis of $\epsilon_{o\overline{\phi}}$ indicates that the error will never be greater than δ or 0.02 degree. This value will then be used in the summation of the error budget.

6.2.2 Antenna Feed Alignment Error

The feed alignment error is the result of the physical alignment of the feed with respect to the reflector and the error of the measuring equipment. The feed is mechanically aligned and adjusted in the reflector such that when two azimuth patterns are taken at polarization angles of zero and 180 degrees the peak of the beams coincide in the azimuth and elevation planes as displayed on the antenna chart recorder. The total error therefore is a combination of the physical alignment and error introduced by the chart recorder. The antennas were aligned on the antenna range using a Scientific-Atlanta Model 1520 chart recorder with a maximum error of ±0.03 degree. After the final alignment the maximum readout error of both polarizations was 0.03 degree which respresents the resolution of the chart readout. Therefore, the maximum error which could occur would be 0.06 degree. Another error was introduced by the Model 1848 Synchro to Digital unit of 0.01 degree in elevation and 0.03 degree in azimuth.

6.2.3 Array Fabrication Error

In a system like the PAMS which utilizes several antennas having parallel boresights, there is an unavoidable fabrication error associated with the physical location of the apertures with respect to each other and the plane of attachment to the positioner. The fabrication of the antenna array back-up structure which is fastened to the positioner was shimmed such that each of the antennas apertures lay in a plane which varied no more than 0.031 inch from an idealized plane containing the interface of the positioner and the antenna array back-up structure. The worst case error introduced by the Band IV antenna assuming a maximum deviation of 0.31 inch over a distance of 24 inches gives a maximum error of 0.0013 radian or 0.074 degree. For the larger reflector, this error becomes much smaller. For instance, the maximum error associated with the 6-foot reflector would be 1/6 this value or 0.012 degree.

6.2.4 Wind Loading/Deflection

The effect of wind loading on the beam pointing accuracy was done experimentally. The drag force was calculated at the maximum operating wind velocity of 40 MPH and then

weights were attached to the antenna to simulate the wind condition. The deflection of the antenna array was then measured to derive the degree of beam pointing error.

The drag force can be calculated using the following

$$D = C_d \frac{1}{2} \rho v^2 A \tag{17}$$

where ρ = air density

v = air velocity

A = area of structure

C_d = drag coefficient (1.55 for most applications)

A more useful form of the above is

$$D = C_d Q A \tag{18}$$

where Q is the dynamic pressure in pounds per square foot.

For the PAMS array the maximum drag force for each antenna for an ambient temperature of 70°F and a 40 MPH wind velocity results in a Q of 4.09 pounds per square foot. The results of the calculation are shown below.

Antenna Aperture	Drag Force "D"
6'	180 lbs
3'	45 lbs
2'	20 lbs
1.5'	11.2 lbs

From the above it is seen that the maximum deflection will occur in the 6 foot parabola. The measured deflection was 0.046 degree. The worst case occurs at -40°F due to higher density of air at the lower temperatures. At 70°F the density ρ is 0.0747 pound per cubic foot and increases to 0.0945 pound per cubic foot at -40°F. The resultant dynamic pressure Q at the low temperature increases to 5.1 pounds per square foot. Extrapolation of the new data results in a maximum deflection of 0.0576 degree. However, the proximity of the adjacent reflectors introduce a randomness of wind currents which tend to reduce the maximum deflection. Therefore a value of 0.046 degree will be used for the error budget.

6.2.5 Solar Heating Effects

The heating effects of solar radiation can be a major source of deflection error. In order to reduce the solar effects the antenna array was painted with a light dispersive white paint with a high reflectivity index and the pedestal with a white high gloss enamel. The effects on beam pointing due to solar radiation were derived experimentally as follows.

Precision calibrated levels were utilized to measure the inclination of the top of a vertical steel cylinder as it deflected from unequal expansion due to solar heating.

The walls of the steel cylinder were 3/8-inch thick, and the cylinder was approximately 240 inches long by 66 inches in diameter. The cylinder was rigidly fastened to a concrete foundation. The exterior surface was coated with red Rustoleum paint. The change in inclination across the north-south and east-west directions was measured at intervals during the day from sunrise to sunset, on a clear day, for which the maximum temperature was 73°F.

As expected, the steel cylinder deflected away from the sun, leaning toward west in the morning, toward north at noon, and toward east in the afternoon. The maximum inclination, which occurred between 3 and 5 PM EST, was approximately 125 arc seconds. The maximum difference in inclination between morning and afternoon was approximately 225 arc seconds (over 0.06 degree).

A reasonable estimate for scale factor effects is to consider that the magnitude of solar deflection will be directly proportional to the ratio of cylinder length to diameter.

The test described above gave 0.606 milliradian (1205 arc seconds) deflection for a cylinder with

$$\frac{L}{D} = 3.63$$

The PAMS pedestal has an approximate $\frac{L}{D}$ equal to

$$\frac{L}{D} = 3.05$$

where L is taken as the distance from the bottom of the base extension to the elevation axis and D is equal to the base diameter. The expected maximum solar deflection in the elevation mode will be 0.51 milliradian (0.0292 degree) for conditions similar to those described by the experiment above.

Azimuth pointing error resulting from pedestal solar reflection will be mostly limited to the deflection caused by one antenna support arm being exposed to the sun while the other support arm remains in the shade. Using the length of the support arm versus the distance between the arms as an approximation to an L/D term where

$$\frac{L}{D} = 1.62$$

the maximum azimuth solar deflection is estimated to be

$$\Delta\phi = 0.606\left[\frac{1.62}{3.63}\right]$$

$$\Delta\phi = 0.446 \text{ milliradian} = 0.0256 \text{ degree}$$

6.2.6 Parallax

Since the PAMS array has four antennas, each with a different phase center, parallax is introduced into the system. The maximum spacing from the center of any antenna in the array to the imaginary boresight center of the array is 45 inches. The parallax angle is then the tangent of the angle made by the offset at the antenna center and range to the target. In Section III it was shown that the minimum range the PAMS would be used was on the order of five nautical miles. At this range the parallax of the array is negligible and will not be considered further. However, the problem of parallax was investigated to see what errors were introduced on the 1000 foot antenna test range at Scientific-Atlanta. Here the short distance introduced a parallax angle of 0.143 degree. Using the geometry shown in figure 61 the beam pointing error is defined as

$$\phi' = \cot^{-1}\left(\frac{R' \cos\phi + r_o}{R' \sin\phi}\right) \tag{19}$$

The above equation was the evaluation for values of ϕ ranging up to two degrees. The parallax correction or beam pointing error was found to be on the order of 10^{-4} degree for both vertical and horizontal polarizations. For the purpose of the error budget the beam pointing error is considered to be zero.

6.2.7 Multipath

The geometry of the Scientific-Atlanta test range is such that high frequency antennas (4 GHz and higher) can be evaluated with no multipath effects encountered. However, for lower frequencies the transmit antenna height must be adjusted so that the peak of its first sidelobe is directed at the base of the receiver antenna tower. Thus, any multipath energy would have as its source the first sidelobe of the transmit antenna. An additional 10 db loss is incurred due to reflections. The multipath energy is then equal to the sidelobe level minus 10 db. For the PAMS test the transmit antenna had 20 db sidelobes for a total multipath energy of -30 db.

The mathematical expression used to evaluate beam pointing error is given by

$$\left|\frac{\Delta\theta}{\beta}\right| = \frac{2.78}{E_M}\left|\frac{K\theta\cos(K\theta) - \sin(K\theta)}{(K\theta)^2}\right|\left|\frac{1}{A_N(-m)}\right| \tag{20}$$

where $\left|\frac{\Delta\theta}{\beta}\right|$ = normalized beam pointing error

E_M = ratio of direct energy to multipath energy

K = beamwidth constant

θ = angle interference enters the main beam

$A_N(-m)$ = pattern function of receive antenna

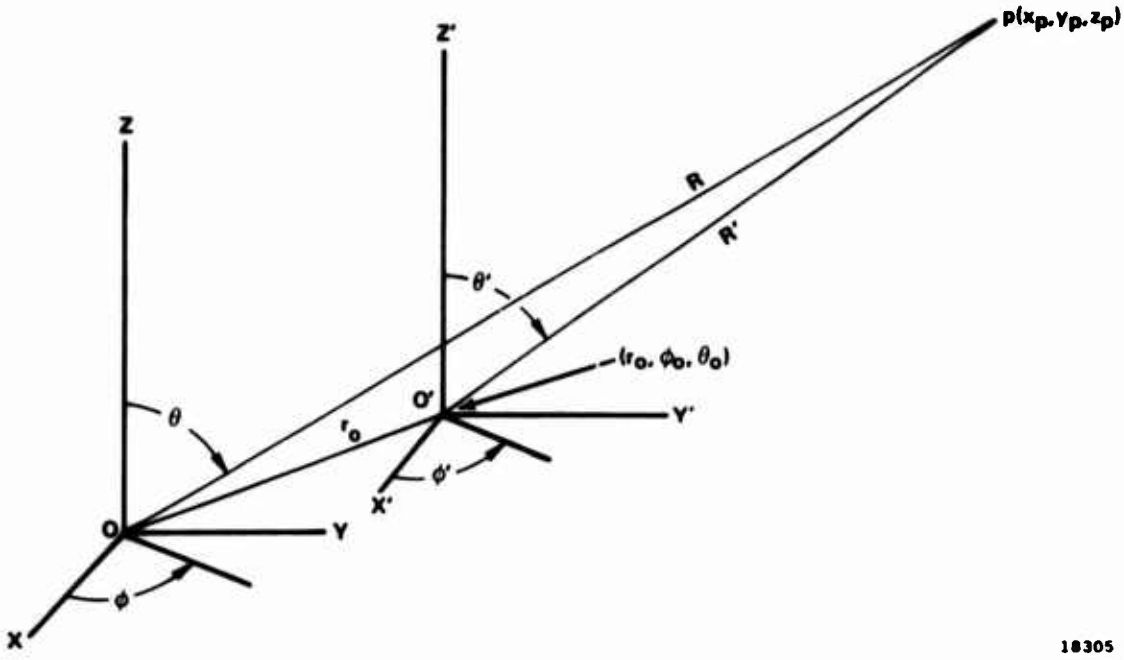

Figure 61. Coordinate Systems Employed for Antenna Measurements, Showing Parallax

The above expression was evaluated on a computer for various angle of θ and the maximum beam pointing error was found to be 0.016 degree on the test range.

6.2.8 Boresight Shift With Frequency

The boresight shift as a function of frequency was determined experimentally. The results of the tests are shown in figure 62. The chart recorder was initially aligned on the K_u-band antenna and no further adjustment was made after the first pattern was measured. The boresight shift was measured using a split lobe technique described in [1]. The boresight shift for the C- and X-band antennas was negligible. The K_u-band antenna exhibited a shift of 0.08 degree and the S-band 0.2 degree. Both of these were in good agreement of the predicted values.

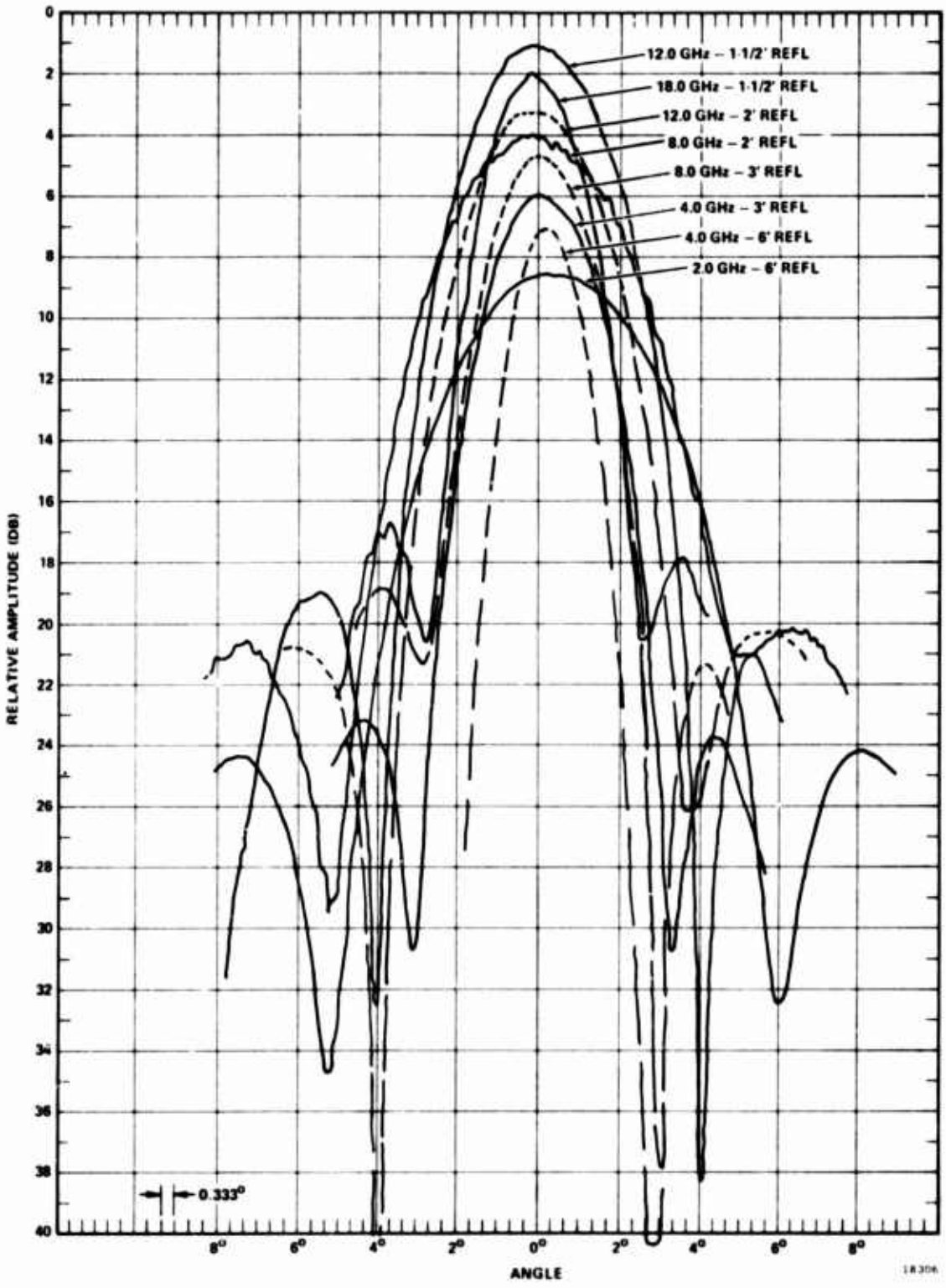

Figure 62. Measurement of Electrical Boresight Shift With Frequency

6.2.9 Summary

The total systematic and random errors are shown in table XII. A Gaussian distribution was assumed for the errors and their Mean Deviation calculated. The total beam pointing error is then the RMS value of these two values. The analysis of the antenna system indicated that even in the worst case conditions the beam pointing error was well within the requirement that the maximum beam pointing error did not exceed one-tenth of a beamwidth. Analyzing the antenna patterns using the values given in table XII indicates that the effect of amplitude variation due to antenna beam pointing error is on the order of 0.25 db in the worst case.

TABLE XII

SUMMARY OF BEAM POINTING ERRORS

Fixed Errors	ΔEl (deg)	ΔAz (deg)
(a) Orthogonality Error	0	0.020
(b) Feed Alignment Error	0.060	0.060
(c) Array Fabrication Error	0.074	0.074
(d) Readout Error	0.010	0.030
Mean Deviation	0.022	0.021
Random Errors		
(a) Wind Loading Error	0.046	0.046
(b) Solar Heating Error	0.029	0.026
(c) Multipath Effects	0.016	0.016
(d) Boresight Shift with Frequency	0.080	0.080
Mean Deviation	0.026	0.026
Total Pointing Error Root Sum Square	0.034	0.033

6.3 RECEIVER GROUP

This Section will discuss the results obtained during acceptance tests and relate them to the performance of the receiver. The results will be summarized and predicted levels of performance given.

It is difficult to address the receiver as an individual subsystem since the output data is a function of the signal processor and computer as well as the receiver. Consequently the reader should keep in mind that the data presented in this Section actually reflects the overall accuracy of the system from the input terminals of the receiver to the computer record.

The results of any measurement program are dependent upon the basic accuracy of the test equipment employed in the measurements. All of the equipment used in the acceptance tests was calibrated by RADC specifically for the acceptance tests. The basic accuracy of the frequency counter used was ±0.001 percent, and therefore, would contribute very little error to frequency measurements. However, the accuracy of the output attenuator on the signal generators was approximately the same as the accuracy trying to be established. Consequently, extreme care was taken in the amplitude measurements to minimize any error introduced by the test equipment.

6.3.1 Frequency Accuracy

The ability of the PAMS to accurately measure frequency is a function of the accuracy of the frequency markers used during the calibration of the receiver. These markers are derived from an extremely stable 100 MHz crystal oscillator which drives a set of step recovery diodes to produce markers every 100 MHz across each frequency band. (See paragraph 4.5.7.2 for a detailed discussion on frequency calibration.) Table XIII shows the accuracy of the calibrated and uncalibrated frequency markers. From the table it can be seen that calibrated markers exceed by a wide margin the design requirement of one-tenth percent accuracy. The uncalibrated marker accuracy of one percent has also been exceeded in all the receivers. Table IX illustrates a computer readout of the frequency markers. These data are read by the computer in the following manner. The frequency markers are routed through a discriminator and as each zero crossover is detected the computer commands the signal processor to read the level of the frequency sweep voltage at that point. The computer has a priori knowledge as to what voltage level each marker has associated with it. The 2.312 GHz measurement in table IX is recognized by the computer as 2.300 MHz. This voltage is stored in memory and during data reduction any frequency with that level is identified as 2.300 GHz. The frequency listing constitutes a look-up table for the computer to use during data reduction. For frequencies which fall between the markers the computer uses a linear interpolation, and the accuracy is dependent upon the linearity of the ramp voltage. Here a one-percent deviation from the desired slope would introduce a one Megahertz error. At S band this would translate into a frequency error of approximately 0.05 percent at 2.0 GHz. The error is even less at the higher frequencies. The results have shown that all of the design requirements for frequency accuracy have been bettered in the PAMS.

6.3.2 Amplitude Accuracy

This Section will discuss the amplitude measurement capability of the system in both the uncalibrated and calibrated modes of operation. The ability of the system to accurately determine the level of an unknown signal is directly dependent on the accuracy of the internal amplitude reference. The data presented here identifies the accuracy of the reference and therefore the precision with which the unknown can be measured.

TABLE XIII

FREQUENCY MEASUREMENT ERRORS - CALIBRATED AND UNCALIBRATED CW MARKER FREQUENCY

	Frequency (GHz)	Vertical Channel		Horizontal Channel	
		Calibrated (%)	Uncalibrated (%)	Calibrated (%)	Uncalibrated (%)
S-Band					
	2.5	0.004	0.09	0.024	0.06
	3.5	0.003	0.12	0.018	0.13
C-Band					
	4.5	0.025	0.55	0.005	0.17
	7.5	0.007	0.41	0.012	0.41
X-Band					
	8.4	0.002	0.35	0.009	0.35
	9.5	0.001	0.3	0.018	0.33
K_u-Band					
	12.0	0.009	0.26	0.017	0.23
	17.0	0.059	0.23	0.012	0.18

In the measurements which were made, the receiver, data processor, and computer could be treated as a comparator since any error associated with these units was the same for both the reference and input levels. This concept is illustrated in figure 63. As can be seen from figure 63, the error is a combination of the internal amplitude reference and the switch network between the reference and signal inputs. Prior to the final calibration measurements a correction factor was derived to take into account the frequency dependency of the RF coupler and the amplitude and frequency characteristics of the RF detector used in the reference loop. This correction factor is used to compute the calibration amplitude error. In addition, this value is stored in the computer as a look-up table for amplitude correction during data reduction.

The tests used to determine the amplitude accuracy were performed in the following manner. The system was put into the Data Acquisition Mode which activated the console displays and put the computer on line. Next a known level was injected at the signal input and the resultant output, as displayed on the console numeric indicator, was recorded. The difference between the known input and the resultant output is the uncalibrated error. The Root Mean Square (RMS) errors were calculated for the uncalibrated mode and are shown in table XIV(a). Next the internal reference is switched into the measurement channel and its level on the console display is recorded. The correction factor is then added to value recorded above. The calibration error of the system is the difference between the reading of the signal input and the internal reference. The RMS values for the calibrated amplitude error as given in table XIV(b). These tests were performed over the frequency band of each receiver with a constant signal input of -60 dbm.

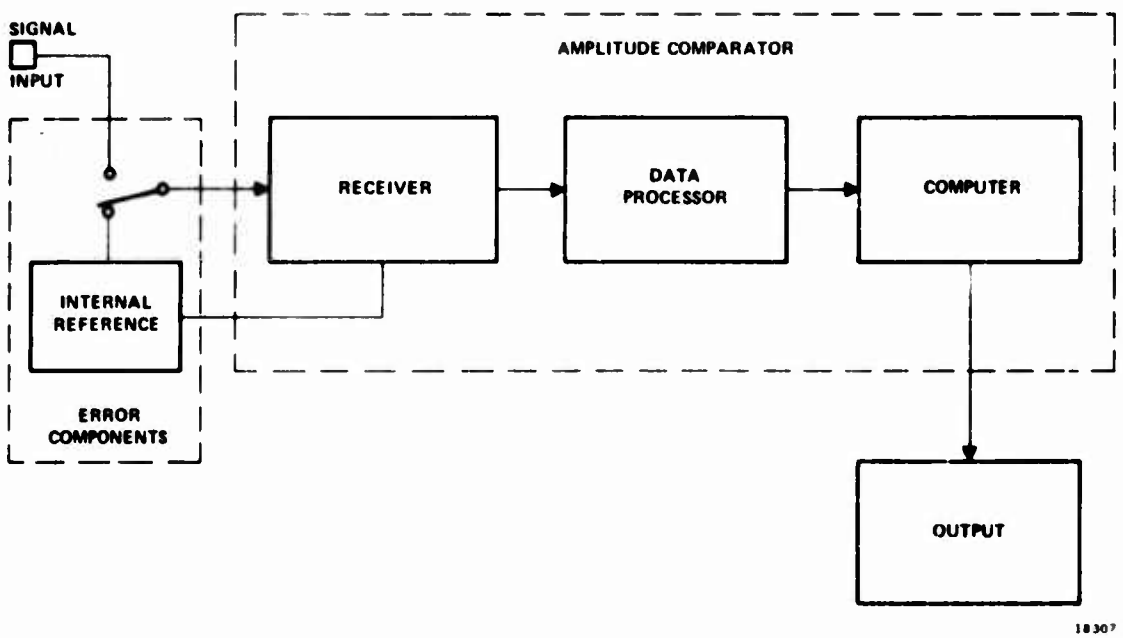

Figure 63. Amplitude Measurement Loop

TABLE XIV

UNCALIBRATED AND CALIBRATED RMS AMPLITUDE ERROR

(a) Uncalibrated RMS Amplitude Error

Receiver	Vertical Channel	Horizontal Channel
S-Band	1.45 db	1.72 db
C-Band	2.05 db	2.2 db
X-Band	1.77 db	1.8 db
K_u-Band	2.4 db	2.7 db

(b) Calibrated RMS Amplitude Error

Receiver	Vertical Channel	Horizontal Channel
S-Band	0.466 db	0.495 db
C-Band	0.28 db	0.44 db
X-Band	0.734 db	0.904 db
K_u-Band	0.66 db	1.9 db

The results of table XIV(a) show that the uncalibrated RMS error was below the design goal of 3 db. The 3 db level was exceeded on a few individual measurements but did not affect the overall RMS value. Due to the roll-off of filter performance in the K_u band receiver as described in paragraph 5.1 the results above 16.5 GHz were not included in the uncalibrated data since they tend to distort the overall performance of the receiver. However, the calibrated error does include the amplitude data above 16.5 GHz. Table XIV(b) shows that the large error encountered in the uncalibrated mode has been corrected for by the calibration loop.

The data shown here corresponds extremely well with data taken during pre-acceptance tests conducted at Actron. The only adjustment made of the reference loop at RADC prior to final acceptance was in the S-band receiver which was required by the replacement of the RF detector. Consequently, the long term stability of the calibration system appears to be very good. In order to establish a dynamic calibration error for the system, the above tests were repeated with the exception that the input level was varied from -40 dbm to -94 dbm in 6 db increments. The results generally followed those with a constant level input and are shown in table XV. These results indicate that the RMS calibration errors are within the specified limits over the dynamic range where the majority of actual pattern measurements will be made.

TABLE XV

DYNAMIC RMS UNCALIBRATED AND CALIBRATED AMPLITUDE ERROR

(a) Uncalibrated RMS Amplitude Error

Receiver	Vertical Channel	Horizontal Channel
S-Band (3 GHz)	1.76 db	1.63 db
C-Band (6 GHz)	1.5 db	2.52 db
X-Band (10 GHz)	2.57 db	2.62 db
K_u-Band (15 GHz)	2.9 db	1.9 db

(b) Calibrated RMS Amplitude Error

Receiver	Vertical Channel	Horizontal Channel
S-Band (3 GHz)	0.398 db	0.597 db
C-Band (6 GHz)	0.886 db	0.845 db
X-Band (10 GHz)	0.708 db	0.921 db
K_u-Band (15 GHz)	0.988 db	1.14 db

The L-Band converter has not been included in the following measurements since it is outside the calibration loop of the receivers. Instead gain curves have been established by individual tests and this data is then used in the system gain curve to correct for the errors introduced by the converter. This technique has resulted in calibrated RMS errors on the order of 2 db and uncalibrated RMS errors of 4 db.

C.3.3 Amplitude Summary

The results of the tests described above will form the basis for establishing an overall predicted level of performance for the PAMS. Reviewing the results of the frequency calibration tests, it can be stated with a high degree of confidence that RMS frequency accuracy of the system will be 0.05 percent under all conditions.

The overall amplitude accuracy of the system is a function of the antennas, transmission lines, and the receiver. In actual operation a gain curve as a function of frequency was generated for the complete system and was transferred to paper tape so that it could be read into the computer. This gain tape includes antenna gain, cable loss from antenna to receiver, L-Band converter gain, receiver gain, and receiver amplitude correction factors. The primary reason this data is on paper tape is so that it can be periodically updated to account for aging, re-alignment, and new measurement data without altering the master program.

We are now in a position to assign RMS values to each factor which contributes to the amplitude accuracy of the system. This will establish the expected level of accuracy for the amplitude measurement capability of the system. This data is presented in table XVI. The value assigned to receiver drift and fluctuation is the result of long time observations made during the pre-test and final test phases. The antenna gain error for the 0.1 to 1.0 GHz band was estimated and the rest of the antenna gain values were provided by the antenna vendor. The remaining values in the table are the direct result of the final acceptance and support tests.

The final RMS system accuracy shown in table XVI indicates a high degree of success for the program. The original goal of 1 db RMS system error was achieved within approximately 0.5 db for all the receivers. The L-band converter would require an internal amplitude reference in order to achieve the same level of accuracy as the receivers. Further overall accuracy could be obtained with the use of high precision test equipment. (Output amplitude accuracies of ±0.1 db or better from 0 to -100 dbm). The ability to establish the amplitude error to approximately one-half of that shown in table XVI and the drift rate to 0.25 db results in an improvement of 0.25 to 0.4 db for all the receivers.

TABLE XVI

PAMS SYSTEM AMPLITUDE ACCURACY

Receiver	Receiver System RMS Amplitude Error (db)	RMS Antenna Gain Error (db)	RMS Transmission Line Error (db)	RMS Receiver Drift and Fluctuation Error (db)	Overall RMS Accuracy of System
L-Band Coverter					
(0.1 - 1.0 GHz)					
Vert & Horiz Channels	2.0	1.5	0.5	0.5	2.60 db
(1. - 2.0 GHz)					
Vert & Horiz Channels	2.0	1.0	0.5	0.5	2.35 db
S-Band					
Vert Channel	0.398	1.0	0.5	0.5	1.29 db
Horiz Channel	0.597	1.0	0.5	0.5	1.37 db
C-Band					
Vert Channel	0.886	0.75	0.6	0.5	1.40 db
Horiz Channel	0.845	0.75	0.6	0.5	1.38 db
X-Band					
Vert Channel	0.708	0.75	0.7	0.5	1.35 db
Horiz Channel	0.921	0.75	0.7	0.5	1.47 db
K_u-Band					
Vert Channel	0.988	0.75	0.8	0.5	1.56 db
Horiz Channel	1.14	0.75	0.8	0.5	1.66 db

SECTION VII

CONCLUSIONS AND RECOMMENDATIONS

7.1 CONCLUSIONS

This report has described the design, development, and fabrication of a developmental "Precision Antenna Measurement System" (PAMS). The most significant result of the program was the successful measurement of airborne antennas and the plotting of their patterns and calculations of their "Effective Radiated Power" (ERP). The patterns, in general, had the predicted shape and the ERP was within 3 db to 4 db of the calculated values. During the program, tests were performed which showed that the frequency measurement accuracy was 0.05 percent and the RMS amplitude measurement accuracy was 1.5 db. The airborne pattern measurements successfully demonstrated that the design concept and goals were met.

Considering the complexity of a system such as the PAMS there were relatively few problems encountered during the development and test phases of the program. The only major problem encountered during the development phase was the tracking capability in the X and K_u band YIG filter assemblies. This was the result of the oscillator and reference channel having different magnetic structures and thereby introducing offset in the tracking. The non-linearities were for the most part compensated for; however, this caused some rolloff of filter performance at the high end of both units resulting in some decrease in receiver sensitivity. The test phase introduced a few new problems. The lack of precision amplitude test equipment (0.1 db or better from 0 to -100 dbm) resulted in slightly higher RMS amplitude errors (0.5 db) than were initially anticipated. During the flight test program, cloverleaf flight patterns provided too few data points which resulted in erroneous pattern plots because of the three-point interpolation used by the computer for curve fitting. A significant improvement was obtained by going to parallel flybys. Associated with the flight pattern problem was the lack of knowledge as to the exact attitude of the aircraft. This caused some of the data to be stored in the wrong data bins resulting in non-existent peaks and valleys in the antenna pattern. Although not really a problem, the two-dimensional plotting formats introduce some restrictions in pattern evaluation. This comes about from the fact that at each common angle plotted, the computer reads the highest power level at that angle and then plots over a 40 db dynamic range down from that point. This negates using overlays for analyzing the patterns since each plot has a different amplitude axis.

7.2 RECOMMENDATIONS

During the course of the program a number of areas were identified which would improve the overall accuracy of the system and extend the present capability. Some of the recommendations listed in the following paragraphs were mentioned briefly in preceding discussions and some have been implemented.

7.2.1 Airborne Monitoring System (AMS)

The AMS system will provide accurate aircraft attitude during the flight program. The information will be used during data reduction and will remove angular ambiguities from the storage of the data. Actron is currently under contract to provide an AMS

device. The system will store positional data from a stable platform on digital tape and will be synchronized by a time code generator referenced to the PAMS clock. The data tape will be used during the Tape Merger Computer program.

7.2.2 Flight Path Study

Provide an analysis to define flight paths to minimize flight time and increase the amount of data collected. With the addition of an AMS a large number of flight patterns can be run. The output of this analysis will optimize the quanity of data as a function of flight economics. In conjunction with the AMS, Actron will provide a flight path study.

7.2.3 Programming

Initiate a program to modify and update existing software. Remove restrictions from existing programs to provide greater flexibility. Generate new programs to satisfy special requirements by the PAMS user.

7.2.4 Propagation and Site Analysis

A problem inherent to all measurement systems which utilize free space as the transmission media is the lack of a good propagation model. This is particularly true for the PAMS which has a measurement capability over a 180:1 bandwidth. Accurate data are required on fading, atmospheric absorption, turbulence effects over the frequency, range, and altitude, where measurements are performed. Associated with this effort would be an evaluation of the Verona test site to provide an RF screening profile, identify all interference sites, and establish lobing profiles for measurements requiring low elevation angles of the PAMS and tracker antennas.

7.2.5 System Analysis

Perform a complete and detailed analysis of the overall PAMS system. This would include the track radars, propagation effects, aircraft scintillation, and would define the overall capability and accuracy.

7.2.6 PAMS Collimation/Calibration

A precision system such as the PAMS requires precision test equipment and facilities to maintain and update the measurement capability of the system. This facility would include an antenna collimation range to provide precise antenna alignment of both the PAMS and the track radars, and to make antenna gain measurements. The use of stable sources would allow system sensitivity and measurement accuracy to be evaluated in a dynamic mode.

7.2.7 L-Band Converter Reference Loops

The L-band converter was added to the system after the receivers were fabricated. As a result the converter has some reduced amplitude accuracy in comparison with the receivers. If greater accuracy is required in the low frequency range, an internal amplitude reference loop could be incorporated into the converter.

7.2.8 Chaff Measurements

Perform an analysis to define the problems involved in making precision measurements of chaff density and dispersion rates. Identify the modifications required in the hardware and software to make these measurements.

7.2.9 Colocated TWT Transmitters

Develop a set of high-power, octave tuning TWT sources which could replace a PAMS receiver. This would locate an active source on the PAMS which could be used as an illuminator for reflectivity and chaff measurements. The source could utilize a separate antenna, or be diplexed with a receiver on a common antenna. The addition of variable modulation circuitry would permit the user to perform a number of ECM measurements and evaluations.

7.2.10 IR Capability

Incorporate IR sensors and receivers into the PAMS to provide the same capability in the IR spectrum as now exists in the RF spectrum.

APPENDIX

ACTIVE RCS MEASUREMENTS WITH PAMS

1.1 INTRODUCTION

The Precision Antenna Measurement System (PAMS) is a highly precise receiver system that was developed by Actron Industries principally to measure dynamic antenna patterns of airborne emitters. The present design is directed primarily at this requirement.

With an auxiliary transmitter, PAMS can operate as a radar to measure the radar cross section (RCS) of physically small targets such as aircraft or the RCS distribution of extended targets such as chaff. In this report, we will discuss what active measurements are of interest, whether PAMS can be used in its present configuration to perform these measurements, and what modifications to PAMS would be necessary to make certain measurements.

We have already distinguished between an RCS measurement of a small target and an RCS distribution measurement of an extended target. The distinction is based on the resolution cell size of the radar (in angle and range). Any target that fits within a resolution cell can be considered a point target as far as the resolution properties are concerned. An extended target is thus larger than one resolution cell. For convenience, we will denote a measurement on a "point-target" as an "RCS measurement." Otherwise, if the target is larger than a resolution cell, the measurement will be an "RCS distribution measurement." Note that both aircraft and chaff can fall into either category, depending on the size of the resolution cell.

2.1 RADAR MEASUREMENTS OF INTEREST

In this section, we will discuss the radar measurements on aircraft (a category that we define to also include all rigid bodies) and chaff (which also includes weather) that are of interest to radar system engineers. In the following discussion, we will always assume that the radar is ground-based and the aircraft or chaff is dynamic.

2.2 RADAR MEASUREMENT ON AIRCRAFT

The following radar measurements on targets are of interest to radar system engineers:

RCS vs. Aspect
Frequency Diversity
Polarization Diversity
Phase
Glint
Bistatic Response
High-Resolution Response in Range
High-Resolution Response in Doppler

The list is not necessarily in the order of importance since all items are not independent. For example, if we know the amplitude and phase of the received signal for all aspects, frequencies, and polarizations, we could derive the glint characteristics and the high-resolution responses in both range and Doppler. In general, this type of measurement is extremely difficult to make, even on a test range. What is usually done is of a much more limited scope. We will now discuss each item in the above list in more detail.

2.2.1 RCS vs. Aspect

This is the fundamental measurement that is usually performed on a target in a test range. Samples of the RCS are taken over many aspects of the target at a fixed frequency and polarization. It is expensive, however, to take enough samples of the RCS pattern to completely describe the target response including all detail in the fine structure of the sidelobes.

In order to estimate the maximum sample spacing in angle so that all information is retained in the RCS pattern, let us place two scatterers a distance Δx apart on a baseline that is normal to the radar line of sight. These scatterers will be in phase. Now let us rotate the baseline so that the scatterers are separated in range by Δr. The phase difference between the scatterers, using the two-way range difference, is

$$\Delta\varphi = (4\pi/\lambda)\,\Delta r \tag{1}$$

The maximum sampling increment in range to retain all information in the response corresponds to a π-radian phase change. Thus by setting $\Delta\varphi=\pi$, we obtain

$$\Delta r = \lambda/4 \tag{2}$$

Since the two scatterers are separated by a distance Δx, the maximum sampling increment in angle is given by

$$\Delta\theta = \Delta r/\Delta x$$

$$= \lambda/4\Delta x \tag{3}$$

For a complex target, the strong scattering centers are not usually located on the extremities of the target. A more reasonable value for the maximum sampling increment would be obtained if we assumed that the strong scattering centers are separated by about L/2 where L is the length of the target. If we make this substitution in (3), we obtain

$$\Delta\theta = \lambda/2L \tag{4}$$

Thus for a 50-ft. target at X-band (λ=0.1 ft.), we require samples every .001 rad if all information in the RCS pattern is to be measured. Over 4π=steradians of solid angle, the total number of samples required is

$$N = 4\pi/(\Delta\theta)^2$$

$$= 16\pi L^2/\lambda^2 \tag{5}$$

For the above example, N is larger than 10^7 samples. Even at L-band (λ=1 ft.), the number of samples required is larger than 10^5.

In practice, one cannot usually afford to obtain so many samples. In many cases, the target aspect is always confined to a limited region so that samples over many aspects of the targets are not really needed. Even if all aspects are of interest, some experimenters just sample the RCS pattern through the principal axes of the target. Others simply sample more coarsely than that specified by (4). In either case, much information is lost.

There is a way to circumvent this dilemma. It is possible to construct good mathematical models of the target and use limited measurement data to establish parameter values in the model and demonstrate validity. The model can then be exercised relatively inexpensively in those situations where detailed information is required on the RCS pattern.

2.2.2 Frequency Diversity

The detailed structure of the RCS pattern is a strong function of small changes in frequency. This is of practical importance because operational radars are capable of operating at many frequencies within a given band. In a generalized measurement program, one does not usually know the exact frequencies of interest in advance. Therefore, it is important to sample the frequency band of interest at fine enough increments to cover all frequencies of interest.

The maximum frequency increment that can be used to retain all information in the RCS response is easy to derive. In (1), we have the phase difference of two scatterers separated by Δr. Since $f\lambda=c$ where f is the frequency and c the propagation velocity, we can write this phase difference as

$$\varphi = (4\pi f/c)\,\Delta r \tag{6}$$

where we have replaced $\Delta\varphi$ by φ. Now if we differentiate φ with respect to f, we obtain

$$\Delta\varphi = (4\pi\Delta r/c)\,\Delta f \tag{7}$$

we can use the sample π-radian criterion to solve for the maximum Δf as

$$\Delta f = c/4\Delta r \tag{8}$$

Again, dominant scatterers are seldom located on the extremities of a target. Therefore, if we set $\Delta r = L/2$ where L is the length of the target, we obtain a more reasonable frequency sampling increment of

$$\Delta f = c/2L \tag{9}$$

Note that this is independent of frequency. For a 50-ft. target, Δf = 10 MHz. Thus, to cover a 1-GHz band of frequencies (at X-band for example), we would need 100 frequency samples to obtain all information in the RCS pattern.

2.2.3 Polarization Diversity

Polarization is a useful discriminant in radar. Targets with lineal features exhibit strong polarization dependencies while rough surfaces tend to depolarize the electromagnetic wave. Thus, polarization is an important parameter in a measurements program. In order to completely specify the polarization properties of a target, we must have both linear components (or both circular components) on transmit and receive. But we only need to record one of the cross terms since they are identical.

2.2.4 Phase Measurements

Phase measurements on targets are routine under well-controlled conditions on a test range where both the radar and target are fixed. With a target in motion, the reference phase ($4\pi r/\lambda$) is always changing, usually in a manner that is not too well predicted. No accelerometer is accurate enough to record absolute position of a moving target to within a fraction of a wavelength over the duration of the measurement. One possible solution would be to use a laser ranging device. But this would be an expensive solution. For this reason, we do not recommend that absolute phase measurements be made on moving targets.

2.2.5 Glint

Slight changes in the target aspect can cause an apparent change in the center of reflected energy from the physical center of the target. This phenomenon is known as glint. It gives rise to an angle noise in an angle tracking radar. With high signal-to-noise ratio on a test range, glint can be measured to about 10% of the beamwidth of the radar antenna, providing the antenna scans across the target. The best way to measure glint with a single antenna beam is to slowly scan the beam past the target, and record the location of the peak response. The glint angle is then determined by the deviation of this peak response from the target centroid predicted on the basis of the flight geometry.

2.2.6 Bistatic Response

In a conventional radar system, the transmitting and receiving antennas are either colocated or they are the same antenna. The radar receives energy radiated only in the backward direction (unless, of course, there are multiple reflections from surfaces other than on the target). By moving the receiving antenna away from the transmitting antenna, we have a bistatic radar where the angle formed by the incident and reflected rays is denoted as the bistatic angle. There are many military applications of a bistatic radar that take advantage of the fact that it is not possible for the target under observation to locate the receiver.

The bistatic response is a function of not only the target aspect with respect to either the transmitter or receiver, but also the bistatic angle. The same rules for sampling should be used as developed in subsection 2.2.1.

2.2.7 High-Resolution Response in Range

A short-pulse radar with a range-gated receiver has a response in range for a point target that is triangular in shape (if the receiver is matched to the transmitted pulse). The resolution capability of this configuration is approximately the length of the pulse. In many high-resolution applications, the transmitted pulse is frequency or phase modulated to improve range resolution without reducing energy. A correlation-type receiver is used to compress the pulse. Irrespective of the waveform, the delay resolution is always approximately

$$\Delta\tau = 1/B \tag{10}$$

where B is the bandwidth of the waveform. Since $c\tau/2=r$, where r is range, we can write the range resolution as

$$\Delta r = c/2B \tag{11}$$

If Δr is much smaller than the range extent of the target, it will be possible to resolve isolated scattering centers on the target. The resulting range profile of RCS (or the RCS distribution in range) can be used for target discrimination, identification, and classification. It should be emphasized that the range profile is a function of target aspect, frequency, and polarization.

2.2.8 High-Resolution Response in Doppler

On a rotating or spinning target, it is possible to resolve isolated scattering centers on the target on the basis of Doppler frequency. The resolution capability is determined by the duration of the coherently processed signal T_c and is given approximately by

$$\Delta f = 1/T_c \tag{12}$$

As an example, consider two scattering centers fixed at each end of a rod of length L that is rotating in a plane that contains the radar line of sight. If Ω is the rotation rate in rad/sec with respect to the radar, the maximum differential range rate between the two scatterers is

$$\Delta\dot{r} = L\Omega \tag{13}$$

Since the Doppler frequency f is related to range rate $\dot{r}$ as

$$f = 2\dot{r}/\lambda \tag{14}$$

we can write the maximum differential Doppler between the two scatterers as

$$\Delta f = 2L\Omega/\lambda \tag{15}$$

For a 50-ft target at X-band ($\lambda = 0.1$ ft) that is rotating at 1-rpm (about 0.1 rad/sec), the maximum differential Doppler between scatterers at each end is thus about 100 Hz. We, therefore, require at least a coherent signal duration of 10 msec for resolution.

There is a slight variation of this technique that can be applied to targets moving with constant velocity even though there is no absolute rotational motion. Over an extended period of time, the target will present different aspects to the radar and appear to rotate. This type of application is usually denoted as inverse synthetic aperture radar. The maximum apparent rotation occurs when the target motion is normal to the radar line of sight and the target is at the intersection. The apparent rotation rate is then given by

$$\Omega = V/r \tag{16}$$

where r is the range and V is the velocity of the target. If we have two scattering centers separated by Δx in the direction of motion (and hence in the cross-range direction), we obtain a differential Doppler by the use of (15) and (16) as

$$\Delta f = \frac{2V\Delta x}{\lambda r} \tag{17}$$

If we substitute $T_c = 1/\Delta f$, we obtain the cross-range resolution capability of approximately

$$\Delta x = \frac{\lambda r}{2VT_c} \tag{18}$$

For an aircraft velocity of 500 ft/sec, a range of 10,000 ft., a wavelength of 0.1 ft., and a coherent processing time of 0.1 sec, we obtain a cross-range resolution capability of 10 ft. Note that this resolution is much better than what is usually obtainable on the basis of the azimuth antenna beam (in the above example, the antenna would have to be 100 ft. in size to obtain comparable resolution).

2.3 RADAR MEASUREMENTS ON CHAFF

The following radar measurements on chaff are of interest to radar system engineers:

Total RCS
RCS Distribution
Polarization Diversity
Frequency Diversity
Doppler Shift and Doppler Spread
Bistatic Responses

These items are generally independent measurements, except that total RCS can be derived from the RCS distribution. It should be emphasized that chaff is a dynamic scattering medium. Any measurements will fluctuate rapidly with time. This dynamic

nature of chaff is of primary interest. Therefore, we will assume that in any measurements program, samples will be obtained continuously throughout a time interval of interest. We will concentrate the discussion here on the type of measurement.

The measurement properties of a cloud of chaff depend on the properties of each chaff element or dipole. In Section 5 of this Appendix, we give a discussion of the backscattering properties of a single dipole.

2.3.1 Total RCS

Although it is theoretically possible to derive the average RCS for an entire cloud of chaff on the basis of the number of elements and the scattering responses of a single element, there are many factors that affect the total RCS in practice that are not analytically tractable. The most important of these factors is an effect called "bird-nesting", where several chaff dipoles come in mutual contact to create a lower overall RCS. In addition, the dipoles can become bent or broken to alter the ideal scattering response. Therefore, it is important to measure the total RCS of a chaff cloud to determine the effectiveness of the type of chaff or the dispensing mechanism.

To measure the total RCS of a chaff cloud with a single measurement, the radar resolution cell determined by the antenna beam and the range gate must be much larger than the extent of the cloud. Since the precise location of the chaff cloud is usually unknown, the radar must search over angle and range to locate the cloud. The total RCS is derived in the same manner as if the chaff were concentrated at a point.

2.3.2 RCS Distribution

In certain applications, it is sometimes desirable to distribute chaff uniformly over a cloud and in other cases in strips, layers, or in some nonuniform manner. In any case, it would be desirable to measure the RCS distribution of chaff over some volume to determine the effectiveness of the distribution technique and the deleterious effects of turbulent winds.

To measure the RCS distribution of a chaff cloud, it is necessary to have resolution capability in at least one of the three dimensions of azimuth, elevation, and range. It would be preferable to have all three. It is most difficult to resolve on the basis of the antenna beam, unless the ranges involved are short (if the receiver location is fixed, it would be possible to move the transmitter close to the chaff to improve angular resolution). It is generally easier to resolve on the basis of range, since this measurement is independent of the actual range.

The antenna beam acts as a lowpass filter on the angle distribution of chaff. For example, if we denote the one-dimensional distribution of chaff RCS in angle as $\sigma(\theta)$, which has the dimensions of RCS per unit angle, the measured response in angle is given by the convolution of $\sigma(\theta)$ with the two-way antenna power pattern $P(\theta)$ as

$$S(\theta) = \int \sigma(\theta')P(\theta-\theta')d\theta' \qquad (19)$$

For a two-dimensional beam, we can define θ to be a coordinate pair, $\sigma(\theta)$ to be the RCS distribution per unit solid angle, and the integration to be over solid angle.

To recover the estimate of the actual RCS distribution $\sigma(\theta)$ from the measured distribution $S(\theta)$, we are forced to use some kind of "deconvolution" technique, practically all of which are basically unstable with noise-type data. A preferable approach would be to compare the measured response $S(\theta)$ with several responses computed on hypothetical RCS distributions to determine which resulted in a best fit. In any case, it is desirable to have beams with low sidelobes to minimize the mutual interference of scatterers.

For resolution in range, we are interested in the receiver response to a point target. In a correlation-type receiver, this point-target response is the autocorrelation function of the waveform if the receiver is matched to the transmitted waveform; otherwise the point-target response is the cross correlation function. Let us denote this point-target response by $X(r)$. Then the measured response in range for distributed chaff is given by the convolution as

$$S(r) = \int \sigma(r')X(r-r')dr' \tag{20}$$

where $\sigma(r)$ is the chaff RCS distribution per unit range. For simultaneous resolution in angle and range, we can combine (19) and (20) as

$$S(r,\theta) = \iint \sigma(r',\theta')P(\theta-\theta')X(r-r')dr'd\theta' \tag{21}$$

where $\sigma(r,\theta)$ is the chaff RCS distribution per unit range per unit solid angle.

If we integrate (21) over range and angle, we obtain the total integrated power as

$$\begin{aligned} S_{TOT} &= \iint S(r,\theta)dr\,d\theta \\ &= \iint \sigma(r,\theta)dr\,d\theta \cdot \int P(\theta)d\theta \cdot \int X(r)dr \end{aligned} \tag{22}$$

The double integral is the total chaff RCS as

$$\sigma_{TOT} = \iint \sigma(r,\theta)dr\,d\theta \tag{23}$$

Now if we define the following two constants

$$K_P = \int P(\theta) d\theta \tag{24}$$

$$K_X = \int X(r) dr \tag{25}$$

we can relate the total integrated power S_{TOT} to the total chaff RCS as

$$S_{TOT} = K_p K_X \sigma_{TOT} \tag{26}$$

where the two constants are just scale factors and are dependent only on system parameters.

2.3.3 Polarization Diversity

A chaff cloud composed of dipoles exhibits strong polarization characteristics. For example, we show in Section 5 of this Appendix that a chaff cloud of randomly oriented dipoles has a cross-polarization ratio for linear polarization of 5 dB (the ratio of the parallel component, HH or VV, to the cross component, HV). This can be used to discriminate dipole chaff from other types of targets or scattering environments.

2.3.4 Frequency Diversity

Dipole chaff exhibits a strong frequency dependence. The most efficient length of dipole chaff in terms of average RCS per unit weight is achieved if the dipole is about one-half wavelength long. The dipole is then matched to the wavelength or frequency. The effective band of frequencies over which the RCS per unit weight is still high is about 11% as we show in Section 5 of this Appendix. To cover a larger band, it is expedient to use dipoles cut to several different lengths. Although it is possible to compute the frequency response of a cloud of mixed-length dipoles, it is necessary to make measurements in practice to determine the effectiveness of the dispensing mechanism and the environmental effects on the cloud as a whole (the heavier dipoles will fall faster, for example).

2.3.5 Doppler Shift and Doppler Spread

Chaff dipoles are usually light in weight and hence tend to move with the local wind. A measurement of Doppler shift is, therefore, a measurement of the local wind conditions. This measurement has often been implemented on rain by radar meteorologists.

Since wind velocities are relatively low, long coherent processing times are required to resolve the Doppler shift imposed by the wind. Even longer times are required to resolve the shape or spread of the Doppler spectrum in high-resolution applications.

We relate Doppler frequency, coherent processing time, and range rate by the use of (12) and (14). To resolve a differential range rate of $\Delta \dot{r}$, we, therefore, require the coherent processing time to be at least as large as

$$T_C = \frac{\lambda}{2\Delta \dot{r}} \tag{27}$$

At X-band (λ = 0.1 ft), we need a coherent processing time of 50 msec to resolve the spectrum to 1 ft/sec.

2.3.6 Bistatic Responses

The bistatic radar response of chaff is important in any bistatic radar application where chaff is a potential ECM technique. In Section 6 of this Appendix, we derive the bistatic radar response of a randomly oriented dipole. With linear polarization, we show that there is a significant difference between HH and VV as a function of the bistatic angle. This feature can be used as a discriminant.

3.1 CAPABILITY OF PAMS

In this section, we will discuss the capabilities and limitations of PAMS in its present configuration on both aircraft and chaff RCS measurements. We will also describe modifications to PAMS to improve the performance in certain areas.

Before we begin the evaluation of PAMS, we should point out that PAMS is presently configured to detect energy in a narrow spectral band that is being swept over a larger band of interest (the bandwidth of this larger band can be varied). The detected energy is then sampled over uniform increments in time. When PAMS is used to measure RCS of either aircraft or chaff, the energy will be confined to the spectral band of the transmitted waveform plus any Doppler shift imposed by the target or chaff motion. Therefore, unless Doppler information is needed, it will not be necessary to sweep the spectrum in PAMS. For frequency diversity, PAMS should sweep or step the spectrum in synchronism with the transmitted waveform.

3.2 PAMS MEASUREMENTS ON AIRCRAFT

In its present configuration, PAMS is adequate to measure aircraft RCS vs. aspect. No modifications will be necessary other than to solve receiver isolation problems.

The finite sampling time of PAMS places certain restrictions on the aircraft roll and turn rates and on the minimum range. In Subsection 2.2.1, we derived the maximum aspect angle to sample the RCS so that no information in the response is lost. If we denote this angle as $\Delta\theta$ and the sampling time by Δt, then the maximum roll or turn rate is $\Delta\theta/\Delta t$. In the example in Subsection 2.2.1 for a 50-ft. target at X-band, $\Delta\theta$ = 0.001 rad. If Δt = 32 msec as in the present PAMS configuration, then the maximum roll or turn rate is 0.030 rad/sec or one turn in 200 sec. At L-band, the maximum rate would be 10-times greater, or one turn in 20 sec.

In Subsection 2.2.8; we indicated that targets flying at uniform velocity over a linear path appear to rotate. This phenomenon sets a lower limit to the range. The maximum

rate of apparent rotation occurs at the minimum range to the flight path and is given by (16) as V/r where V is the aircraft velocity and r is the minimum range. Hence

$$\frac{\Delta\theta}{\Delta t} = \frac{V}{r} \tag{28}$$

We can solve for the minimum range as

$$r = V\,\Delta t/\Delta\theta \tag{29}$$

For the above example of $\Delta\theta = 0.001$ rad. $\Delta t = 32$ msec and for V = 300 ft/sec, the minimum range is 10^4 ft. Note that this requirement is less severe than the one on roll or turn rates.

In its present configuration, PAMS is also capable of measuring the frequency and polarization dependence of the RCS response of aircraft. Glint and bistatic radar measurements are also possible with the present configuration. Thus, in its present configuration, PAMS has a wide range of application on target measurements.

To make high-resolution measurements in range, the received signal must be sampled at a rate corresponding to the bandwidth of the signal. For 10-ft range resolution, the bandwidth is 50 MHz. If phase modulated signals are used, both the relative phase and amplitude or the quadrature video components of the received signal must be either processed in real time or recorded at the full bandwidth for pulse compression at a later time. PAMS is presently configured to sample only the peak response as a function of range. For high-resolution in range, PAMS must be modified to sample continuously in range at a rate equal to the signal bandwidth.

For high-resolution Doppler measurements, the amplitude and phase (here phase is most important) of the received pulses must be sampled over the coherent processing time. The transmitter must also be phase-locked over this time. The sampling rate is determined by the pulse repetition frequency. It appears that extensive modifications to PAMS will be necessary to make high-resolution measurements in either range or Doppler.

3.3 PAMS MEASUREMENTS ON CHAFF

PAMS is presently capable of measuring the total RCS of a chaff cloud. To avoid difficulties in the measurement, the chaff should be dispensed at a range sufficiently large so that it is completely within the antenna beam. In addition, the bandwidth should be low enough so that all chaff is within a range resolution cell. The peak received power is then proportional to the total chaff RCS and the ordinary point-target radar range equation given by

$$\frac{P_R}{P_T} = \frac{G_1 G_2 \lambda^2}{(4\pi)^3 r^4}\,\sigma \tag{30}$$

can be used to scale the RCS, where G_1 and G_2 are the antenna gains of the transmitting and receiving antennas.

PAMS can be used to resolve the chaff with the antenna beam, providing either the receiving or transmitting antenna (or both) is close to the chaff cloud. If the ranges to each antenna are unequal, the radar range equation in (30) must be modified by replacing r^4 with $r_1^2 r_2^2$ where r_1 and r_2 are the respective ranges. This result also applies for bistatic angles.

PAMS is also capable of providing polarization and frequency diversity in its present configuration. To cover wide frequency bands, several transmitters will probably be required.

Just as in the case of high-resolution range or Doppler measurements on aircraft, PAMS will also require extensive modifications to measure chaff RCS at high-resolution in range or Doppler. However, it is more important for chaff measurements that PAMS have resolution capability in other than angle in order to extend the utility of PAMS. Because of the restrictions on the minimum range that result in poor angle resolution, PAMS will have only limited applicability in chaff measurement programs without high-resolution in range. Resolution of at least 50 ft. (10 MHz bandwidth) is necessary in most chaff measurements where RCS distribution is desired.

4.1 CONCLUSIONS

In its present configuration, PAMS can be used in a wide variety of applications to measure RCS and RCS distributions of aircraft (and other rigid bodies) and chaff. The principal features of PAMS that would be attractive in an RCS measurement program are

(a) precision and good calibration

(b) automatic data processing

(c) extremely wide frequency range

(d) polarization diversity

The following applications are well within the capability of the present configuration of PAMS:

(a) RCS vs. aspect on aircraft

(b) total RCS of chaff

(c) frequency diversity

(d) polarization diversity

(e) glint on aircraft

(f) bistatic responses on aircraft and chaff

The principle limitation of the present configuration of PAMS is the lack of range resolution, especially in chaff measurement applications. One other limitation of less importance is the fixed time sampling increment in PAMS.

To extend the capability of PAMS, it is recommended that range gating be added in the receiver for use with unmodulated pulses. This improvement will provide range resolution capability in those applications where the ranges are short and the target RCS is strong.

For chaff RCS measurements, it is recommended that a portable version of PAMS be constructed since the chaff must usually be dispensed in remote areas. To make this feasible, the antennas will probably have to be smaller than the present design. But with high range-resolution capability, some loss in angular resolution could be tolerated.

5.1 BACKSCATTERING CHARACTERISTICS OF A RESONANT WIRE (BY J. L. WONG)

The scattering characteristics of a thin wire may be derived from the transmitting and receiving properties of a wire antenna (i.e., as if the wire were used as an antenna). When an electromagnetic wave is impinging upon an antenna, part of the incident energy is absorbed and part is reradiated or scattered. The amount of energy scattered depends on, among other factors, the load impedance connected across the antenna terminals. Thus, a wire scatterer may be regarded as a short circuited dipole antenna.

The equivalent circuit for an antenna is a simple two-terminal network as shown in Figure 1. The impedance of the antenna is denoted by Z_a, and the terminating impedance is presented by Z_t. The real part of the antenna impedance R_a generally consists of a radiation resistance R_r and a loss resistance R_ℓ. The voltage induced at the antenna terminals by the incident electromagnetic wave is represented by V. The antenna current is thus given by

$$I = \frac{V}{Z_a + Z_t} \tag{31}$$

The power delivered to the load is $R_t|I|^2$, and the power dissipated in the antenna impedance is $R_a|I|^2$. The former is related to the receiving cross section of the antenna, while the latter is related to the scattering cross section of the antenna; e.g., for a lossless antenna the power dissipated in the antenna impedance may be interpreted as the power re-radiated or scattered by the antenna. For maximum power transfer to the load, the terminating impedance is set equal to the complex conjugate of the antenna impedance, i.e., $Z_t = Z_a^*$, and under this matched condition the receiving cross section of the antenna is maximum. If the antenna is lossless, an equal amount of power is dissipated in the antenna radiation resistance. Thus, under matched load conditions the scattering cross section is equal to the receiving cross section. It is known that the maximum receiving cross section of any lossless antenna is given by $(\lambda^2/4\pi)G$, where λ is the wavelength and G is the antenna gain function.

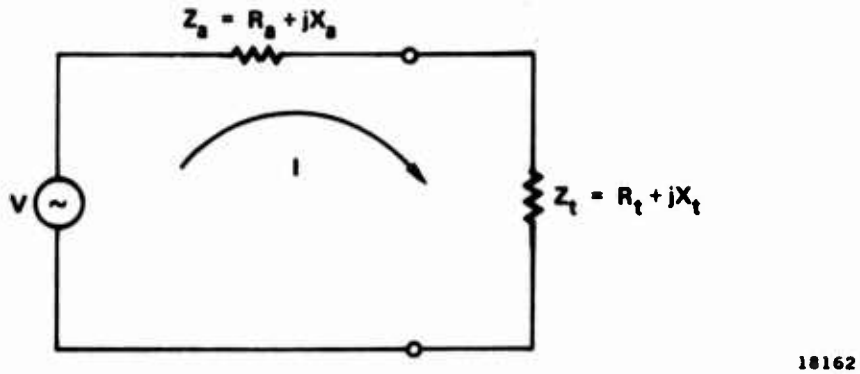

Figure 1. Equivalent Circuit of an Antenna

Hence, the scattering cross section of a lossless antenna under matched load conditions is given by

$$\sigma_{sm} = \frac{\lambda^2}{4\pi} G \tag{32}$$

If the antenna is loaded by an arbitrary impedance, the scattering cross section is given by

$$\sigma_s = \frac{P}{P_m} \sigma_{sm} = \frac{\lambda^2}{\pi} G \left| \frac{R_r}{Z_a + Z_t} \right|^2 \tag{33}$$

where

$P = R_r |I|^2$ = Power scattered with an arbitrary load

$P_m = R_r |I_m|^2$ = Power scattered with a matched load

$I_m = \frac{V}{2R_r}$ = Antenna current with a matched load

Since the antenna has transmitting gain as well as receiving gain, and if only back-scattering is considered, the cross section of the antenna is

$$\sigma = G\sigma_s = \frac{\lambda^2}{\pi} G^2 \left| \frac{R_r}{Z_a + Z_t} \right|^2 \tag{34}$$

Equation (34) is identical to that given by Harrington [1] and derived by using a different approach. It should be noted that the derivation which led to (34) is only approximately correct; e.g., (34) implies that an open-circuited antenna would scatter no field. However, it should be correct if the power scattered by the open-circuited antenna is small compared to that of the terminated antenna. Such is the case for a half-wavelength dipole.

For an unloaded wire, we set $Z_t = 0$, and Equation (34) reduces to

$$\sigma = \frac{\lambda^2}{\pi} G^2 R_r^2 / |Z_a|^2 \tag{35}$$

where

$$|Z_a| = \sqrt{(R_r + R_\ell)^2 + X_a^2} \tag{36}$$

Maximum cross section is observed when $R_\ell = 0$ (lossless) and $X_a = 0$ (resonant). The resonant condition occurs when the dipole is slightly less than half wavelength rather than exactly half wavelength.[2] The maximum gain of a half-wavelength dipole is equal to 1.64 and hence the maximum cross section is equal to $0.86\lambda^2$. Other properties can be established by examination of the scattering geometry (Figure 2) and by consideration of the parameters in Equations (35) and (36).

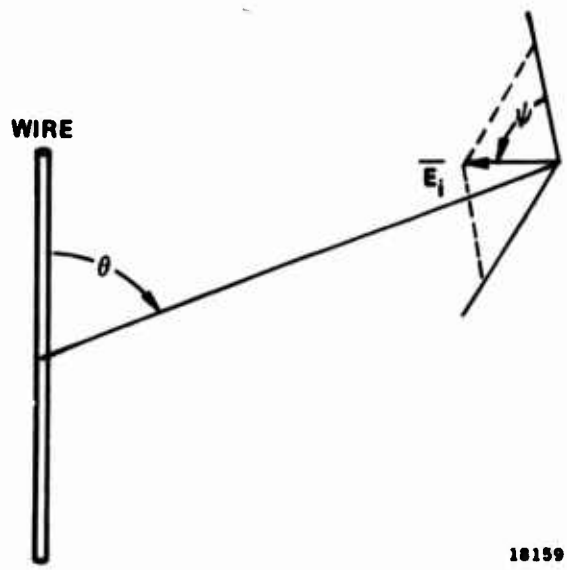

Figure 2. Wire Scattering Geometry

For oblique incidence the radar cross section is modified by the angular response of the wire. If a sinusoidal current distribution is assumed, the gain function is given by

$$G(\theta) = (1.64)\left[\frac{\cos(\frac{\pi}{2}\cos\theta)}{\sin\theta}\right]^2 \tag{37}$$

where θ is measured from the wire axis. In addition, if the transmitter polarization (direction of the electric field) makes an angle ψ with the plane of incidence (the plane formed by the wire axis and the direction of incidence), the received backscattered field is modified by $\cos^2\psi$ and hence the backscattering cross section is modified by $\cos^4\psi$. The backscattering cross section of a lossless resonant $\frac{\lambda}{2}$ - dipole then becomes

$$\sigma(\theta,\psi) = \sigma_o\left[\frac{\cos(\frac{\pi}{2}\cos\theta)}{\sin\theta}\right]^4 \cos^4\psi \tag{38}$$

where $\sigma_o = 0.86\lambda^2$ is the maximum cross section.

When a resonant wire is used as a chaff element, its orientation in space is generally not known. For the spherical random case, every orientation in space is equally likely, the average cross section is given by

$$\bar{\sigma} = \frac{1}{4\pi}\int_0^{2\pi}\int_0^{\pi}\sigma(\theta,\psi)\sin\theta\, d\theta\, d\psi \tag{39}$$

For a half-wave lossless resonant dipole, Equation (39) gives

$$\sigma \approx 0.17\,\lambda^2 \tag{40}$$

The bandwidth of a chaff dipole generally depends on the conductivity and thickness of the wire. In Equation (35) the radar cross section of a wire antenna is expressed in terms of the antenna impedance parameters. The bandwidth characteristics can be determined by observing the impedance variations with frequency[3]. For a perfectly conducting wire, the 3-dB bandwidth is about 11%. When the conductivity of the wire is finite, part of the incident energy will be dissipated in the wire resistance. Consequently, the backscattering cross section will be reduced. The effect of finite wire conductivity can be accounted for by incorporating the wire loss resistance in the calculation of radar cross section. Two assumptions are made:

1. The current distribution on the wire is the same as that of a perfectly conducting wire.

2. For a given frequency, the wire length can be adjusted to achieve the resonant condition.

At resonance the broadside backscattering cross section is given by

$$\sigma = (0.86\lambda^2)\left[\frac{R_r}{R_r + R_\ell}\right]^2 \tag{41}$$

For a sinusoidal current distribution, i.e $I=I_0 \sin k(\ell - z)$ where I_0 is the current at the center of the wire and ℓ is the half length of the wire, the effective loss resistance of the wire is given by

$$R_\ell = \int_{-\ell}^{+\ell} R_i \sin^2 k(\ell - |z|)dz = R_i \ell \tag{42}$$

where

R_i is the internal resistance per unit length, [4]

$$R_i = \frac{\sqrt{\frac{\pi f \mu}{2G}}}{\pi a}\left[\frac{\text{Ber } q \text{ Bei}'q - \text{Bei } q \text{ Ber}'q}{(\text{Ber}'q)^2 + (\text{Bei}'q)^2}\right] \tag{43}$$

G = conductivity (mhos/m)

$\mu = 4\pi \times 10^{-7}$

a = wire radius

$q = \sqrt{2}\, a/\delta$

$\delta = \frac{1}{\sqrt{\pi f \mu_o G}}$ = skin depth

$\text{Ber } q = \text{Re}[J_o(q/\sqrt{j})]$

$\text{Bei } q = \text{Im}[J_o(q/\sqrt{j})]$

$\text{Ber}' q = \frac{d}{dq} \text{Ber } q$

$\text{Bei}' q = \frac{d}{dq} \text{Bei } q$

$J_o(x)$ = Zero order Bessel function of first kind

Thus, the loss resistance can be calculated once the conductivity, wire size, and frequency are specified. Figure 3 shows the effect of wire losses on the peak cross section of a resonant dipole for a frequency of 3 GHz and a wire diameter of 1 mil,

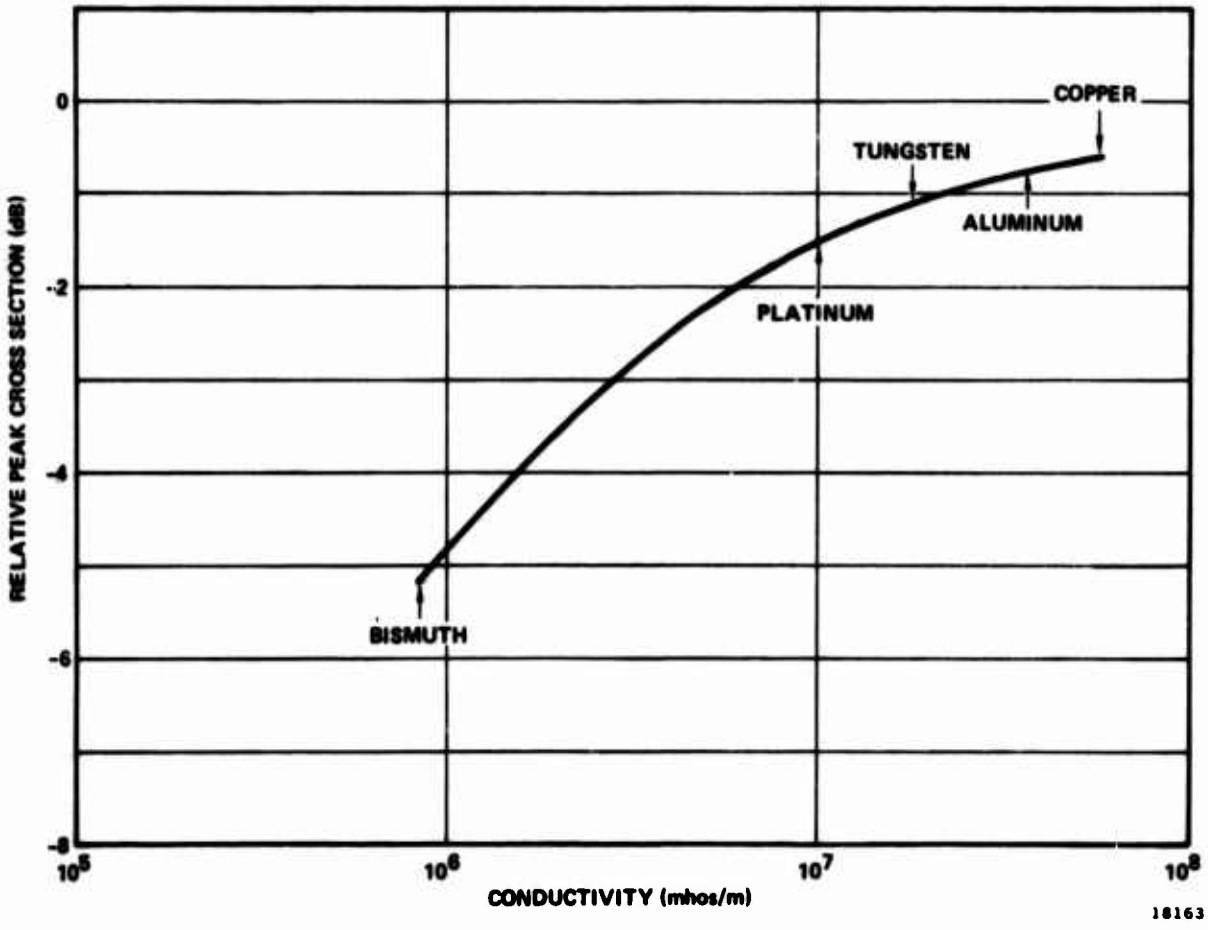

Figure 3. Effect of Wire Losses on the Peak Cross Section of a Resonant Wire. Frequency = 3 GHz; Wire Diameter = 1 mil

and Figure 4 shows the normalized peak cross section as a function of wire diameter for copper, platinum, and bismuth wires at 3 GHz.

Since the gain-bandwidth product for a small resonant scatterer is unchanged by losses, the radar cross section and bandwidth characteristics are related by

$$\sqrt{\sigma}\,\beta = \sqrt{\sigma}_o\,\beta_o = \text{constant} \tag{44}$$

A derivation of this relation has been given by Harrington.[5] A plot of the bandwidth characteristics for a half-wave dipole as a function of conductivity for a 1 mil wire at 3 GHz is given in Figure 5. The general effect of wire losses is to reduce the scattering cross section and to widen the bandwidth.

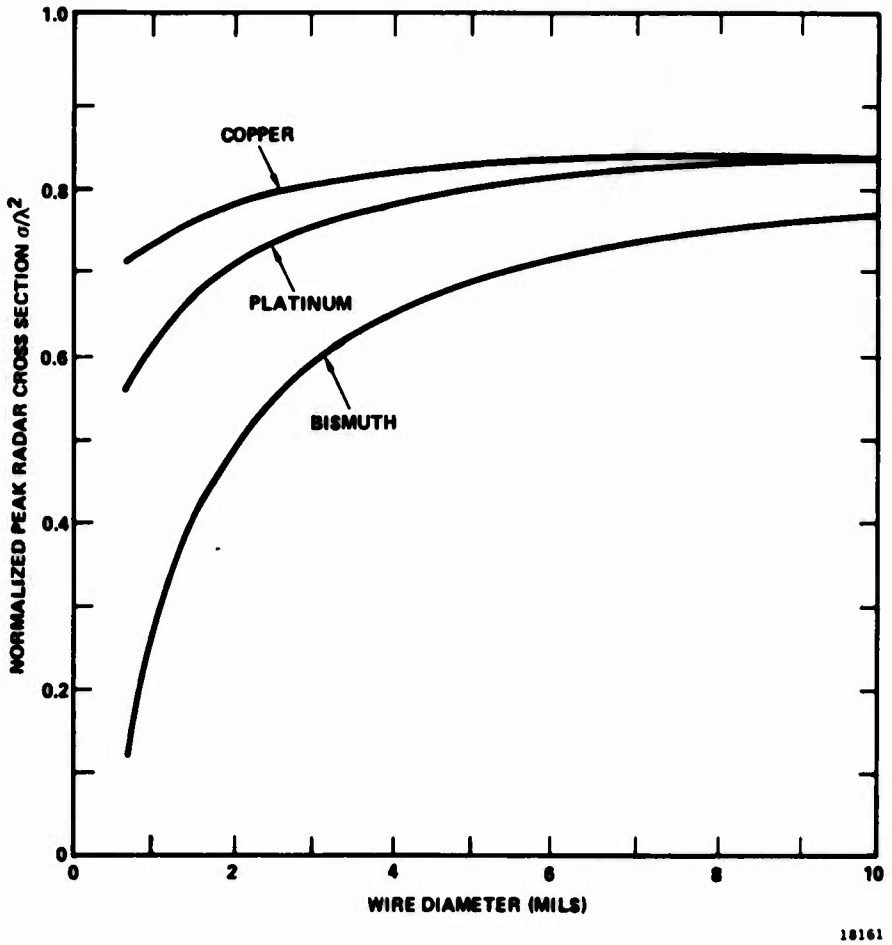

Figure 4. Radar Cross Section as a Function of Wire Diameter. Frequency = 3 GHz

REFERENCES TO SECTION 5 OF THIS APPENDIX

1. R.F. Harrington, "Electromagnetic Scattering by Antennas," IEEE Trans. on Antennas and Propagation, Vol. AP-11, September 1963, pp. 595-596.

2. J.D. Kraus, Antennas, McGraw-Hill Book Co., New York, 1950.

3. S.A. Schelkunoff and H.T. Friis, Antennas - Theory and Practice, John Wiley and Sons, Inc., New York, 1952.

4. S. Ramo and J.R. Whinnery, Fields and Waves in Modern Radio, John Wiley and Sons, Inc., New York, 1953.

5. R.F. Harrington, "Some Bounds on the Behavior of Small Resonant Scatterers," IEEE Trans. on Antennas and Propagation, Vol. AP-12, January 1964, p. 126.

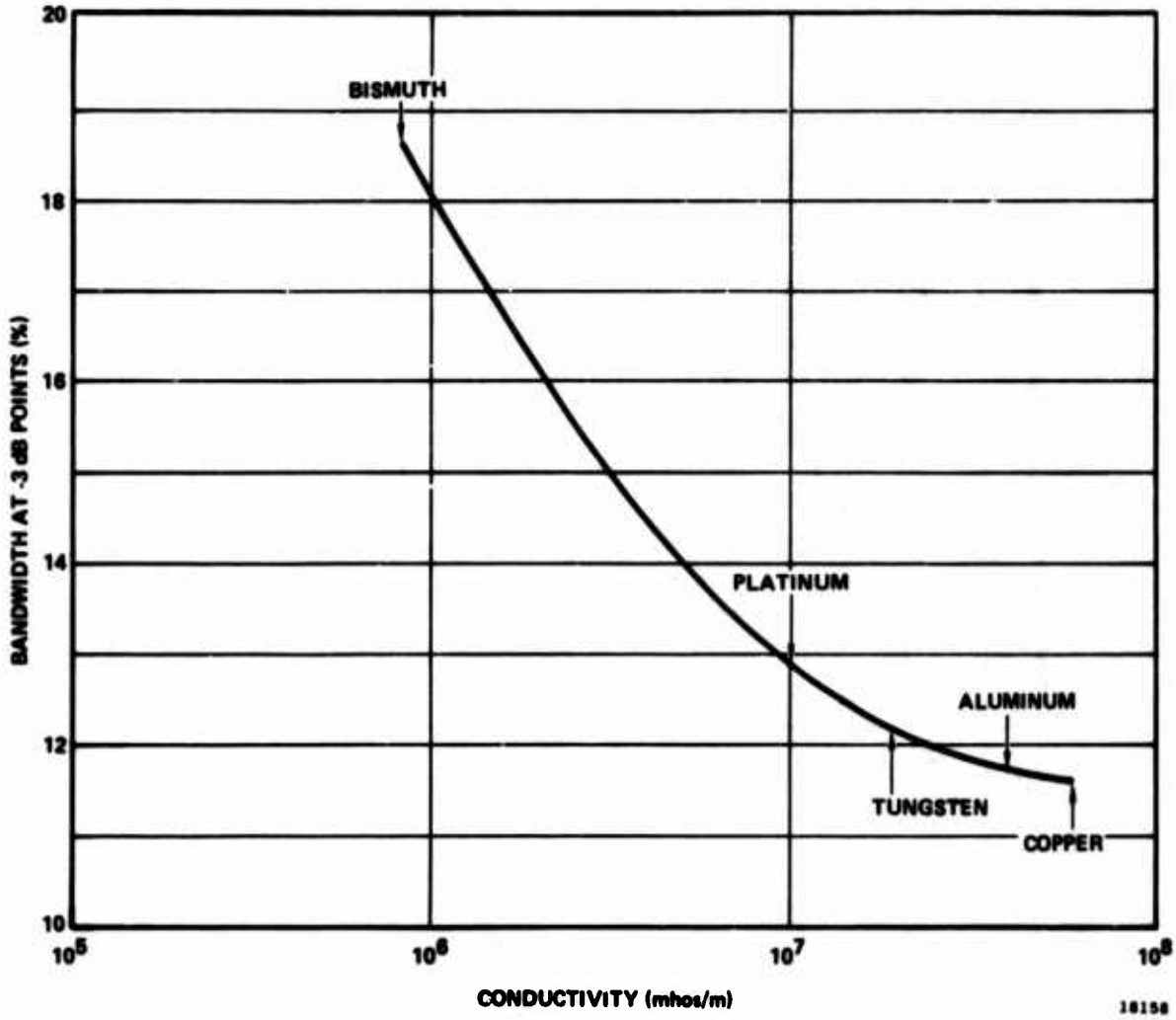

Figure 5. Bandwidth of a Chaff Dipole as a Function of Conductivity. Frequency = 3 GHz; Wire Diameter = 1 mil

6.1 BISTATIC RADAR CROSS SECTION OF A CHAFF DIPOLE (BY J. L. WONG)

In this section, we derive an expression for the average bistatic radar cross section of a randomly oriented dipole. Variable transmitter and receiver polarizations are considered. Numerical results are given for the special case when the transmitter and receiver are similarly or orthogonally polarized.

The bistatic scattering geometry is shown in Figure 6. The transmitter and receiver are separated by the angle β. The incident wave is assumed to be propagating along the positive Z-axis of the transmitter (unprimed) coordinate system, and the scattered wave is observed in the direction of the negative Z'-axis of the receiver (primed)

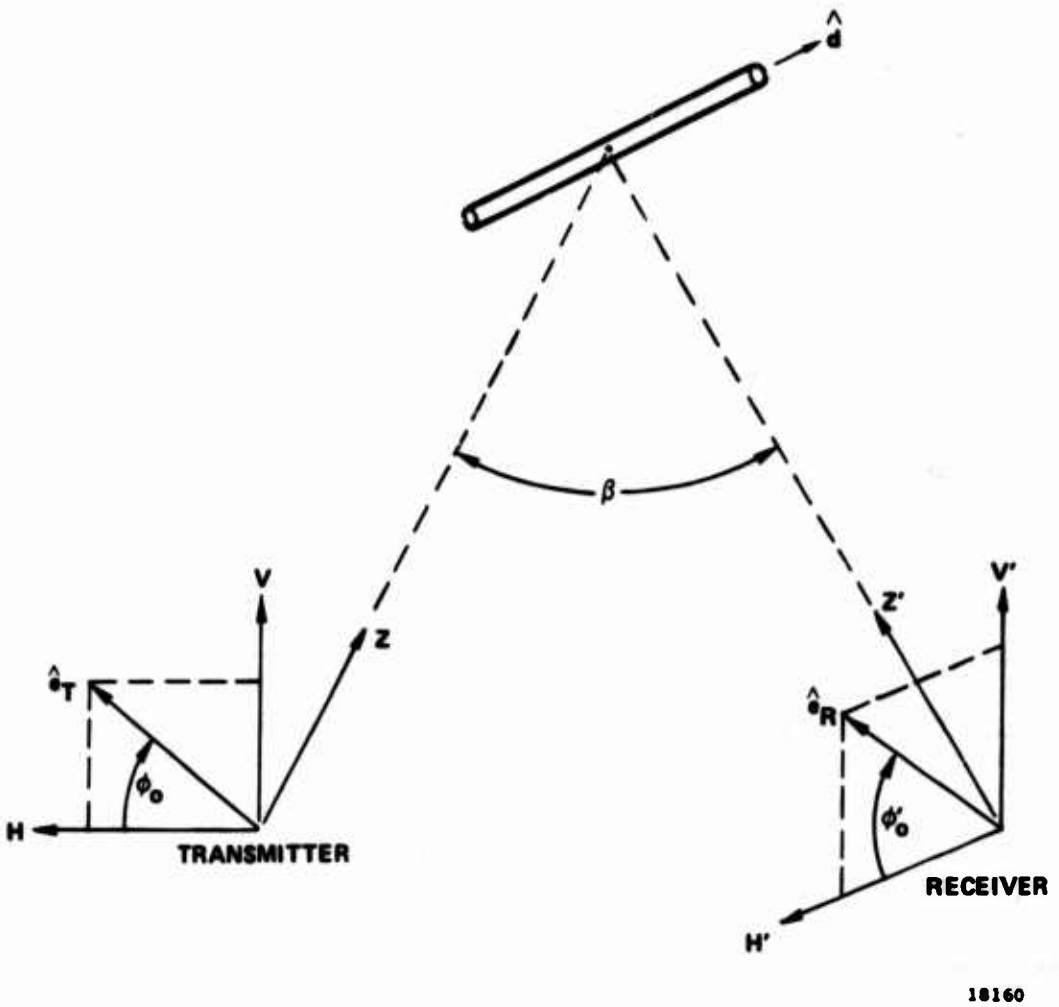

Figure 6. Bistatic Scattering Geometry for a Chaff Dipole

coordinate system. If the polarization vector of the transmitter is $\hat{e}_T$ and that of the receiver is $\hat{e}_R$, the radar cross section may be expressed as

$$\sigma = \sigma_o \left| (\hat{d} \cdot \hat{e}_T)\,(\hat{d} \cdot \hat{e}_R) \right|^2 \tag{45}$$

where σ_o is the maximum cross section and $\hat{d}$ is a unit vector parallel to the dipole axis. For a half-wavelength resonant dipole,

$$\sigma_o \approx 0.86\,\lambda^2 \tag{46}$$

In order to compute the exact radar cross section it is necessary to express the dipole orientation and the polarization vectors in one common coordinate system. However, some simplifications can be made if the dipole is randomly oriented and only the average cross section is desired. Consider the localized dipole coordinate system shown in Figure 7. The orientation of the dipole is described by the spherical angles θ and φ. For simplicity, we choose the polarization vector $\hat{e}_T$ to be parallel to the x-axis and assume that both $\hat{e}_T$ and $\hat{e}_R$ lie in the xy-plane. With these simplifications, we find

$$\hat{d} \cdot \hat{e}_T = \sin\theta \cos\varphi \tag{47}$$

$$\hat{d} \cdot \hat{e}_R = \sin\theta \cos(\varphi - \gamma) \tag{48}$$

and the average radar cross section is given by

$$\bar{\sigma} = \frac{\sigma_o}{4\pi} \int_0^{2\pi} \int_0^{\pi} |(\hat{d} \cdot \hat{e}_T)(\hat{d} \cdot \hat{e}_R)|^2 \sin\theta \, d\theta \, d\varphi \tag{49}$$

If both the transmitter and receiver are linearly polarized, the polarization vectors are real and (49) yields

$$\bar{\sigma} = \sigma_o \left[\frac{1}{15} + \frac{2}{15} (\hat{e}_T \cdot \hat{e}_R)^2 \right] \tag{50}$$

Using Figure 6, we have

$$\hat{e}_T = \hat{H} \cos\varphi'_o + \hat{V} \sin\varphi'_o \tag{51}$$

$$\hat{e}_R = \hat{H}' \cos\varphi_o + \hat{V}' \sin\varphi_o \tag{52}$$

For simplicity, we choose the coordinate axes such that the transmitter and receiver coordinate systems are rotated in the HZ-plane by the bistatic angle β. Hence, the unit vectors $(\hat{H}', \hat{V}', \hat{Z}')$ in the receiver coordinate system are related to the unit vectors $(\hat{H}, \hat{V}, \hat{Z})$ in the transmitter coordinate system by the rational transormation,

$$\begin{pmatrix} \cos\beta & 0 & \sin\beta \\ 0 & 1 & 0 \\ -\sin\beta & 0 & \cos\beta \end{pmatrix} \tag{53}$$

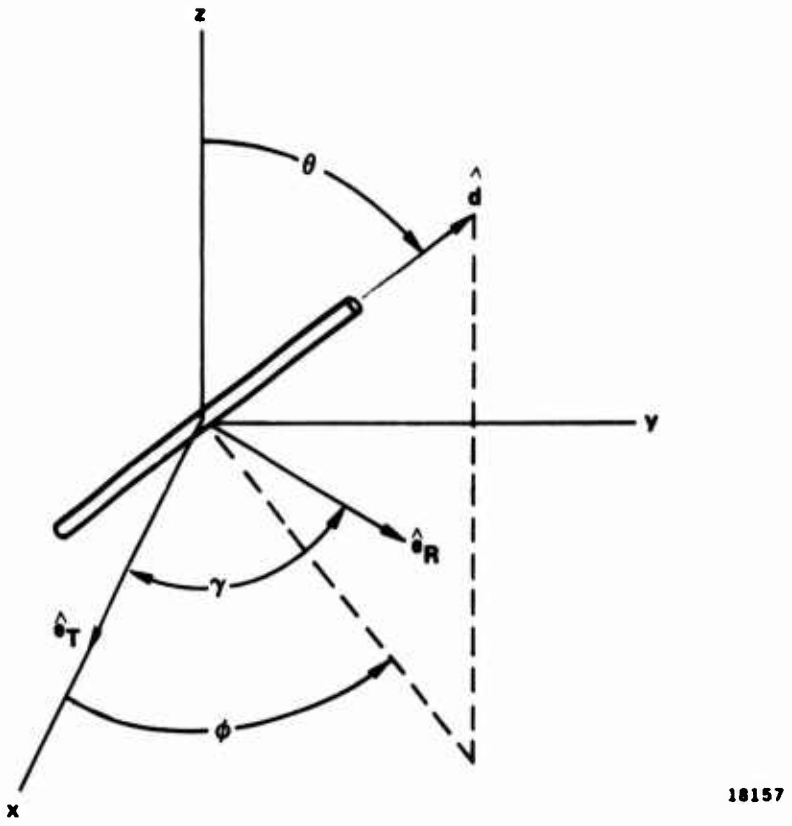

Figure 7. Localized Coordinate System for a Chaff Dipole with Transmitter Polarization $\hat{e}_T$ and Receiver Polarization $\hat{e}_R$

Using (51) to (53), we find

$$\bar{\sigma} = \frac{\sigma_o}{15}\left[1 + 2\,(\sin\varphi_o \sin\varphi_o' + \cos\beta\,\cos\varphi_o \cos\varphi_o')^2\right] \tag{54}$$

Thus, for linear polarization, the average radar cross section varies between $\sigma_o/15$ and $\sigma_o/5$ depending on the relative orientation of the transmitter and receiver polarization vectors.

For circular polarization, the polarization vectors are complex. Thus, we let

$$\hat{R} = \frac{1}{\sqrt{2}}(\hat{H} - j\hat{V})$$

(Right Hand Circular) (55)

$$\hat{R}' = \frac{1}{\sqrt{2}}(\hat{H}' - j\hat{V}')$$

and

$$\hat{L} = \frac{1}{\sqrt{2}}(\hat{H} + j\hat{V})$$

(Left Hand Circular) (56)

$$\hat{L}' = \frac{1}{\sqrt{2}}(\hat{H}' + j\hat{V}')$$

where the primed and unprimed vectors refer to the receiver and transmitter coordinate systems, respectively. Following a similar procedure, we find

$$\bar{\sigma} = \frac{\sigma_o}{30}(3 + \cos^2\beta) \tag{57}$$

In this case the average radar cross section is independent of the sense of polarization and depends only on the bistatic angle.

Of practical interest is the case when the transmitter and receiver polarizations are similarly or orthogonally polarized. The following results are obtained:

$$\bar{\sigma}_{VV'} = \frac{1}{5}\sigma_o \tag{58}$$

$$\bar{\sigma}_{HH'} = \frac{2}{15}\sigma_o\,(1/2 + \cos^2\beta) \tag{59}$$

$$\bar{\sigma}_{HV'} = \sigma_{VH'} = \frac{1}{15}\sigma_o \tag{60}$$

The average radar cross section as a function of bistatic angle for a half-wavelength resonant dipole is shown graphically in Figure 8.

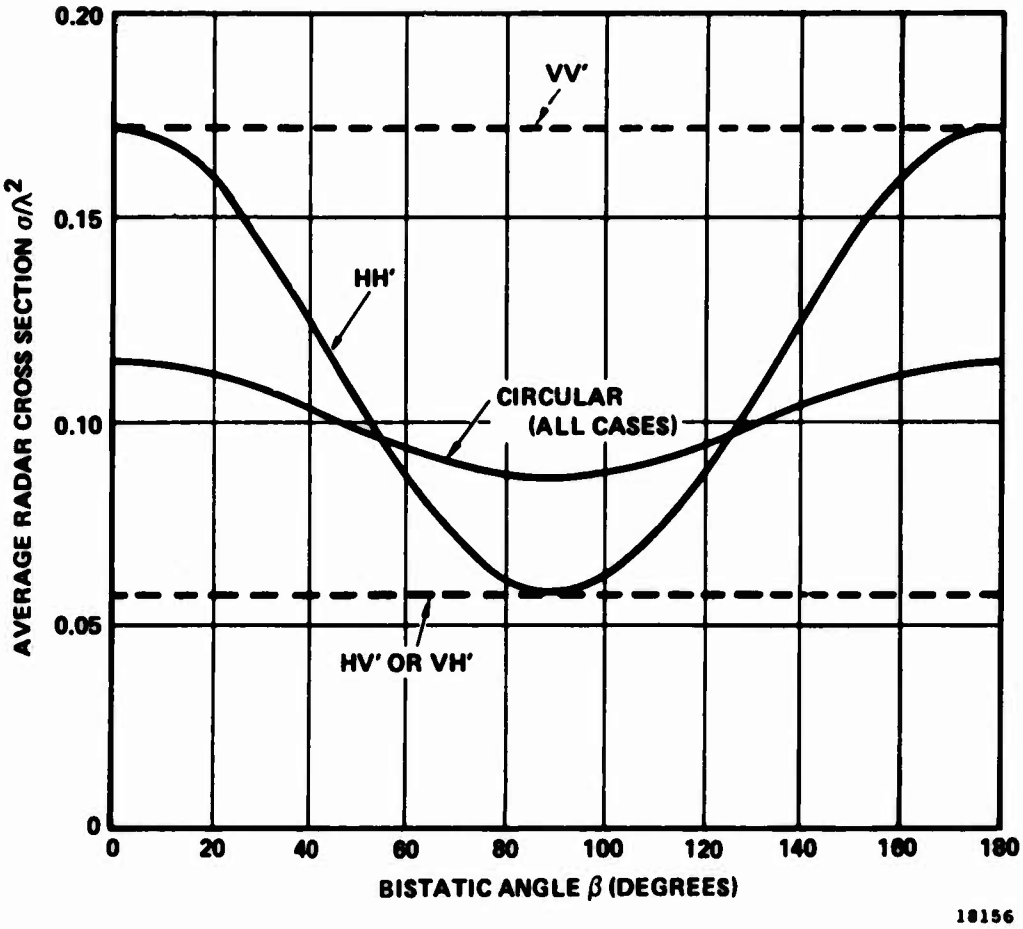

Figure 8. Average Bistatic Radar Cross Section of a Half-Wavelength Dipole with Spherical Random Orientation

REPORT DOCUMENTATION PAGE

READ INSTRUCTIONS BEFORE COMPLETING FORM

1. REPORT NUMBER: RADC-TR-73-233	2. GOVT ACCESSION NO.
3. RECIPIENT'S CATALOG NUMBER	
4. TITLE (and Subtitle): PRECISION ANTENNA MEASUREMENT SYSTEM (PAMS)	5. TYPE OF REPORT & PERIOD COVERED: Final - January 70 - February 72
6. PERFORMING ORG. REPORT NUMBER: 2101-03-3000	
7. AUTHOR(s): Graham A. Walker	8. CONTRACT OR GRANT NUMBER(s): F30602-70-C-0011
9. PERFORMING ORGANIZATION NAME AND ADDRESS: Actron Industries, Inc. 700 Royal Oaks Monrovia, California 91016	10. PROGRAM ELEMENT, PROJECT, TASK AREA & WORK UNIT NUMBERS: 65100015
11. CONTROLLING OFFICE NAME AND ADDRESS: Rome Air Development Center (TUTV) Griffiss AFB, NY 13441	12. REPORT DATE: August 1973
	13. NUMBER OF PAGES: 196
14. MONITORING AGENCY NAME & ADDRESS (if different from Controlling Office): Same	15. SECURITY CLASS. (of this report): Unclassified
	15a. DECLASSIFICATION/DOWNGRADING SCHEDULE: N/A

16. DISTRIBUTION STATEMENT (of this Report)

Distribution limited to U. S. Government Agencies only; Test and Evaluation; August 1973. Requests for this document must be referred to RADC, (TUTV), GAFB, NY 13441.

17. DISTRIBUTION STATEMENT (of the abstract entered in Block 20, if different from Report)

N/A

18. SUPPLEMENTARY NOTES

RADC Project Engineer: Merton E. Cook (TUTV)
Griffiss AFB, NY 13441

19. KEY WORDS (Continue on reverse side if necessary and identify by block number)

Antennas
Airborne Antennas
Antenna Measurements
Antenna Patterns
Data Processing
Receivers
Dynamic Measurements
Test Facilities

20. ABSTRACT (Continue on reverse side if necessary and identify by block number)

This technical report documents the design, development, and performance of a Precision Antenna Measurement System (PAMS) which is used to perform dynamic measurements and evaluate the radiation characteristics of airborne antennas.

The PAMS operates over the frequency range of 100 MHz through 18 GHz and can be used to measure the cross section of aircraft and chaff. The system is slaved to either an AN/MSQ-1A or AN/FPS-16

20. (Continued)

track radar for aircraft acquisition.

The report details the design parameters and covers the data acquisition and computer programs used in the data reduction. The system performance is presented and actual antenna patterns given for various antenna configurations on a C-131 aircraft.

SAC--Griffiss AFB NY